

**Quantitative Mineralogic Evaluation of the Transition Zone: Ore
Characterization Study at the Cerro Colorado Porphyry Cu- (Mo-)
Deposit, Region I, Northern Chile.**

**by
Jason David Odette**

**Submitted as partial fulfillment of the
Requirements for the Degree of
Master of Science in Geology
April 26, 2005**

**Department of Earth and Environmental Science
New Mexico Institute of Mining and Technology
Socorro, NM**

ABSTRACT

The ca 51.8 to 55.8 Ma Cerro Colorado porphyry Cu- (Mo) deposit is located approximately 120 km east-northeast of the port city of Iquique, Región I, northern Chile. Hypogene pyrite (py)-chalcopyrite (cp)-(bornite) (bn) and py-bn mineralization at Cerro Colorado is associated with multiple shallow-level, generally felsic to intermediate composition, Eocene age intrusions and associated breccias that cross cut late Cretaceous age andesitic volcanic rocks of the Cerro Empexa Formation. Sulfur isotopic compositions of pyrite display $\delta^{34}\text{S}$ values from +0.2 to +2.9‰ and a mean of +2.0‰ indicating that the primary source of sulfur during hypogene mineralization at Cerro Colorado was magmatic.

As part of a characterization of the “transition zone”, the rock volume comprising the geochemical change from supergene metals accumulation to essentially unoxidized hypogene sulfides, the relative volume percents of chalcocite (cc), covellite (cv), py, cp, and bn were calculated for one hundred thirty-five 10-meter composite pulp samples from fourteen drill holes representing the Cerro Colorado deposit. Using mineral ratios (py:cp, cc+cv:cp+bn, py:cc+cv, and cc:cv) three distinct mineralogic zones were delineated: 1) Supergene enrichment zone; 2) Transition zone; and 3) Hypogene zone.

The supergene enrichment zone at Cerro Colorado is defined as a volume of rock having a cc+cv:cp+bn ratio ≥ 2 and having $\geq 80\%$ of the copper contained in cc+cv. This zone is characterized by very strong cc/cv replacement of py and cp and absence of bn.

The upper parts of the supergene enrichment zone are predominantly cc, whereas the lower intervals are generally dominated by cv.

The transition zone is defined as a rock volume having a cc+cv:cp+bn ratio ≥ 0.1 and < 2 and having $\geq 15\%$ but $< 80\%$ of the copper contained in cc+cv. This zone is characterized by a mixed hypogene/supergene mineral assemblage represented by the incomplete replacement of bn, cp, and py by cc and cv. From base of enrichment to the top of unenriched hypogene mineralization, cc and cv replacement of cp and bn gradually weakens. This is manifested initially as lesser replacement of cp, then bn, by paragenetically latest cv.

The hypogene zone is defined as the volume of rock having a cc+cv:cp+bn ratio ≤ 0.1 and $< 15\%$ of the copper contained in cc+cv. This zone is characterized by an essentially unoxidized py+cp±bn mineral assemblage having a py:cp ratio between 0.5 to 5. Near the center of the deposit this zone is characterized by a py+bn mineral assemblage. Where cc/cv enrichment as is developed in the py+bn assemblage, a supergene profile may appear as a deeply penetrating enrichment zone within the hypogene and/or transition zones due to the absence of hypogene chalcopyrite.

The transition zone varies in thickness from 10 to 20-meters along the western margins of the deposit, thickening to 40 to 60-meters in the west-central and eastern parts of the deposit. This is attributable to a variety of factors that include: variations in hypogene mineralization and wall-rock alteration intensity; pre-oxidation total pyrite content of the leached capping; variations in fracture development; and structural history of fault-bounded regimes. This study found a strong correlation between transition zone thickness and wall-rock alteration mineral assemblages. Where this zone is developed

within less reactive quartz-sericite alteration it is typically up to 60-meters thick; in a more reactive quartz-sericite-chlorite alteration assemblage it is generally 20 to 40-meters thick; and in a very reactive biotitic alteration it is ≤ 10 -meters thick. In addition, the top of the transition zone and the top of the hypogene zone are coincident with a change in alteration type from quartz-sericite to quartz-sericite-chlorite or from quartz-sericite-chlorite to biotitic alteration. These trends clearly support buffering of acidic, supergene copper-bearing solutions by chlorite and biotite as the dominant control of transition zone occurrence and thickness at Cerro Colorado.

ACKNOWLEDGEMENTS

First and foremost I would like to thank BHP-Billiton for providing the majority of the funding for this project and the Society of Economic Geologists (SEG) and the New Mexico Tech Graduate Student Association (NMT-GSA) for their contributions towards this project. I would like to thank John Larson of the BHP office in Santiago for suggesting that we approach Cerro Colorado with this work. A special thanks to Eduardo Fernández L., Gonzalo Mendoza S., and Luís Aedo S. at Cerro Colorado for all of their insightful comments during this study, coordinating all of the in-mine transportation and sampling, and not forcing me to speak Spanish. The successful completion of this study is a tribute to all of your help over the past two-years.

There are many people at New Mexico Tech that have also given enormous contributions to this work. First I would like to thank my thesis advisor William “Billy” X. Chávez Jr. for all the time, hard work and patience he has put into me and this project. Your insightful comments and discussions have added so much to this study and to my experience at New Mexico Tech. You are not only a fantastic advisor, but also an inspirational instructor, great friend, and a terrific traveling companion. It has been a privilege working with you and I look forward to working with you again in the future. To the other members of my committee, Andy Campbell, Virgil Lueth, and Philip Kyle, who have also been instrumental in the timely completion of this work, thanks for all of your comments throughout the past two-years, especially during the past few months; I have enjoyed working with you all.

To my friends at New Mexico Tech and friends and family back at home (you all know who you are!): you have been a source of constant distractions and tremendous support these past few years and it has been an adventure to say the least. This is only one chapter and I'm looking forward to many more. A very special thanks to Rob Sanders and Amber McIntosh (a.k.a. "Romber") my personal editorial staff. You guys are the best, and if my thesis committee hasn't thanked you yet (with beer) they should.

Finally I'd like to thank my parents Susan Dahlke and William Odette for always letting me know that I could do anything I want in life. I don't think you guys ever knew where I was going, and most of the time neither did I, but you were always there with endless support. I want you to know that this is all for you...

TABLE OF CONTENTS

	Page
TITLE PAGE	i
ABSTRACT	
ACKNOWLEDGEMENTS	ii
LIST OF TABLES	3
LIST OF FIGURES	4
LIST OF APPENDICES	7
LIST OF MINERAL ABBREVIATIONS	8
CHAPTER 1: INTRODUCTION	9
CHAPTER 2: BACKGROUND	11
CHAPTER 3: REGIONAL GEOLOGY: MAMIÑA AND JUAN DE MORALES QUADRANGLES	14
CHAPTER 4: DISTRICT GEOLOGY: CERRO COLORADO PORPHYRY COPPER MOLYBDENUM DEPOSIT	19
CHAPTER 5: METHODS	32
Quantitative Methods	
<i>Heavy Mineral Separates</i>	32
Analytical Methods	
<i>Isotope Geochemistry</i>	36
<i>Lithogeochemistry</i>	38
CHAPTER 6: RESULTS	39
Transition Zone Ore Characterization	39
Isotope Geochemistry	40
Lithogeochemistry	40
CHAPTER 7: DISCUSSION	61
Mineral Ratios	61

Ore Zone Characterization	
<i>Supergene Enrichment Zone</i>	68
<i>Transition Zone</i>	68
<i>Hypogene Zone</i>	79
Atypical Enrichment Profiles	79
Wall-Rock Alteration and the Transition Zone	86
Ore Zone Stratigraphy: Margin to Center of Deposit	96
Sulfur Source	100
Trace Element Lithologic Discrimination	112
CHAPTER 8: CONCLUSIONS	114
REFERENCES CITED	118
APPENDIX A: MINERAL RATIO RESULTS	121
APPENDIX B: INTERPRETED MINERAL RATIO RESULTS	136
APPENDIX C: QUALITATIVE MINERALOGIC OBSERVATIONS AND PHOTOMICROGRAPHS OF HEAVY MINERAL SEPARATIONS	151
APPENDIX D: POLISHED THINSECTION PETROGRAPHY	172
APPENDIX E: INTERPRETED LITHOLOGIC, ALTERATION, AND MINERALOGIC ZONE COLUMNS	194

LIST OF TABLES

Table 1: Heavy Mineral Separation Quantitative Results	44
Table 2: Stable Sulfur Isotopic Results	56
Table 3: XRF Lithochemical Results	60

LIST OF FIGURES

Figure 2.1: Generalized Diagram of a Supergene Enrichment Profile	12
Figure 3.1: Metallogenic Belts of Northern Chile and Southern Peru	15
Figure 3.2: Regional Geologic Map: Mamiña and Juan de Morales Quadrangles	16
Figure 4.1: Geologic Map of the Cerro Colorado District	20
Figure 4.2: Geologic Map of the Cerro Colorado Deposit	23
Figure 4.3: East-West Geologic Cross-Sections of Lithology	24
Figure 4.4: East-West Geologic Cross-Sections of Alteration	27
Figure 4.5: East-West Geologic Cross-Sections of Mineralization	30
Figure 5.1: Location of Sampled Drill Holes	33
Figure 5.2: Sample Preparation Schematic for Heavy Mineral Separates	35
Figure 5.3: Line Integration Technique Schematic	37
Figure 6.1(a-b): Range of Mineral Ratio Results	41
Figure 6.1(c-d): Range of Mineral Ratio Results	42
Figure 6.1(e): Range of Mineral Ratio Results	43
Figure 6.2: Histogram of $\delta^{34}\text{S}$ Pyrite Values	57
Figure 6.3: Zr/TiO_2 – Ga Discrimination Diagram of Analyzed Samples	58
Figure 6.4: Zr/TiO_2 – Nb/Y Discrimination Diagram of Analyzed Samples	59
Figure 7.1: Hypothetical Mineral Ratio Diagram	62
Figure 7.2: Mineral Ratio Diagram with Photomicrographs for Drill Hole DDH-02-03	65

Figure 7.3: Generalized Enrichment Profile Based on Qualitative and Quantitative Observations	69
Figure 7.4: Interpreted Mineral Ratio Plot for Drill Hole DDH-02-04	70
Figure 7.5: Interpreted Mineral Ratio Plot for Drill Hole RC-F6-28	71
Figure 7.6: Cv-Cc-Cp+Bn Ternary Diagram of Heavy Mineral Separates	72
Figure 7.7: Cp+Bn-Cc+Cv-Py Ternary Diagram of Heavy Mineral Separates	73
Figure 7.8: Cp-Bn-Cc+Cv Ternary Diagram of Heavy Mineral Separates	74
Figure 7.9: Interpreted Mineral Ratio Plot for Drill Hole RC-CC160	75
Figure 7.10: Interpreted Mineral Ratio Plot for Drill Hole RC-02-24	77
Figure 7.11: Interpreted Mineral Ratio Plot for Drill Hole DDH-03-09	78
Figure 7.12: Interpreted Mineral Ratio Plot for Drill Hole DDH-03-14	81
Figure 7.13: Interpreted Mineral Ratio Plot for Drill Hole DDH-02-08	82
Figure 7.14: Interpreted Mineral Ratio Plot for Drill Hole RC-F6-17	83
Figure 7.15: Generalized Diagram Illustrating the Preferential Supergene Enrichment along Zones with Higher Permeability	85
Figure 7.16: Drill Hole Column for Hole DDH-02-03 Showing the Relationship Between Lithology and Alteration to the Defined Mineral Zones	87
Figure 7.17: Drill Hole Column for Hole DDH-02-04 Showing the Relationship Between Lithology and Alteration to the Defined Mineral Zones	88
Figure 7.18: Drill Hole Column for Hole DDH-03-09 Showing the Relationship Between Lithology and Alteration to the Defined Mineral Zones	89
Figure 7.19: Drill Hole Column for Hole DDH-02-11 Showing the Relationship Between Lithology and Alteration to the Defined Mineral Zones	90
Figure 7.20: Drill Hole Column for Hole DDH-02-08 Showing the Relationship Between Lithology and Alteration to the Defined Mineral Zones	91
Figure 7.21: Drill Hole Column for Hole DDH-03-14 Showing the Relationship Between Lithology and Alteration to the Defined Mineral Zones	92

Figure 7.22: Drill Hole Column for Hole RC-02-30 Showing the Relationship Between Lithology and Alteration to the Defined Mineral Zones	93
Figure 7.23: Drill Hole Column for Hole RC-02-21 Showing the Relationship Between Lithology and Alteration to the Defined Mineral Zones	94
Figure 7.24: East-West Cross-Section across the Northern Part of the Cerro Colorado Deposit Showing the Distribution of Mineralization and Alteration Types	97
Figure 7.25: East-West Cross-Section across the Central Part of the Cerro Colorado Deposit Showing the Distribution of Mineralization and Alteration Types	98
Figure 7.26: East-West Cross-Section across the Southern Part of the Cerro Colorado Deposit Showing the Distribution of Mineralization and Alteration Types	99
Figure 7.27: Drill Hole Column for Hole DDH-02-01 Showing the Relationship Between Lithology and Alteration to the Defined Mineral Zones	101
Figure 7.28: Drill Hole Column for Hole RC-02-24 Showing the Relationship Between Lithology and Alteration to the Defined Mineral Zones	102
Figure 7.29: Drill Hole Column for Hole RC-F6-28 Showing the Relationship Between Lithology and Alteration to the Defined Mineral Zones	103
Figure 7.30: Drill Hole Column for Hole RC-F6-17 Showing the Relationship Between Lithology and Alteration to the Defined Mineral Zones	104
Figure 7.31: Drill Hole Column for Hole RC-CC160 Showing the Relationship Between Lithology and Alteration to the Defined Mineral Zones	105
Figure 7.32: Drill Hole Column for Hole DDH-03-13 Showing the Relationship Between Lithology and Alteration to the Defined Mineral Zones	106
Figure 7.33: Map of North-Central Chile Showing the Generalized Geology from 194 to 108 Ma, and the Location of Major Porphyry Copper Deposits	108
Figure 7.34: Map of North-Central Chile Showing the Generalized Geology from 194 to 108 Ma, and the Location of Major Porphyry Copper Deposits	111

LIST OF APPENDICES

APPENDIX A: MINERAL RATIO RESULTS	121
APPENDIX B: INTERPRETED MINERAL RATIO RESULTS	136
APPENDIX C: QUALITATIVE MINERALOGIC OBSERVATIONS AND PHOTOMICROGRAPHS OF HEAVY MINERAL SEPARATIONS	151
APPENDIX D: POLISHED THINSECTION PETROGRAPHY	172
APPENDIX E: INTERPRETED LITHOLOGIC, ALTERATION, AND MINERALOGIC ZONE COLUMNS	194

LIST OF MINERAL ABBREVIATIONS

Chalcocite – Cu_2S – cc

Covellite – CuS – cv

Pyrite – FeS_2 – py

Chalcopyrite – CuFeS_2 – cp

Bornite – Cu_5FeS_4 – bn

Molybdenite – MoS_2 – mo

This Thesis is accepted on behalf of the faculty
of the Institute by the following committee:

Andrew Campbell

Academic Adviser

William X. Davis

Research Advisor

Vigil W.

Committee Member

Philip R. Kyle

Committee Member

Committee Member

April 26 2005

Date

I release this document to New Mexico Institute of Mining and Technology

Joan Davis

Students Signature

April 26, 2005

Date

CHAPTER 1

INTRODUCTION

The ca 51.8 to 55.8 Ma (Bouzari and Clark, 2002; Cotton, 2003) Cerro Colorado porphyry copper deposit is centered at 20° 2' 41"S; 69° 15' 35" W within the Atacama Desert in northern Chile, at an elevation of 2,600 meters a.m.s.l. Hydrothermal alteration and hypogene mineralization is associated with the emplacement of numerous Eocene-age porphyritic intrusions. From ~42 Ma through ~19 Ma (Bouzari and Clark, 2002) subsequent uplift and weathering of the deposit lead to the development of a supergene enrichment profile. The “classic” enrichment profile, described in detail by Bouzari and Clark (2002) consists, simply, of a leached capping, oxide zone, and supergene enrichment zone that have developed from a 0.3 to 0.6% Cu (pyrite-chalcopyrite-bornite) protore.

Cerro Colorado and many other porphyry copper deposits are made economically viable as a result of supergene enrichment processes that: 1. increase copper grades, many times by a factor of 2 or more; and 2. place this copper in an easily recoverable phase as supergene sulfides (chalcocite-covellite) and/or as oxides (chrysocolla-brochantite-atacamite). For many deposits, continued depletion of “leachable” ore reserves (e.g. oxide and supergene sulfide ores) has created interest in the mixed zone or “transition zone” and hypogene zone resources that currently contain marginally economic copper. The “transition zone” is of particular interest because it generally

contains elevated copper values relative to protore and, more importantly, contains a mixed copper sulfide assemblage of chalcocite-covellite-chalcopyrite-bornite. Copper is currently recoverable from chalcocite and covellite by Solvent Extraction Electrowinning or SX/EW.

Although this study represents a detailed quantitative evaluation of the “transition zone” at Cerro Colorado, the implications of this work extend far beyond the deposit itself. Currently many other deposits are evaluating transitional and hypogene resources to replace depleting ore reserves. As an example, Phelps Dodge is actively testing a proprietary technique at Bagdad that allows for concentrate leaching of hypogene pyrite-chalcopyrite ore. More importantly this quantitative technique used at Cerro Colorado could be employed to characterize and define sulfide mineralization at any deposit.

The primary goal of this study is to provide quantitative mineralogic data that can aid geologists and metallurgists in deciding how these ores could be processed in the future (e.g. modified SX/EW or as a concentrate). The detailed mineralogical study of these environments has also allowed for a more complete understanding of: 1. the mineralogical changes that occur within the supergene enrichment zone, “transition zone”, and hypogene zone environments, and 2. the occurrence and thickness of the “transition zone” relative to wall-rock alteration that may have some implications to future modeling.

CHAPTER 2

BACKGROUND

The processes associated with the development of supergene enrichment from hypogene ore (e.g. geochemical conditions and mineralogic changes) have been the subject of numerous studies (Titley, 1982; Lichtner and Biino, 1992; Chavez, 2000; and Patricio and Gonzalo, 2001). Descriptive studies have documented enrichment profiles from many porphyry copper deposits throughout the American Cordillera establishing a well-documented characterization of the different mineralogic zones that develop in the supergene weathering environment (Swayne and Trask, 1960; Sillitoe, 1973; Titley, 1982; Ojeda, 1990; Atkinson et al., 1996; Virtue, T.L., 1996; Ossandón et al., 2001; and Bouzari and Clark, 2002). The supergene environment has been historically subdivided into four distinct geochemical zones; the leached capping, oxide zone, supergene enrichment zone, and hypogene zone (Figure 2.1). Each zone, because of the unique geochemical conditions that exist there, are generally characterized by distinct mineral assemblages.

The leached capping contains abundant iron and manganese oxides, minor pyrite, and has low total copper values (<0.0X% Cu). The oxide zone is defined as the zone containing abundant copper oxide and oxyanion (e.g. CO₃ and PO₄) minerals, and can contain variable copper grades (0.X to >1% Cu). The supergene enrichment zone contains the sulfides chalcocite and covellite, and trace quantities of hypogene sulfides.

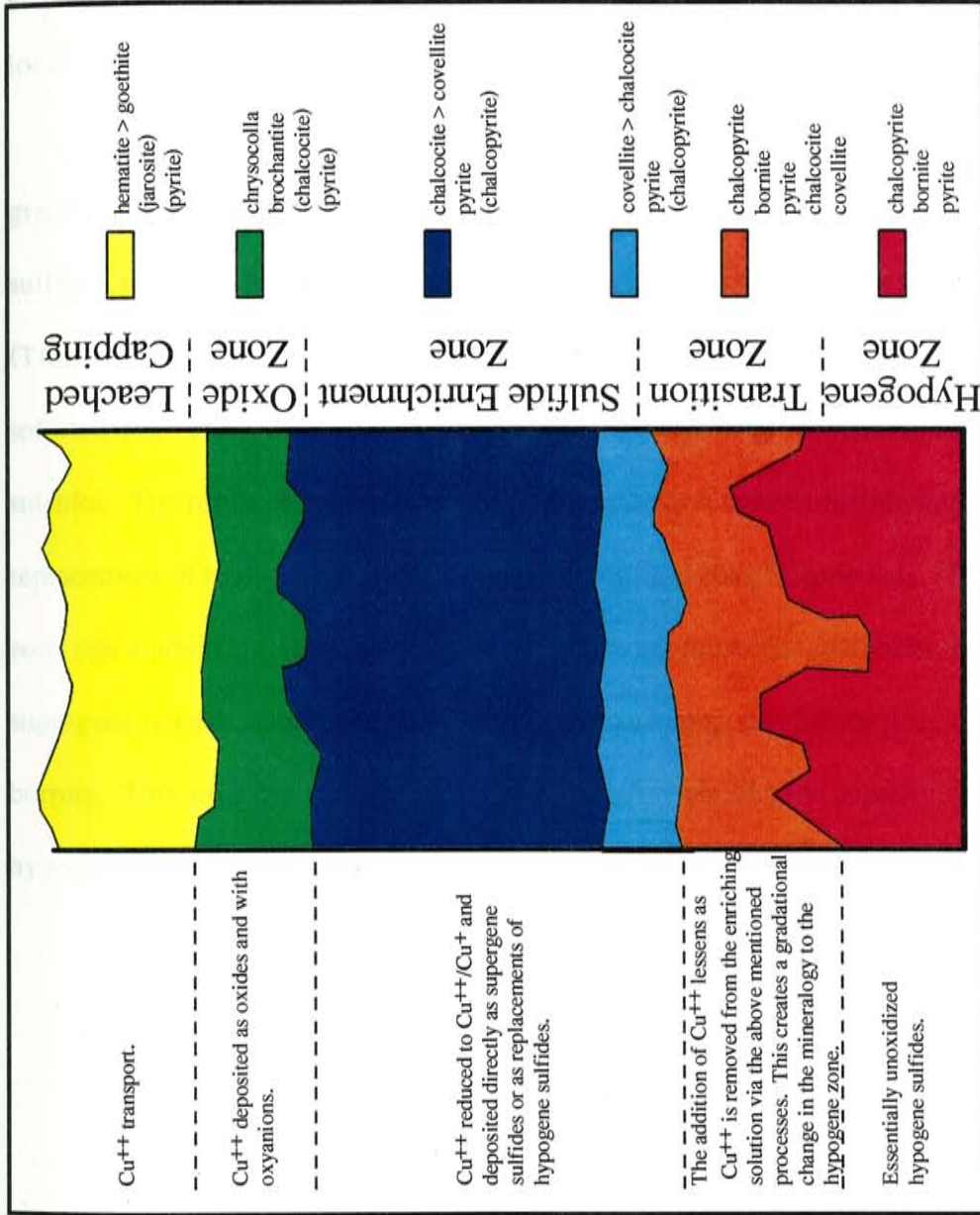


Figure 2.1: A schematic diagram of the supergene weathering profile showing the relationship between the leached capping, oxide, supergene enrichment, transition, and hypogene zones.

This zone is enriched (0.X to >1% Cu) in copper relative to hypogene ore grades.

Finally, the hypogene zone is predominantly composed of unoxidized hypogene sulfides pyrite, chalcopyrite, bornite, and in some cases hypogene chalcocite and covellite. It can also contain variable copper grades typically ranging from 0.3% to 0.6% Cu and can locally exceed 1% Cu in the core of the systems.

The contact between the supergene enrichment and hypogene zone can be gradational. As copper-rich, downward percolating groundwater interacts with hypogene sulfides, reactions result in the formation of supergene sulfides below the water table (Titley, 1982). The formation of supergene sulfides decreases the copper activity of the solution that in turn decreases the ability of the solution to produce more supergene sulfides. The result of this process is the formation of a zone of incomplete to partial replacement of hypogene sulfides called the transition zone (Figure 6.1). The transition zone can contain variable quantities of the following minerals: chalcocite, covellite, supergene bornite, supergene chalcopyrite, pyrite, hypogene chalcopyrite, and hypogene bornite. This zone can also be weakly to moderately enriched in copper relative to hypogene ore grades (0.2% up to 1% Cu).

CHAPTER 3

REGIONAL GEOLOGY: MAMIÑA AND JUAN DE MORALES

QUADRANGLES

The Cerro Colorado Porphyry Cu- (Mo-) Deposit is one of numerous productive porphyry systems located between 16° and 27° south latitude within the Eocene to Oligocene porphyry belt of northern Chile and southern Perú (Figure 3.1). This metallogenic belt includes the Cerro Verde, Santa Rosa, Cuajone, Quellaveco, and Toquepala porphyries in southern Perú; and the Spence, Lomas Bayas, and Carmen porphyries, and the Sierra Gorda breccia-hosted system in northern Chile (Figure 3.1). Regional mapping of the Mamiña and Juan de Morales quadrangles, which cover the Cerro Colorado District, was conducted by Thomas (1967) and Galli (1968), and the following summary of the regional geology is based on their work as reported by Garcia (1967), Cepeda et al. (1982), Bouzari and Clark (1997; 2002), and Cotton (2003). In general, the Cerro Colorado region consists of a rather simple suite of rocks including Paleozoic shallow marine sediments, Jurassic sandstone and shale, Cretaceous volcanic, intrusive and sedimentary rocks, Eocene intrusions, and Miocene volcanic rocks (Figure 3.2).

Paleozoic sediments represent the oldest and least exposed rocks in the area, found only along the eastern side of the Sierra Juan de Morales, manifested as >1,500 m

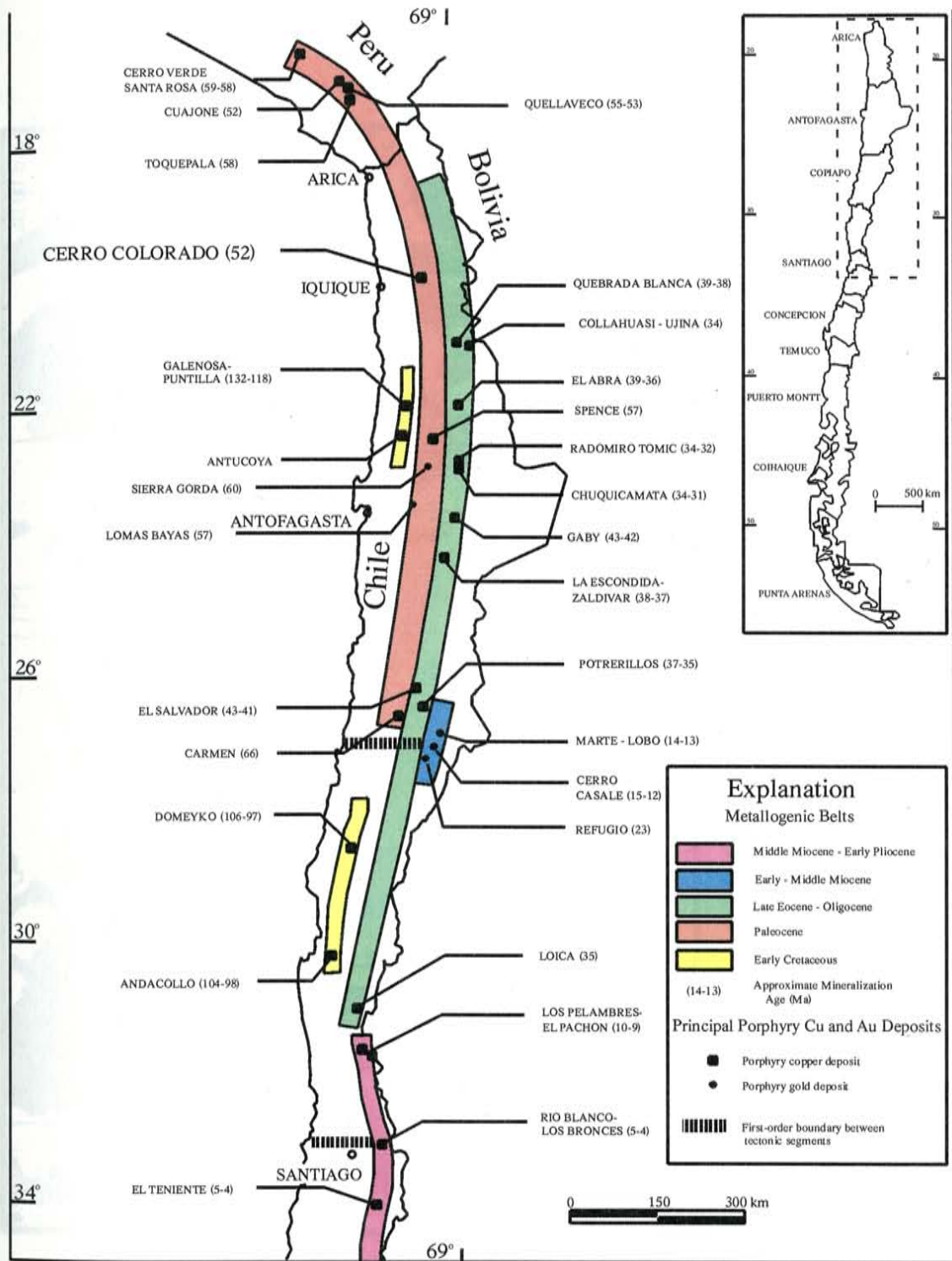


Figure 3.1: Regional map of Region I, northern Chile and southern Perú showing the location and age of numerous productive porphyry-related systems and their associated metallogenetic belts (Compiled from numerous sources and modified after Cotton, 2002).

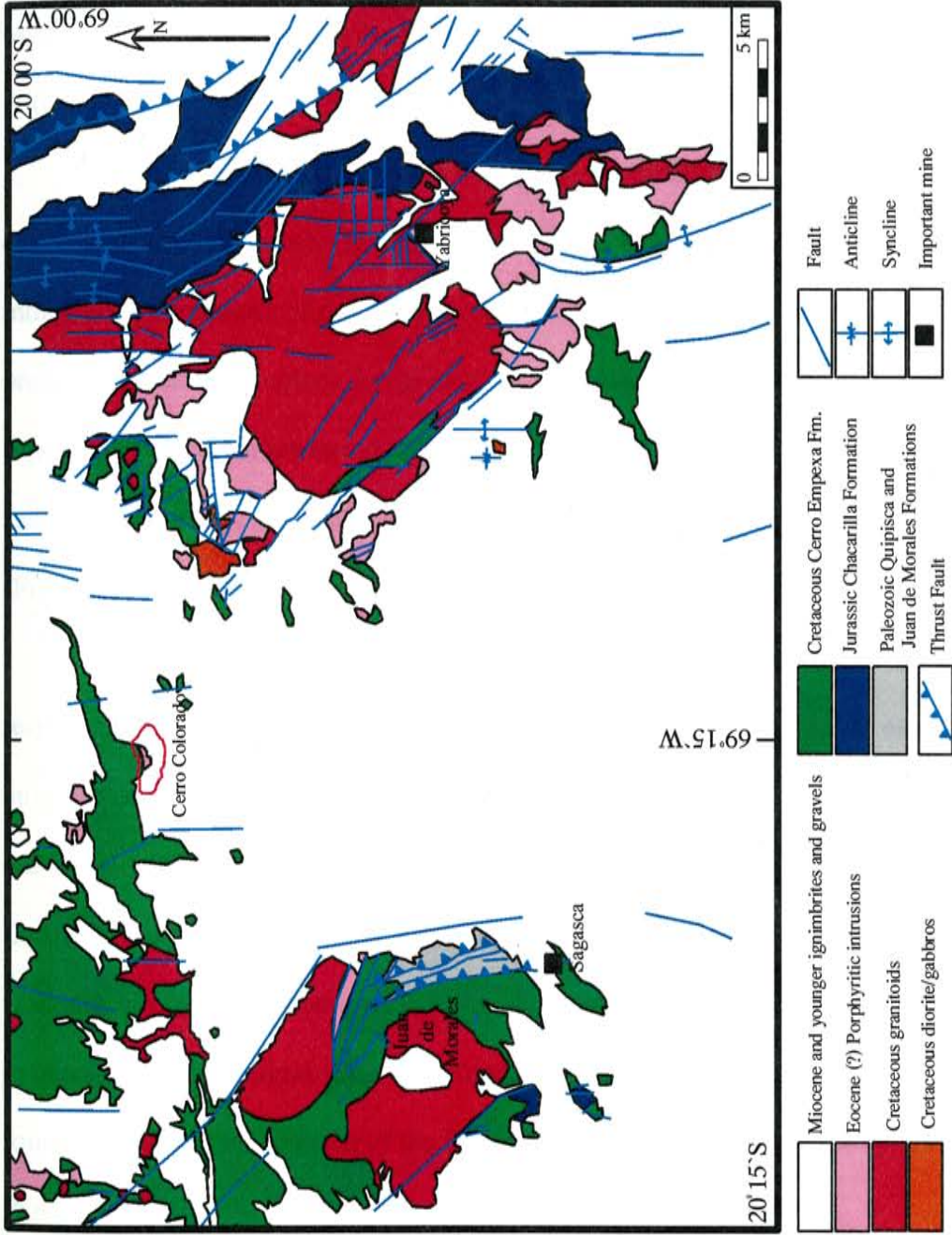


Figure 3.2: Generalized regional geologic map modified after Cotton (2003), compiled from the Mamina and Juan de Morales 15-minute quadrangle maps by Thomas (1967) and Galli (1968).

thick sequence of the Quipisca and Juan de Morales Formations (Figure 3.2). The Quipisca Formation consists of Paleozoic volcanic rocks, which is overlain by sandy breccia, conglomerate, and, in the uppermost parts of the stratigraphic section, interbedded marine shales of the Late Carboniferous Juan de Morales Formation (Cotton, 2003).

During the Jurassic, a large marine back-arc basin (the Domeyko Basin) developed throughout much of central Chile (Prinz et al., 1994; Ardill et al., 1998), as indicated by sequences of marine shale, sandstone, conglomerate, and evaporates preserved within the region. Large exposures of sandstone and shale of the Jurassic Chacarilla Formation are found to the east and north of the Yabricoya mine in the Cordón Lallinca Mountains, and also found in the southern part of the Sierra Juan de Morales (Figure 3.2).

From the Late Jurassic to the Cretaceous the volcanic arc migrated eastward in response to changing plate movements (Jaillard et al., 2000). As a result extensive outcrops of Cretaceous andesite, tuffs, and agglomerates of the Cerro Empexa Formation are found around the Sierra Juan de Morales, within the Quebrada de Parca, north of Cerro Colorado, and west of the Yabricoya igneous complex. These Late Cretaceous volcanic and volcano-sedimentary rocks were intruded by a series of Cretaceous granitoids. The intrusions range in composition from granite to diorite, and are also found around and to the north of the Sierra Juan de Morales, within the Quebrada de Parca, and around the Yabricoya mine (Cotton, 2003) (Figure 3.2).

Eocene-age intrusive rocks are found within and to the north of the Sierra Juan de Morales, at Cerro Colorado, and surrounding the Yabricoya igneous complex. These

quartz-rich, shallow-level porphyries generally trend northwest and intrude Jurassic and Late Cretaceous volcanic and intrusive rocks. These lithologies represent the final expression of a volcano-plutonic arc developed throughout central Chile during the latest Cretaceous to Eocene time (Bouzari and Clark, 2002).

Miocene conglomerates and ignimbrites of the Altos de Pica Formation, as well as Pliocene and younger gravels, are found throughout the area described by the Mamiña and Juan de Morales quadrangles (Cepeda et al., 1982). Volcanism and sedimentation during Altos de Pica Formation time is constrained by $^{40}\text{Ar}/^{39}\text{Ar}$ age dates (ca 19 Ma for sanidine, Bouzari and Clark, 2000); Miocene and Paleocene erosion has covered much of the bedrock in the area including the central part of the Cerro Colorado district (Figure 3.2).

CHAPTER 4

DEPOSIT GEOLOGY: THE CERRO COLORADO PORPHYRY COPPER SYSTEM

Hydrothermal alteration and mineralization at Cerro Colorado is associated with the emplacement of numerous, typically quartz-rich, porphyritic, hypabyssal stocks and associated breccias within the Cretaceous volcanic rocks of the Cerro Empexa Formation (Cepeda et al., 1982; Bouzari and Clark, 1997; 2002; Cotton, 2003) (Figure 4.1). Subsequent uplift and weathering of the hypogene (0.4% to 0.5% Cu as chalcopyrite + bornite) mineralization has created a supergene enrichment profile that contains the 193 MT, 1.08% Cu Reserves (Bouzari and Clark, 1997).

The late Cretaceous Cerro Empexa Formation is a gently south-dipping sequence of vesicular porphyritic andesite volcanic rocks, and volcanic-sandstones and conglomerates. The Cerro Empexa Formation consists of a lower volcanosedimentary dominated member and an upper volcanic-volcanoclastic dominated member based on the detailed work done by Thomas (1967), Garcia (1967), and Galli (1968). The lower member is typically 340-meters thick and consists of a sequence of volcanic-sandstone and conglomerate, shale, and locally interbedded andesite lavas. The upper member of the Cerro Empexa Formation is up to 220-meters thick and is comprised of andesite and

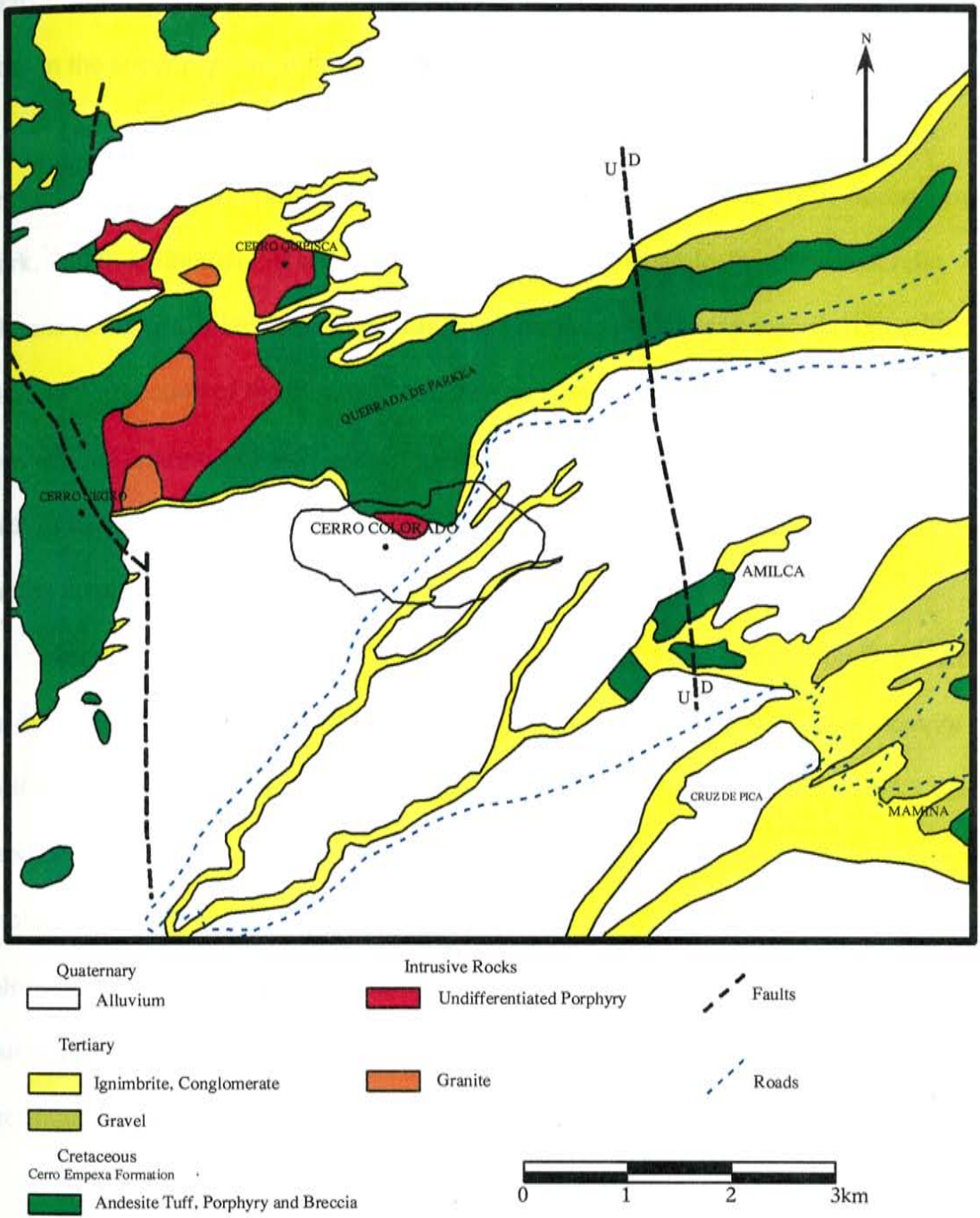


Figure 4.1: Generalized geologic map of the Cerro Colorado District. Modified after Cepeda et al (1982).

trachyandesite lavas, tuff, sandstone, and conglomerate. Overall there are more volcanic rocks in the upper portions of the Cerro Empexa Formation.

The intensely biotitized host rocks at Cerro Colorado are the altered upper member of the Cerro Empexa Formation (Cepeda et al, 1982; Cotton, 2003; Bouzari and Clark, 2002). Although this relationship has not been geochemically supported, relic volcanic textures similar to the Cerro Empexa Formation have been described in drill core and thin section of the biotitized andesites at Cerro Colorado (Cepeda et al, 1982). Least-altered andesites of the Cerro Empexa Formation have been mapped immediately north of Cerro Colorado within the Quebrada Parca and 3 km to the west at Cerro Negro, placing them in location compatible with the assumption (Figure 4.1).

Intrusive activity at Cerro Colorado began about ca 51.8 Ma based on $^{40}\text{Ar}/^{39}\text{Ar}$ age determinations of hydrothermal and magmatic biotite and hydrothermal muscovite (Cotton, 2003; Bouzari and Clark, 2002), with hydrothermal mineralization ca 55.8 Ma based on Re/Os age determinations on molybdenite (Cotton, 2003). Numerous intrusive lithologies ranging from tonalite to quartz monzonite have been described at Cerro Colorado, although intense hypogene and supergene alteration and mineralization have destroyed much of the original petrologic textures and mineralogy making protolith determination difficult.

Detailed mapping and petrography of intrusive lithologies at Cerro Colorado have led to the recognition of numerous distinct intrusive units. The recent work by Bouzari and Clark (1997), using a non-genetic classification scheme utilizing phenocryst type and abundance, have recognized four intrusions and associated breccias at Cerro Colorado: (QPP) Quartz Plagioclase Porphyry; (BQFP) Biotite Quartz Feldspar Porphyry; (EWBC)

Eastern and Western Breccia Complexes; and (PAFP) Plagioclase Alkali Feldspar Porphyry Dike (Figure 4.2 and 4.3).

The Quartz Plagioclase Porphyry (QPP) is the most abundant intrusive unit at Cerro Colorado. This rock is texturally similar to the andesites of the Cerro Empexa Formation with abundant 2-4 mm feldspar phenocrysts, except that the QPP contains some larger (>5 mm) feldspar phenocrysts. This unit correlates with the “Productive Tonalite” described by Cepeda et al. (1982), the “Quartz Feldspar Porphyry” described by Cotton (2003), and possibly to the “Feldspar Porphyry Tonalite” described by Campbell (1994). This porphyry has undergone both potassic and chloritic alteration.

The Biotite Quartz Feldspar Porphyry (BQPP) is typically found in the deeper portions of, and to the east of, the main pit. It contains abundant feldspar, quartz, and biotite phenocrysts. Biotite phenocrysts occur as ≥ 5 mm books. Bouzari and Clark (2002) interpreted this unit as being post-biotization, as they describe this unit intruding into biotitized andesite and only containing minor chlorite veins. The “Biotite Quartz Plagioclase Porphyry”, a possibly correlative mapped unit described by Cotton (2003), is interpreted as a pre-biotitization intrusion. It is unclear if these represent the same intrusive units with different interpretations, or entirely different intrusions all together.

The Eastern and Western Breccia Complexes (EWBC) represent a very complex rock type at Cerro Colorado. The Eastern Breccia Complex, of Bouzari and Clark (2002), consists of breccias that occur around and below the central and eastern parts of the mine and are correlative to the “Central Breccia and Quartz Monzonite Microbreccia” as defined by Cotton (2003). The eastern complex is essentially an igneous breccia or fragmental porphyry and is characterized by phyllic-altered quartz-feldspar porphyry

Geology 2400 m Level

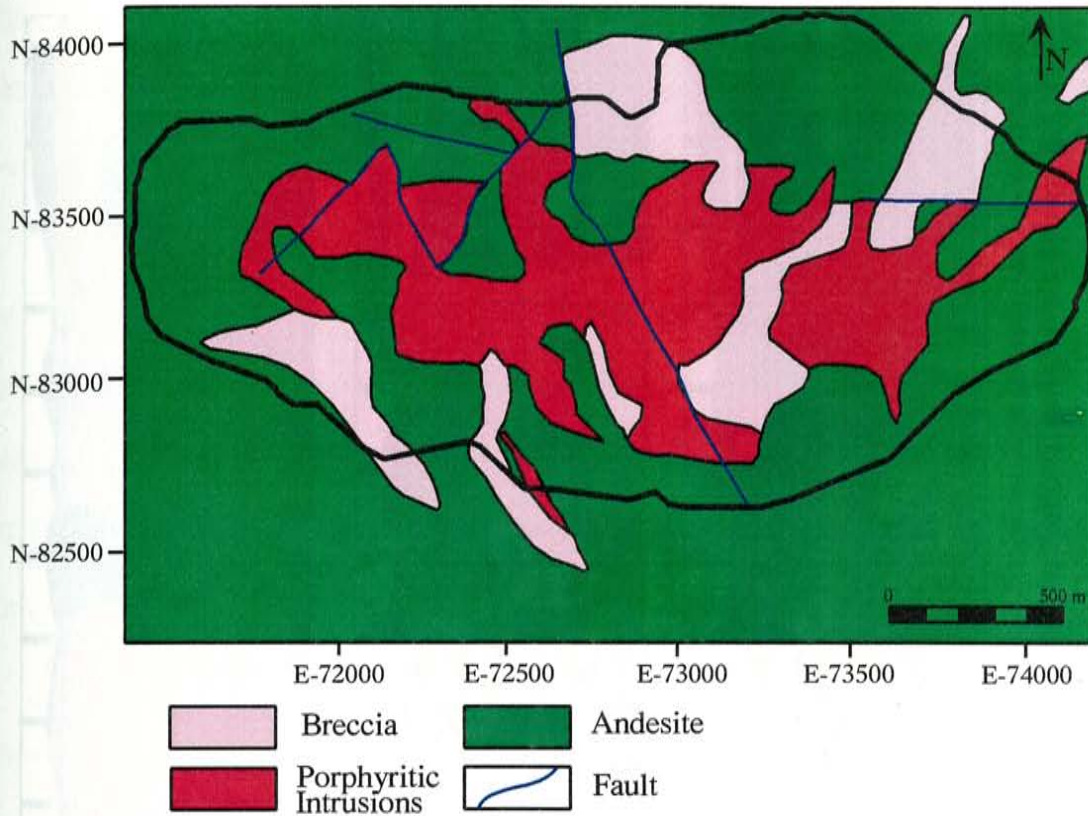


Figure 4.2: Generalized geologic map of the Cerro Colorado deposit showing the distribution of the Cerro Empexa Formation, undifferentiated porphyritic intrusives, and undifferentiated breccias. Modified after Cotton (2003).

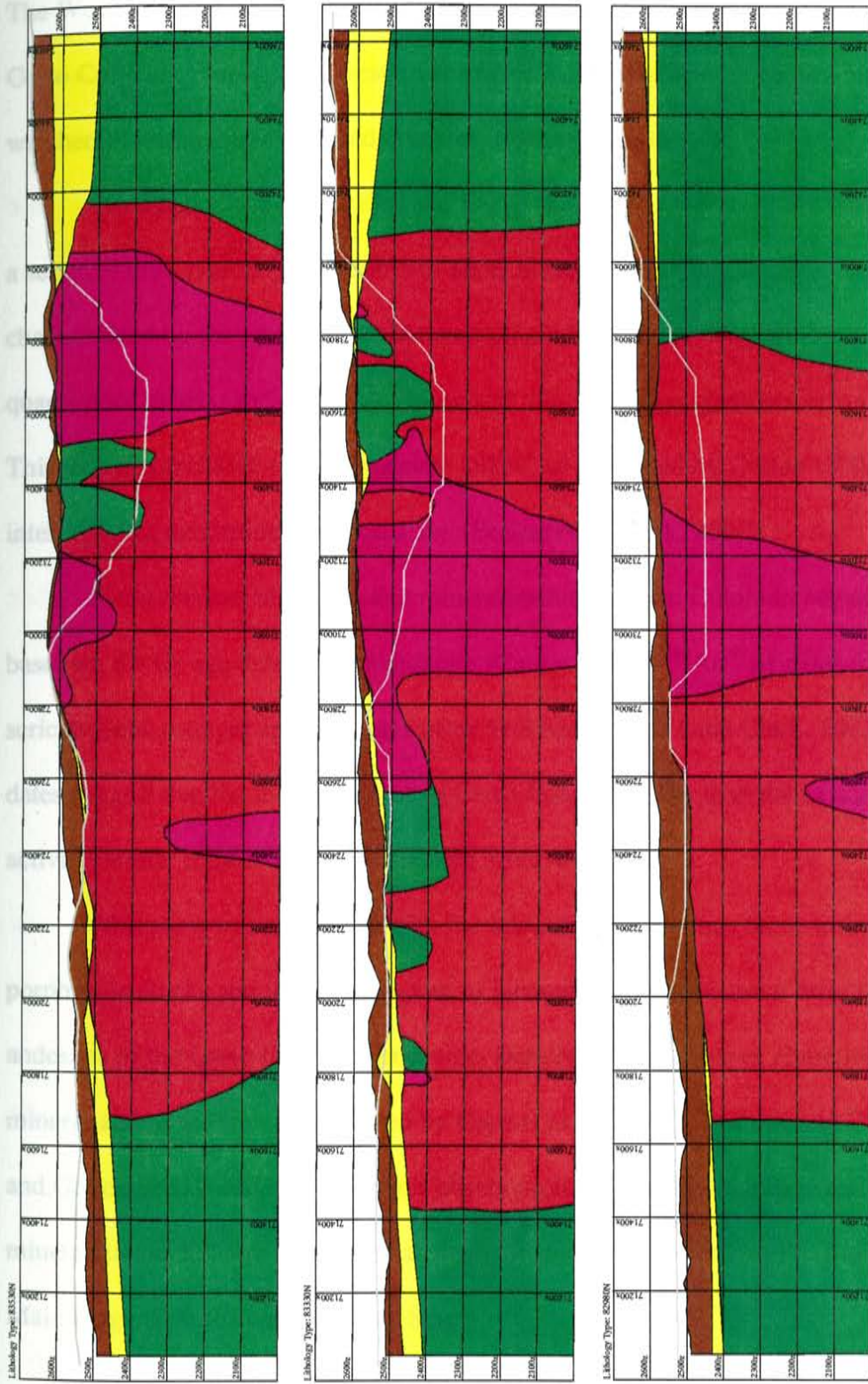


Figure 4.3: Generalized east-west cross-sections of lithology illustrating the relationships between the Andesite (green), Undifferentiated porphyry (red), Undifferentiated breccia (purple), Ignimbrite (yellow), and Gravels (brown) at Cerro Colorado. It is important to note that due to the intense alteration at Cerro Colorado only undifferentiated porphyry and breccia are recognized.

clasts surrounded by silicified rims in a fine-grained, dark gray, phyllic altered matrix. The Western Breccia Complex, as defined by Bouzari and Clark (2002), crop out atop Cerro Colorado proper. The western complex is characterized by barren, highly weathered, tourmaline-cemented breccias (Figures 4.2 and 4.3).

The Plagioclase Alkali Feldspar Dikes (PAFP) is a late intrusive unit consisting of a series of thin, typically less than 5 m wide, northwest-trending dikes. These dikes are characterized by the presence of abundant plagioclase and pink alkali feldspars in a quartz-poor matrix, and cut all alteration and mineralization types at Cerro Colorado. This unit is correlative to the “Andesite Dikes” as described by Cotton (2003) and are interpreted as post-mineralization dikes (Bouzari and Clark, 2002).

Hydrothermal alteration and mineralization at Cerro Colorado began ca 55.8 Ma based on Re-Os age dates of molybdenite (Cotton, 2002). $^{40}\text{Ar}/^{39}\text{Ar}$ dates for biotite and sericite yield younger apparent ages of ca 51.8 Ma (Bouzari and Clark, 2002). These age dates suggest that the mineralization at Cerro Colorado older than the causative intrusive activity, which is incorrect based on field observations.

Alteration was associated with the intrusion of numerous felsic to intermediate porphyritic stocks and the development of igneous and hydrothermal breccias within the andesites of the Cerro Empexa Formation. Detailed descriptions of alteration and mineralization are well documented by Cepeda et al. (1982), Bouzari and Clark (2002), and Cotton (2003) and based on their observations, hypogene alteration and mineralization at Cerro Colorado has been divided into four stages; Pre-Main Stage, Main Stage, Transitional, and Late Stage.

Pre-main stage alteration and mineralization is characterized by extremely intense, deposit-scale (~2.5 x ~1.5 km), potassium and sodium metasomatism in the form of fine-grained, shreddy-biotite and albite. Potassic alteration, or biotitization, has strongly affected the host rock andesites at Cerro Colorado (Figure 4.4). Quantitative XRD analysis by Cotton (2003) has shown that altered host rocks can locally contain over 45 wt. % biotite. No sulfide mineralization has been attributed to this alteration type (Cepeda et al, 1982; Bouzari and Clark, 2002; Cotton, 2003). Vein types associated with this alteration include: biotite veinlets, albite ± biotite ± quartz ± K-feldspar veinlets, thin granular quartz veinlets with albite or K-feldspar haloes, and K-feldspar veinlets (Cotton, 2003). Relic textures in drill core and thin section suggest that this metasomatic event had originally affected a larger rock volume than what is currently preserved; but later overprinting of hypogene and supergene alteration, and mineralization has reduced the occurrence of this alteration type to the deeper portions of the deposit.

Main stage alteration and mineralization is characterized by the development of a quartz-chlorite-sericite mineral assemblage (Figure 4.4). This intermediate argillic alteration is associated with the development of quartz + chlorite + sericite + pyrite + chalcopyrite veins. Main stage veins are responsible for most of the hypogene copper mineralization at Cerro Colorado (Cepeda et al, 1982; Bouzari and Clark, 2002; Cotton, 2003). Main stage alteration is clearly later and overprints Pre-Main stage alteration as magnetite is destroyed, biotite is replaced by chlorite and/or sericite, and albite is replaced by sericite. Main stage alteration and mineralization dominates all other alteration types.

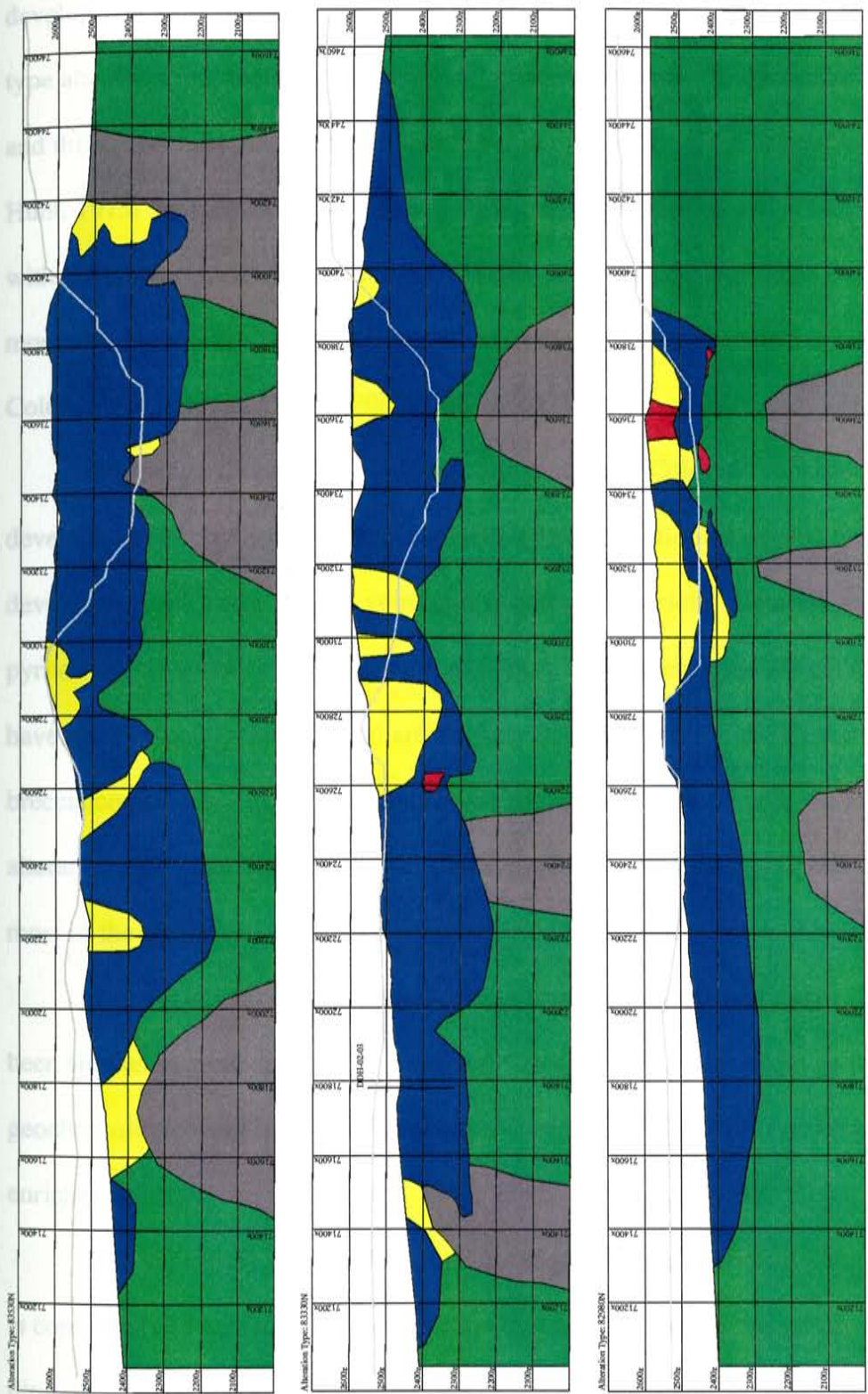


Figure 4.4: Generalized east-west cross-sections of mineral zones illustrating the relationships between the hypogene zone (red), transition zone (orange), supergene sulfide zone (blue), oxide zone (green), and the leached capping (brown) at Cerro Colorado. Note that the relationship between mineral zones is more complex in the eastern part of the property in the main pit relative to the western expansion area.

Transitional stage alteration and mineralization is characterized by the development of a quartz-sericite-pyrite mineral assemblage (Figure 4.4). This phyllic-type alteration is associated with the development of quartz + molybdenite + pyrite veins, and thick, generally sulfide barren quartz veins. These “B-veins” (after Gustafson and Hunt, 1975) are most abundant in the central part of the deposit and are closely associated with the emplacement of the QPP and EWBG. Transitional stage veins introduced moderate copper, as chalcopyrite, and most of the molybdenum mineralization at Cerro Colorado (Bouzari and Clark, 2002; Cotton, 2003).

Late stage alteration and mineralization at Cerro Colorado consisted of continued development of phyllic-style, quartz-sericite-pyrite alteration associated with the development of quartz + pyrite veins and veinlets with sericite alteration halos. These pyrite-rich “D-veins” (after Gustafson and Hunt, 1975) are commonly centimeters thick, have a very planar geometry, and are strongly developed within the Eastern and Western breccia complexes. The extreme hydrolytic alteration associated with the Late Stage alteration and mineralization remobilized some copper mineralization and introduced most of the pyrite into the system (Bouzari and Clark, 2002; Cotton, 2003).

The evolution of supergene alteration and mineralization at Cerro Colorado has been studied in great detail by Bouzari and Clark (2002). Their recent geologic and geochronologic work has helped to unravel Cerro Colorado’s uplift and supergene enrichment history.

The supergene profile of Cerro Colorado as defined by Bouzari and Clark (2002) is composed of four facies; 1) the Leached Cap which is mainly hematitic and lies directly beneath the Choja pediplain; 2) the Upper Supergene Ore which is dominantly

composed of the copper oxides brochantite, atacamite, and chrysocolla; 3) the Lower Leached Zone which is also dominantly hematitic; and 4) the Lower Supergene Ore which is dominantly composed of chalcocite. This supergene profile overlays the transitional and 0.4 to 0.5% copper hypogene zones (Figure 4.5).

Detailed $^{40}\text{Ar}/^{39}\text{Ar}$ geochronology of alunite, natroalunite, and jarosite collected from the supergene profile have outlined the uplift and enrichment history of the deposit over the last 20 m.y. A brief discussion of these events are included herein, but the reader is referred to Bouzari and Clark (2002) for a more detailed discussion.

Following the development of hypogene mineralization between ca 51.8 Ma (Bouzari and Clark, 2002) and ca 55.8 Ma (Cotton, 2003), the deposit was uplifted ~42 Ma during the initiation of the Incaic orogeny. By 35.26 ± 0.68 Ma (Bouzari and Clark, 2002) the deposit was oxidizing in the near-surface, and enrichment processes had begun. From 35.26 ± 0.68 Ma to 22.42 ± 1.6 Ma (Bouzari and Clark, 2002), continued uplift and exhumation of the deposit lead to the continued development of the leached zone accompanied by thickening of the Upper Supergene Ore. From 21.49 ± 0.49 Ma to 19.25 ± 0.43 Ma (Bouzari and Clark, 2002) uplift rates accelerated due to the onset of Pehuenchean (Aymara) tectonism and the Lower Leached Zone developed due to rapid drop of the water table, that subsequently lead to the development of the Lower Supergene Ore. At 19.25 ± 0.43 Ma, ignimbrites of the Altos de Pica Formation covered the deposit, and may have interrupted supergene activity at Cerro Colorado. Between 19.25 ± 0.43 Ma and 14.59 ± 2.46 Ma (Bouzari and Clark, 2002) lateral movement of ground-water from Cerro Colorado formed small exotic copper showings, composed predominantly of chrysocolla coating of gravels and conglomerates, within the base of

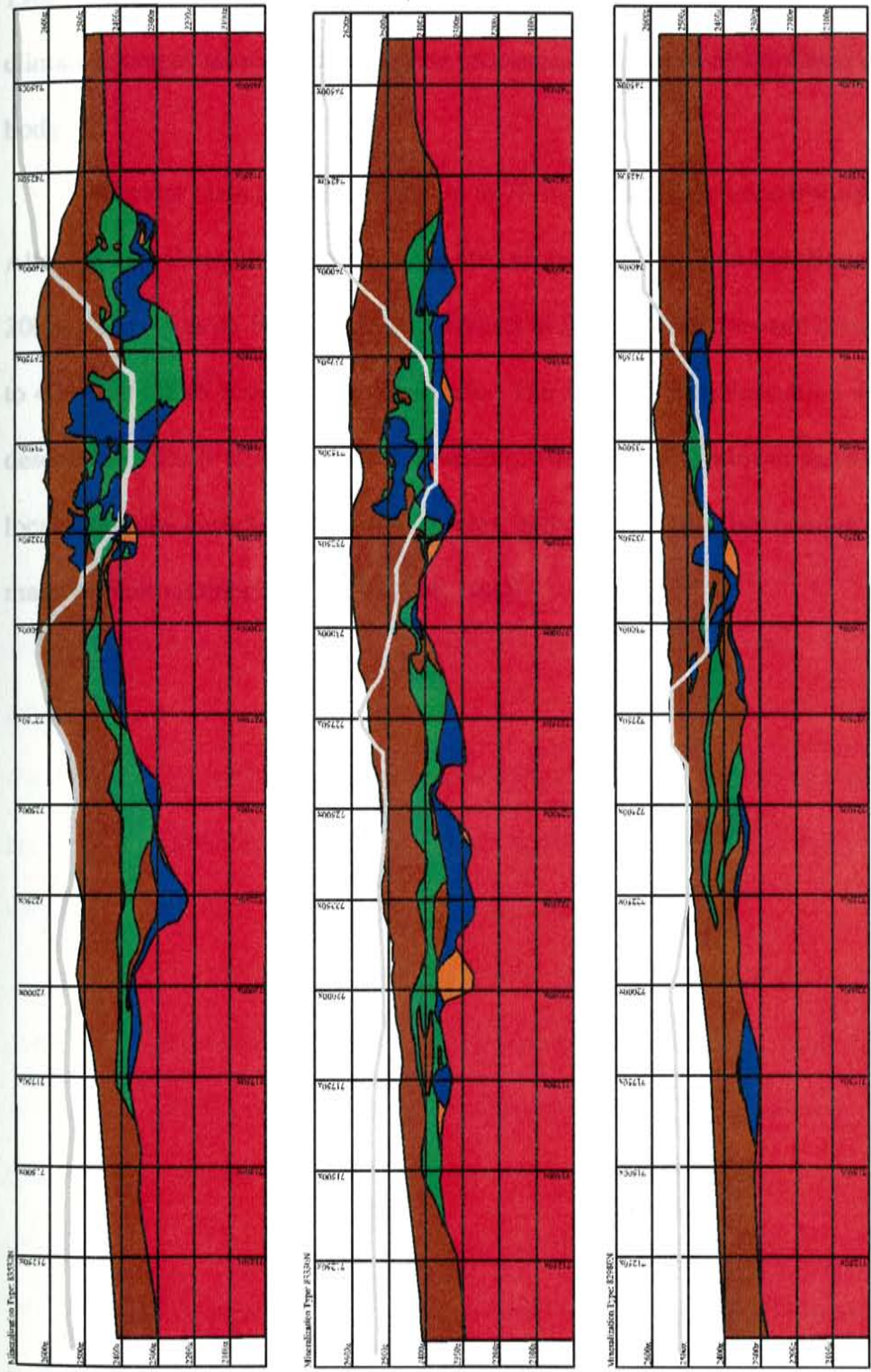


Figure 4.5: Generalized east-west cross-sections of alteration illustrating the relationships between the biotite-albite-magnetite alteration (dark grey), sericite-chlorite alteration (green), sericite-quartz alteration (blue), and white clay alteration (yellow) at Cerro Colorado. It is important to note that the current contact between the sericite-chlorite and sericite-quartz alteration zones has been lowered due to supergene weathering and preferential removal of chlorite over sericite.

the Altos de Pica formation to the north and south of Cerro Colorado (Cepeda et al., 1982). Finally, around 14.59 ± 2.46 Ma (Bouzari and Clark, 2002) continued uplift and climatic changes terminated supergene processes and preserved the Cerro Colorado ore body.

Alluvial plain gravel deposits up to 70-meters thick lie unconformably on the Altos de Pica Formation that was deposited around 19.25 ± 0.43 Ma (Bouzari and Clark, 2002). The Altos de Pica Formation consists of tuffs, ignimbrites and conglomerates, up to 40-meters thick around Cerro Colorado. The Altos de Pica Formation was first described by Galli (1968) and is composed of two members; a lower member containing locally derived unsorted red conglomerates, and an upper member composed of a massive pink ignimbrite (Cepeda et al, 1982).

CHAPTER 5

METHODS

Quantitative Methods

Heavy Mineral Separates

One hundred-thirty-five, ten-meter composite pulp samples, from 14 drill holes were collected in two phases from across the deposit; the pulp samples corresponded to mine benches. Forty-six samples were obtained from 3 drill holes in the main pit and 3 drill holes from the western zone (Figure 5.1). This sampling strategy was designed to test if 10-meter composite samples could effectively characterize the transition zone at Cerro Colorado. Drill holes were sampled from the base of significant supergene sulfide accumulation through the transition zone and into hypogene ore based by visual inspection of the drill core and review of drill core logs.

A second phase of sampling consisted of 89 additional samples; 6 samples were collected from previous drill holes and 83 samples were collected from 7 new holes (Figure 5.1). This second round of sampling was designed to: 1) obtain better spatial coverage over the deposit; 2) better understand the mineralogical character of the hypogene zone; 3) characterize the supergene sulfide zone; and 4) to recognize the effect of changing alteration and lithologic types on the occurrence and thickness of the transition zone. The second round of sampling was extended higher up into the

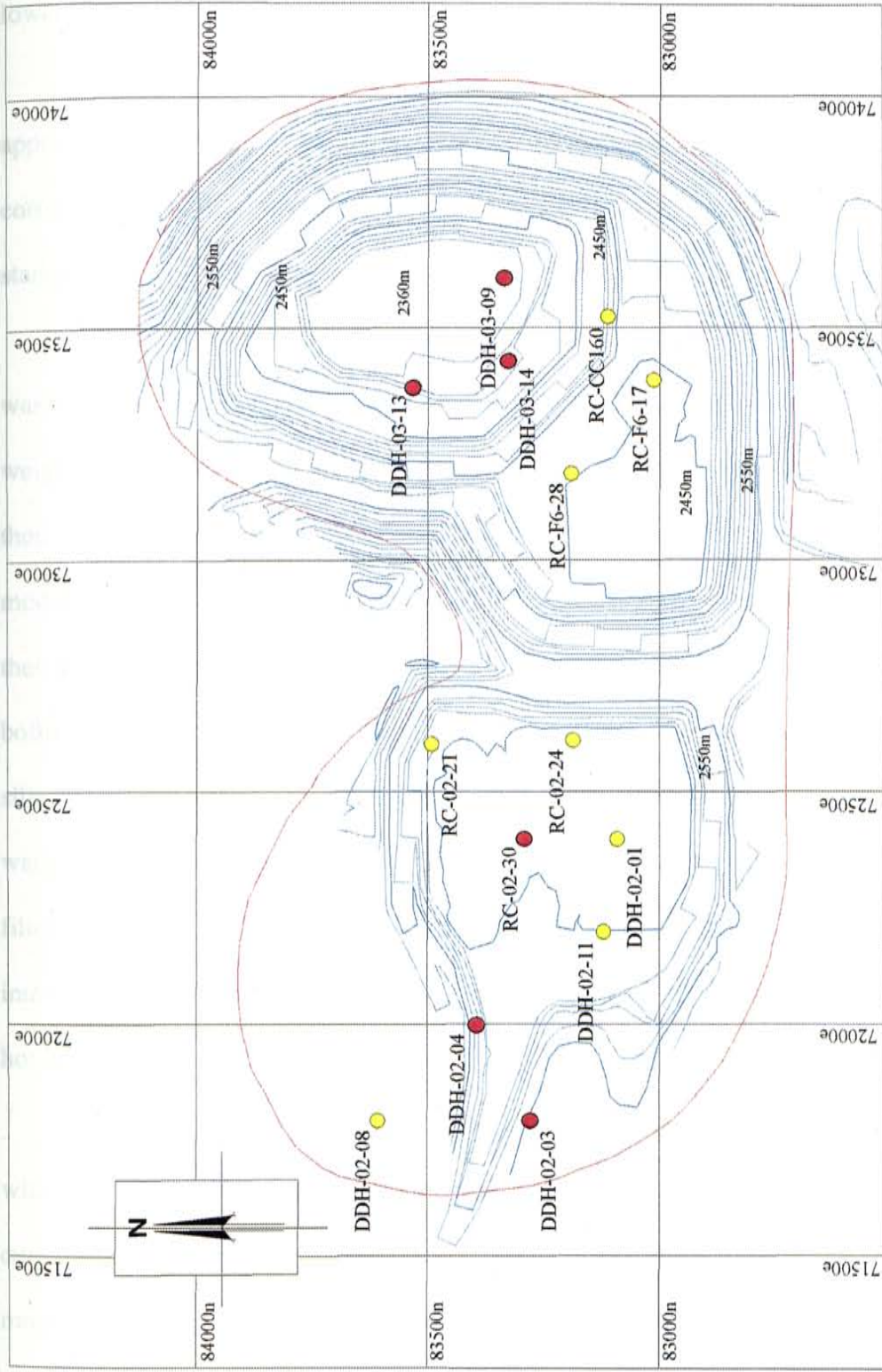


Figure 4.1: Location of drill holes sampled during the first (in red) and second (in yellow) round of sampling. Contour interval is 10-meters; red line represents the outline of the final pit.

supergene profile to include the supergene sulfide zone. Sampling was also extended lower in the profile into the hypogene zone.

Ten-meter composite pulp samples were compiled at Cerro Colorado by sampling approximately 50 grams of material from each of the five 2-meter coarse pulp rejects corresponding to that particular interval. This material was mixed and placed into a standard paper sample envelope and generally weighed 250 to 350 grams.

At The New Mexico Institute of Mining and Technology, 30 grams of material was combined with sodium polytungstate in a 250 ml centrifuge bottle to a combined weight of approximately 410 grams (Figure 5.2). Two 250 ml centrifuge bottles were then agitated by hand for 15 to 30 seconds and placed into an International Centrifuge model CM Cabinet Stand at 800 r.p.m. for 10-minutes. Each centrifuged sample was then placed in approximately one-inch of liquid nitrogen for 1 to 2 minutes, or until the boiling pitch changed. The unfrozen upper portion of the liquid containing the light silicate fraction was decanted and the centrifuge bottle was rinsed using warm distilled water to remove excess liquid and light fraction partials into a glass funnel containing filter paper. The remaining heavy fraction was then rinsed using warm distilled water into another glass funnel containing filter paper. Samples were continually rinsed with hot distilled water until all of the heavy liquid was recovered and the samples were clean.

A few grams of the heavy fraction, containing the sulfides, were then combined with a few grams of epoxy, poured into small, half-moon shaped Teflon[®] molds, and cured in an oven at 40 °C (Figure 5.2). Three cured samples are then placed into a probe-mount with the settling profile face down and covered with additional epoxy and allowed



Figure 5.2: Sample preparation schematic for the heavy mineral separations. Each sample followed this separation procedure as illustrated above.

to cure for 24-hours. The probe-mounted samples were then polished to P# 2,400-grit using a polishing wheel, and finished on a carpet using a 0.05 μ aluminum oxide polish.

Quantitative mineralogical analyses of heavy mineral separates were completed at The New Mexico Institute of Mining and Technology. Sulfide species were identified using standard reflective light techniques. Line integration, a point counting technique that integrates the total volume of each sulfide species intersecting a transecting line was employed (Brimhall, 1977) (Figure 5.3). This allowed the volume percent to be calculated for pyrite (py), chalcopyrite (cp), bornite (bn), covellite (cv), chalcocite (cc), and molybdenite (mo). Ten line traverses usually spaced at 1 mm were performed at 100x magnification for each sample. Traverses were oriented perpendicular to the settling column of each sample. The number of sulfide points counted from each sample varied between 100 and 1,000 depending on the sulfide yield for a particular heavy mineral separate.

Analytical Methods

Isotope Geochemistry

Pyrite grains were collected from eighteen 10-meter composite heavy mineral separates from the six initially sampled drill holes. Samples were collected from the transition and hypogene zones where pyrite grains were not replaced by supergene sulfide minerals. Samples were collected to identify if the sulfur from the mineralizing intrusions at Cerro Colorado is of a magmatic or sedimentary source (Jurassic-age evaporates).

The $\delta^{34}\text{S}$ measurements of the pyrite mineral separates were made at The New Mexico Institute of Mining and Technology using a Thermo Finnigan Delta Plus XP

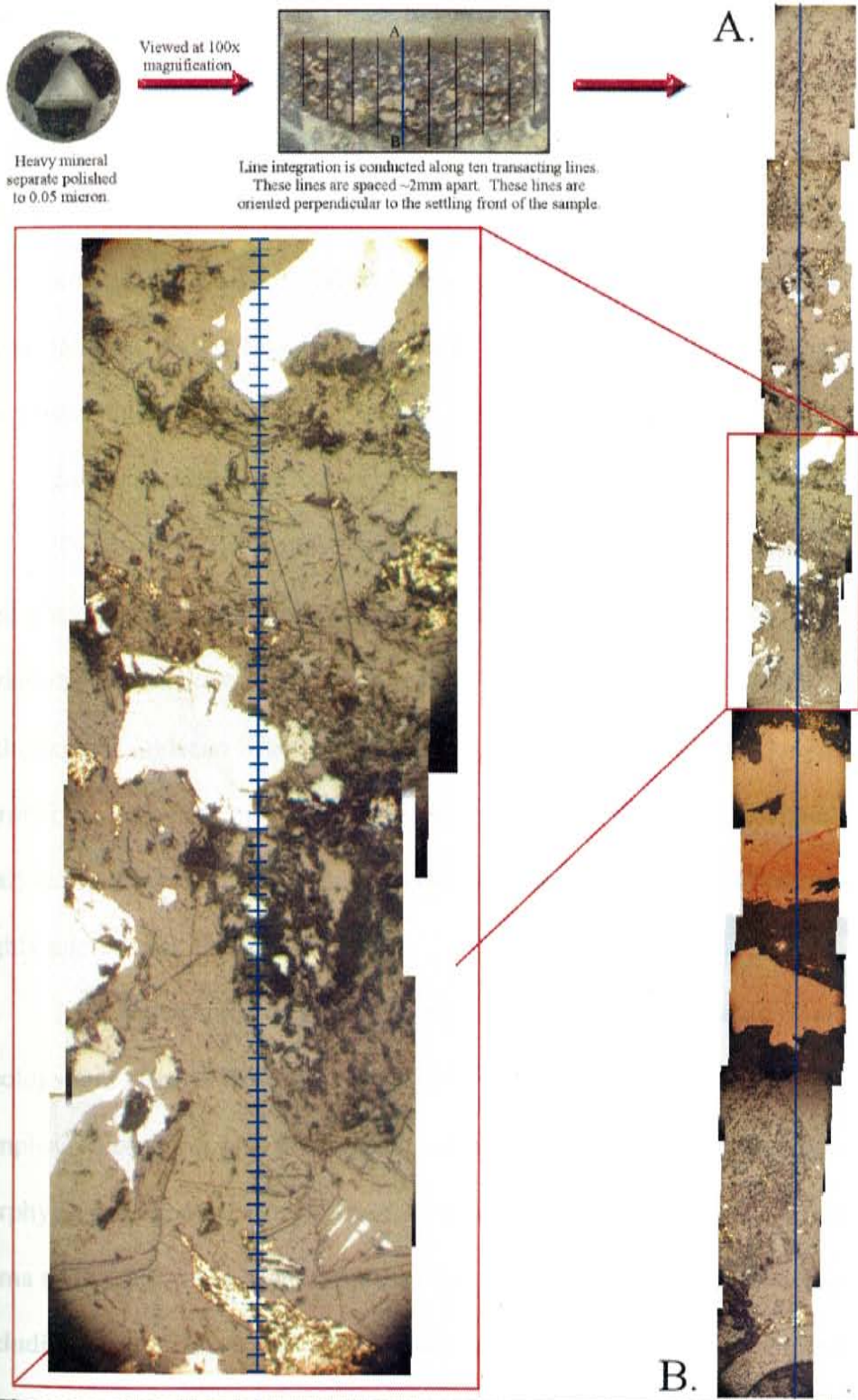


Figure 5.3: Schematic illustrating the line integration technique used to calculate the volume percent of the sulfide species. Line A-B is a photomosaic of one traversing line from the above pictured sample. Each intersected tick-mark, as pictured in the red-outlined inset, is counted for each sulfide and integrated over the entire line.

Continuous Flow Isotope Ratio Mass Spectrometer (CFIRMS) interfaced to an Elemental Analyzer (EA). Each dried sample was weighted on an analytical microbalance in small tin cups (3.5 x 5.0mm). Sample size ranged from 0.51 mg to 0.69 mg. To maintain quality standard protocol standard materials, NBS ZnS, NBS Ag₂S, NBS 127 BaSO₄, and in-house standard FeS were analyzed with the samples at the start, between, and at the end of samples. In addition to the standard materials three pyrite duplicates were also analyzed with the samples.

Lithochemistry

Twenty-one core samples were analyzed by x-ray fluorescence spectroscopy for their trace element compositions. These samples were selected to test if trace element variations could be used to discriminate the various rock-types at Cerro Colorado including the Andesite (Cerro Empexa Formation), Feldspar Porphyry, Quartz-Feldspar Porphyry (Micro Breccia), and Quartz-Feldspar-Biotite Porphyry. Samples were analyzed to examine if immobile trace elements could be used to differentiate these highly altered rock-types.

XRF geochemical analyses were conducted at the New Mexico Bureau of Geology and Mineral Resources (NMBGMR) using a Phillips PW 2400 XRF. Core samples representing four lithologic units: Andesite, Feldspar Porphyry, Quartz-Feldspar Porphyry, and Quartz-Feldspar-Biotite Porphyry, prior to analysis were crushed using a Tema swing mill, a hardened stainless steel container, for two-minutes. Samples, including one duplicate, one triplicate, and one sand standard, were prepared as pressed powder pellets (to 10 tons) and analyzed, using NMBGMR standard operating procedures (Hallett and Kyle, 1993).

CHAPTER 6

RESULTS

Transition Zone Ore Characterization

Data was collected for 135 ten-meter composite samples from 14 drill holes. For each sample, the relative volume percents of pyrite (py), chalcopyrite (cp), bornite (bn), chalcocite (cc), covellite (cv), and molybdenite (mo) were determined using the line integration technique. The mineral ratios cc/cv, py/cp, py/cc+cv, and cc+cv/bn+cp, allow relative changes in the volume percents of sulfide minerals to be observed. In addition to these mineral ratios, the relative volume percent of copper sulfides were also calculated for each sample using the following equation:

$$\left\{ \frac{[Cc + Cv + Bn + Cp]}{[Cc + Cv + Bn + Cp + Py]} \right\} \times 100$$

Quantitative mineralogical results are separated into three categories (Category 1, Category 2, and Category 3) based on the amount of copper contained in the supergene sulfide phase (as chalcocite + covellite) using the following equation:

$$\left\{ \frac{[(Cc \times 0.80) + (Cv \times 0.67)]}{[(Cc \times 0.80) + (Cv \times 0.67) + (Cp \times 0.35) + (Bn \times 0.63)]} \right\} \times 100$$

Category 1 is defined as $\geq 80\%$ copper as chalcocite and covellite, Category 2 is defined as $< 80\%$ to $\geq 15\%$ copper, and Category 3 is defined as $< 14\%$ copper as chalcocite and covellite.

The range of mineral ratio values and relative percent copper sulfides for each category are listed below and presented for each group in Figures 6.1a through 6.1e, and for each drill hole in Appendix A: Category 1, $cc/cv = 100$ to 0.01 , $py/cp = 100$ to 5.2 , $py/cc+cv = 100$ to 0.01 , $cc+cv/bn+cp = 100$ to 2.0 , and $vol\% \text{ Cu sulfides} = 100\%$ to 1% ; Category 2, $cc/cv = 100$ to 0.01 , $py/cp = 100$ to 0.91 , $py/cc+cv = 100$ to 2.3 , $cc+cv/bn+cp = 3.1$ to 0.09 , and $vol\% \text{ Cu sulfides} = 58\%$ to 2% ; and Category 3, $cc/cv = 100$ to 0.13 , $py/cp = 41$ to 0.45 , $py/cc+cv = 100$ to 8.7 , and $cc+cv/bn+cp = 0.07$ to 0.01 , and $vol\% \text{ Cu sulfides} = 71\%$ to 3% . All quantitative mineralogical data is presented in Table 1.

Isotope Geochemistry

Stable isotopic pyrite data was collected from 18 samples representing 6 drill holes. The range of stable isotopic pyrite values (Table 2) is $\delta^{34}\text{S} = +0.2$ to $+2.9\%$, and form a normal distribution centered over $+2.0\%$ (Figure 6.2).

Lithochemistry

Twenty-element whole-rock lithochemical data were collected from 21 samples representing 10 drill holes. The samples are separated into four different categories (andesite, feldspar porphyry, quartz-feldspar porphyry, and quartz-feldspar-biotite porphyry) based on lithology. These data are plotted according to these four categories and will be discussed following the same convention.

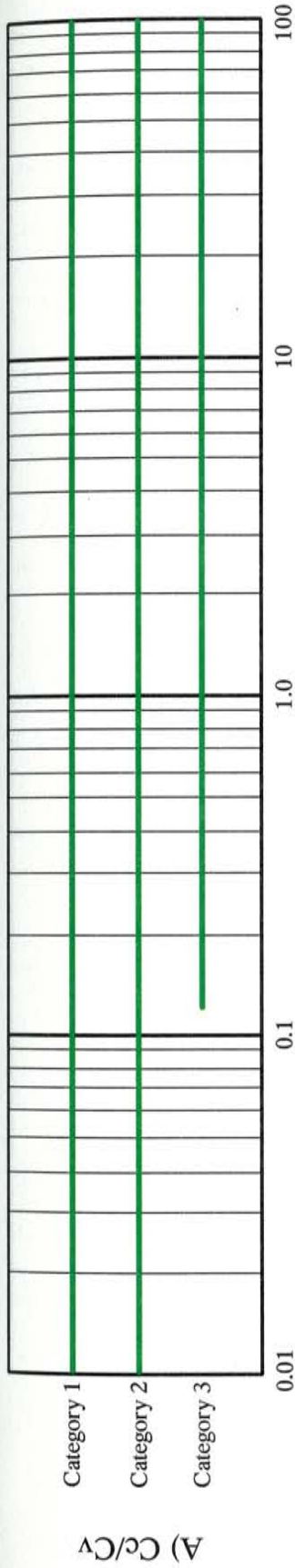


Figure 6.1a: Logarithm plot showing the Cc/Cv ranges for Category 1 through Category 3 samples.

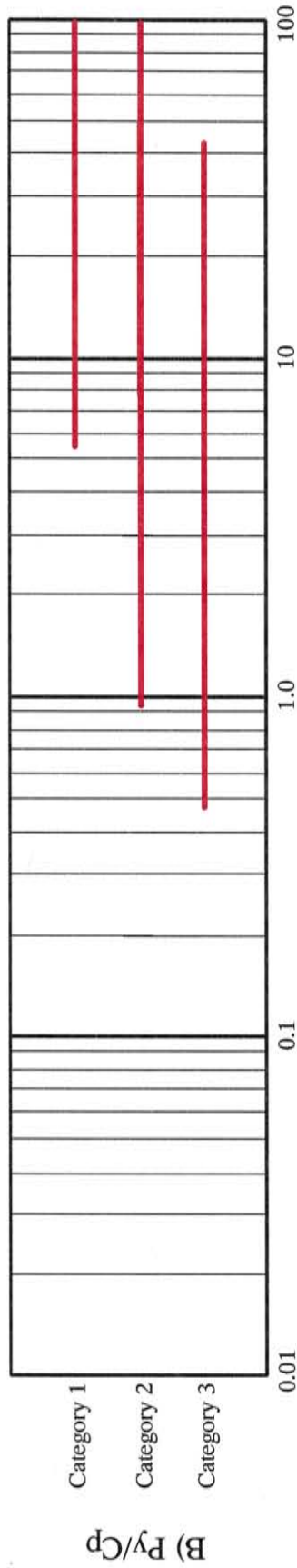


Figure 6.1b: Logarithm plot showing the Py/Cp ranges for Category 1 through Category 3 samples.

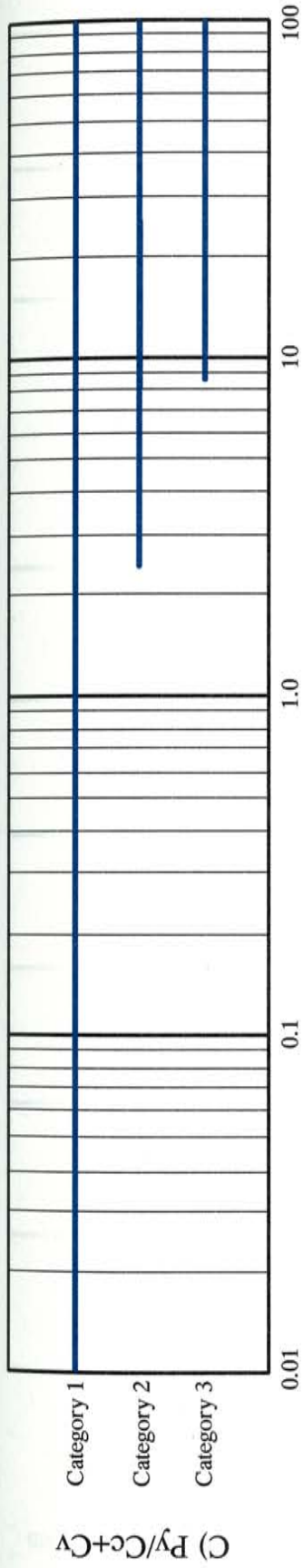


Figure 6.1c: Logarithm plot showing the $\frac{Py}{Cc+Cv}$ ranges for Category 1 through Category 3 samples.

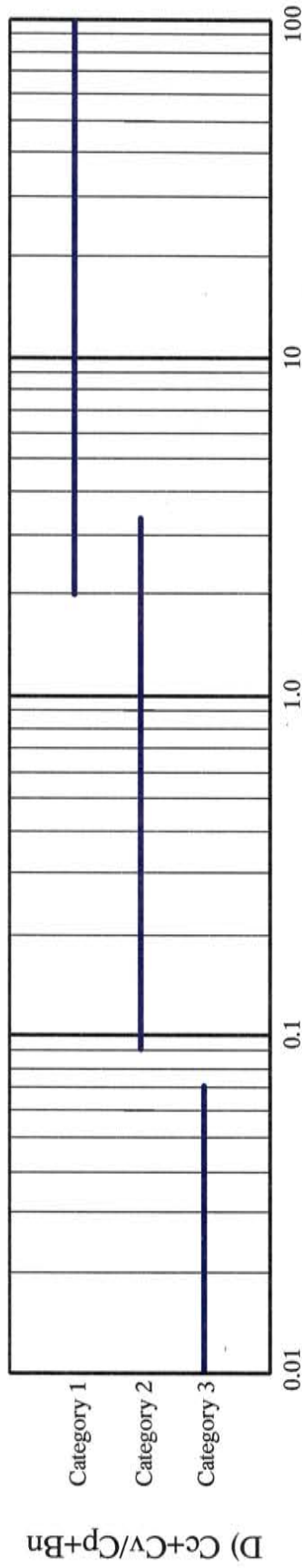


Figure 6.1d: Logarithm plot showing the $\frac{Cc+Cv}{Bn+Cp}$ ranges for Category 1 through Category 3 samples.

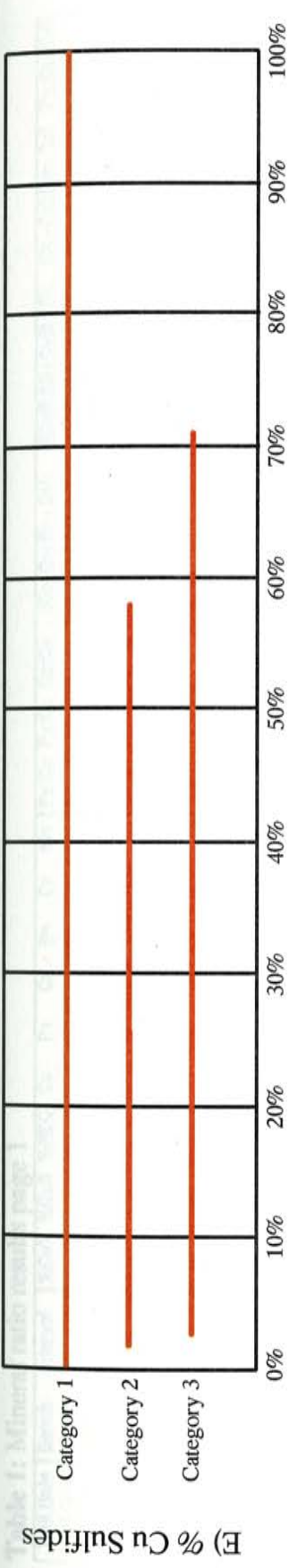


Figure 6.1e: Diagram illustrating the range of percent copper sulfides contained in Category 1 through Category 3 samples.

Table 1: Mineral ratio results page 1

Drill Hole	Bench	Interval	%CuT	%CuS	%REC	Cc	Py	Cp	Bn	Cv	Mo	Py:Cb	Py:Cc	Cc:Cv	(Cc+Cv+Bn+Cp): (Cc+Cv+Bn+Cp+Py)	(Cc(0.80)+Cv(0.67)): (Cc(0.80)+Cv(0.67) +Cp(0.35)+Bn(0.63))	(Cc+Cv):(Bn+Cp)	(Py:Cc+Cv)
DDH-02-01	2600																	
	2590																	
Collar	2580																	
	2570	0-8m	N/A	N/A	N/A													
	2560	8-18m	N/A	N/A	N/A													
UTME	2550	18-28m	N/A	N/A	N/A													
	2540	28-38m	N/A	N/A	N/A													
	2530	38-48m	N/A	N/A	N/A													
UTMN	2520	48-58m	N/A	N/A	N/A													
	2510	58-68m	N/A	N/A	N/A													
83080	2500	68-78m	N/A	N/A	N/A													
	2490	78-88m	N/A	N/A	N/A													
	2480	88-98m	0.10	0.03	30%													
	2470	98-108m	0.35	0.24	69%													
	2460	108-118m	0.35	0.20	57%													
	2450	118-128m	0.18	0.08	44%													
	2440	128-138m	0.98	0.86	88%													
	2430	138-148m	1.29	1.18	91%													
	2420	148-158m	0.19	0.13	68%													
	2410	158-168m	0.13	0.04	31%													
	2400	168-178m	0.14	0.05	36%													
	2390	178-188m	0.61	0.55	90%													
	2380	188-198m	0.95	0.88	93%													
	2370	198-208m	0.13	0.07	54%													
	2360	208-218m	0.18	0.08	44%													
	2350	218-228m	0.08	0.02	25%	0.25	0.25	0	0	0.25	0	100	100	100	75%	81%	100	0.01
	2340	228-238m	0.08	0.02	13%	121	94	18	0.25	0.25	0	5.2	0.78	100	60%	94%	6.6	0.78
	2330	238-248m	2.31	0.34	15%	135	292	26	13	1	0	11	2.2	100	37%	86%	3.5	2.1
	2320	248-258m	0.98	0.07	7%	49	151	116	0.25	4	0	1.3	3.1	12	53%	51%	0.46	2.8
	2310	258-268m	0.81	0.05	6%	50	346	95	7	0.25	0.25	3.6	6.9	100	31%	52%	0.49	6.9
	2300	268-278m	0.66	0.06	9%	17	99	104	7	1	0	0.95	5.8	17	57%	26%	0.16	5.5
	2290	278-288m	0.52	0.04	8%	31	269	179	33	0.25	0	1.5	8.7	100	47%	23%	0.15	8.6
	2280	288-290m	0.67	0.04	6%													

Table 1: Mineral ratio results page 2

Drill Hole	Bench	Interval	%CuT	%CuS	%REC	Cc	Py	Cp	Bn	Cv	Mo	Pv:Cb	Py:Cc	Cc:Cv	(Cc+Cv+Bn+Cp): (Cc+Cv+Bn+Cp+Py)	(Cc(0.80)+Cv(0.67)): (Cc(0.80)+Cv(0.67) +Cp(0.35)+Bn(0.63))	(Cc+Cv):(Bn+Cp)	(Py:Cc+Cv)
DDH-02-03	2580					420	232	0	0	7	0	100	0.55	60	65%	100%	100	0.54
	2570					167	332	25	0	84	0	13	2.0	2.0	45%	96%	10	1.3
Cellar	2560	0-4m	N/A	N/A	N/A	21	245	60	0.25	51	0	4.1	12	0.41	35%	71%	1.2	3.4
2550	2540	4-14m	N/A	N/A	N/A	29	574	56	1	65	0	10	20	0.45	21%	77%	1.6	6.1
2530	2520	14-24m	N/A	N/A	N/A	1	297	192	1	1	0	1.5	100	1.0	40%	2%	0.01	100
UTME	71781	24-34m	N/A	N/A	N/A	9	235	196	0	0.25	0.25	1.2	26	36	47%	10%	0.05	25
2510	2500	34-44m	N/A	N/A	N/A	0.25	217	127	0	0	0	1.7	100	100	37%	0.4%	0.01	100
UTMN	83268	44-54m	N/A	N/A	N/A	0	510	67	2	0	0	7.6	100	100	12%	0.1%	0.01	100
2490	2480	54-64m	N/A	N/A	N/A													
2470	2460	64-74m	N/A	N/A	N/A													
2450	2440	74-84m	N/A	N/A	N/A													
2430	2420	84-94m	N/A	N/A	N/A													
2410	2400	94-104m	0.08	0.01	13%													
2390	2380	104-114m	0.10	0.01	10%													
2370	2360	114-124m	0.22	0.03	14%													
2350	2340	124-134m	0.10	0.02	20%													
2330	2320	134-144m	0.13	0.04	31%													
2310	2300	144-154m	0.27	0.21	78%													
	2290	154-164m	1.30	0.41	32%													
	2280	164-174m	3.56	0.95	27%													
	2270	174-184m	2.15	0.19	9%													
	2260	184-194m	1.16	0.09	8%													
	2250	194-204m	0.85	0.06	7%													
	2240	204-214m	0.59	0.04	7%													
	2230	214-224m	0.78	0.04	5%													
	2220	224-234m	0.52	0.02	4%													
	2210	234-242.7m	0.42	0.02	5%													

Table 1: Mineral ratio results page 3

Drill Hole	Bench	Interval	%CuI	%CuS	%REC	Cc	Py	Cp	Bn	Cv	Mo	Py:Cp	Py:Cc	Cc:Cv	(Cc+Cv+Bn+Cp): (Cc+Cv+Bn+Cp+Py)	(Cc(0.80)+Cv(0.67)): (Cc(0.80)+Cv(0.67) +Cp(0.35)+Bn(0.63))	(Cc+Cv):(Bn+Cp)	(Py:Cc+Cv)
DDH-02-04	2580					227	209	18	0	29	0	12	0.92	7.8	57%	97%	14	0.82
	2570					11	656	274	0	20	20	2.4	60	0.6	32%	19%	0.11	21
Cellar	2560					25	536	255	6	3	30	2.1	21	8.3	35%	19%	0.11	19
2555m	2550	0-5m	N/A	N/A	N/A	3	478	546	1	24	23	0.88	100	0.13	55%	9%	0.05	18
	2540	5-15m	N/A	N/A	N/A	4	624	365	3	0.25	3	1.7	100	16	37%	3%	0.01	100
UTME	2530	15-25m	N/A	N/A	N/A	4	481	226	0.25	0.25	0.25	2.1	100	16	32%	4%	0.02	100
71997	2520	25-35m	N/A	N/A	N/A	3	478	246	0.25	0	0.25	1.9	100	100	34%	3%	0.01	100
	2510	35-45m	N/A	N/A	N/A	0.25	601	459	0.25	0	1	1.3	100	100	43%	1%	0.00	100
UTMN	2500	45-55m	N/A	N/A	N/A													
83379	2490	55-65m	0.11	0.05	45%													
	2480	65-75m	0.13	0.05	38%													
	2470	75-85m	0.82	0.70	85%													
	2460	85-95m	0.61	0.41	67%													
	2450	95-105m	0.30	0.04	13%													
	2440	105-115m	0.61	0.26	43%													
	2430	115-125m	0.65	0.40	62%													
	2420	125-135m	0.36	0.24	67%													
	2410	135-145m	1.16	0.92	79%													
	2400	145-155m	0.58	0.48	83%													
	2390	155-165m	0.35	0.26	74%													
	2380	165-175m	0.86	0.38	45%													
	2370	175-185m	0.92	0.05	5%													
	2360	185-195m	0.92	0.03	3%													
	2350	195-205m	0.99	0.03	3%													
	2340	205-215m	0.68	0.02	2%													
	2330	215-225m	0.66	0.02	3%													
	2320	225-235m	0.60	0.02	3%													
	2310	235-245m	0.62	0.01	2%													
	2300	245-248.5m																

Table 1: Mineral ratio results page 4

Drill Hole	Bench	Interval	%CuT	%CuS	%REC	Cc	Py	Cp	Bn	Cv	Mo	Py:Cb	Py:Cc	Cc:Cv	(Cc+Cv+Bn+Cp): (Cc+Cv+Bn+Cp+Py)	(Cc(0.80)+Cv(0.67): (Cc(0.80)+Cv(0.67) +Cp(0.35)+Bn(0.63))	(Cc+Cv):(Bn+Cp)	(Py:Cc+Cv)	
DDH-02-08	2580					12	363	5	1	16	0.25	73	30	0.75					
	2570					11	362	36	0	0.25	0	10	33	44		90%	4.7	13	
Collar	2560	0-10m	N/A	N/A	N/A														
2560m	2550	10-20m	N/A	N/A	N/A														
	2540	20-30m	N/A	N/A	N/A	19	453	82	0	0.25	0	5.5	24	76		42%	0.31	32	
UTME	2530	30-40m	N/A	N/A	N/A	0.25	184	23	0.25	0	0	8.0	100	100		35%	0.23	24	
71783	2520	40-50m	N/A	N/A	N/A	0.25	329	24	0.25	0	0	14	100	100		2%	0.01	100	
	2510	50-60m	N/A	N/A	N/A	5	322	43	3	0	0	7.5	64	100		2%	0.01	100	
UTMN	2500	60-70m	N/A	N/A	N/A	3	205	46	1	0	0	4.5	68	100		19%	0.11	64	
83609	2480	70-80m	N/A	N/A	N/A														
	2470	80-90m	N/A	N/A	N/A														
	2460	90-100m	0.03	0.01	20%														
	2450	100-110m	0.05	0.01	14%														
	2440	110-120m	0.06	0.01	17%														
	2430	120-130m	0.11	0.02	18%														
	2420	130-140m	0.48	0.29	60%														
	2410	140-150m	0.82	0.58	71%														
	2400	150-160m	0.46	0.36	78%														
	2390	160-170m	0.46	0.27	59%														
	2380	170-180m	0.26	0.14	54%														
	2370	180-190m	0.17	0.07	41%														
	2360	190-200m	0.53	0.13	25%														
	2350	200-210m	0.59	0.05	8%														
	2340	210-220m	0.47	0.03	6%														
	2330	220-230m	0.36	0.02	6%														
	2320	230-240m	0.36	0.01	3%														
	2310	240-250m	0.35	0.03	9%														
	2300	250-260m	0.43	0.03	7%														

Table 1: Mineral ratio results page 5

Drill Hole	Bench	Interval	%CuT	%CuS	%REC	Ce	Py	Gp	Bn	Cv	Mo	Py:Gp	Py:Ce	Cc:Cv	(Cc+Cv+Bn+Cp): (Cc+Cv+Bn+Cp+Py)	(Cc(0.80)+Cv(0.67)): (Cc(0.80)+Cv(0.67) +Cp(0.35)+Bn(0.63))	(Cc+Cv):(Bn+Cp)	(Py:Cc+Cv)
DDH-02-11	2560					114	585	0	0	0	0	100	5.1	100		100%	100	5.1
	2550					19	623	63	0	20	0	9.9	33	0.95		56%	0.62	16
Cellar	2540					7	446	103	0	4	0	4.3	64	1.8		19%	0.11	41
2530		0-8m	N/A	N/A	N/A	12	550	193	0.25	8	0.25	2.8	46	1.5		18%	0.10	28
2520		8-18m	N/A	N/A	N/A	29	219	211	1	11	0.25	1.0	7.6	2.6		29%	0.19	5.5
2510		18-28m	N/A	N/A	N/A	16	354	75	1	2	0.25	4.7	22	8.0		34%	0.24	20
2500		28-38m	N/A	N/A	N/A	1	425	121	0	0.25	0	3.5	100	4.0		2.2%	0.01	100
2490		38-48m	N/A	N/A	N/A	0.25	395	198	0	0	0	2.0	100	100		0.29%	0.01	100
2480		48-58m	N/A	N/A	N/A													
2470		58-68m	N/A	N/A	N/A													
2460		68-78m	0.08	0.02	25%													
2450		78-88m	0.09	0.01	11%													
2440		88-98m	0.22	0.10	45%													
2430		98-108m	0.17	0.06	35%													
2420		108-118m	0.83	0.75	90%													
2410		118-128m	0.78	0.72	92%													
2400		128-138m	0.21	0.10	48%													
2390		138-148m	0.21	0.11	52%													
2380		148-158m	0.18	0.13	72%													
2370		158-168m	0.22	0.14	64%													
2360		168-178m	0.72	0.53	74%													
2350		178-188m	0.95	0.18	19%													
2340		188-198m	0.94	0.08	9%													
2330		198-208m	0.47	0.04	9%													
2320		208-218m	0.62	0.05	8%													
2310		218-228m	0.63	0.08	13%													
2300		228-238m	0.44	0.04	9%													
2290		238-248m	0.37	0.01	3%													
2280		248-258m	0.46	0.01	2%													
2270		258-260m	0.49	0.01	2%													

Table 1: Mineral ratio results page 6

Drill Hole	Bench	Interval	%CuI	%CuS	%REC	Cc	Py	Cp	Bn	Cy	Mo	Py:Cp	Py:Cc	Cc:Cv	(Cc+Cv+Bn+Cp): (Cc+Cv+Bn+Cp+Py)	(Cc(0.80)+Cv(0.67)): (Cc(0.80)+Cv(0.67) +Cp(0.35)+Bn(0.63))	(Cc+Cv):(Bn+Cp)	(Py:Cc+Cv)	
DDH-03-09	2410																		
	2400																		
Collar	2390																		
2390m	2380	0-10m	0.56	0.47	84%	68	146	0	0	1	0	100	2.1	68	32%	100%	100	2.1	
	2370	10-20m	0.57	0.26	46%	53	84	2	0	0.25	0	42	1.6	100	40%	98%	27	1.6	100
UTME	2360	20-30m	0.46	0.19	41%	62	248	50	2	0.25	4	5.0	4.0	100	32%	73%	1.2	4.0	100
73601	2350	30-40m	0.56	0.06	11%	31	463	111	25	0	26	4.2	15	100	27%	31%	0.23	15	100
	2340	40-50m	0.72	0.03	4%	41	269	59	10	0	0	4.6	6.6	100	29%	55%	0.59	6.6	100
UTMN	2330	50-60m	0.66	0.05	8%	9	149	165	14	0	1	0.90	17	100	56%	10%	0.05	17	100
83325	2320	60-70m	0.62	0.04	6%	8	306	302	5	0	216	1.0	38	100	51%	5.6%	0.03	38	100
	2310	70-80m	0.46	0.02	4%	40	479	55	29	0.25	15	8.7	12	100	21%	46%	0.48	12	100
	2300	80-90m	0.70	0.04	6%	102	674	48	37	0.25	5	14	6.6	100	22%	67%	1.2	6.6	100
	2290	90-100m	0.78	0.05	6%	100	535	36	46	0.25	3	15	5.4	100	25%	66%	1.2	5.3	100
	2280	100-110m	0.60	0.04	7%	38	482	4	11	4	0.25	121	13	9.5	11%	80%	2.8	11	100
	2270	110-120m	0.58	0.04	7%	11	383	102	77	14	10	3.8	35	0.79	35%	18%	0.14	15	100
	2260	120-130m	0.66	0.04	6%	0.25	153	94	0	0.25	104	1.6	100	1.0	38%	1%	0.01	100	100
	2250	130-140m	0.33	0.01	3%	0	172	159	0	0.25	6	1.1	100	100	48%	0.3%	0.01	100	100
	2240	140-150m	0.30	0.01	3%														

Drill Hole	Bench	Interval	%CuI	%CuS	%REC	Cc	Py	Cp	Bn	Cy	Mo	Py:Cp	Py:Cc	Cc:Cv	(Cc+Cv+Bn+Cp): (Cc+Cv+Bn+Cp+Py)	(Cc(0.80)+Cv(0.67)): (Cc(0.80)+Cv(0.67) +Cp(0.35)+Bn(0.63))	(Cc+Cv):(Bn+Cp)	(Py:Cc+Cv)	
DDH-03-13	2410																		
	2400																		
Collar	2390																		
2390m	2380	0-10m	0.29	0.04	14%	54	414	26	1	4	0.25	16	7.7	13.5	17%	83%	2.1	7.1	100
	2370	10-20m	0.43	0.02	5%	1	331	114	7	0	0	2.9	100	100	27%	2%	0.01	100	100
UTME	2360	20-30m	0.41	0.01	2%	16	271	113	0.25	0	0.25	2.4	100	100	30%	2%	0.01	100	100
73378	2350	30-40m	0.41	0.03	7%	12	412	93	11	0	0	4.0	23	100	24%	24%	0.15	23	100
	2340	40-50m	0.48	0.04	8%	5	515	98	1	0	3	3.6	34	100	26%	16%	0.09	34	100
UTMN	2330	50-60m	0.33	0.02	6%	9	1397	146	1	0	0	5.3	100	100	17%	10%	0.05	100	100
83541	2320	60-70m	0.34	0.02	6%	0.25	386	153	9	0	0	9.6	100	100	10%	12%	0.06	100	100
	2310	70-77.4m	N/A	N/A	N/A							2.5	100	100	30%	0.3%	0.01	100	100

Table 1: Mineral ratio results page 7

Drill Hole	Bench	Interval	%CuT	%CuS	%REC	Cc	Py	Cp	Bn	Cy	Mo	Pv:Cp	Pv:Cc	Cc:Cv	(Cc+Cv+Bn+Cp): (Cc+Cv+Bn+Cp+Py)	(Cc(0.80)+Cv(0.67)): (Cc(0.80)+Cv(0.67) +Cp(0.35)+Bn(0.63))	(Cc+Cv):(Bn+Cp)	(Py:Cc+Cv)
RC-02-21	2620					0	0	0	0	0	0.25	N/A	N/A	N/A	N/A	N/A	N/A	N/A
	2610					0.25	0	0	0	0	0	100	0.01	100	100%	N/A	100	0.01
Cellar	2600					21	10	0	0	0.25	0	100	0.48	84	68%	100%	100	0.47
2597m	2590	0-8m	N/A	N/A	N/A	45	125	21	2	1	0	6.0	2.8	45	36%	81%	2.0	2.7
	2580	8-18m	N/A	N/A	N/A	14	190	64	1	1	0	3.0	14	14	30%	34%	0.23	13
UTME	2570	18-28m	N/A	N/A	N/A	16	117	11	1	1	0	11	7.3	16	20%	75%	1.4	6.9
72606	2560	28-38m	N/A	N/A	N/A	7	86	12	2	0.25	0.25	7.2	12	28	20%	51%	0.52	12
	2550	38-48m	N/A	N/A	N/A	25	628	21	16	5	18	30	25	5.0	10%	57%	0.81	21
UTMN	2540	48-58m	0.04	0.00	5%	8	140	11	4	1	0.25	13	18	8.0	15%	53%	0.60	16
83482	2530	58-68m	0.03	0.00	10%	27	304	49	17	6	40	6.2	11	4.5	25%	48%	0.50	9.2
	2520	68-78m	0.04	0.00	10%													
	2510	78-88m	0.06	0.01	17%													
	2500	88-98m	0.07	0.01	14%													
	2490	98-108m	0.22	0.15	68%													
	2480	108-118m	0.21	0.08	38%													
	2470	118-128m	0.09	0.01	11%													
	2460	128-138m	0.06	0.00	7%													
	2450	138-148m	0.09	0.01	6%													
	2440	148-158m	0.05	0.00	6%													
	2430	158-168m	0.07	0.01	14%													
	2420	168-178m	0.28	0.20	71%													
	2410	178-188m	0.19	0.13	68%													
	2400	188-198m	0.89	0.80	90%													
	2390	198-208m	0.59	0.54	92%													
	2380	208-218m	0.65	0.61	94%													
	2370	218-228m	1.25	1.09	87%													
	2360	228-238m	0.83	0.11	13%													
	2350	238-248m	0.52	0.04	8%													
	2340	248-258m	0.55	0.04	7%													
	2330	258-268m	0.51	0.04	8%													
	2320	268-278m	0.42	0.05	12%													
	2310	278-288m	0.60	0.06	10%													
	2300	288-298m	0.61	0.06	10%													
	2290	298-300m	0.38	0.05	13%													

Table 1: Mineral ratio results page 8

Drill Hole	Bench	Interval	%CuT	%CuS	%REC	Cc	Py	Cp	Bn	Cy	Mo	Pv:Op	Pv:Oc	Cc:Cv	(Cc+Cv+Bn+Op): (Cc+Cv+Bn+Op+Py)	(Cc(0.80)+Cv(0.677): (Cc(0.80)+Cv(0.677) +Cp(0.35)+Bn(0.63))	(Cc+Cv):(Bn+Cp)	(Py:Cc+Cv)	
RC-02-24	2600					230	110	1	2	0	0.25	100	0.48	100					
	2590					123	376	76	24	0.25	0.25	4.9	3.1	100					
Cellar	2580					27	217	238	13	0	0	0.91	8.0	100					
2580m	2570	0-10m	N/A	N/A	N/A														
	2560	10-20m	N/A	N/A	N/A														
UTME	2550	20-30m	N/A	N/A	N/A														
72603	2540	30-40m	N/A	N/A	N/A	6	432	164	2	0.25	0	2.6	72	24					
	2530	40-50m	N/A	N/A	N/A	31	438	220	7	1	1	2.0	14	31					
	2520	50-60m	N/A	N/A	N/A	145	421	120	59	0	0	3.5	2.9	100					
UTMN	2510	60-70m	N/A	N/A	N/A	76	1192	40	28	0	13	30	16	100					
83177	2500	70-80m	N/A	N/A	N/A	36	802	48	25	0.25	0	17	22	100					
	2490	80-90m	N/A	N/A	N/A	20	174	388	25	0	0.25	0.45	8.7	100					
	2480	90-100m	N/A	N/A	N/A	10	181	143	19	0	0.25	1.3	18	100					
	2470	100-110m	N/A	N/A	N/A														
	2460	110-120m	N/A	N/A	N/A														
	2450	120-130m	0.01	0.00	10%														
	2440	130-140m	0.01	0.00	10%														
	2430	140-150m	0.02	0.00	10%														
	2420	150-160m	0.37	0.25	68%														
	2410	160-170m	0.50	0.20	40%														
	2400	170-180m	0.95	0.50	53%														
	2390	180-190m	1.16	0.88	76%														
	2380	190-200m	1.51	1.17	77%														
	2370	200-210m	1.38	0.55	40%														
	2360	210-220m	1.12	0.10	9%														
	2350	220-230m	0.65	0.04	6%														
	2340	230-240m	0.57	0.04	7%														
	2330	240-250m	0.57	0.06	11%														
	2320	250-260m	0.80	0.10	13%														
	2310	260-270m	0.40	0.06	15%														
	2300	270-280m	0.39	0.07	18%														
	2290	280-290m	0.55	0.04	7%														
	2280	290-300m	0.38	0.03	8%														

Table 1: Mineral ratio results page 9

Drill Hole	Bench	Interval	%CuT	%CuS	%REC	Cc	Py	Cp	Bn	Cv	Mo	Py:Sp	Py:Ce	Cc:Cv	(Cc+Cv+Bn+Cp): (Cc+Cv+Bn+Cp+Py)	(Cc(0.80)+Cv(0.67)): (Cc(0.80)+Cv(0.67) +Cp(0.35)+Bn(0.63))	(Cc+Cv):(Bn+Cp)	(Py:Cc+Cv)
RC-02-30	2600					113	171	0	0	10	0	100	1.5	11				
	2590					146	198	0	0	4	0	100	1.4	37	42%	100%	100	1.4
Collar	2580																	
	2570	0-8m	N/A	N/A	N/A													
	2560	8-18m	N/A	N/A	N/A													
UTME	2550	18-28m	N/A	N/A	N/A													
	2540	28-38m	N/A	N/A	N/A													
	2530	38-48m	N/A	N/A	N/A													
UTMN	2520	48-58m	0.43	0.32	74%													
	2510	58-68m	0.13	0.08	62%													
	2500	68-78m	0.35	0.28	80%													
	2490	78-88m	0.34	0.25	74%													
	2480	88-98m	0.44	0.32	73%													
	2470	98-108m	0.16	0.02	13%													
	2460	108-118m	0.21	0.07	33%													
	2450	118-128m	0.12	0.04	33%													
	2440	128-138m	0.21	0.15	71%													
	2430	138-148m	0.15	0.07	47%													
	2420	148-158m	0.20	0.1	50%													
	2410	158-168m	0.31	0.21	68%													
	2400	168-178m	1.24	1.09	88%													
	2390	178-188m	0.83	0.74	89%													
	2380	188-198m	0.06	0.02	33%													
	2370	198-208m	0.96	0.15	16%													
	2360	208-218m	2.42	0.38	16%													
	2350	218-228m	1.42	0.21	15%													
	2340	228-238m	1.03	0.18	17%													
	2330	238-248m	0.81	0.10	12%													
	2320	248-258m	0.68	0.09	14%													
	2310	258-268m	0.90	0.07	8%													
	2300	268-278m	0.89	0.05	6%													
	2290	278-288m	0.64	0.07	11%													
	2280	288-296m	0.67	0.05	7%													

Table 1: Mineral ratio results page 10

Drill Hole	Bench	Interval	%CuI	%CuS	%REC	Cc	Py	Cp	Bn	Cv	Mo	Py:Cp	Py:Cc	Cc:Cv	[Cc+Cu+Bn+Cp]: [Cc+Cu+Bn+Cp+Py]	[Cc(0.80)+Cv(0.67)]: [Cc(0.80)+Cv(0.67) +Cp(0.35)+Bn(0.63)]	[Cc+Cu+Bn+Cp]: [Cc+Cu+Bn+Cp+Py]	[Cc(0.80)+Cv(0.67)]: [Cc(0.80)+Cv(0.67) +Cp(0.35)+Bn(0.63)]	[Py:Cc+Cv]
SRC-F6-17	2560					266	291	0	0	0.25	0	100	1.1	100	48%	100%	100	1.1	
	2550					41	240	0	0.25	3	0	100	5.9	14	16%	100%	100	5.9	5.5
Collar	2540					53	305	5	0.25	8	2	61	5.8	6.6	18%	96%	12	5.8	5.0
2540m	2530	0-10m	0.04	0.00	0%	3	151	26	4	7	0.25	5.8	50	0.43	21%	38%	0.33	50	15
UTME	2510	20-30m	0.02	0.00	0%	3	238	60	0.25	1	0.25	4.0	79	3.0	21%	13%	0.07	79	60
73384	2500	30-40m	0.02	0.00	0%	11	187	10	12	0.25	0.25	19	17	44	15%	45%	0.51	17	17
	2490	40-50m	0.02	0.00	0%	24	366	85	7	0.25	0.25	4.3	15	96	24%	36%	0.26	15	15
UTMN	2480	50-60m	0.78	0.73	94%	19	578	60	1	1	0.25	9.6	30	19	12%	42%	0.33	30	29
83018	2470	60-70m	3.03	0.76	25%														
	2460	70-80m	1.78	0.10	6%														
	2450	80-90m	1.29	0.08	6%														
	2440	90-100m	0.49	0.03	6%														
	2430	100-110m	0.45	0.02	4%														
	2420	110-120m	0.50	0.04	8%														
	2410	120-130m	0.36	0.04	11%														
	2400	130-140m	0.34	0.02	6%														

Drill Hole	Bench	Interval	%CuI	%CuS	%REC	Cc	Py	Cp	Bn	Cv	Mo	Py:Cp	Py:Cc	Cc:Cv	[Cc+Cu+Bn+Cp]: [Cc+Cu+Bn+Cp+Py]	[Cc(0.80)+Cv(0.67)]: [Cc(0.80)+Cv(0.67) +Cp(0.35)+Bn(0.63)]	[Cc+Cu+Bn+Cp]: [Cc+Cu+Bn+Cp+Py]	[Cc(0.80)+Cv(0.67)]: [Cc(0.80)+Cv(0.67) +Cp(0.35)+Bn(0.63)]	[Py:Cc+Cv]
DDH-03-14	2400					27	473	101	24	0.25	7	4.7	18	100	24%	30%	0.22	18	17
	2390					9	670	31	0	1	0	22	74	9.0	6%	42%	0.32	74	67
Collar	2380					19	900	83	7	0.25	4	11	47	76	11%	31%	0.21	47	47
2380m	2370	0-10m	0.36	0.04	11%	18	592	5	2	1	0.25	100	33	18	4%	83%	2.7	33	31
UTME	2360	10-20m	0.46	0.05	11%	24	942	1	7	0.25	0.25	100	39	96	3%	80%	3.0	39	39
73439	2350	20-30m	0.53	0.05	9%	3	636	6	1	4	1	100	100	0.75	2%	65%	1.0	100	91
	2340	30-40m	0.64	0.08	13%	12	345	60	6	0.25	1	5.8	29	48	18%	28%	0.19	29	28
UTMN	2330	40-50m	0.21	0.04	19%	4	309	188	0	0	4	1.6	77	100	38%	5%	0.02	77	77
83321	2320	50-60m	0.33	0.05	15%														
	2310	60-70m	0.43	0.05	12%														
	2300	70-80.0m	0.35	0.02	6%														

Table 1: Mineral ratio results page 11

Drill Hole	Bench	Interval	%CuI	%CuS	%REC	Cc	Py	Cp	Bn	Cv	Mo	Py:Cb	Py:Cc	Cc:Cv	(Cc+Cv+Bn+Cp): (Cc+Cv+Bn+Cp+Py)	(Cc(0.80)+Cv(0.67)): (Cc(0.80)+Cv(0.67) +Cp(0.35)+Bn(0.63))	(Cc+Cv):(Bn+Cp)	(Py:Cc+Cv)
SRC-F6-28	2550					198	482	0	0	14	0	100	2.4	14.1	31%	100%	100	2.3
	2540					2	574	2	0.25	12	0	100	100	0.17	3%	92%	6.2	41
<u>Collar</u>	2530					57	444	1	0	9	0	100	7.8	6.3	13%	99%	66	6.7
	2520	0-10m	0.03	0.00	0%	81	681	1	0	4	0	100	8.4	20	11%	99%	85	8.0
	2510	10-20m	0.01	0.01	100%	234	537	0.25	0.25	14	0	100	2.3	17	32%	100%	100	2.2
<u>UTME</u>	2500	20-30m	0.01	0.00	0%	85	909	1	0	16	0	100	11	5.3	10%	100%	100	9.0
	2490	30-40m	0.01	0.00	0%	24	990	1	0	43	0	100	41	0.56	6%	99%	67	15
	2480	40-50m	0.48	0.16	33%	9	1522	1	4	60	0	100	100	0.15	5%	94%	14	22
	2470	50-60m	0.64	0.12	19%	0.50	1105	1	8	27	0	100	100	0.02	3%	77%	3.1	40
<u>UTMN</u>	2460	60-70m	0.43	0.06	14%	6	774	1	0.25	62	0	100	100	0.10	8%	99%	54	11
83180	2450	70-80m	0.56	0.09	16%	1	1072	0.25	0.25	42	0	100	100	0.02	4%	99%	86	25
	2440	80-90m	0.69	0.07	10%	0	1155	0	3	15	0	100	100	0.01	2%	84%	5.0	77
	2430	90-100m	1.24	0.09	7%	1	1290	64	0.25	172	0	20	100	0.01	16%	84%	2.7	7.5
	2420	100-110m	0.81	0.05	6%	0.25	1795	6	0.25	17	0	100	100	0.01	1%	84%	2.8	100
	2410	110-120m	0.57	0.04	7%	5	1028	5	2	5	0	100	100	1.0	2%	71%	1.4	100
	2400	120-130m	0.56	0.06	11%													
	2390	130-140m	0.33	0.05	15%													
	2380	140-150m	0.37	0.08	22%													
	2370	150-160m	0.34	0.06	18%													
	2360	160-170m	0.32	0.06	19%													
	2350	170-180m	0.44	0.05	11%													
	2340	180-190m	0.25	0.04	16%													
	2330	190-198m	0.16	0.02	13%													

Table 1: Mineral ratio results page 12

Drill Hole	Bench	Interval	%CuT	%CuS	%REC	Cc	Py	Cp	Bn	Cv	Mo	Py:Cb	Py:Ce	Cc:Cv	(Cc+Cv+Bn+Cp): (Cc+Cv+Bn+Cp+Py)	(Cc(0.80)+Cv(0.67)): (Cc(0.80)+Cv(0.67) +Cp(0.35)+Bn(0.63))	(Cc+Cv):(Bn+Cp)	(Py:Cc+Cv)	
RC-CC160	2600	0-10m	N/A	N/A	N/A	13	209	1	0	34	0	100	16	0.38	19%	99%	47	4.4	
	2590	10-20m	N/A	N/A	N/A	118	357	1	0.25	14	0	100	3.0	8.4	27%	100%	100	2.7	
Cellar	2580	20-30m	N/A	N/A	N/A	55	367	0	0	44	0.25	100	6.7	1.3	21%	100%	100	3.7	
2610m	2570	30-40m	N/A	N/A	N/A	136	571	4	0	23	0.25	100	4.2	5.9	22%	99%	40	3.6	
	2560	40-50m	N/A	N/A	N/A	27	275	2	0	78	0.25	100	10	0.35	28%	99%	53	2.6	
UTME	2550	50-60m	N/A	N/A	N/A	63	455	4	0	65	0.25	100	7.2	0.97	22%	99%	32	3.6	
73532	2540	60-70m	N/A	N/A	N/A	27	448	5	0	40	1	90	17	0.68	14%	97%	13	6.7	
UTMN	2530	70-80m	N/A	N/A	N/A	0.25	500	2	0	28	22	100	100	0.01	6%	96%	14	18	
83114	2520	80-90m	N/A	N/A	N/A	0.25	230	18	0	7	8	13	100	0.04	10%	44%	0.40	32	
	2510	90-100m	N/A	N/A	N/A	0	343	40	0	2	1	8.6	100	0.01	11%	9%	0.05	172	
	2500	100-110m	0.05	0.02	40%	0.25	674	6	0.25	13	0.25	100	100	0.02	3%	80%	2.1	51	
	2490	110-120m	0.94	0.86	91%	0.25	897	22	0	1	2	41	100	0.25	3%	10%	0.06	100	
	2480	120-130m	1.38	0.24	17%	0	604	48	0	7	0.25	13	100	0.01	8%	22%	0.15	86	
	2470	130-140m	1.88	0.17	9%	0	419	9	0	1	0.25	47	100	0.01	2%	18%	0.11	100	
	2460	140-150m	1.49	0.10	7%														
	2450	150-160m	2.01	0.14	7%														
	2440	160-170m	1.89	0.15	8%														
	2430	170-180m	1.48	0.14	9%														
	2420	180-190m	0.84	0.12	14%														
	2410	190-200m	0.63	0.04	6%														
	2400	200-210m	0.50	0.06	12%														
	2390	210-220m	0.40	0.04	10%														
	2380	220-230m	0.33	0.03	9%														
	2370	230-240m	0.24	0.03	13%														
	2360	240-250m	0.33	0.03	9%														
	2350	250-260m	0.35	0.03	9%														
	2340	260-264m	0.17	0.02	12%														

Table 2: $\delta^{34}\text{S}$ results for pyrite page 1

Sample	Mineral	$\delta^{34}\text{S}$ (py) vs CDT
DDH-02-03-214-224	py	2.0
DDH-02-03-224-234	py	2.7
DDH-02-03-234-242.70	py	2.4
DDH-02-04-235-225	py	2.9
DDH-02-04-235-245	py	2.4
DDH-02-04-245-248.65	py	1.8
DDH-03-09-110-120	py	1.9
DDH-03-09-120-130	py	2.1
DDH-03-09-140-150	py	1.6
DDH-03-13-50-60	py	1.9
DDH-03-13-70-60	py	2.2
DDH-03-13-70-77.70	py	2.3
DDH-03-14-50-60	py	1.9
DDH-03-14-60-70	py	2.0
DDH-03-14-70-80.75	py	2.6
RC-02-30-268-278	py	1.2
RC-02-30-278-288	py	1.1
RC-02-30-288-296	py	0.2

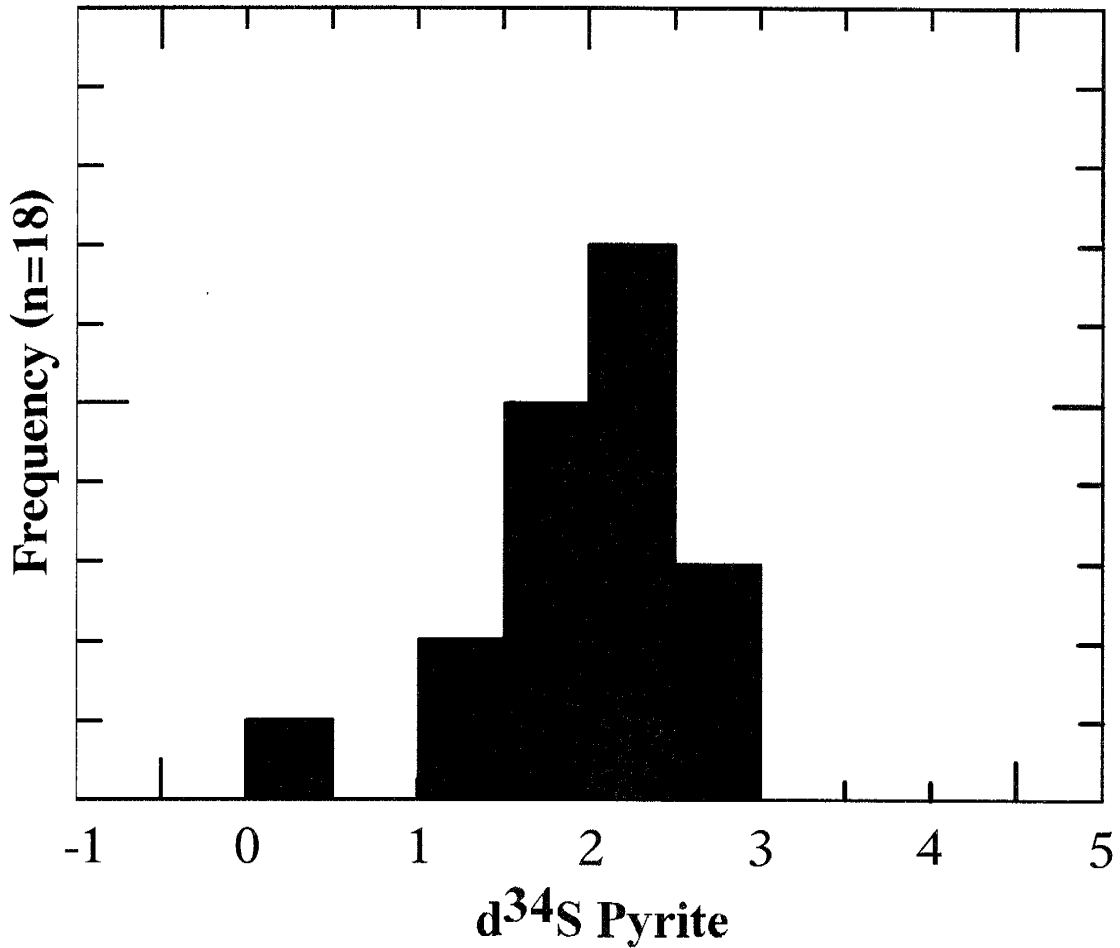


Figure 6.2: Histogram of $\delta^{34}\text{S}$ pyrite values. Note the normal distribution of the samples over $\sim 2.0\text{‰}$

The range of selected element and element ratios for each sample are listed below and presented in Figures 6.3 and 6.4: andesite, $\text{Zr}/\text{TiO}_2 = 0.018$ to 0.012 , $\text{Ga}(\text{ppm}) = 19$ to 2 , $\text{Nb}/\text{Y} = 0.44$ to 0.36 ; feldspar porphyry, $\text{Zr}/\text{TiO}_2 = 0.023$ to 0.017 , $\text{Ga}(\text{ppm}) = 19$ to 15 , $\text{Nb}/\text{Y} = 0.56$ to 0.40 ; quartz feldspar porphyry, $\text{Zr}/\text{TiO}_2 = 0.030$ to 0.020 , $\text{Ga}(\text{ppm}) = 23$ to 13 , $\text{Nb}/\text{Y} = 4.50$ to 0.25 ; quartz feldspar biotite porphyry, $\text{Zr}/\text{TiO}_2 = 0.032$ to 0.013 , $\text{Ga}(\text{ppm}) = 24$ to 16 , $\text{Nb}/\text{Y} = 1.50$ to 0.38 . Data for all analyzed elements, element-element ratios, detection limits, and calculated standard errors are presented in Table 3.

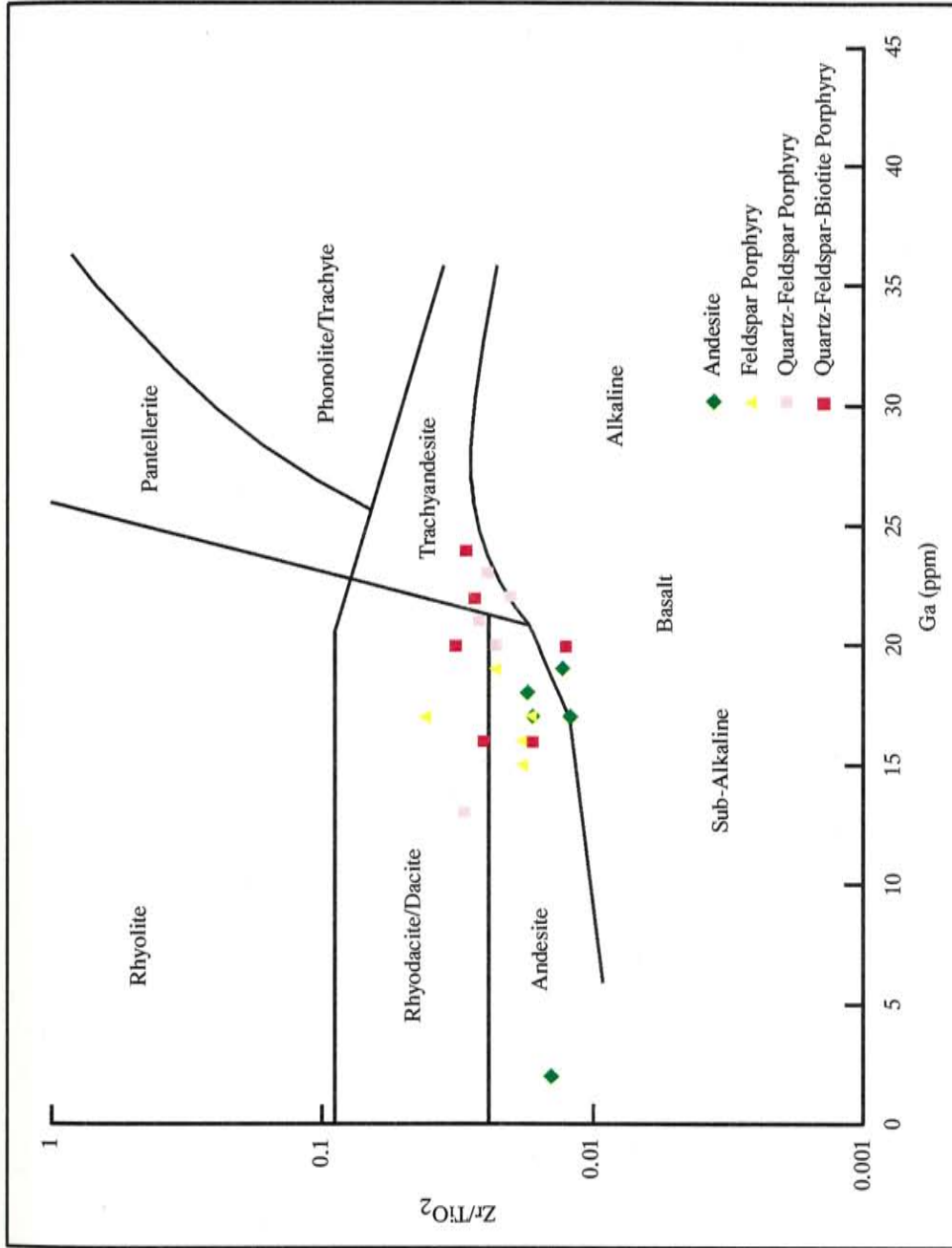


Figure 6.3: Zr/TiO₂ – Ga diagram showing the delimited fields for common volcanic rocks after Winchester and Floyd (1976). Andesite and Feldspar Porphyry generally plot within the andesite field, whereas, the Quartz-Feldspar and Quartz-Feldspar-Biotite Porphyries tend to plot within the Rhyodacite/Dacite-Trachyandesite fields.

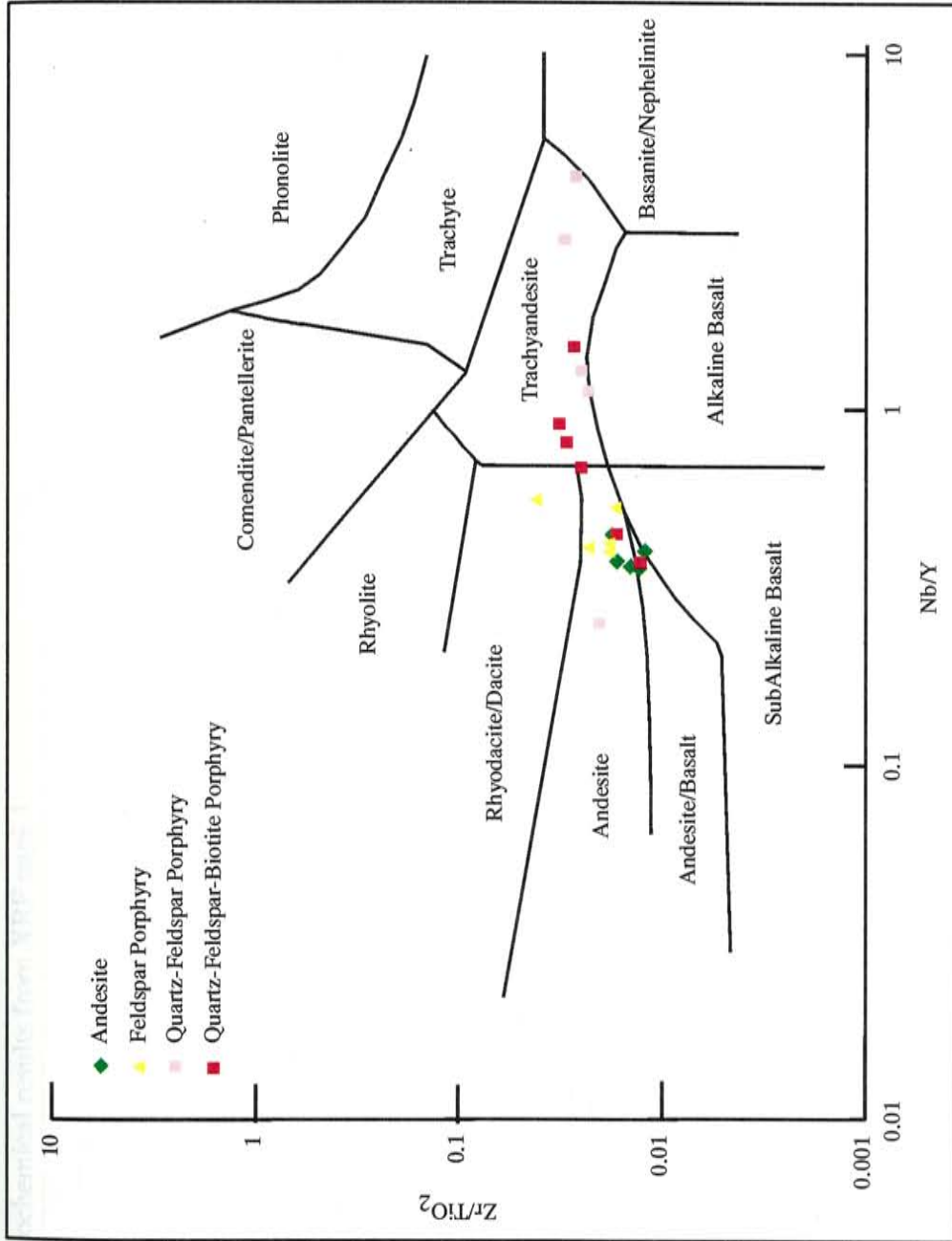


Figure 6.4: Zr/TiO₂ – Nb/Y diagram showing the delimited fields for common volcanic rocks after Winchester and Floyd (1976). Andesite and Feldspar Porphyry cluster within the Andesite field, whereas, Quartz-Feldspar and Quartz-Feldspar-Biotite Porphyries plot more within the Trachyandesite field.

Table 3: Lithochemical results from XRF page 1

Sample	Rock Type	TiO ₂	Fe ₂ O ₃ -I	MnO	V	Cr	Ni	Cu	Zn	Ga	As	Rb	Sr	Y	Zr	Nb	Ba	Mo	Pb	Th	U
02-04-201.40M	Andesite	0.69	3.76	0.03	139	116	19	4267	92	18	ND	37	86	23	121	10	207	10	6	4	4
03-09-142.60M	Andesite	0.86	4.56	0.03	236	88	21	2900	25	17	ND	98	318	20	105	8	312	41	4	ND	3
03-13-6.70M	Andesite	0.97	5.72	0.28	51	12	952	68	20	2	ND	83	437	25	139	9	514	6	7	ND	3
03-13-75.00M	Andesite	0.92	6.58	0.04	202	81	8	949	61	19	ND	85	360	22	120	8	302	6	5	3	2
03-14-73.80M	Andesite	0.76	3.64	0.02	186	93	10	6800	96	17	ND	73	199	24	127	9	516	30	8	ND	4
02-04-175.10M	F porphyry	0.38	1.63	0.02	88	46	8	746	49	17	ND	70	113	18	168	10	335	26	13	3	4
02-08-191.80M	F porphyry	0.71	5.80	0.03	147	96	19	2503	112	19	ND	54	340	22	164	9	334	12	38	3	4
02-08-245.80M	F porphyry	0.68	5.64	0.04	149	91	14	1300	66	17	ND	27	123	17	115	9	290	19	4	4	3
03-09-44.25M	F porphyry	0.73	3.20	0.03	124	149	9	8100	238	16	ND	35	212	19	134	8	259	62	5	ND	4
03-14-18.30M	F porphyry	0.66	2.38	0.02	183	64	11	1530	53	15	ND	28	211	20	121	8	186	15	4	ND	5
02-03-191.30M	QF porphyry	0.54	2.92	0.02	75	155	7	1520	54	22	ND	28	175	36	109	9	264	11	3	ND	3
02-03-217.10M	QF porphyry	0.49	3.00	0.02	70	205	11	2900	77	20	ND	19	245	8	111	9	277	14.5	6.5	ND	2
CC31-144.40M	QF porphyry	0.48	1.67	0.02	53	53	4	5300	26	21	3	12	351	2	127	9	232	10	13	5	2
CC32-193.40M	QF porphyry	0.51	3.51	0.02	109	200	8	11000	14	23	21	68	609	7	126	9	444	14	8	3	2
CC32-247.50M	QF porphyry	0.48	1.29	0.01	78	95	4	7000	4	13	13	17	233	3	144	9	164	13	9	3	2
99-01-212.10M	QFB porphyry	0.48	1.92	0.03	91	155	9	1800	78	16	ND	101	284	13	120	9	1010	217	25	4	4
CC31-192.00M	QFB porphyry	0.48	1.99	0.02	65	84	9	4400	80	22	ND	21	487	6	130	9	266	8	8	ND	3
99-T7-225.40M	QFB porphyry (?)	0.42	3.62	0.02	106	75	16	1700	85	24	3	75	318	11	123	9	634	8	9	4	6
99-T7-299.20M	QFB porphyry (?)	0.41	2.19	0.02	114	84	8	1013	21	20	7	79	96	13	131	12	580	9	3	4	5
99-01-180.20M	QFB porphyry (?)	0.73	4.07	0.04	128	87	7	999	56	16	ND	93	237	20	121	9	377	10	7	ND	4
99-01-227.20M	QFB porphyry (?)	0.84	9.43	0.04	132	61	25	1800	62	20	ND	142	275	24	106	9	611	24	6	ND	4
Quartz sand		0.04	0.38	0.01	21	227	8	13	14	2	ND	ND	2	4	94	4	33	17	2	ND	3

CHAPTER 7

DISCUSSION

Mineral Ratios

To examine the mineralogical changes from the supergene enrichment zone through the transition zone to the hypogene zone, sulfide mineral ratios are employed. Mineral ratios are a means of viewing the relative changes in the mineralogy of a sample using two or more minerals. This study used the following mineral ratios: py:cp, cc+cv:bn+cp, py:cc+cv, and cc:cv. There are two assumptions associated with the use of these mineral ratios: 1. all chalcocite and covellite is supergene in origin; and 2. all chalcopyrite and bornite is hypogene in origin. Although hypogene chalcocite and covellite and supergene chalcopyrite and bornite have been identified at Cerro Colorado, volumetrically the occurrence of these minerals is minor making these assumptions reasonable.

A brief discussion of each ratio is included below, but in general, these mineral ratios were selected to define and characterize the supergene enrichment, transition, and hypogene zones; and any mineralogical changes within each zone. The expected changes for each mineral ratio from the leached capping to the hypogene zone based on the general mineralogy of each zone are presented in Figure 7.1.

The preferential oxidation of chalcopyrite over pyrite is shown by the py:cp ratio. As the hypogene zone (typical ratio of ~0.5 to 5 at Cerro Colorado) becomes oxidized,

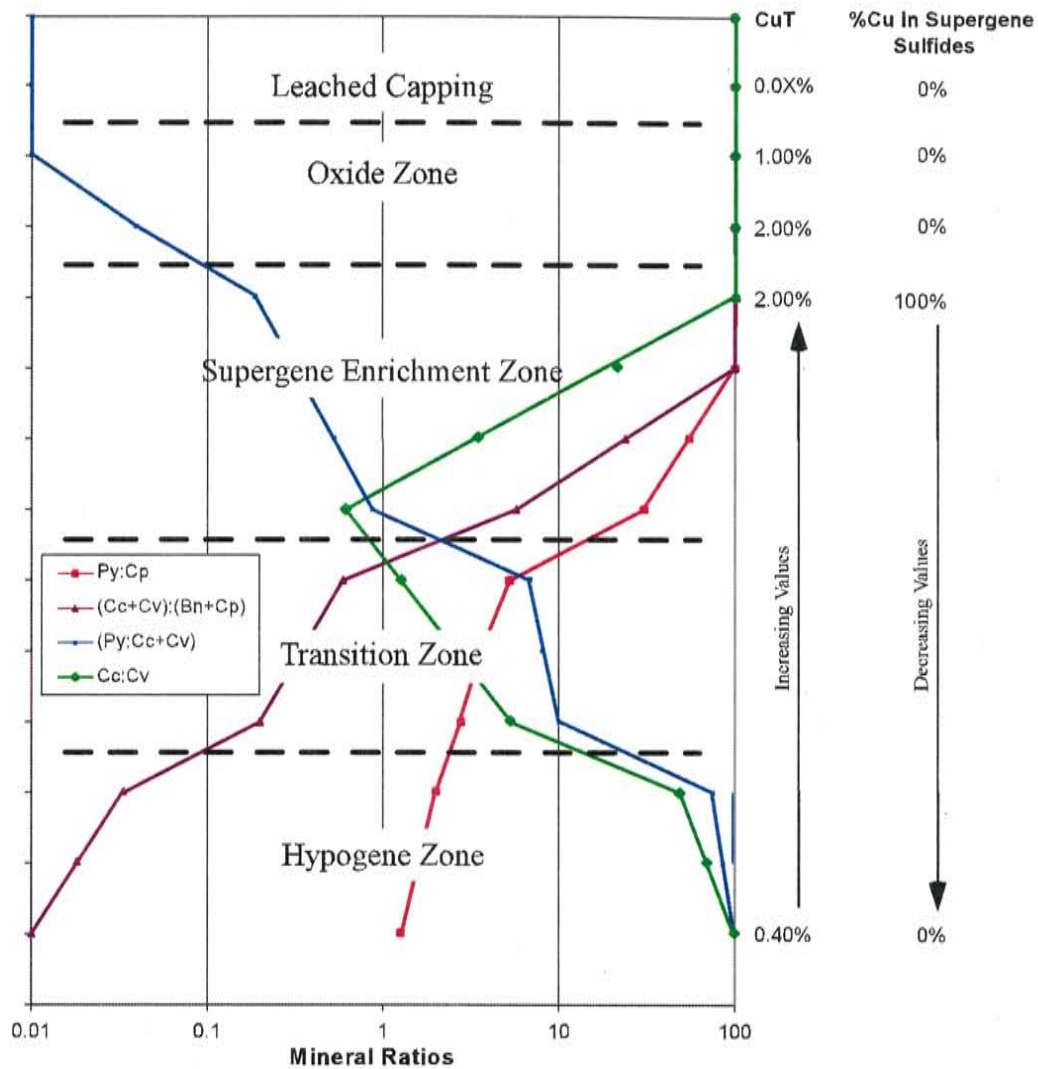


Figure 7.1: A hypothetical mineral ratio diagram illustrating the change in copper values assuming a 0.40% Cu protore grade, the change in percent copper in supergene sulfides, and the generalized mineralogical changes between and with in each mineral zone from the leached capping to the hypogene zone based on the general mineralogy of each zone as observed in numerous weathered porphyry systems.

chalcopyrite is preferentially replaced by chalcocite and/or covellite (Anderson, 1950; and Chavez, 2000). When this occurs the py:cp ratio will increase, relative to hypogene ratios, as the replacement of chalcopyrite goes to completion.

The cc+cv:cp+bn ratio tracks the change from the supergene enrichment zone to the hypogene zone. Hypogene chalcopyrite-bornite mineralization will have a low ratio (~0.01). As this mineralization becomes enriched in copper, chalcopyrite and bornite are replaced by chalcocite and/or covellite and the ratio increases. If this replacement continues to completion only chalcocite and covellite will remain and the ratio will approach infinity.

The py:cc+cv ratio tracks the replacement of pyrite by chalcocite and covellite. Pyrite enrichment generally occurs after chalcopyrite and bornite have been replaced by chalcocite and covellite (Chavez, 2000). This typically only occurs in the well-developed portions of the enrichment profile, near and within the supergene enrichment zone. As the enrichment of pyrite goes to completion, the ratio will move to lower values (generally <1 in moderate to low py assemblages and <10 in a high py assemblage). In addition, the py:cc+cv ratio used in combination with the py:cp ratio can indicate high or low py assemblages.

Lastly the cc:cv ratio tracks the mineralogy of the enrichment species. In the lower parts of a well-developed supergene enrichment zone covellite will be the dominant copper sulfide species (ratios <1), whereas in the upper portions of a well-developed supergene enrichment zone chalcocite will be the dominant copper sulfide species (Flores, 1985).

As an example of how mineral ratios were interpreted, drill hole DDH-02-03 is discussed in more detail. This drill hole was selected because it illustrates many of the general mineral ratio trends observed in most drill holes. In general two types of changes were observed in the mineral ratio data, order of magnitude shifts and small less than an order of magnitude shifts. These shifts in the mineral ratio data represent relative changes between 10 m composite samples in a particular drill hole.

In drill hole DDH-02-03 the top sample (2380 m level) was collected from the base of the supergene enrichment zone based on drill core logs and sampled to the end of the hole (Figure 7.2). Three order-of-magnitude shifts in the mineral ratios were identified between samples. The first was from the 2380 to the 2370 m level where there is an order of magnitude decrease in the py:cp, cc:cv, and cc+cv:cp+bn ratios. The second was from the 2370 to the 2360 m level where there is an order of magnitude decrease in the cc+cv:cp+bn ratio. The third was from the 2350 m level to the 2340 m level where there is a two order of magnitude decrease in the cc+cv:cp+bn ratio and an order of magnitude increase in the py:cc+cv ratio.

The first mineral ratio shift between the 2380 m and 2370 m levels is interpreted to represent the change from the upper chalcocite-rich member of the supergene enrichment zone to the lower covellite-rich member of the supergene enrichment zone. These mineralogical changes are shown in photomicrographs (a) and (b) Figure 7.2. The second shift in the mineral ratios is between the 2370 m and 2360 m levels and is interpreted to represent the change from the base of the supergene enrichment zone to the top of the transition zone. Mineralogic changes between these zones can be seen in photomicrographs (b) and (c) Figure 7.2. The third shift in the mineral ratios between the

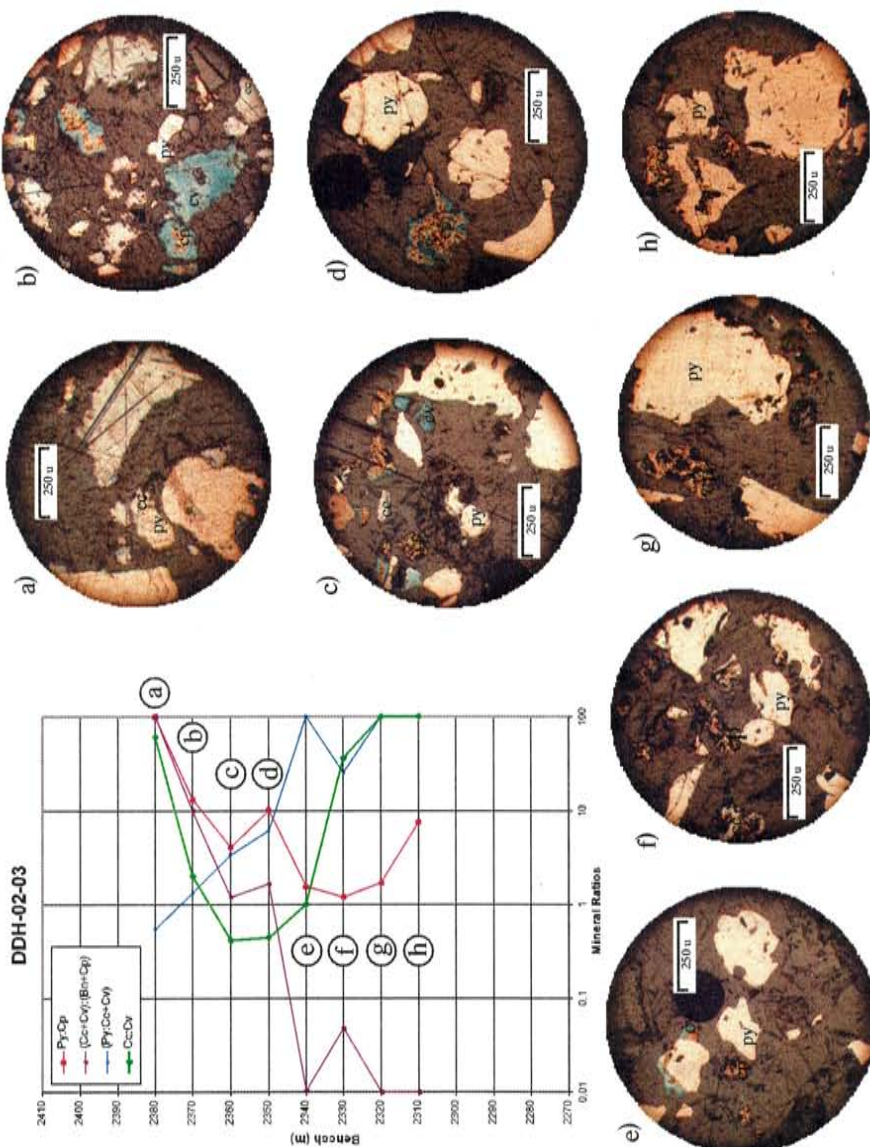


Figure 7.2: A mineral ratio diagram of drill hole DDH-02-03 and representative photo micrographs of each ten-meter composite sample. Note that samples corresponding to photo micrographs a and b are dominated by supergene sulfides, whereas the samples corresponding to photo micrographs e through h are dominated by hypogene sulfides, in addition, the samples corresponding to photomicrographs c and d are composed of a mixed supergene/hypogene mineral assemblage.

2350 m and 2340 m levels and is interpreted as the change from the base of the transition zone to the top of the hypogene zone. This mineralogic change is illustrated in photomicrographs (d) and (e) Figure 7.2.

There are also smaller shifts in the mineral ratio data. In drill hole DDH-02-03 these changes occur between the 2360 m and 2350 m levels and from the 2340 m to the 2310 m level. From the 2360 m to the 2350 m level there are small increases in the py:cc+cv and py:cp ratios; the cc+cv:cp+bn and the cc:cv ratios remain relatively unchanged. From the 2340 m to the 2330 m level there is a moderate increase in the cc+cv:cp+bn ratio, a large order of magnitude increase in the cc:cv ratio, and a moderate decrease in the py:cc+cv ratio; the py:cp ratio remains relatively unchanged. From the 2330 m to the 2320 m level there is a moderate increase in the py:cc+cv ratio, a moderate decrease in the cc+cv:cp+bn ratio, and a small increase in the cc:cv ratio; again the py:cp ratio remains relatively unchanged. From the 2320 m to the 2310 m level there is only a moderate increase in the py:cp ratio, all other ratios remain relatively unchanged.

The small changes in the mineral ratios from the 2360 m to the 2350 m levels are interpreted to represent variations within the transition zone as illustrated by photomicrographs (c) and (d) Figure 7.2. The moderate changes in the cc+cv:cp+bn and py:cc+cv ratios from the 2340m to the 2320 m level are interpreted to represent a zone of minor enrichment within the hypogene zone. These mineralogical changes are illustrated by photomicrographs (e), (f), and (g) Figure 7.2. The large increase in the py:cp ratio from the 2320 m to the 2310 m level is interpreted to represent a change in the mineralogic character of the hypogene zone from a pyrite-chalcopyrite mineral

assemblage to a pyrite-(chalcopyrite) mineral assemblage. This is illustrated in photomicrographs (g) and (h) Figure 7.2.

Large, order of magnitude changes in the mineral ratios were observed in each drill hole. In ten of fourteen drill holes an order of magnitude change in the $cc+cv:cp+bn$ ratio occurred between samples that had a ratio >2 and samples that had a ratio <1.2 . Based on this consistent pattern in the data, a change in $cc+cv:cp+bn$ ratios from greater than 2 to those that are less than 2 are interpreted to represent the upper boundary of the transition zone. In nine of fourteen drill holes another order of magnitude change occurred in the $cc+cv:cp+bn$ ratio between samples that had a ratio >0.11 and samples that had a ratio of <0.07 . Based on this consistent pattern in the data, a change in $cc+cv:cp+bn$ ratios from greater than 0.10 to those that are less than 0.10 are interpreted to represent the lower boundary of the transition zone.

In some drill holes large changes in mineral ratios such as those previously discussed are not always observed. In these cases, to ensure the same cutoff was applied for each mineral zone, the percent copper in supergene sulfides was calculated. The percent copper in supergene sulfides cutoff values were determined by identifying those values that correspond to the 2.0 and 0.1 cutoffs defined by the $cc+cv:cp+bn$ ratio, and can also be used to define the upper and lower boundaries of the transition zone. The percent copper in supergene sulfides cutoff values used for each zone are: supergene enrichment zone 100% to $\geq 80\%$; transition zone 79% to $\geq 15\%$; and hypogene zone $<14\%$. Drill holes interpreted using these cutoffs are presented in Appendix B.

Ore Zone Character

Supergene Enrichment Zone

The supergene enrichment zone at Cerro Colorado comprises a zone extending ~3 km east-west and ~1.5 km north-south. Stratigraphically, the enrichment zone resides between the leached capping or oxide zone and the transition zone (Figure 7.3), and varies from ~10-meters thick in the west zone (Figure 7.4) to a maximum of ~130-meters thick in the central zone (Figure 7.5). Copper grades range from ~0.30% to >3.00% Cu, but overall samples examined for this study have a mean grade of 1.08% Cu.

The supergene enrichment zone is characterized qualitatively by the variable but generally widespread replacement of pyrite by chalcocite and/or covellite, the complete to almost complete replacement of chalcopyrite by chalcocite and/or covellite, and typically by the absence of bornite (Figures 7.6 through 7.8). The supergene enrichment zone is defined quantitatively as the volume of rock having a $cc+cv/bn+cp$ ratio ≥ 2 and/or having $\geq 80\%$ of the copper contained in chalcocite + covellite.

Two mineralogic changes are observed within the enrichment zone. The first is an increase in covellite relative to chalcocite from the top to the base of the enrichment zone. This increase in covellite relative to chalcocite is best illustrated in drill holes RC-CC160 (Figure 7.9) and RC-F6-28 (Figure 7.5). The second mineralogic change is the overall increase of hypogene sulfides towards the base of the enrichment zone, as illustrated by drill holes RC-F6-28 (Figure 7.5) and RC-CC160 (Figure 7.9).

Transition Zone

The transition zone at Cerro Colorado comprises a continuous 10 to 60-meter thick zone that may have the same dimensions as the supergene enrichment zone

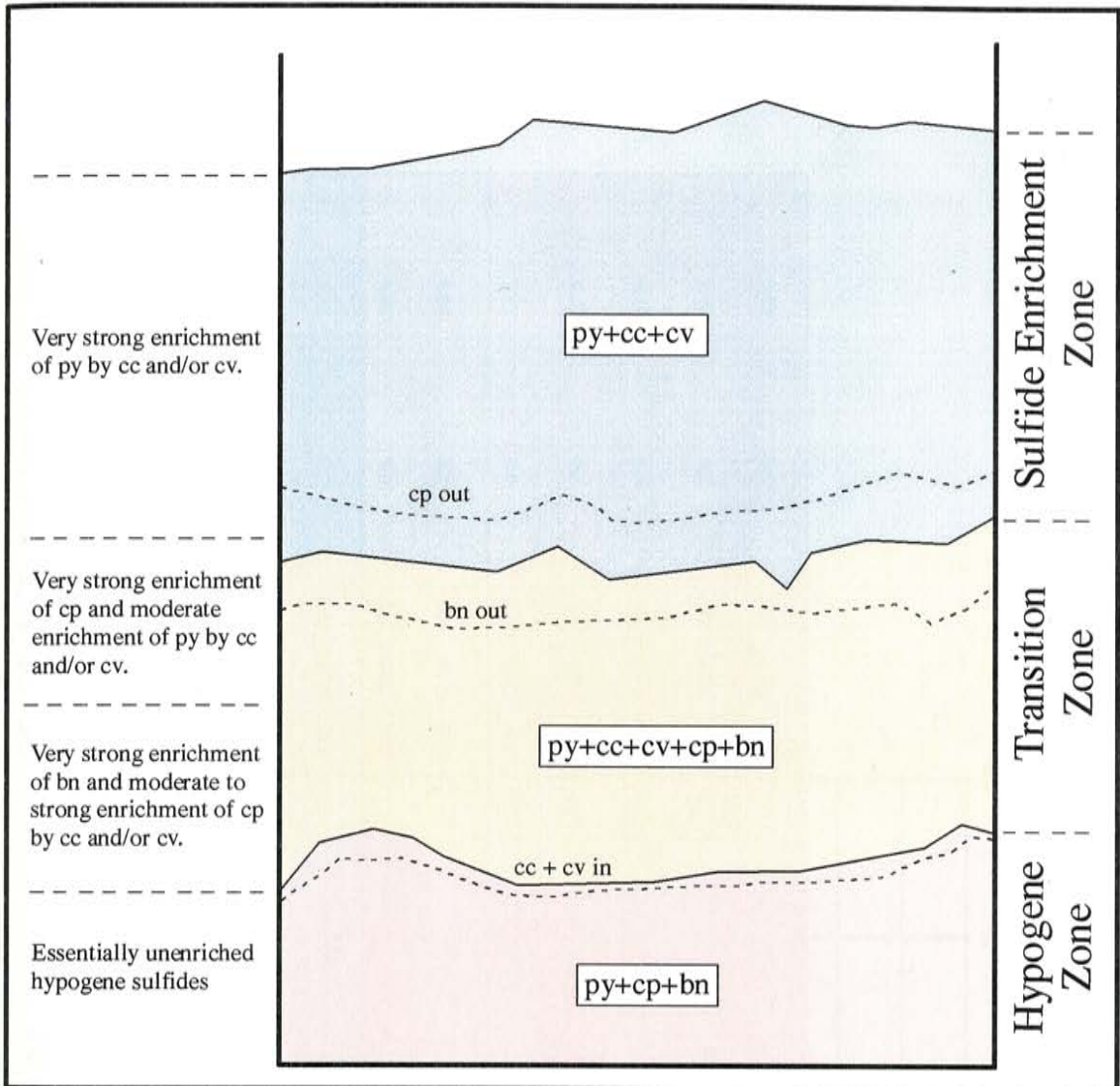


Figure 7.3: Generalized enrichment profile based on all qualitative and quantitative observations. The white boxes show the general sulfide mineral assemblages for each zone. The dashed lines mark the general location where selected copper sulfides appear or disappear from the system.

DDH-02-04

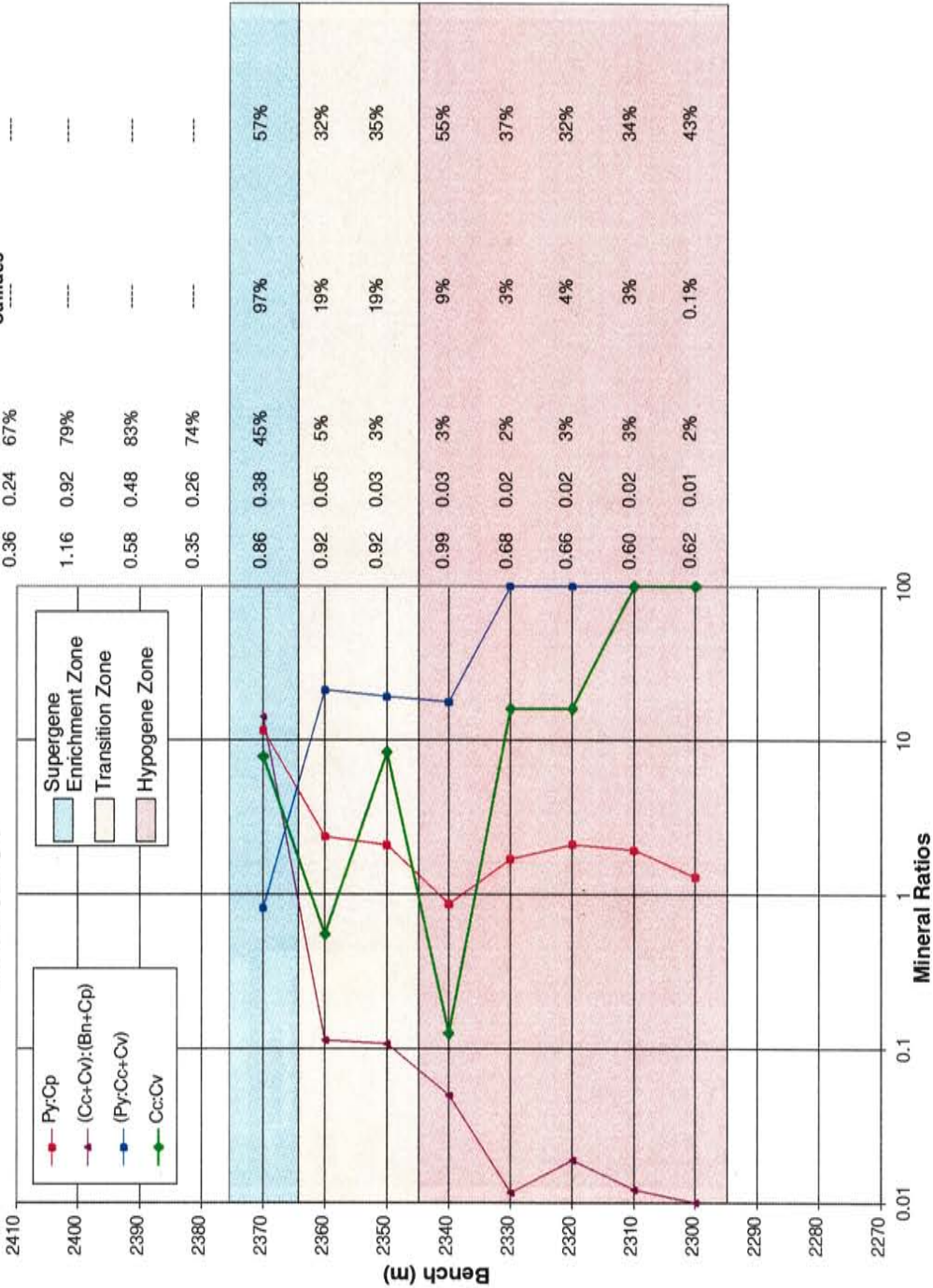


Figure 7.4: Mineral ratio diagram of drill hole DDH-02-04 illustrating the relationship of mineral ratios, relative percent copper sulfides, and percent copper in the supergene sulfide phase to the interpreted mineral zones.

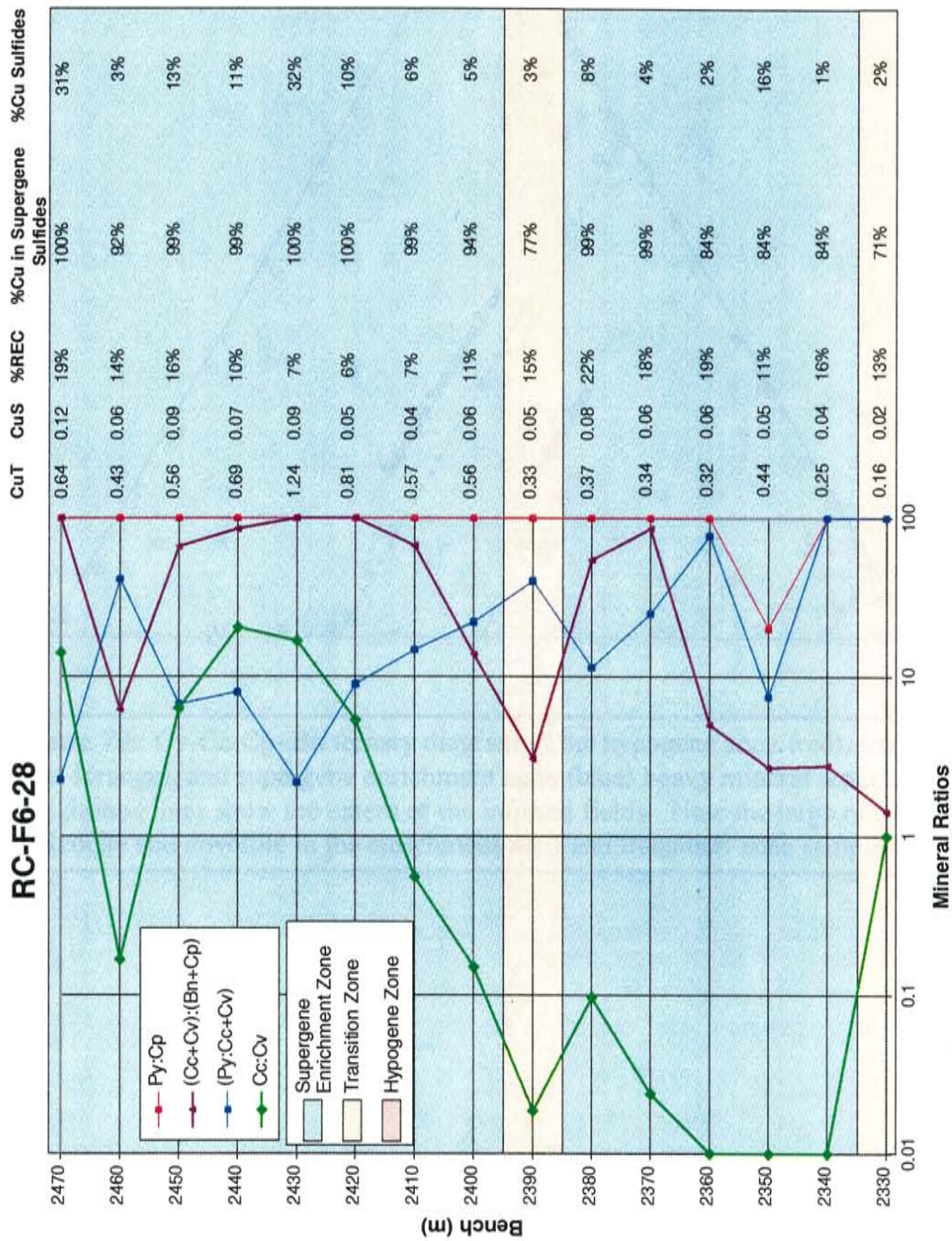


Figure 7.5: Mineral ratio diagram of drill hole RC-F6-28 illustrating the relationship of mineral ratios, relative percent copper sulfides, and percent copper in the supergene sulfide phase to the interpreted mineral zones.

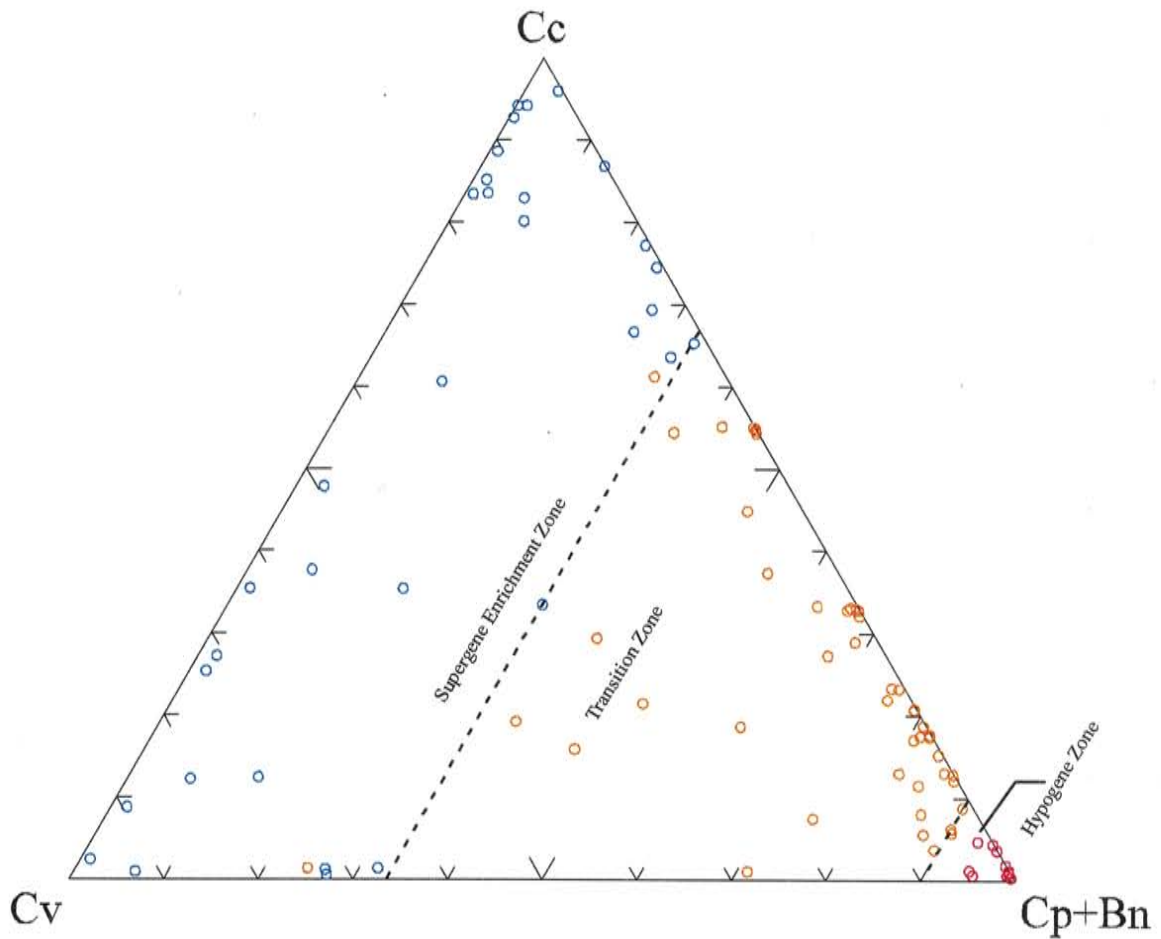


Figure 7.6: Cv-Cc-Cp+Bn ternary diagram of the hypogene zone (red), transition zone (orange), and supergene enrichment zone (blue) heavy mineral separate samples. The dashed lines show the extent of the inferred fields. Note the large range in chalcocite and covellite in the enrichment zone and transition zone samples.

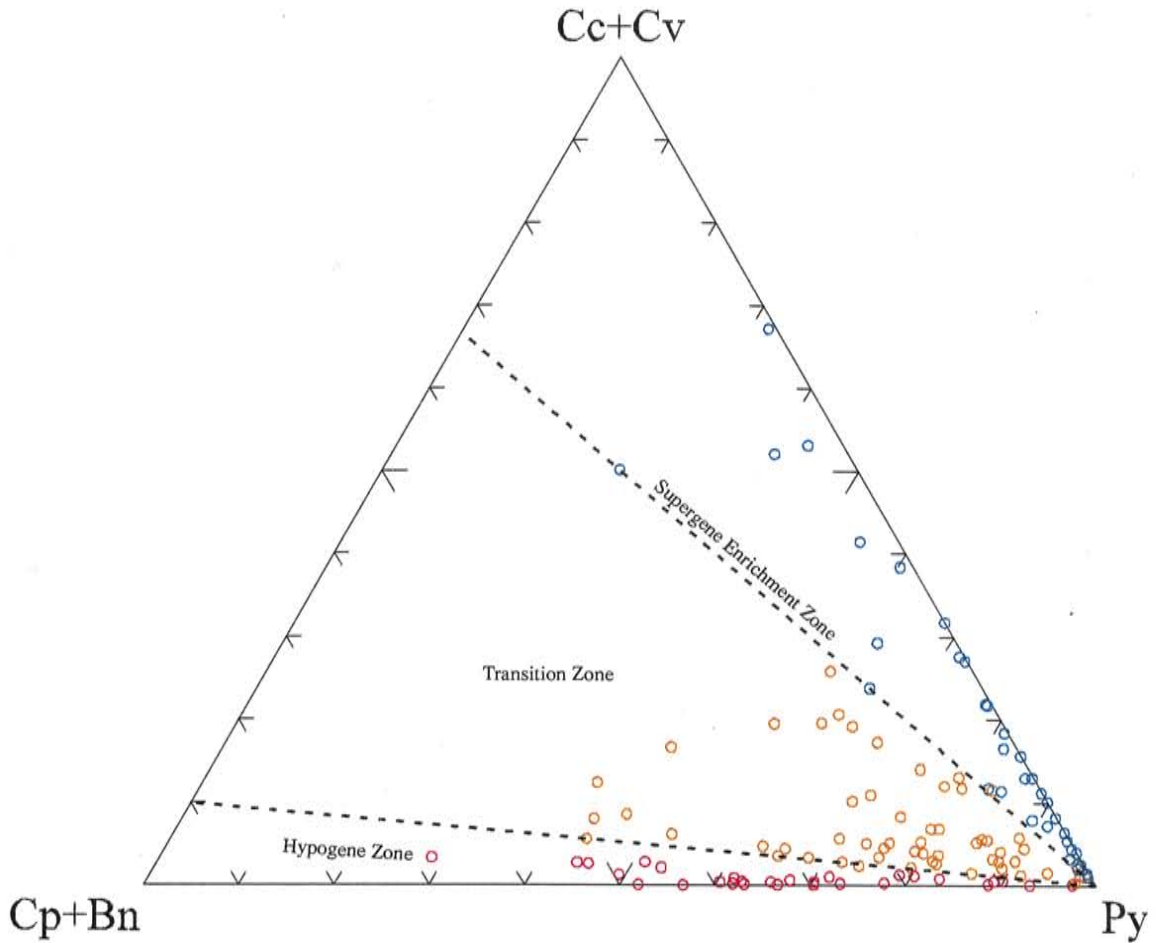


Figure 7.7: Cp+Bn-Cc+Cv-Py ternary diagram of the hypogene zone (red), transition zone (orange), and supergene enrichment zone (blue) heavy mineral separate samples. The dashed lines show the extent of the inferred fields. Note that although all three zones contain relatively high pyrite the supergene sulfide zone has the largest range of pyrite values, reflecting the enrichment of chalcopyrite, bornite, and pyrite by chalcocite and covellite.

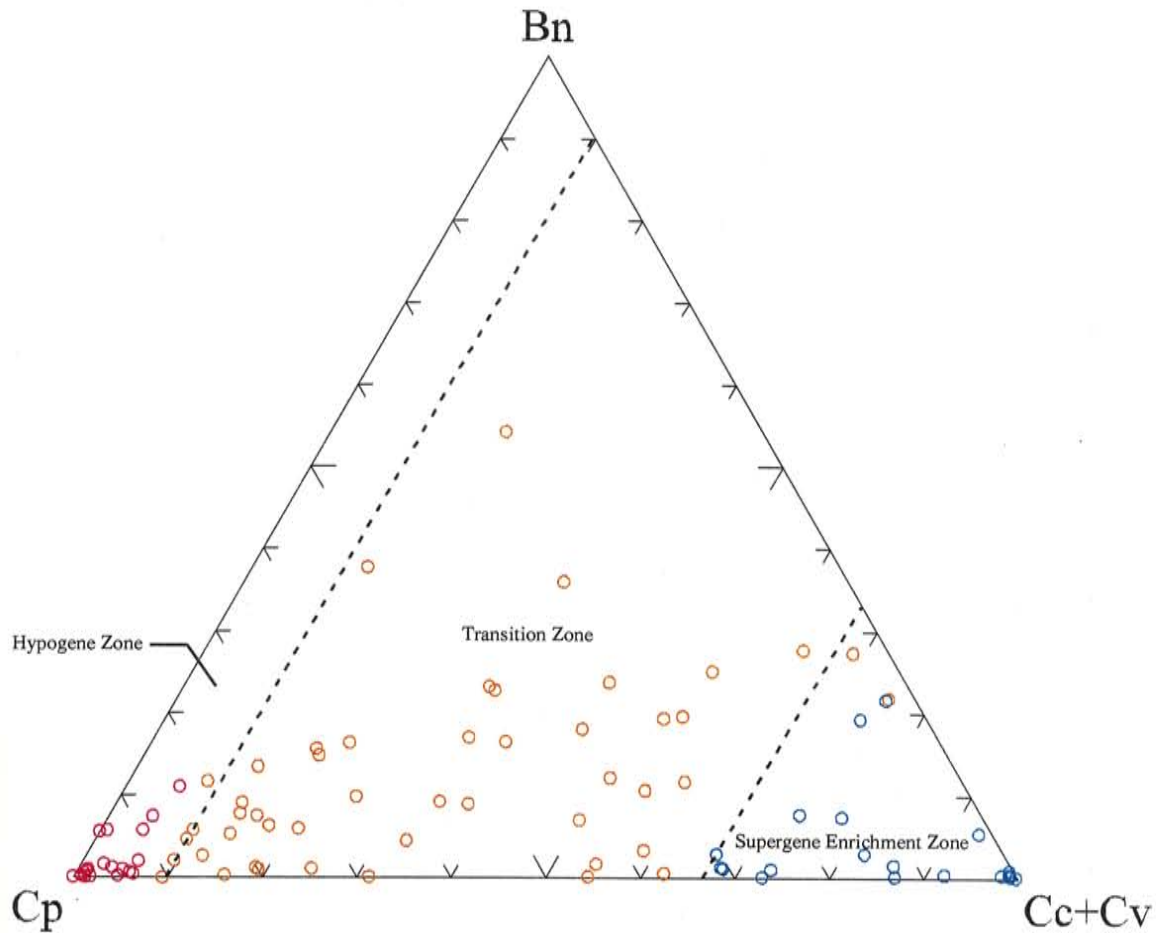


Figure 7.8: Cp-Bn-Cc+Cv ternary diagram of the hypogene zone (red), transition zone (orange), and supergene enrichment zone (blue) heavy mineral separate samples. The dashed lines show the extent of the inferred fields. Note the relatively low bornite content of the hypogene zone relative to the transition zone. Higher bornite in the transition zone is interpreted as reflecting originally higher bornite content of the hypogene mineralization.

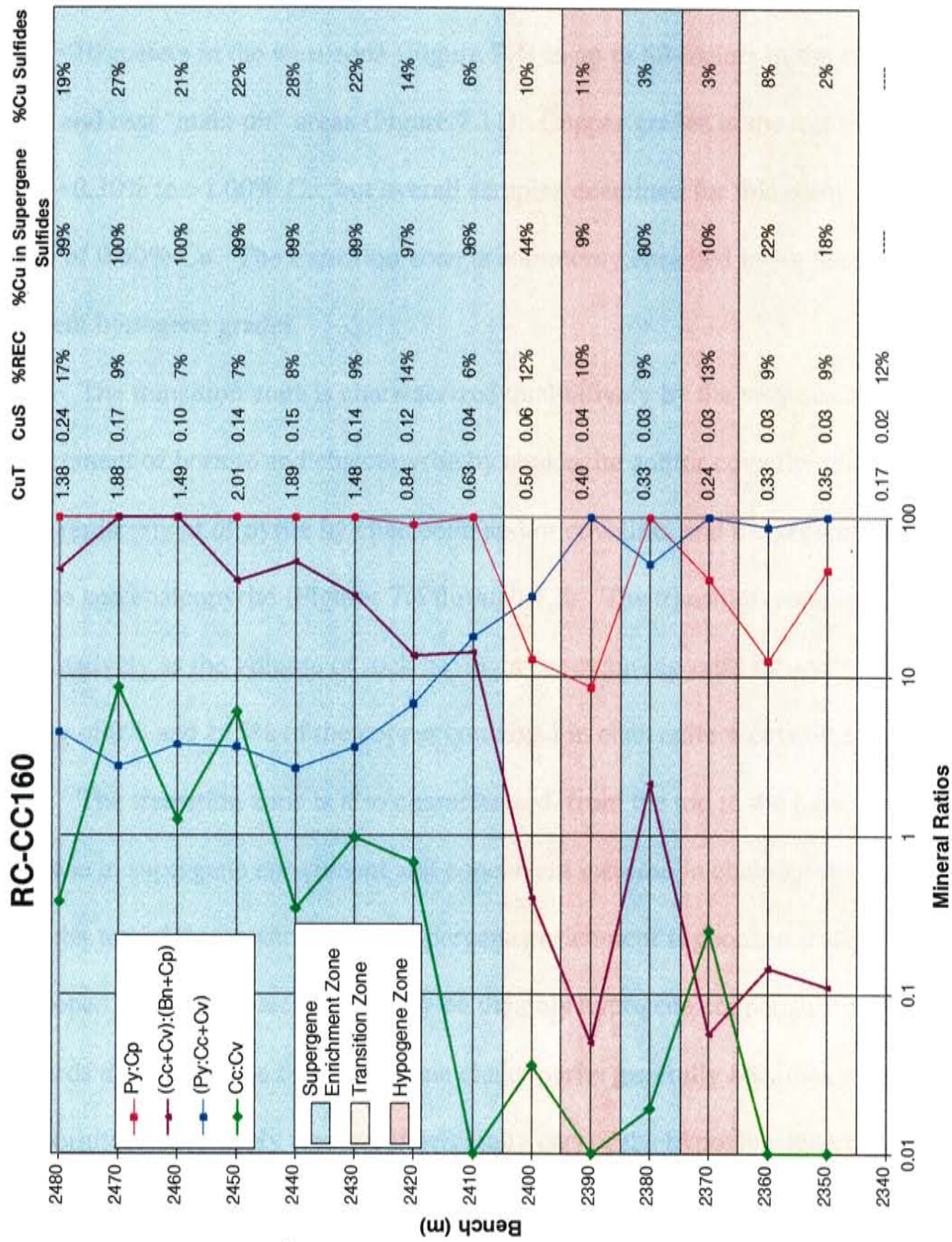


Figure 7.9: Mineral ratio diagram of drill hole RC-CC160 illustrating the relationship of mineral ratios, relative percent copper sulfides, and percent copper in the supergene sulfide phase to the interpreted mineral zones.

extending ~3 km east-west and ~1.5 km north-south. Stratigraphically, the transition zone resides between the supergene enrichment zone and the hypogene zone (Figure 7.3). The thickness of the transition zone based on samples examined during this study varies from ≤ 10 -meters in the west zone (Figure 7.4) to up to 60-meters in the central (Figure 7.10) and east “main pit” areas (Figure 7.11). Copper grades in the transition zone range from ~0.30% to >1.00% Cu, but overall samples examined for this study have a mean grade of 0.60% Cu. The transition zone is commonly enriched in copper relative to adjacent hypogene grades.

The transition zone is characterized qualitatively by the very strong to moderate replacement of bornite and chalcopyrite by chalcocite and/or covellite, the moderate to weak replacement of pyrite by chalcocite and/or covellite, and the presence of supergene bornite and chalcopyrite (Figures 7.6 through 7.8). The transition zone is defined quantitatively as the volume of rock having a $cc+cv:bn+cp$ ratio < 2 and ≥ 0.10 and/or having $< 80\%$ and $\geq 15\%$ of the copper contained in chalcocite + covellite.

The transition zone is also characterized, from the top to the base, by an overall decrease in supergene enrichment and concurrent increase in chalcopyrite and bornite. Near the top of the transition zone supergene enrichment is geochemically well-developed such that chalcopyrite may be the only hypogene copper sulfide present. Towards the base of the transition zone chalcopyrite generally becomes more abundant and bornite is commonly present, if originally part of the hypogene assemblage (Figure 7.3).

RC-02-24

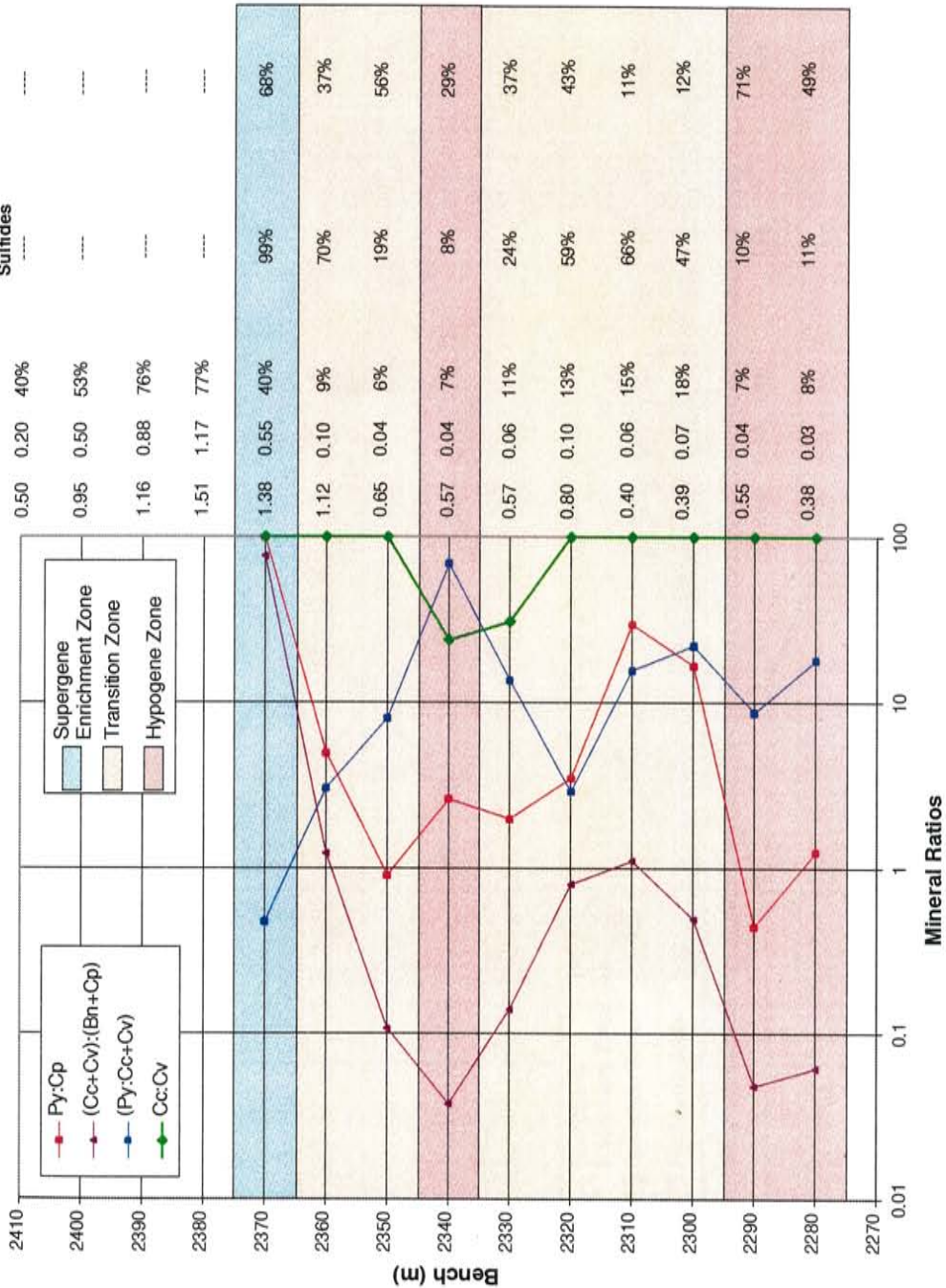


Figure 7.10: Mineral ratio diagram of drill hole RC-02-24 illustrating the relationship of mineral ratios, relative percent copper sulfides, and percent copper in the supergene sulfide phase to the interpreted mineral zones.

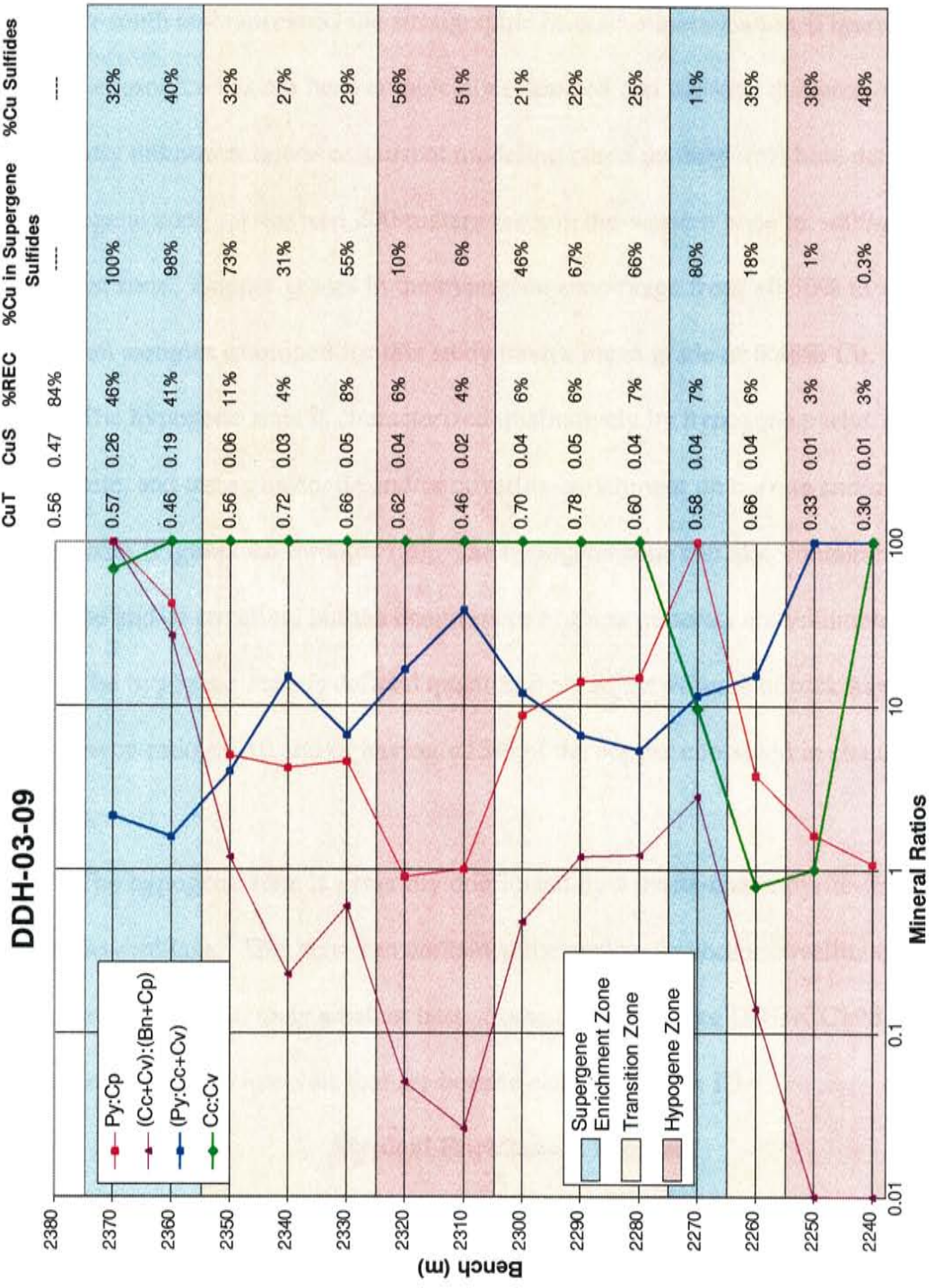


Figure 7.11: Mineral ratio diagram of drill hole DDH-03-09 illustrating the relationship of mineral ratios, relative percent copper sulfides, and percent copper in the supergene sulfide phase to the interpreted mineral zones.

Hypogene Zone

The hypogene zone at Cerro Colorado comprises a zone >3 km east-west and >2 km north-south and represents the stratigraphic base of mineralization (Figure 7.3). The hypogene resource has not been completely evaluated and the total thickness of this zone is currently unknown; however, current modeling based on deep drill hole data show that the hypogene zone varies from 200-meters thick in the western zone to ~400-meters thick in the east zone. Copper grades in the hypogene zone range from ~0.30% to >1.00% Cu, but overall samples examined for this study have a mean grade of 0.48% Cu.

The hypogene zone is characterized qualitatively by hypogene pyrite, chalcopyrite and bornite, and trace chalcocite and/or covellite enrichment on bornite and/or chalcopyrite (Figures 7.6 through 7.8). The hypogene zone can also contain hypogene chalcocite and/or covellite, but the occurrences of these minerals are volumetrically small. The hypogene zone is defined quantitatively as the volume of rock having a $cc+cv:bn+cp$ ratio <0.10 and/or having $<15\%$ of the copper contained in chalcocite + covellite.

The hypogene zone is generally dominated by a pyrite-chalcopyrite-(bornite) mineral assemblage. This zone can contain some chalcocite and/or covellite enrichment, but generally it is extremely weak at best. Some drill holes like DDH-CC198 have intersected hypogene intervals that are bornite-rich (Appendix D).

Atypical Enrichment Profiles

The generalized enrichment profile presented in Figure 7.3 is based on all of the qualitative and quantitative observations made during this study. However most drill holes from this study show some deviation from this generalized profile. Rather eight of

the fourteen drill holes contain abnormal profiles. One type of these profiles is where the supergene enrichment zone occurs within the transition and/or hypogene zones, and the other is where the transition zone occurs within the hypogene zone. In drill holes RC-CC160 (Figure 7.9), DDH-03-14 (Figure 7.14), and DDH-03-09 (Figure 7.11) a 10 to 20-meter thick enrichment zone occurs below the transition and/or hypogene zones and in drill holes DDH-02-08 (Figure 7.13), RC-02-24 (Figure 7.10), RC-F6-17 (Figure 7.14), and RC-CC160 (Figure 7.9) the transition zone is separated by 10 to 20-meters of hypogene mineralization.

In drill holes RC-CC160 (Figure 7.9), DDH-03-14 (Figure 7.12), and DDH-03-09 (Figure 7.11) the occurrence of these atypical enrichment zones are associated with a zone marked by an increase in the percent Cu in supergene sulfides to values near cutoff (80%) and by very high py:cp ratios (100). In these intervals the qualitative observations (Appendix C) show that the occurrence of these intervals are associated with zones containing little to no chalcopryite, abundant pyrite with weak chalcocite/covellite enrichment, and bornite that is almost completely replaced by chalcocite.

In drill holes DDH-02-08 (Figure 7.13), RC-02-24 (Figure 7.10), RC-F6-17 (Figure 7.14), and RC-CC160 (Figure 7.9) the occurrence of these atypical enrichment zones are associated with a zone marked by a decrease in the percent Cu in supergene sulfides to low values (2-13%) and by an increase in the py:cc+cv ratio from values around 30 to values generally greater than 80. In these intervals the qualitative observations (Appendix C) show that their occurrence is associated with an overall decrease in supergene enrichment.

DDH-03-14

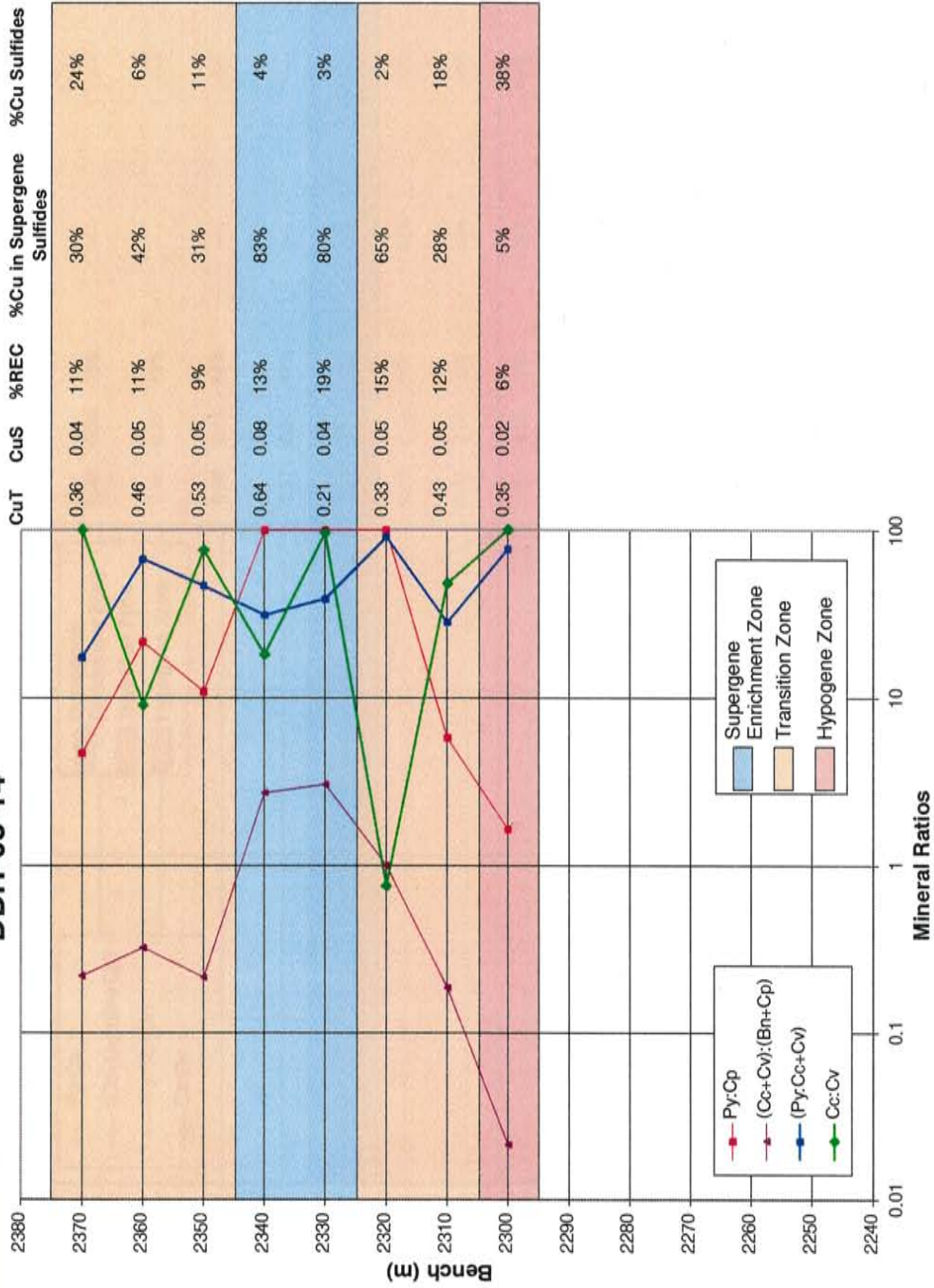


Figure 7.12: Mineral ratio diagram of drill hole DDH-03-14 illustrating the relationship of mineral ratios, relative percent copper sulfides, and percent copper in the supergene sulfide phase to the interpreted mineral zones.

DDH-02-08

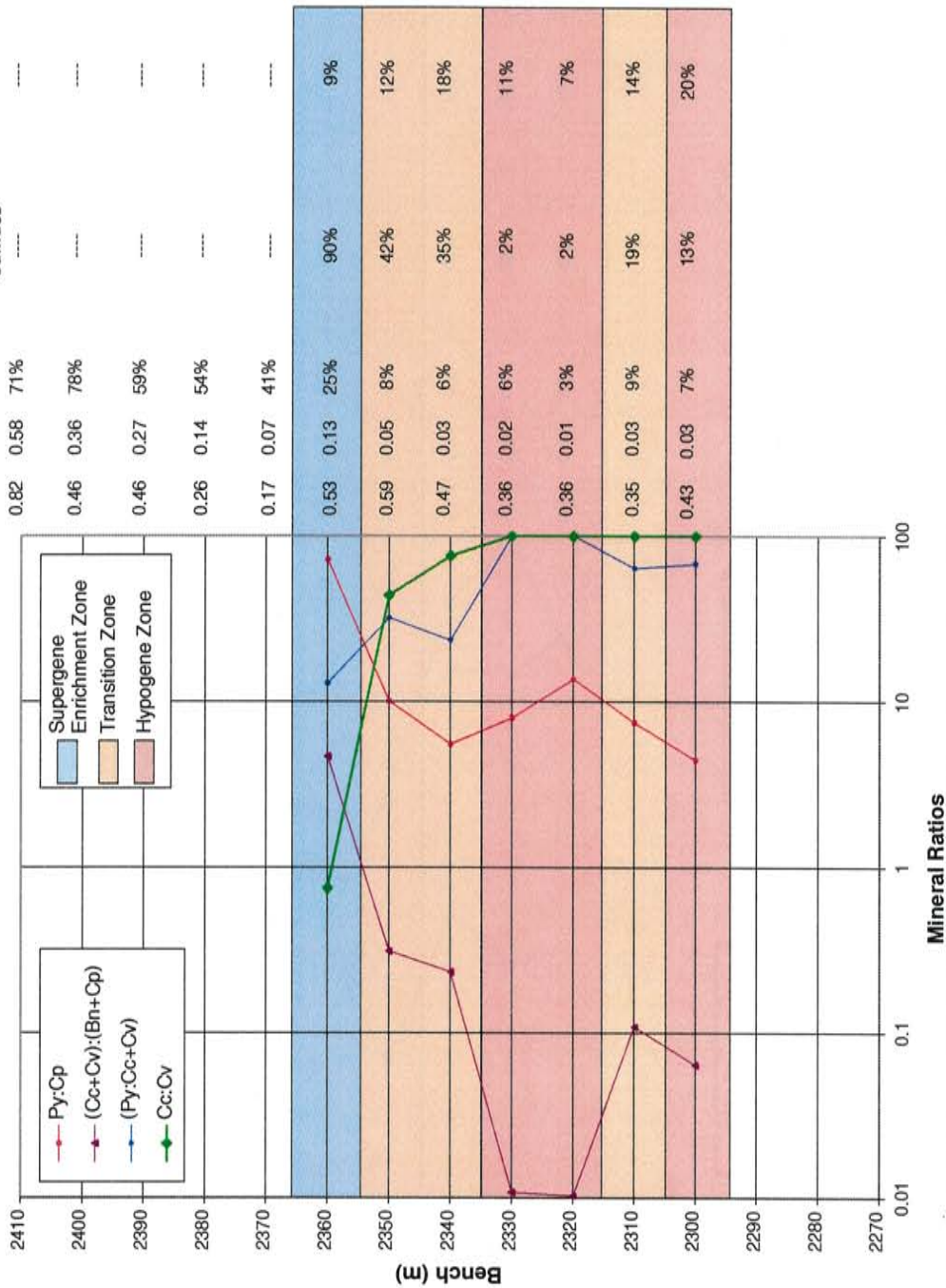


Figure 7.13: Mineral ratio diagram of drill hole DDH-02-08 illustrating the relationship of mineral ratios, relative percent copper sulfides, and percent copper in the supergene sulfide phase to the interpreted mineral zones.

RC-F6-17

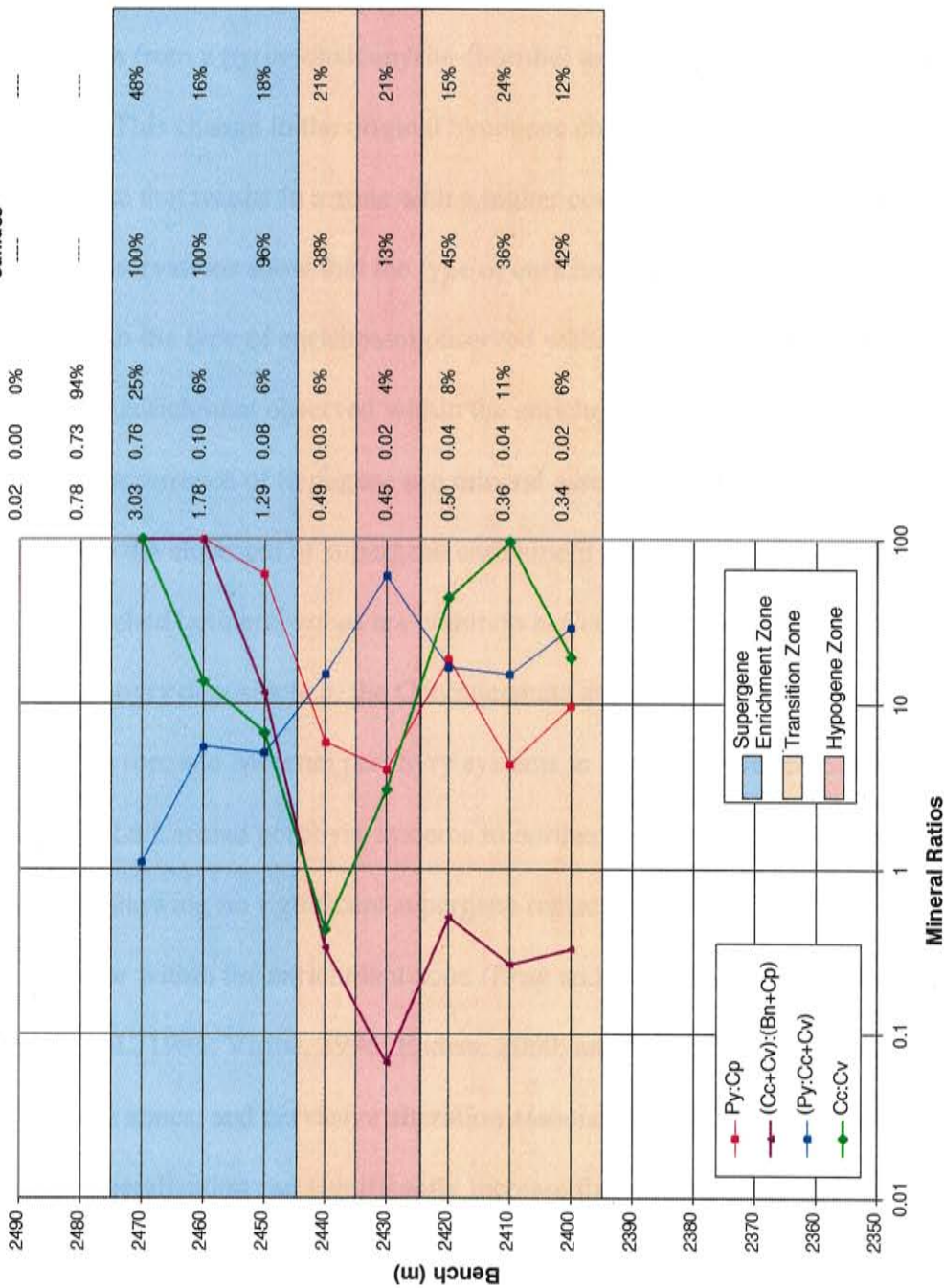


Figure 7.14: Mineral ratio diagram of drill hole RC-F6-17 illustrating the relationship of mineral ratios, relative percent copper sulfides, and percent copper in the supergene sulfide phase to the interpreted mineral zones.

The occurrence of the enrichment zone within the transition and/or hypogene zone is associated, not with an overall increase in enrichment of the interval as it may first appear, but rather, with a change in the character of the pre-enriched hypogene mineralization from a pyrite-chalcopyrite-(bornite) assemblage to a pyrite-bornite assemblage. This change in the original hypogene character leads to an overall decrease in chalcopyrite that results in a zone with a higher $cc+cv:cp+bn$ ratio. In addition, the qualitative observations show that the type of enrichment within these intervals is consistent with the type of enrichment observed within the transition zone and not typical of the type of enrichment observed within the enrichment zone.

The occurrence of hypogene ore mineral assemblages within the transition zone represents the development of supergene enrichment around a “perched” hypogene zone. Relict or “perched” mineral zones are common at Cerro Colorado as well as other enriched porphyry deposits (e.g. the Chuquicamata and Escondida deposits in Chile, the Santa Rita, Tyron, and Morenci porphyry systems in southwest United States, and the Cananea and La Caridad porphyry systems in northern Mexico), where the hypogene assemblages showing no significant supergene replacement may occur within the leached capping and/or within the enrichment zone (Rose and Baltosser, 1966; Ojeda, 1990; DuHamel et al., 1995; Virtue, 1996; Enders, 2000; and Garza et al., 2001). Veins, faults/fracture zones, and pervasive alteration associated with the development of hypogene mineralization can significantly increase the heterogeneity of mineralized rock volumes subject to weathering. Local increase in porosity and permeability, generally along veins and fractures, allows enriching fluids to “by-pass” volumes of rock with lower permeability permitting the development of “perched” mineral zones (Figure 7.15).

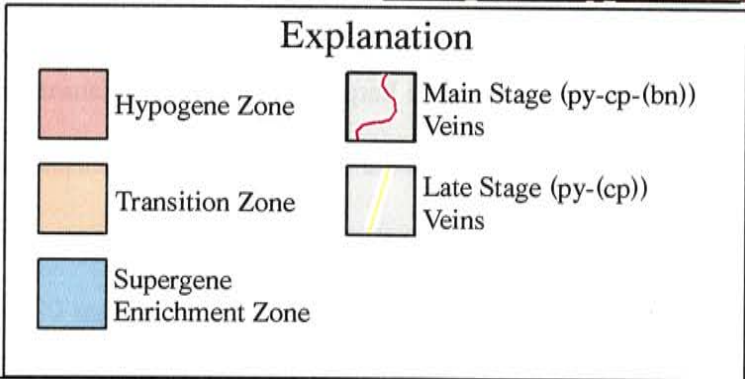


Figure 7.15: A generalized diagram illustrating the preferential supergene enrichment along zones with higher permeability. Note that the development of veins and fractures can locally increase the depth to which enrichment can develop causing an atypical profile as is visible by the hypothetical drill hole.

Wall-Rock Alteration and the Transition Zone

The transition zone forms as copper-rich low pH fluid interacts with hypogene sulfides resulting in the formation of supergene sulfides. The depth to which this zone can develop can be controlled by the porosity and permeability of the mineralized rock. Ultimately, this is a function of the degree to which alteration and mineralization, in the form of veins, have developed. The thickness of this zone can be controlled by the reactivity of the wall-rock where less-reactive alteration assemblages can permit the development of a thicker transition zone.

In drill holes DDH-02-03 (Figure 7.16), DDH-02-04 (Figure 7.17), and DDH-03-09 (Figure 7.18) the occurrence of the top of the transition zone/base of supergene enrichment zone is coincident with a change from quartz-sericite alteration to quartz-sericite-chlorite alteration. In drill hole DDH-02-11 (Figure 7.19) the base of the transition zone/top of the hypogene zone is coincident with a change from quartz-sericite alteration to quartz-sericite-chlorite alteration, and in drill holes DDH-02-08 (Figure 7.20) and DDH-03-14 (Figure 7.21) the base of the transition zone/top of the hypogene zone is also coincident with a change from quartz-sericite-chlorite alteration to biotite-rich potassic alteration.

Where the transition zone is developed in quartz-sericite alteration it is up to 60-meters thick as illustrated in drill holes RC-02-30 (Figure 7.22) and RC-02-21 (Figure 7.23). When the transition zone is developed within quartz-sericite-chlorite alteration it is generally 20 to 30-meters thick as seen in drill holes DDH-02-08 (Figure 7.20) and DDH-02-03 (Figure 7.16), and where the transition zone is developed within the biotite-

DDH-02-03

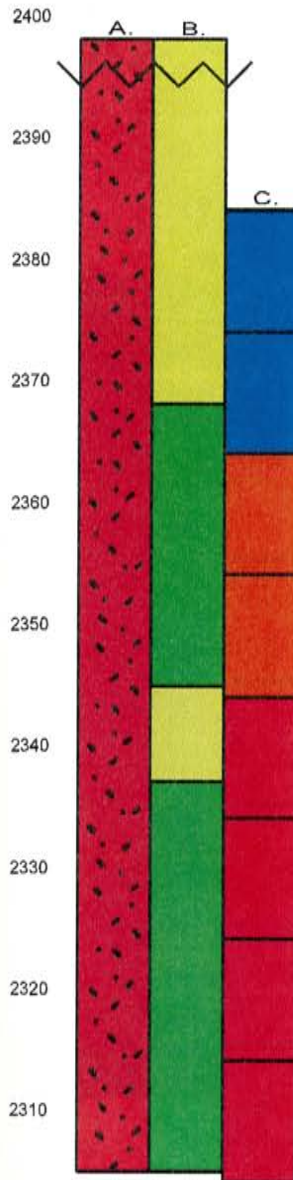


Figure 7.16: Drill hole column showing the relationship between lithology "A" (quartz-feldspar porphyry in red) and alteration "B" (quartz-sericite in yellow and quartz-sericite-chlorite in green) to the occurrence of the defined mineral zones "C" (supergene enrichment zone in blue, transition zone in orange, and the hypogene zone in red).

DDH-02-04

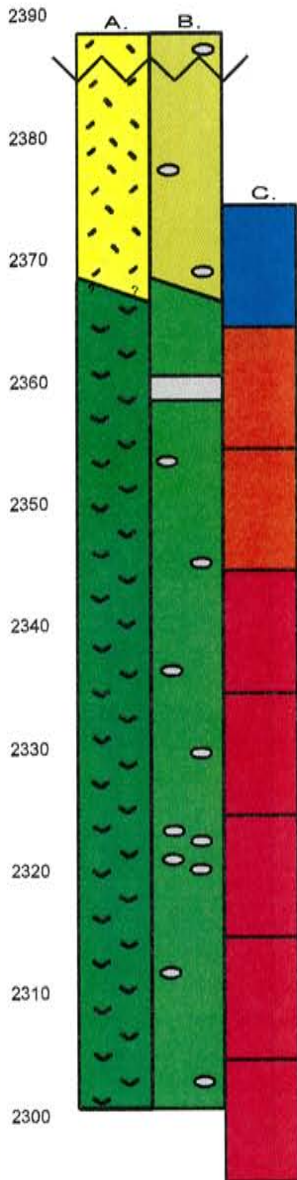


Figure 7.17: Drill hole column showing the relationship between lithology “A” (feldspar porphyry in yellow and the andesite in green) and alteration “B” (quartz-sericite in yellow, quartz-sericite-chlorite in green, and biotite-rich potassic in grey) to the occurrence of the defined mineral zones “C” (supergene enrichment zone in blue, transition zone in orange, and the hypogene zone in red).

DDH-03-09

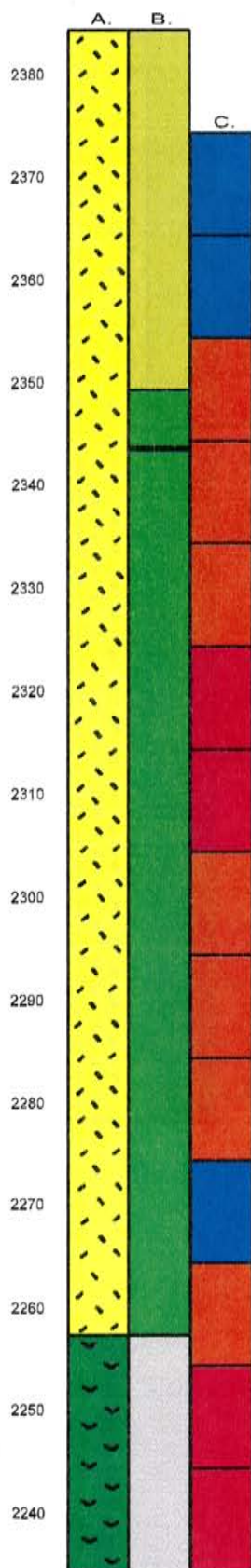


Figure 7.18: Drill hole column showing the relationship between lithology “A” (feldspar porphyry in yellow and the andesite in green) and alteration “B” (quartz-sericite in yellow, quartz-sericite-chlorite in green, and biotite-rich potassic in grey) to the occurrence of the defined mineral zones “C” (supergene enrichment zone in blue, transition zone in orange, and the hypogene zone in red).

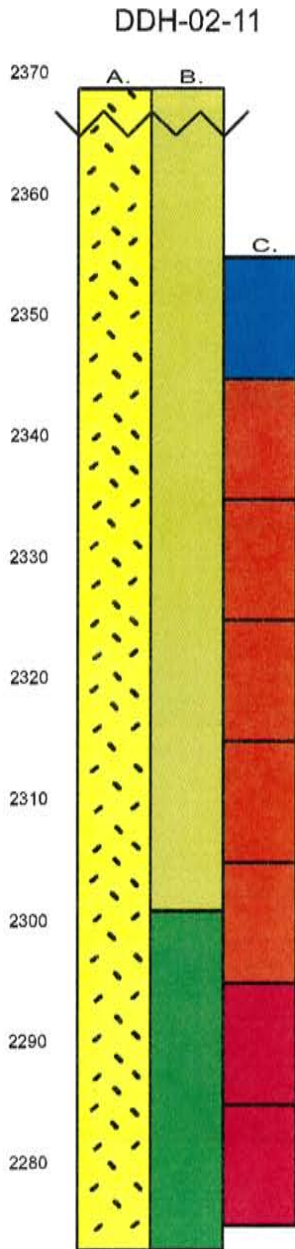


Figure 7.19: Drill hole column showing the relationship between lithology “A” (feldspar porphyry in yellow) and alteration “B” (quartz-sericite in yellow, quartz-sericite-chlorite in green, and biotite-rich potassic in grey) to the occurrence of the defined mineral zones “C” (supergene enrichment zone in blue, transition zone in orange, and the hypogene zone in red).

DDH-02-08

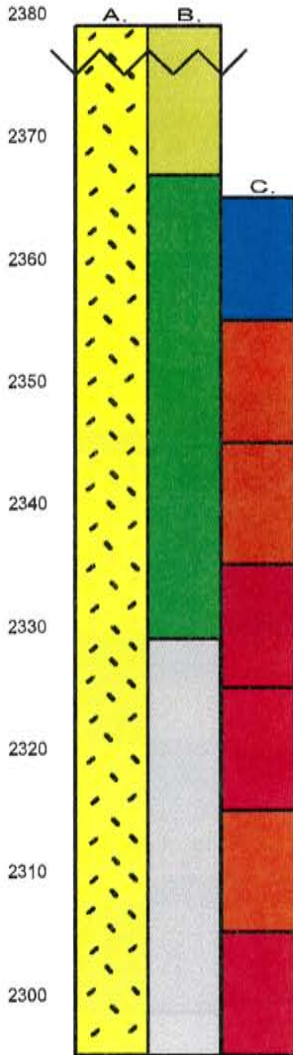


Figure 7.20: Drill hole column showing the relationship between lithology "A" (feldspar porphyry in yellow) and alteration "B" (quartz-sericite in yellow, quartz-sericite-chlorite in green, and biotite-rich potassic in grey) to the occurrence of the defined mineral zones "C" (supergene enrichment zone in blue, transition zone in orange, and the hypogene zone in red).

DDH-03-14

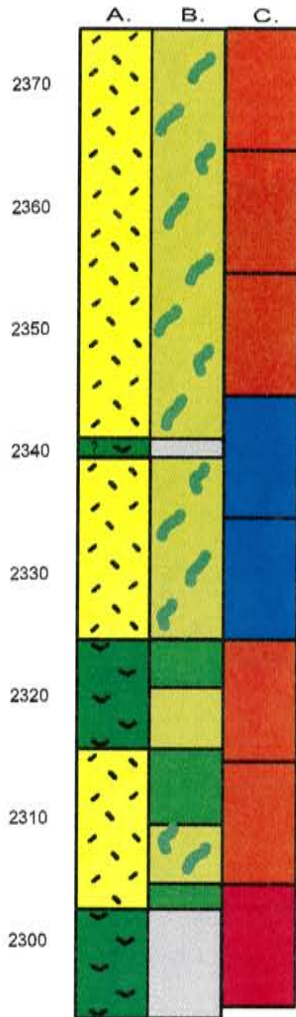


Figure 7.21: Drill hole column showing the relationship between lithology "A" (feldspar porphyry in yellow and the andesite in green) and alteration "B" (quartz-sericite in yellow, quartz-sericite-chlorite in green, and biotite-rich potassic in grey) to the occurrence of the defined mineral zones "C" (supergene enrichment zone in blue, transition zone in orange, and the hypogene zone in red).

RC-02-30

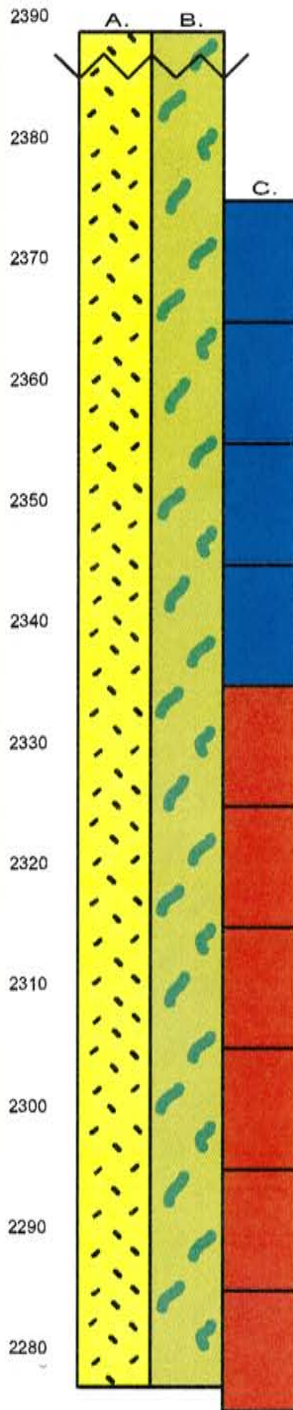


Figure 7.22: Drill hole column showing the relationship between lithology "A" (feldspar porphyry in yellow) and alteration "B" (quartz-sericite in yellow) to the occurrence of the defined mineral zones "C" (supergene enrichment zone in blue and the transition zone in orange).

RC-02-21

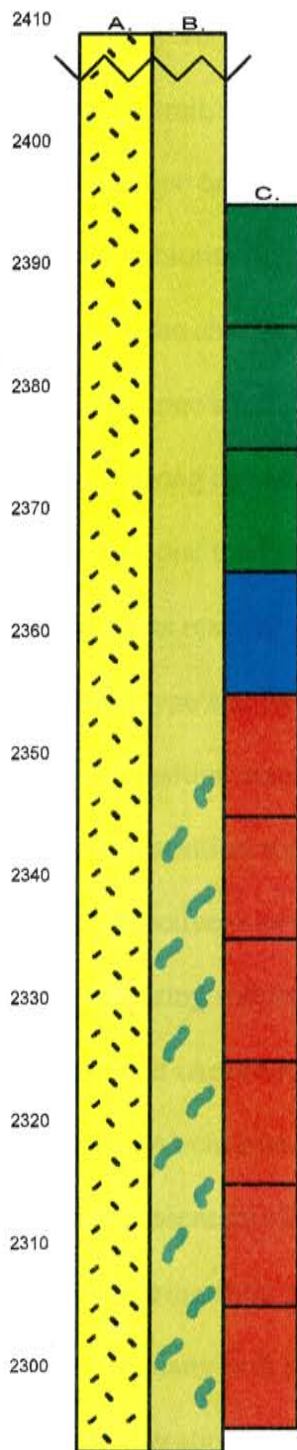


Figure 7.23: Drill hole column showing the relationship between lithology "A" (feldspar porphyry in yellow) and alteration "B" (quartz-sericite in yellow) to the occurrence of the defined mineral zones "C" (oxide zone in green, supergene enrichment zone in blue, and the transition zone in orange).

rich potassic zone, that only occurs in drill hole DDH-02-08 (Figure 7.20), the transition zone is only 10-meters thick.

Overall, these drill holes show a change from a less reactive alteration type to a more reactive one (e.g. quartz-sericite to quartz-sericite-chlorite and quartz-sericite-chlorite to biotite-rich potassic) correlating with a marked decrease in enrichment as is shown by the change in mineral zones from the supergene enrichment zone to the transition zone and/or from the transition zone to the hypogene zone. This data also shows a strong correlation between less reactive alteration types and an increase in transition zone thickness as the transition zone is much thicker where it is developed within a less reactive alteration assemblage. The coincident change in mineral zone and alteration type and the correlation between less reactive alteration assemblages and thicker transition zone development all point to wall-rock reactivity as the controlling factor in transition zone occurrence and development.

Reactive minerals like chlorite and biotite can neutralize acid, raising the pH of copper-bearing solutions. Hydrothermal chlorite and biotite at Cerro Colorado are very fine grained (Appendix D). This increases the potential reactive surface area of these minerals. As chlorite and biotite react with the enriching fluids they act to buffer the acid produced essentially by the oxidation of pyrite that decreases the effectiveness of the copper-bearing fluid to replace hypogene sulfides.

In many drill holes where the transition zone is developed within quartz-sericite-chlorite alteration there is a significant decrease in chlorite relative to the chlorite contained in the hypogene mineralization immediately down hole. In most cases the amount of chlorite is reduced to only trace quantities that results in the development of a

“pseudo” quartz-sericite alteration (Appendix E). Biotite-rich potassic alteration is well developed within the Main-Pit at Cerro Colorado. Very little enrichment occurs within this zone as copper grades in the oxide zone developed here are similar to hypogene ore grades. In this alteration chrysocolla is only developed within vein and vein halos associated with hypogene mineralization where biotite destruction has already taken place. The result of these reactions can also be seen on the deposit-scale where the occurrence of the quartz-sericite-chlorite alteration is coincident with the occurrence of the transition and hypogene zones, and the occurrence of the biotite-rich potassic alteration is coincident with the occurrence with the hypogene zone (Figures 7.24 through 7.26).

Ore Zone Stratigraphy: Margin to Center of Deposit

The ore zone stratigraphy at Cerro Colorado comprises the leached capping, oxide zone, supergene enrichment zone, transition zone, and hypogene zone. The oxide and supergene enrichment zones are much thicker and vertically developed in the east main-pit area, whereas these zones are relatively thin but laterally continuous in the western parts of the deposit (Figures 7.24 through 7.26). The increase in the oxide and supergene enrichment zone thickness is mirrored by the transition zone that also increases in thickness from the western margins of the deposit towards the east main-pit area. The ore zone stratigraphy along the western margins of the deposit, as illustrated by drill holes DDH-02-08 (Figure 7.20), DDH-02-03 (Figure 7.16), and DDH-02-04 (Figure 7.17), is relatively simple where a 10 to 20-meter thick enrichment zone grades into a 20-meter thick transition zone and finally into hypogene ore. The ore zone stratigraphy along the west-central part of the deposit, as illustrated by drill holes DDH-02-11 (Figure 7.19),

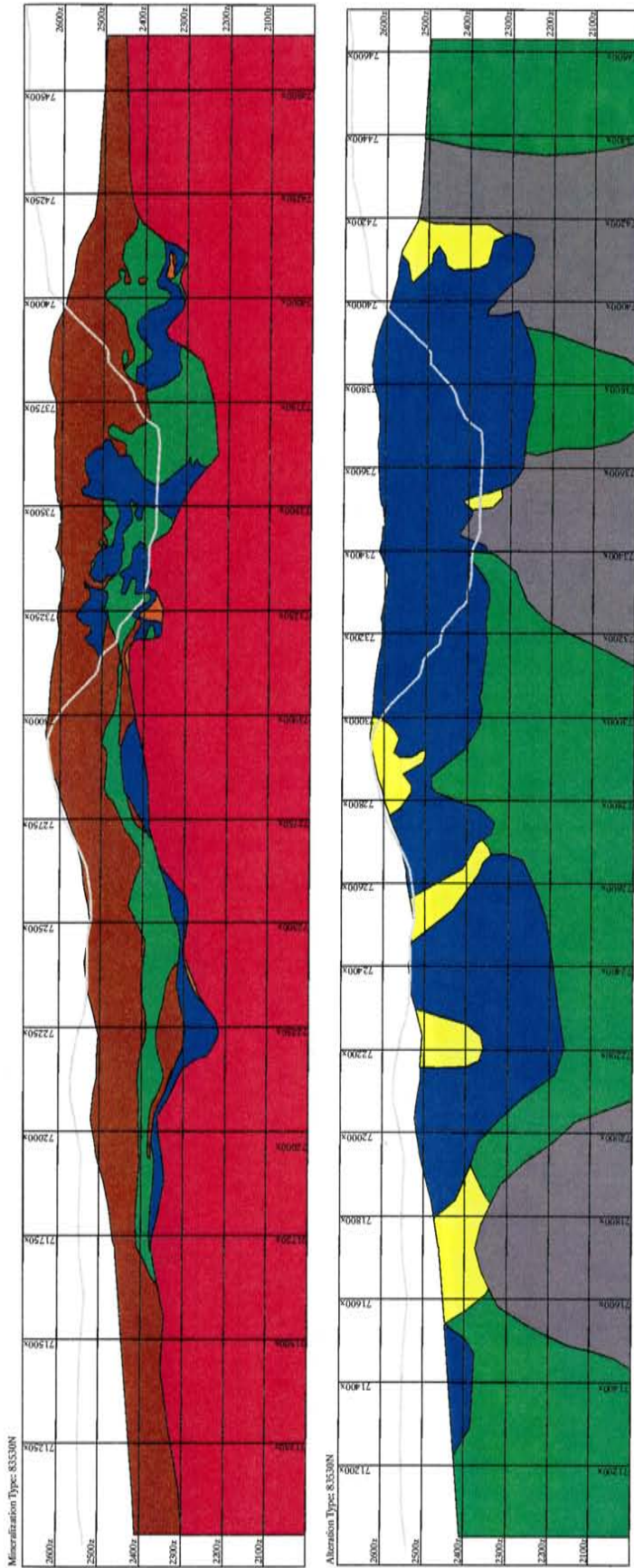


Figure 7.24: An east-west cross-section across the northern part of the Cerro Colorado deposit showing the distribution of mineralization (top) and alteration (bottom) types. Note that the qtz-ser-chl (green) and bio-rich potassic (grey) alteration assemblages define the lower boundary of supergene enrichment.

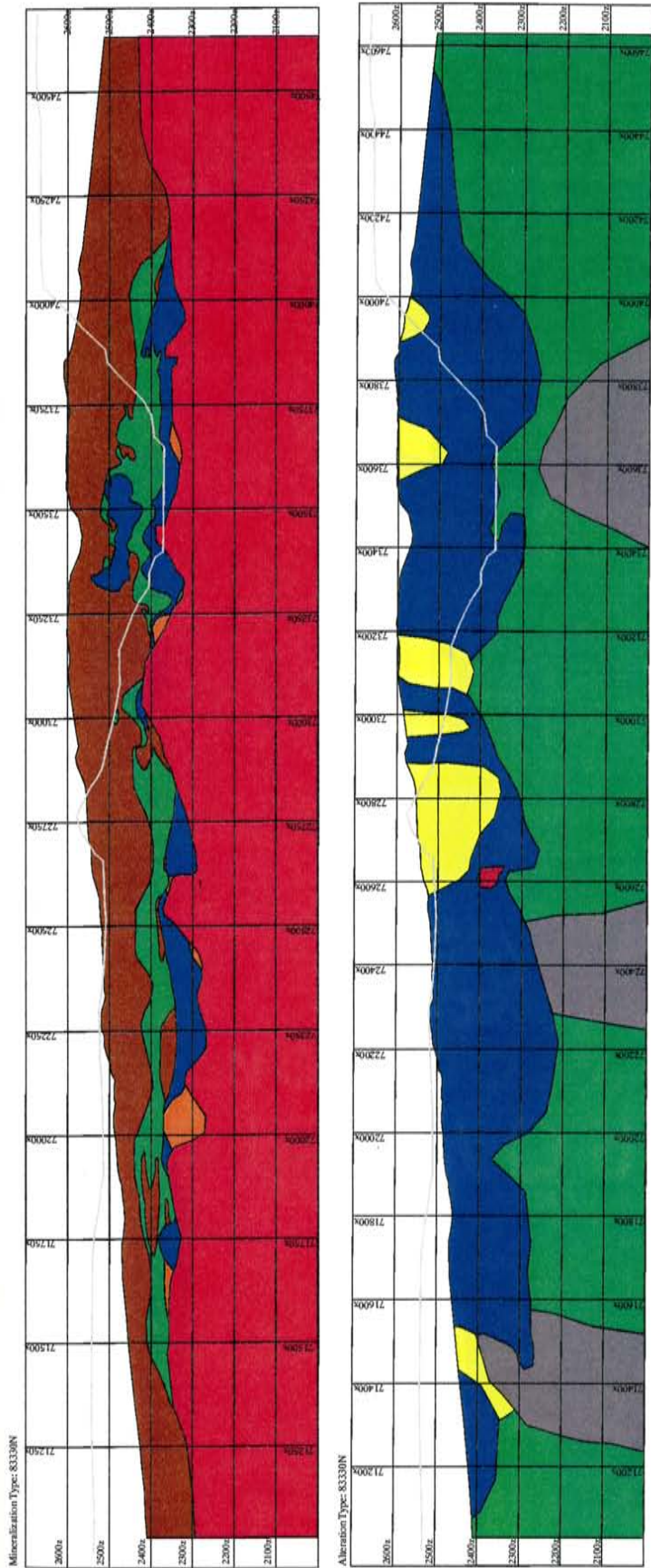


Figure 7.25: An east-west cross-section across the central part of the Cerro Colorado deposit showing the distribution of mineralization (top) and alteration (bottom) types. Note that the qtz-ser-chl (green) and bio-rich potassic (grey) alteration assemblages define the lower boundary of supergene enrichment.

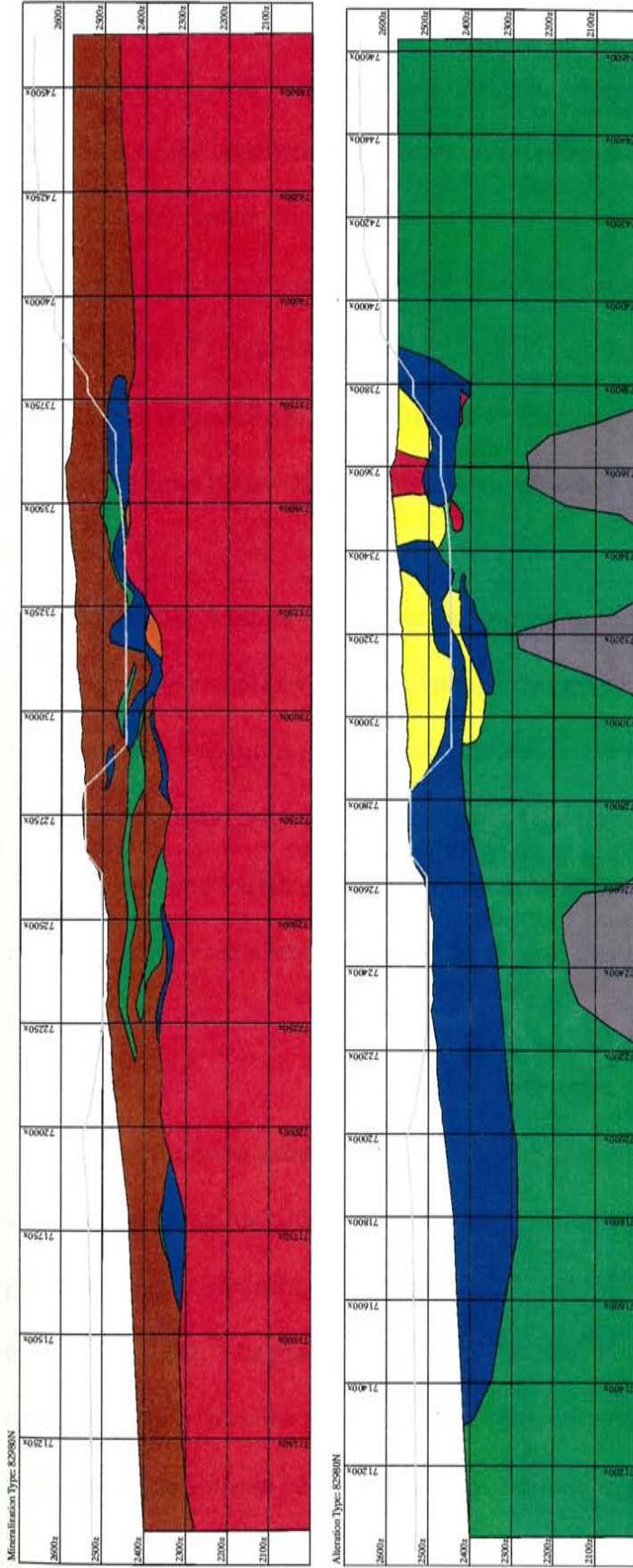


Figure 7.26: An east-west cross-section across the southern part of the Cerro Colorado deposit showing the distribution of mineralization (top) and alteration (bottom) types. Note that the qtz-ser-chl (green) and bio-rich potassic (grey) alteration assemblages define the lower boundary of supergene enrichment.

DDH-02-01 (Figure 7.27), RC-02-30 (Figure 7.22), RC-02-24 (Figure 7.28), and RC-02-21 (Figure 7.23), continues to remain relatively simple but in this zone there is an overall thickening of the supergene enrichment zone (20 to 100-meters thick) and the transition zone (40 to 60-meters thick). In the east main-pit zone there is an increase in stratigraphic thickness and complexity, as illustrated in drill holes RC-F6-28 (Figure 7.29), RC-F6-17 (Figure 7.30), RC-CC160 (Figure 7.31), DDH-03-14 (Figure 7.21), DDH-03-09 (Figure 7.18), and DDH-03-13 (Figure 7.32). Here, the supergene enrichment zone is now 20 to >200-meters thick and the transition zone is now 30 to 70-meters thick.

From the western margins of the deposit to the center there is an overall increase in stratigraphic complexity and thickness. This may be due to a variety of factors that could include: variations in hypogene mineralization intensity; variations in wall-rock alteration intensity; original pyrite content of the leached capping; variations in fracture development; and variable uplift histories to name a few. It is likely that a combination of these processes are responsible for the overall stratigraphic trends seen at Cerro Colorado.

Sulfur Source

In addition to anomalous copper concentrations, porphyry copper deposits are also anomalous sulfur concentrations. There are two general sources of sulfur in the porphyry copper environment; magmatic that has a $\delta^{34}\text{S} \sim 0\%$, and sedimentary that has a $\delta^{34}\text{S} \sim 12$ to 32% . As porphyritic intrusives enter the shallow crust, sedimentary sulfur can be inherited from the surrounding marine sedimentary rocks into the ascending melt and this interaction can be recorded by an increase in the isotopic composition of the

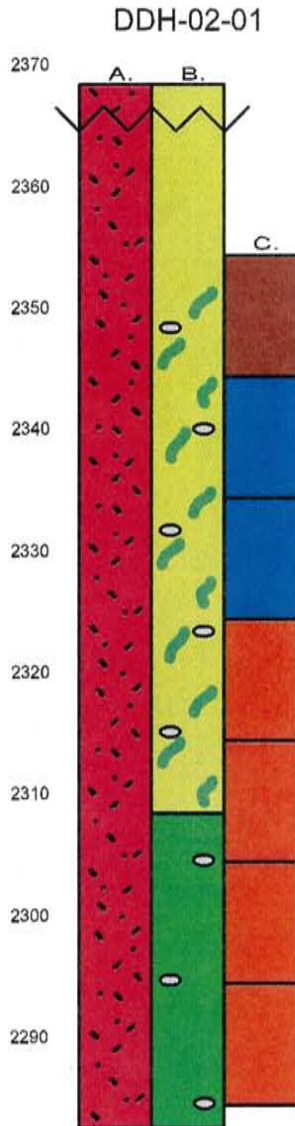


Figure 7.27: Drill hole column showing the relationship between lithology “A” (quartz-feldspar porphyry in red) and alteration “B” (quartz-sericite in yellow, quartz-sericite-chlorite in green, and biotite-rich potassic in grey) to the occurrence of the defined mineral zones “C” (Leached capping in brown, supergene enrichment zone in blue, and the transition zone in orange).

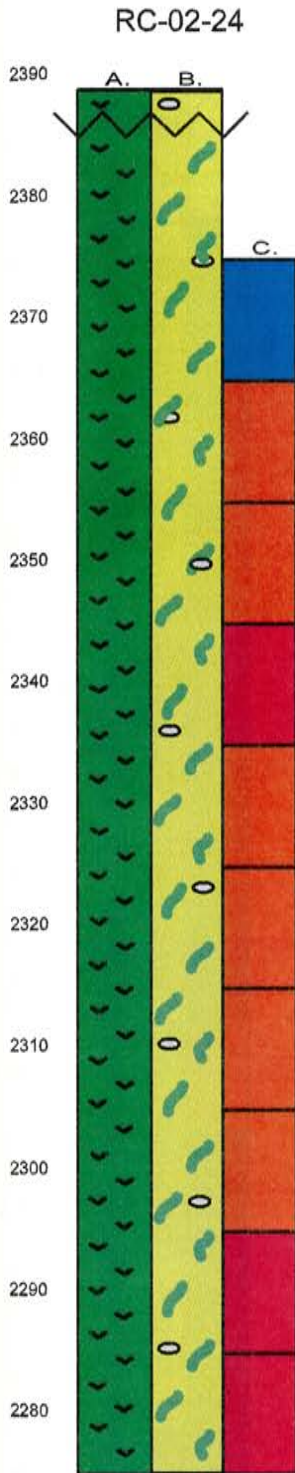


Figure 7.28: Drill hole column showing the relationship between lithology "A" (andesite in green) and alteration "B" (quartz-sericite in yellow and biotite-rich potassic in grey) to the occurrence of the defined mineral zones "C" (supergene enrichment zone in blue, transition zone in orange, and the hypogene zone in red).

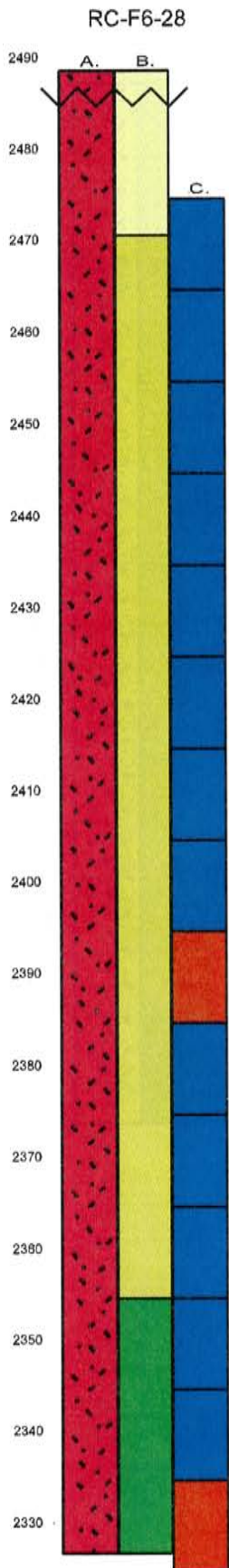


Figure 7.29: Drill hole column showing the relationship between lithology “A” (quartz-feldspar porphyry in red) and alteration “B” (white-clay in tan, quartz-sericite in yellow, and quartz-sericite-chlorite in green) to the occurrence of the defined mineral zones “C” (supergene enrichment zone in blue, and the transition zone in orange).

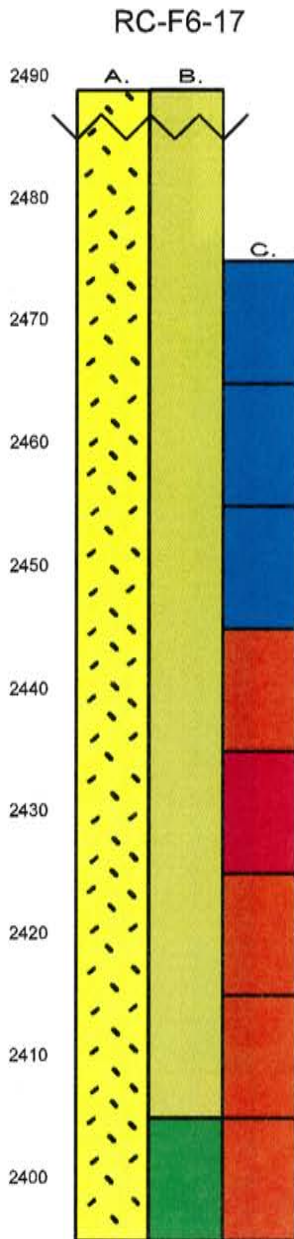


Figure 7.30: Drill hole column showing the relationship between lithology “A” (feldspar porphyry in yellow) and alteration “B” (quartz-sericite in yellow and quartz-sericite-chlorite in green) to the occurrence of the defined mineral zones “C” (supergene enrichment zone in blue, transition zone in orange, and the hypogene zone in red).

RC-CC160



Figure 7.31: Drill hole column showing the relationship between lithology “A” (andesite in green) and alteration “B” (quartz-sericite in yellow) to the occurrence of the defined mineral zones “C” (supergene enrichment zone in blue, transition zone in orange, and the hypogene zone in red).

DDH-03-13

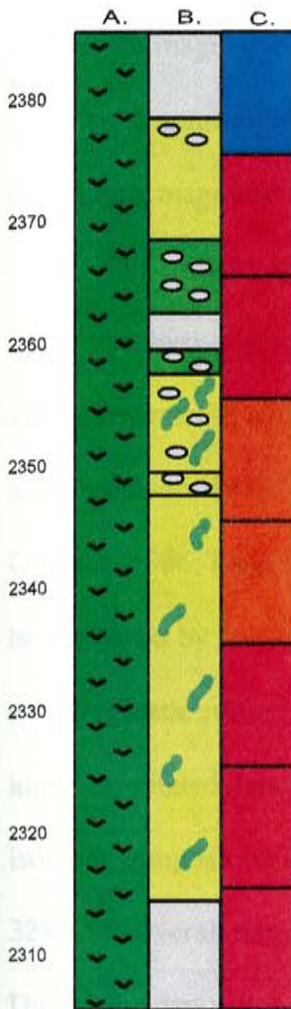


Figure 7.32: Drill hole column showing the relationship between lithology "A" (andesite in green) and alteration "B" (quartz-sericite in yellow, quartz-sericite-chlorite in green, and biotite-rich potassic in grey) to the occurrence of the defined mineral zones "C" (supergene enrichment zone in blue, transition zone in orange, and the hypogene zone in red).

subsequent sulfide mineralization produced by the porphyry system. Because of the large quantity of magmatic sulfur already present in many of these intrusions, a significant quantity of non-magmatic sulfur would be required to raise the isotopic composition beyond the magmatic range.

The primary source of sulfur in most porphyry copper systems is magmatic. Many porphyry copper deposits throughout the American Cordillera report $\delta^{34}\text{S}_{\text{sulfide}}$ values between -5 and 5‰ and are consistent with a magmatic-dominated source (Field and Gustafson, 1976; Ohmoto and Rye, 1979; Shelton and Rye, 1982; Eastoe, 1983; Ohmoto, 1986; Lang et al., 1989). If values outside the range of magmatic sulfur can not be explained by fractionation mechanisms then this may suggest the incorporation of non-magmatic sulfur. An alternative source of sulfur in porphyry copper, as well as other intrusion-related deposit types, is sea-water sulfate. Over the past billion years the isotopic composition of sulfate in equilibrium with sea-water has varied from ~12 to 32‰, but overall has remained enriched in ^{34}S relative to magmatic sulfur (Holser, 1977). During the deposition of marine sediments (e.g. evaporites, limestone, and shale) isotopically heavier sea-water sulfate can be deposited as sulfate minerals within these sediments. If ascending magmas come into contact with these sediments the isotopic composition of the intrusion can become heavier.

During the Early Jurassic through Early Cretaceous, thick sequences of marine limestones, shales, and evaporites were deposited in a large back-arc basin that was present in central Chile (Prinz et al., 1994; Ardill et al., 1998) (Figure 7.33a). The Domeyko Basin that separated the volcanic arc from the mainland developed in the Early

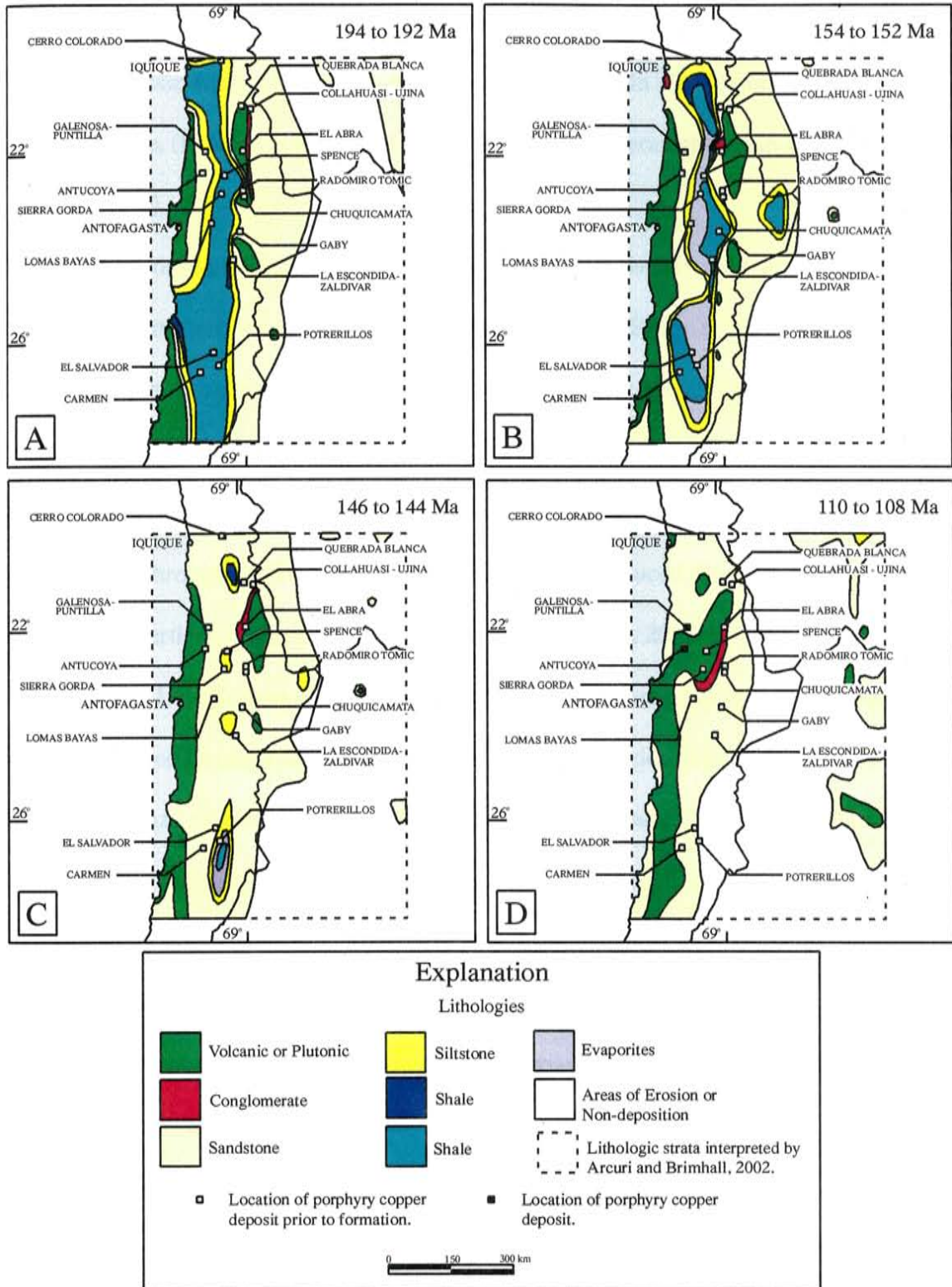


Figure 7.33: Map of north-central Chile showing the generalized geology at different time intervals from 194 to 108 Ma, and the location of major porphyry copper deposits. Modified after Arcuri and Brimhall (2002).

Jurassic in response to numerous transgressive events (Arcuri and Brimhall, 2002). In the Late Jurassic-Early Cretaceous, the basin was reduced in size to only a few small isolated basins (Figure 7.33b-c), and by the Middle Cretaceous the basin was gone (Figure 7.33d).

From the Middle Cretaceous through the Middle Tertiary the Salta Basin developed to the east along the Chilean, Argentinean, and Bolivian borders. In the Middle Cretaceous the volcanic arc migrated east and back-arc rifting initiated (Jaillard et al., 2000) (Figure 7.34e). Continued rifting coupled with a transgression from the east was instrumental in basin development (Figure 7.34f). Eastward migration of the volcanic arc through the Tertiary and subsequent uplift reduced the extent of the basin by the Middle Tertiary (Figure 7.34g-h) (Arcuri and Brimhall, 2002).

In the Late Eocene through the Middle Miocene, numerous porphyry copper deposits formed throughout northern Chile. These porphyries developed after the volcanic arc had migrated east over the Domeyko Basin, and many are located directly over or along the margins of this basin. Because of this spatial association it is likely that the intrusives associated with the development of these systems came into contact with non-magmatic sulfur.

There is evidence for the addition of non-magmatic chloride and bromine from Jurassic evaporates during the development of supergene enrichment (Arcuri and Brimhall, 2001). Elevated bromine (22 to 180 ppm) and stable chloride isotopic ratios near 0‰ from atacamite mineralization are inconsistent with unmineralized biotite-bearing whole rock samples at Radio Tomic that contains low total bromine (<2 ppm) and $\delta^{37}\text{Cl}$ values from 0.1 to 2.5‰, indicating a marine source of these elements (Arcuri

and Brimhall, 2001). The development of abundant atacamite in the oxide zone is not unique to Radio Tomic (Patricio and Gonzalo, 2001), as Montos Blancos (Chávez, 1983), Loma Bayas, and Chuquicamata also contain abundant atacamite in their oxide zones, suggesting the interaction of Jurassic marine sediments during the supergene development of these systems too (Arcuri and Brimhall, 2001).

Evidence to support the addition of non-magmatic sulfur to hypogene mineralization at Cerro Colorado, Chuquicamata, El Salvador, and Potrerillos is scarce. $\delta^{34}\text{S}_{\text{pyrite}}$ values at Cerro Colorado have a range of 0 to 3‰ with a mean of 2‰, $\delta^{34}\text{S}_{\text{sulfide}}$ values at Chuquicamata have a mean of -5‰ (Akira et al., 1984), $\delta^{34}\text{S}_{\text{sulfide}}$ values at El Salvador have a range of -10 to -0.3‰ with a mean of -3‰, and $\delta^{34}\text{S}_{\text{sulfate}}$ values have a range of 7.3 to 17‰ with a mean of 10.7‰ (Field and Gustafson, 1976; and Akira et al., 1984), and $\delta^{34}\text{S}_{\text{sulfide}}$ values at Potrerillos have a range of -4.3 to 0.1‰ with a mean of -3‰, and $\delta^{34}\text{S}_{\text{sulfate}}$ values have a range of 7.2 to 17.4‰ (Marsh, 1997). The isotope ratios of all of these deposits are within the range of other porphyry deposits interpreted to have a magmatic-dominated source of sulfur $\delta^{34}\text{S} = 0 \pm 5\%$ (Akira et al., 1984).

The close proximity of these deposits to Domeyko Basin sediments as is evident from recent basin reconstructions (Arcuri and Brimhall, 2002) and the chloride and bromine work (Arcuri and Brimhall, 2000; 2001) suggesting that the mineralizing intrusions at Cerro Colorado, Chuquicamata, and El Salvador were in contact with Jurassic marine sediments. Sulfur isotopes from these deposits are inconclusive with respect to supporting the introduction of detectible quantities sedimentary sulfur into the system. Rather, this data suggests that if non-magmatic sulfur was introduced, it was minor relative to the magmatic sulfur already present in the mineralizing intrusions.

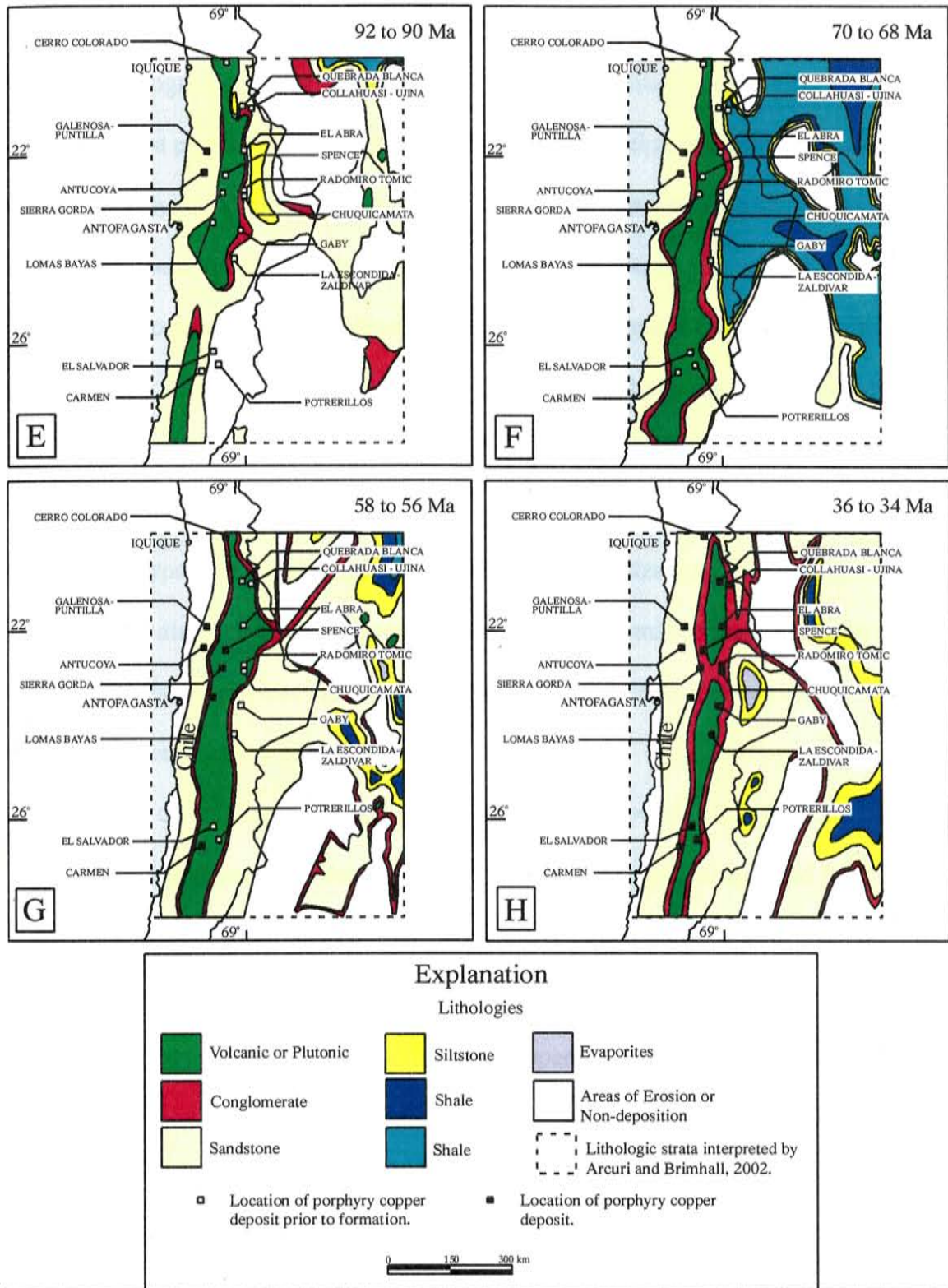


Figure 7.34: Map of north-central Chile showing the generalized geology at different time intervals from 194 to 108 Ma, and the location of major porphyry copper deposits. Modified after Arcuri and Brimhall (2002).

Trace Element Lithologic Discrimination

Lithologic discrimination is a common problem at many porphyry copper deposits. Most porphyry deposits are characterized by multiple episodes of pervasive and overprinting hydrothermal alteration with associated vein and disseminated-type hypogene mineralization. Alteration and mineralization events, that occur throughout the life of these porphyry deposits, commonly destroy the original textures of the lithologic units affected. In addition, the high degree of chemical mobility during hydrothermal alteration can make geochemical identification of these units extremely difficult (Pearce, 1983). At the Cerro Colorado deposit these statements also hold true. In an attempt to see through the hypogene and supergene alteration and mineralization events at Cerro Colorado and discriminate the host-rock Cerro Empexa Formation andesites from the undifferentiated porphyritic intrusives, the use of trace elements in conjunction with phenocryst identification was employed.

Based on drill core logging and petrographic descriptions of the size and type of relic phenocrysts present, the host-rock andesite can be clearly distinguished from the quartz-feldspar (microbreccia) and the quartz-feldspar-biotite porphyries, but not the feldspar porphyry. The host-rock andesite is characterized by ~1 mm feldspar phenocrysts that can appear irregular in shape (Appendix D). This is very similar to the feldspar porphyry that also contains ~1 mm feldspar phenocrysts. Unlike the andesite and feldspar porphyry the quartz-feldspar porphyry is characterized by the presence of ~1 mm β -quartz and quartz-eyes, and two populations of feldspar phenocrysts (~1 mm and a less common 2-5 mm) (Appendix D). The quartz-feldspar-biotite porphyry is also characterized by the presence of ~1 mm β -quartz and quartz-eyes, and two populations of

feldspar phenocrysts (~1 mm and a less common 2-5 mm), but also contains 2-5 mm, euhedral, pseudo-hexagonal biotite-books (Appendix D).

In an attempt to further discriminate the host-rock andesite from the porphyries the geochemical discrimination diagrams $Zr/TiO_2 - Ga$ and $Zr/TiO_2 - Nb/Y$ that delimitate common volcanic rocks defined by Winchester and Floyd (1976) were used (Figures 6.3 and 6.4). Based on the distribution of these lithologic units two observations can be made: 1. the host-rock andesite and the feldspar porphyry plot within the andesite field; 2. the quartz-feldspar (microbreccia) and the quartz-feldspar-biotite porphyries generally plot within the rhyodacite/dacite –trachyandesite fields. This data suggests that the feldspar porphyry is geochemically similar to the host-rock andesite and that the quartz-feldspar and quartz-feldspar-biotite porphyries are somewhat more felsic in composition. At Cerro Colorado the quartz-feldspar and quartz-feldspar-biotite porphyries are easily distinguished from the feldspar porphyry and the andesite based on texture and phenocryst type and size. Where the andesite and feldspar porphyry are highly altered they appear texturally and geochemically similar.

Geochemical discrimination of the different lithologic units present at Cerro Colorado may in fact be possible and provide a useful tool in understanding the distribution of these units and untimely add insight to the intrusive history of this system. In order for this to occur, detailed drill core logging and petrographic study must be undertaken to define these intrusive units where alteration has not completely destroyed original textures. Once these units are defined, a more thorough geochemical investigation may be able to better define geologic contacts.

CHAPTER 8

CONCLUSIONS

- The supergene enrichment zone at Cerro Colorado is defined quantitatively as the volume of rock having a $cc+cv/bn+cp$ ratio ≥ 2 and/or having $\geq 80\%$ of the copper contained in chalcocite + covellite. This zone is characterized by the very strong replacement of pyrite by chalcocite and/or covellite, the complete to almost complete replacement of chalcopyrite by chalcocite and/or covellite, and typically by the absence of bornite. The upper parts of a well-developed supergene enrichment zone are dominated by chalcocite enrichment, whereas the lower parts of the supergene enrichment zone are dominated by covellite enrichment. In addition the lower parts of the supergene enrichment zone are also characterized by an overall increase in hypogene sulfides.
- The transition zone at Cerro Colorado is defined quantitatively as the volume of rock having a $cc+cv:bn+cp$ ratio < 2 and ≥ 0.10 and/or having $< 80\%$ and $\geq 15\%$ of the copper contained in chalcocite + covellite. This zone is characterized by the incomplete replacement of hypogene sulfides by chalcocite and covellite, by the very strong to moderate replacement of bornite and chalcopyrite by chalcocite and/or covellite, the moderate to weak replacement of pyrite by chalcocite and/or covellite, and by the presence of supergene bornite and chalcopyrite. The transition zone is also characterized

by an overall decrease in supergene enrichment towards the base and subsequent increase in chalcopyrite followed by bornite.

- The hypogene zone at Cerro Colorado is defined quantitatively as the volume of rock having a $cc+cv:bn+cp$ ratio <0.10 and/or having $<15\%$ of the copper contained in chalcocite + covellite. This zone is characterized by the presence of dominantly un-enriched hypogene pyrite, chalcopyrite and lesser bornite mineralization. Locally, hypogene mineralization at Cerro Colorado is characterized by a pyrite-bornite assemblage. Trace chalcocite and/or covellite enrichment on bornite and/or chalcopyrite can occur in the upper parts of the hypogene zone. This zone can also contain hypogene chalcocite and/or covellite, but the occurrences of these minerals are volumetrically small.
- The occurrence of the enrichment zone within the transition and/or hypogene zone is associated with a change in the character of the pre-enriched hypogene mineralization from a pyrite-chalcopyrite-(bornite) assemblage to a pyrite-bornite assemblage. This change in the original hypogene character leads to an overall decrease in chalcopyrite that results in a zone with a higher $cc+cv:cp+bn$ ratio. In addition, qualitative observations show that the type of enrichment within these intervals is consistent with the type of enrichment observed within the transition zone and not typical of the type of enrichment observed within the enrichment zone. These intervals should ultimately be considered as part of the transition zone.
- The occurrence of the hypogene zone within the transition zone is associated with the development of a relict “perched” hypogene zone. Veins, faults/fractures, and pervasive alteration associated with the development of hypogene mineralization can

significantly increase the heterogeneity of the mineralized rock. The large increase in porosity and permeability, generally along veins and fractures, allows enriching fluids to “by-pass” volumes of rock with lower permeability permitting the development of these “perched” mineral zones.

- The thickness of the transition zone is controlled by the reactivity of the wall-rock alteration mineral assemblage. Detailed study of the transition zone shows that where the transition zone is developed in a less reactive quartz-sericite alteration it is generally up to 60-meters thick, whereas where this zone is developed in a more reactive quartz-sericite-chlorite alteration it is generally 20 to 40-meters thick, and where it is developed in a very reactive biotite-rich potassic alteration it is only 10-meters thick. In addition, the top of the transition zone and the top of the hypogene zone commonly occur with a change in alteration type from quartz-sericite to quartz-sericite-chlorite alteration or from quartz-sericite-chlorite to biotite-rich potassic alteration. These trends clearly support acid buffering of copper-bearing solutions by chlorite and biotite as the dominant control on transition zone occurrence and thickness at Cerro Colorado.

- From the western margins of the deposit to the center there is an overall increase in geochemical stratigraphic complexity and thickness. The oxide and supergene enrichment zones are much thicker and vertically developed in the east main-pit area, whereas these zones are relatively thin but laterally continuous in the western parts of the deposit. The increase in the oxide and supergene enrichment zone thickness is mirrored by the transition zone. These trends may be attributable to a variety of factors that include: variations in hypogene mineralization intensity; variations in wall-rock alteration

intensity; pre-oxidation total pyrite content of the leached capping; variations in fracture development; or structural history of fault-bounded regimes.

- Basin reconstructions place numerous porphyry Cu deposits within or along the margins of the Domeyko Basin. A marine transgressive basin was host to a large quantity of sedimentary sulfur. Stable chloride and bromine work shows that these some of these porphyries had interacted with these marine sediments during their supergene development. Stable isotopic analysis of sulfides and sulfates from the Cerro Colorado, Chuquicamata, El Salvador, and Potrerillos deposits returned values within the range of sulfide-sulfate fractionation of a magmatic source. It is believed that due to the large quantity of magmatic sulfur already present in these mineralizing porphyries, a significant quantity of sedimentary sulfur, enough to raise the isotopic composition beyond the magmatic range, was not incorporated.

- At Cerro Colorado the quartz-feldspar and quartz-feldspar-biotite porphyries are easily distinguished from the feldspar porphyry and the andesite based on the presence of ~1 mm β -quartz and quartz-eyes 2-5 mm feldspar phenocrysts, and from each other by the presence of 2-5 mm, euhedral, pseudo-hexagonal biotite-books. Geochemically the quartz-feldspar and quartz-feldspar-biotite porphyries are generally more felsic than the feldspar porphyry and the andesite. Where the andesite and feldspar porphyry are highly altered they appear texturally and geochemically similar. Discrimination of these units in highly altered parts of the deposit would require a more thorough investigation.

REFERENCES CITED

- Anderson, C.A., 1950, Alteration and Metallization in the Bagdad Porphyry Copper Deposit, Arizona: *Economic Geology and the Bulletin of the Society of Economic Geologists*, v. 45, p. 609-628.
- Arcuri, T.L., and Brimhall, G.H., 2000, Jurassic to Mid-Miocene Back-Arc Evaporative Basin Evolution of Northern Chile and Argentina: Potential Influences on Porphyry Copper Emplacement, Mineralogy, and Mineralization [abs.]: *Geological Society of America Abstracts with Programs*, v. 32, p. A-86.
- , 2001, Chlorine Isotope and Bromine Evidence of a Jurassic Sedimentary Chloride Source for Atacamite Mineralization at the Radomiro Tomic Porphyry Copper Deposit, Northern Chile [abs.]: *Geological Society of America Abstracts with Programs*, v. 33, p. A-359.
- , 2002, Animation Model of West Central South America from the Early Jurassic to Late Miocene, with Some Oil and Gas Implications: *Search and Discovery Article #10033*.
- Ardill, J., Flint, S., Chong, G., and Wilke, H., 1998, Sequence stratigraphy of the Mesozoic Domeyko Basin, Northern Chile: *Journal of the Geological Society of London*, v. 155, p. 71-88.
- Atkinson, W.W., Jr., Souviron, A., Vehrs, T.I., and Faunes, A., 1996, Geology and Mineral Zoning of the Los Pelambres Porphyry Copper Deposit, Chile: "Andean Copper Deposits: New Discoveries, Mineralization, Styles and Metallogeny", *Society of Economic Geologists Special Publication No. 5*, p. 131-156.
- Bouzari, F., and Clark, A.H., 1997, The Cerro Colorado Porphyry Copper Deposit, Chile: (1) Field Observations: Internal Report for Rio Algom Exploration Inc.
- , 2000, Definition of a Protracted History of Supergene Alteration in the Cerro Colorado Porphyry Copper Deposit, Chile, Through Ar-Ar Dating of Alunite-Group Minerals [abs.]: *Geological Society of America Abstracts with Programs*, v. 32, p. A-110.
- , 2002, Anatomy, Evolution, and Metallogenic Significance of the Supergene Orebody of the Cerro Colorado Porphyry Copper Deposit, I Región, Northern Chile: *Economic Geology*, v. 97, 1701-1740 p.
- Brimhall, G.H., 1977, Early Fracture-Controlled Disseminated Mineralization at Butte, Montana: *Economic Geology*, v. 72, p. 37-59.
- Cepeda A., 1982, Geological Assessment of the Cerro Colorado Project, Chile: Internal Report for CIA. Minera Riochilex Ltda.
- Chávez, W.X., 1983, Zoning and Compositions of Hypogene and Supergene Sulfides, Mantos Blancos District, Northern Chile [abs.]: *Geological Society of America Abstracts with Programs*, v. 15, p. 542.

- Chávez, W.X., 2000, Supergene Oxidation of Copper Deposits: Zoning and Distribution of Copper Oxide Minerals: Society of Economic Geologists Newsletter, no. 41, p. 1, 10-21.
- Cotton, W.B. III, 2003, Near Infrared and XRD Quantification of Porphyry Copper Alteration at Cerro Colorado and Spence, Chile: University of Colorado PhD Thesis.
- DuHamel, J.E., Cook, S.S., and Kolessar, J., 1995, Geology of the Tyrone Copper Deposit, New Mexico: Arizona Geological Society Digest, v. 20, p. 464-472.
- Eastoe, C.J., 1983, Sulfur Isotope Data and the Nature of the Hydrothermal Systems at the Panguna and Frieda Porphyry Copper Deposits, Papua New Guinea: Economic Geology and the Bulletin of the Society of Economic Geologists, v. 78, p. 201-213.
- Field, C.W., and Gustafson, L.B., 1976, Sulfur Isotopes in the Porphyry Copper Deposit at El Salvador, Chile: Economic Geology and the Bulletin of the Society of Economic Geologists, v. 71, p. 1533-1548.
- Flores, R., 1985, Control de Enriquecimiento Supérgeno en el Yacimiento Chuquicamata, Chile: Cuarto Congreso Geológico Chileno, v. 2, p. 3-228 to 3-249.
- Galli O.C., 1968, Carta Geológica de Chile: Cuadrángulo Juan de Morales, Provincia de Tarapacá: Instituto de Investigaciones Geológicas de Chile, Carta 18, escala 1:50,000, 53 p.
- García A., F., 1967, Geología del Norte Grande de Chile: Sociedad Geológica de Chile Symposium Sobre el Geosinclinal Andino 1962 Santiago (Chile).
- Garza, R.A., Titley, S.R., and Pimentle, F., 2001, Geology of the Escondida Porphyry Copper Deposit, Antofagasta Region, Chile: Economic Geology and the Bulletin of the Society of Economic Geologists, v. 96, p. 307-324.
- Gustafson, L.B., and Hunt, J.P., 1975, The Porphyry Copper Deposit at El Salvador, Chile: Economic Geology and the Bulletin of the Society of Economic Geologists, v. 70, p. 857-912.
- Hallett, R.B., and Kyle, P.R., 1993, XRF and INAA Determinations of Major and Trace Elements in Geologic Survey of Japan Igneous and Sedimentary Rock Standards: Geostandards Newsletter, v. 17, p. 127-133.
- Holser, W.T., 1977, Catastrophic Chemical Events in the History of the Ocean: Nature, v. 267, p. 403-408.
- Jaillard, E., Héral, G., Monfret, T., Díaz-Martínez, E., Baby, P., Lavenu, A., and Dumont, J.F., 2000, Tectonic Evolution of the Andes of Ecuador, Peru, Bolivia and Northernmost Chile: Tectonic Evolution of South America, p. 481-559.
- Lang, J.R., Yin, G., and Eastoe, C.J., 1989, Stable Isotopic Studies of Sulfates and Sulfides in the Mineral Park Porphyry Cu-Mo System, Arizona: Economic Geology and the Bulletin of the Society of Economic Geologists, v. 84, p. 650-662.
- Lichtner, P.C., and Biino, G.G., 1992, A First Principles Approach to Supergene Enrichment of a Porphyry Copper Protore: I Cu-Fe-S Subsystem: *Geochimica et Cosmochimica Acta*, v. 56, p. 3987-4013.
- Marsh, T.M., 1997, Geochronology, Thermochronology, and Isotope Systematics of the Cu-Au and Au-Ag Deposits of the Potrerillos District, Atacama Region, Chile: Doctoral Thesis, Stanford University.
- Ohmoto, H., 1986, Stable Isotope Geochemistry of Ore Deposits: Stable Isotopes in High Temperature Geological Processes Reviews in Mineralogy, v. 16, p. 491-559.

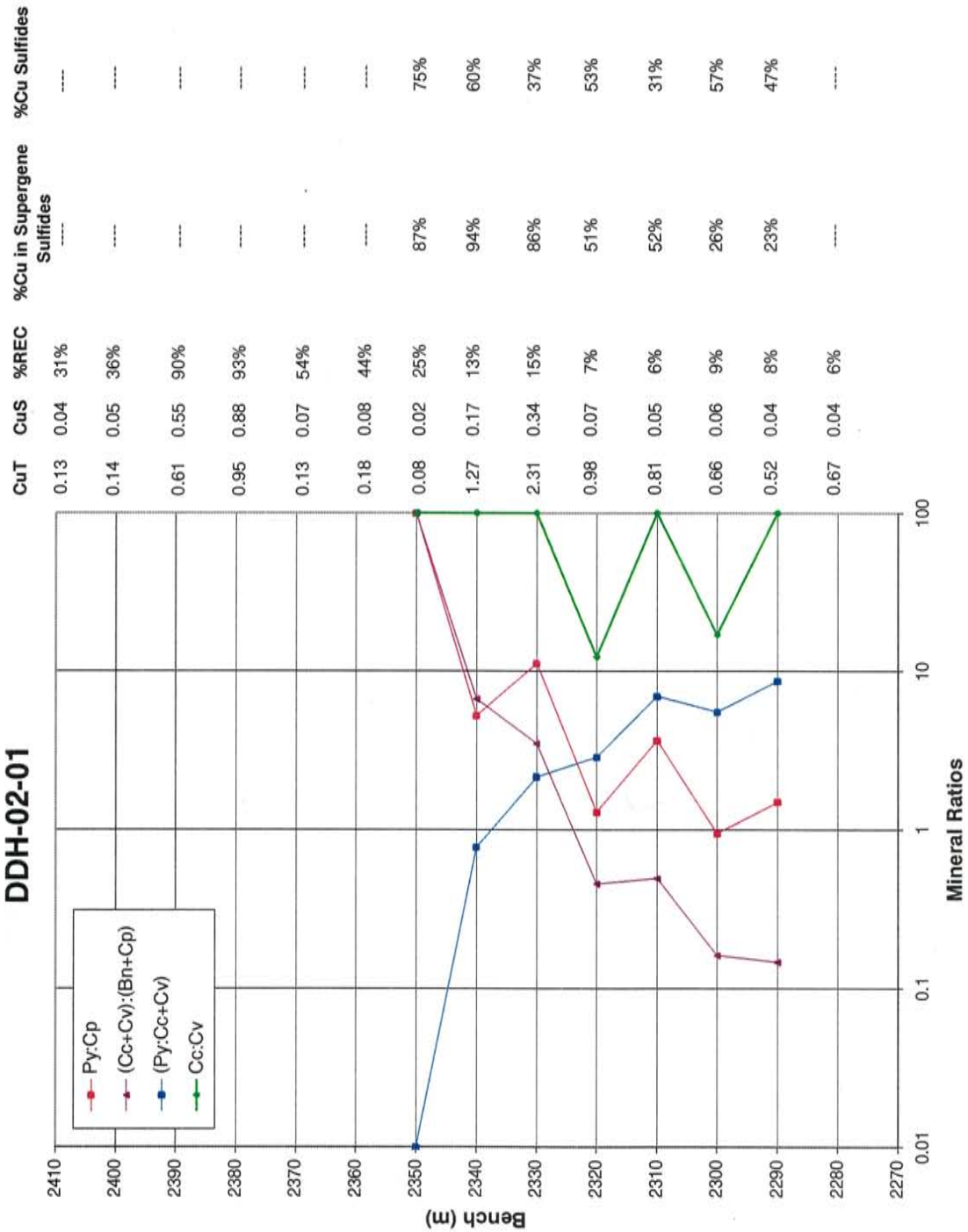
- Ohmoto, H., and Rye, R.O., 1979, Isotopes of Sulfur and Carbon: Geochemistry of Hydrothermal Ore Deposits: In *Geochemistry of Hydrothermal Ore Deposits*, p. 509-567.
- Ojeda, J.M., 1990, Geology of the Escondida Porphyry Copper Deposit, II Region, Chile: *Proceedings of the Pacific Rim Congress 90*, p. 473-483.
- Ossandón, G., Fréaut, R., Gustafson, L.B., Lindsay, D.D., and Zentilli, M., 2001, Geology of the Chuquicamata Mine: A Progress Report: *Economic Geology and the Bulletin of the Society of Economic Geologists*, v. 96, p. 249-270.
- Patricio, C.C., and Gonzalo, R.S., 2001, Oxide Mineralization at the Radio Tomic Porphyry Copper Deposit, Northern Chile: *Economic Geology and the Bulletin of the Society of Economic Geologists*, v. 96, p. 387-400.
- Prinz, P., Wilke, H., and Hillebrandt, A., 1994, Sediment Accumulation and Subsidence History in the Mesozoic Marginal Basin of Northern Chile: *Tectonics of the Southern Central Andes; Structure and Evolution of an Active Continental Margin*.
- Rose, A.W., and Baltosser, W.W., 1966, The Porphyry Copper Deposit at Santa Rita, New Mexico: *Geology of the Porphyry Copper Deposits, Southwest North America*, p. 205-220.
- Sasaki, A., et al., 1984, Sulfur Isotope Reconnaissance of Porphyry Copper and Manto-Type Deposits in Chile and the Philippines: *Bulletin of the Geological Survey of Japan*, v. 35, p. 615-622.
- Shelton, K.L., and Rye, D.M., 1982, Sulfur Isotopic Compositions of Ores from Mines Gaspé, Quebec: An Example of Sulfate-Sulfide Isotopic Disequilibria in Ore-Forming Fluids with Applications to Other Porphyry-type Deposits.
- Sillitoe, R.H., 1973, Geology of the Los Pelambres Porphyry Copper Deposit, Chile: *Economic Geology and the Bulletin of the Society of Economic Geologists*, v. 68, p. 1-10.
- Swayne, W.H., and Trask, F., 1960, *Geology of El Salvador: Mining Engineering*, p. 344-348.
- Thomas N., A., 1967, Carta geológica de Chile: Cuadrángulo Mamiña, Provincia de Tarapacá: Instituto de Investigaciones Geológicas de Chile, carta 17, escala 1:50,000, 49 p.
- Titley, S.R., 1982, Characteristics of Leached Capping and Techniques of Appraisal: *Advances in Geology of the Porphyry Copper Deposits Southwest North America*, p. 275-295.
- Virtue, T.L., 1996, Geology, Mineralogy, and Genesis of Supergene Enrichment at the Cananea Porphyry Copper Deposit, Sonora, Mexico: Department of Geological Sciences, University of Texas at El Paso.
- Winchester, J.A., and Floyd, P.A., 1977, Geochemical Discrimination of Different Magma Series and Their Differentiation Products Using Immobile Elements: *Chemical Geology*, v. 20, p. 325-343.

APPENDIX A

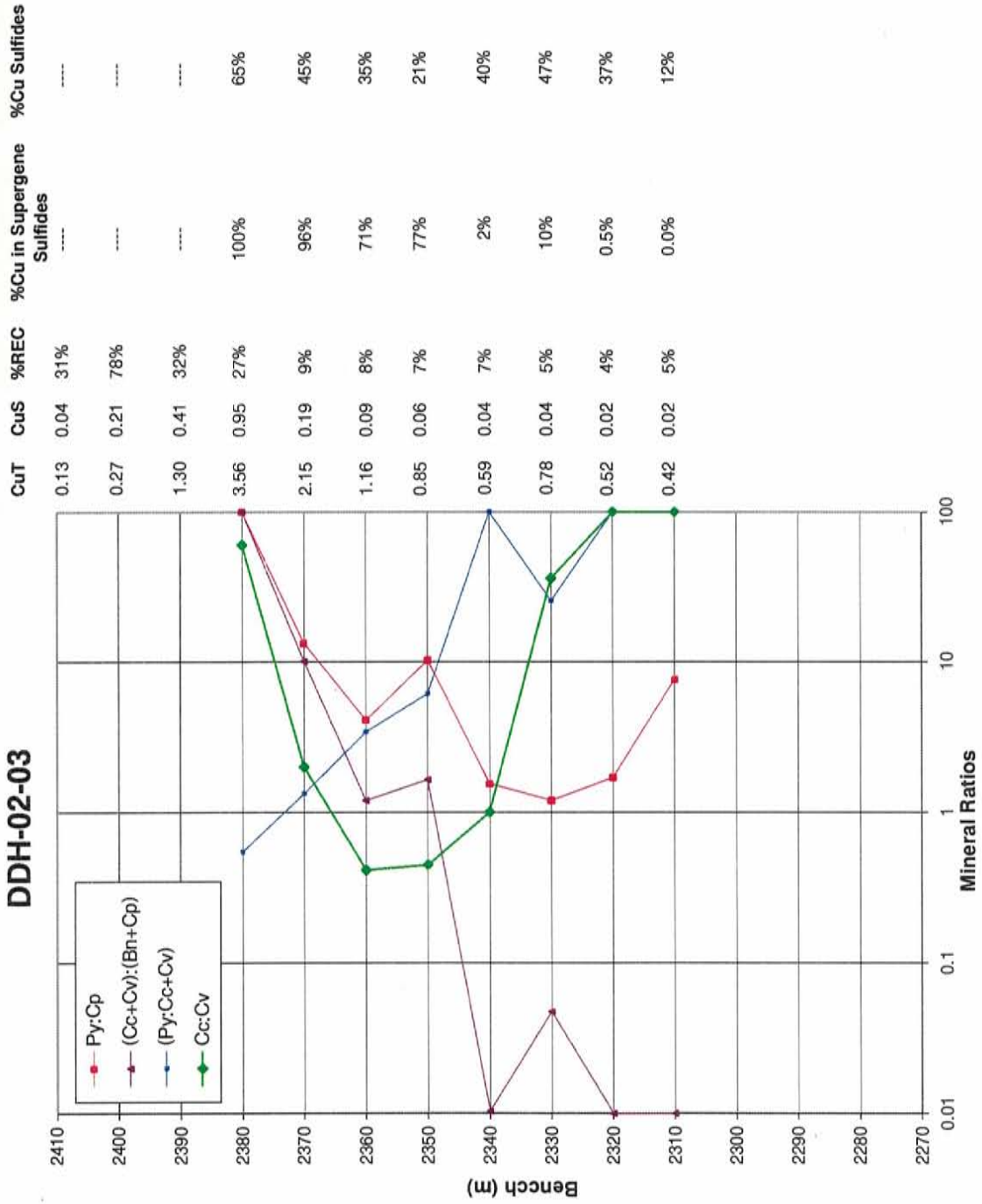
Logarithmic mineral ratio plots of the selected mineral ratios for the below mentioned drill holes. For each drill hole total copper (CuT), soluble copper (CuS), and percent recoverable copper (%REC) are displayed to the immediate right of the diagram and are compiled for each bench from two-meter assay samples. Farther to the right, the calculated values of percent copper in supergene sulfides and the relative percent copper sulfides for each sample are presented.

Drill Holes: DDH-02-01, DDH-02-03, DDH-02-04, DDH-02-08, DDH-02-11, DDH-03-09, DDH-03-13, DDH-03-14, RC-02-21, RC-02-24, RC-02-30, RC-F6-17, RC-F6-28, and RC-CC160.

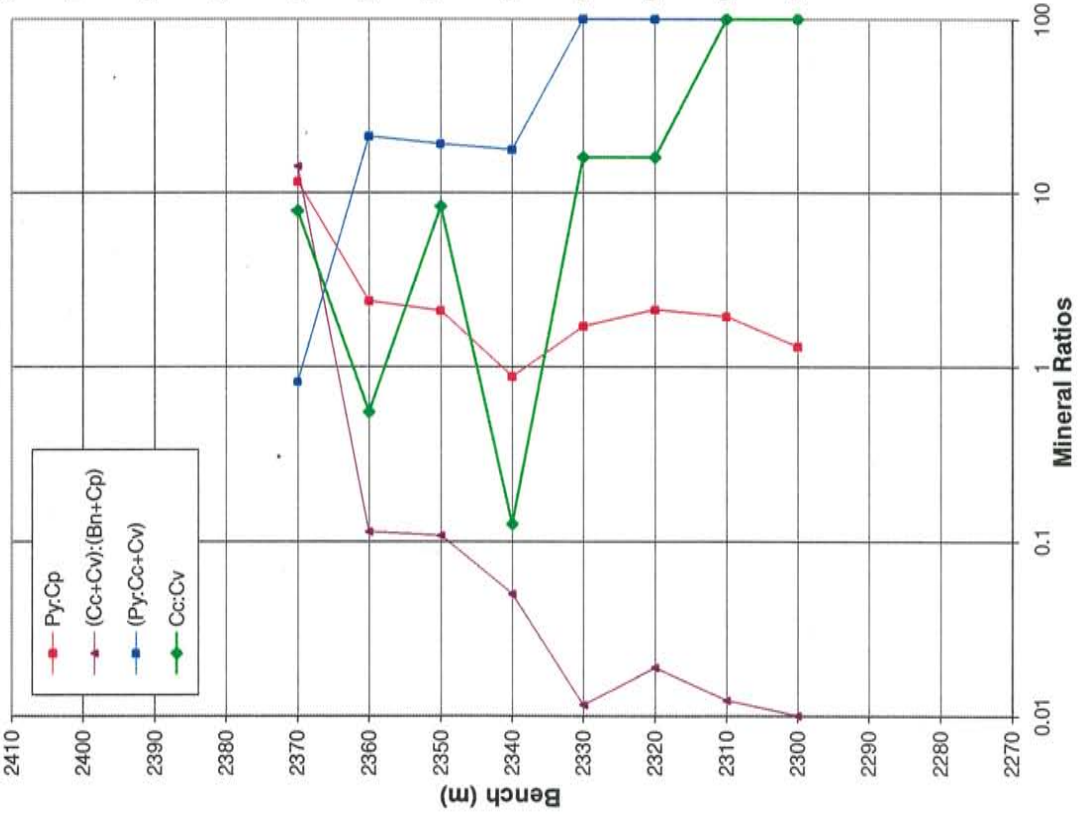
DDH-02-01



DDH-02-03

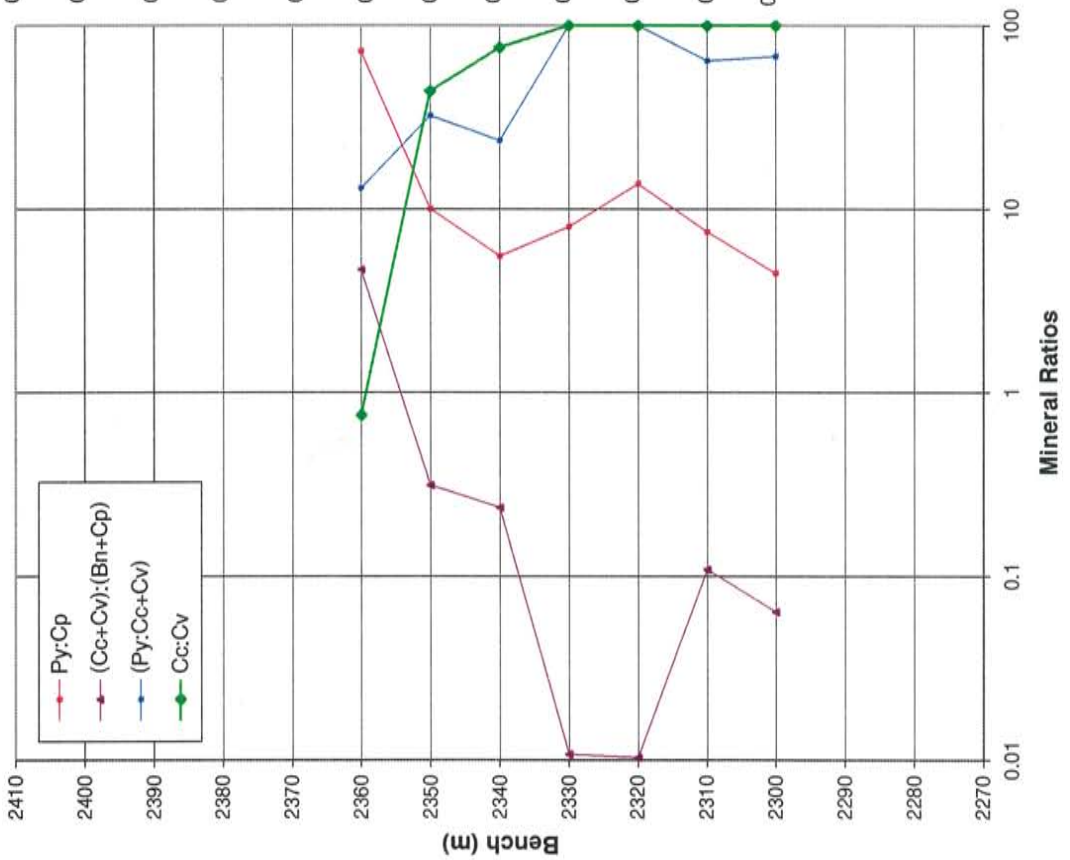


DDH-02-04



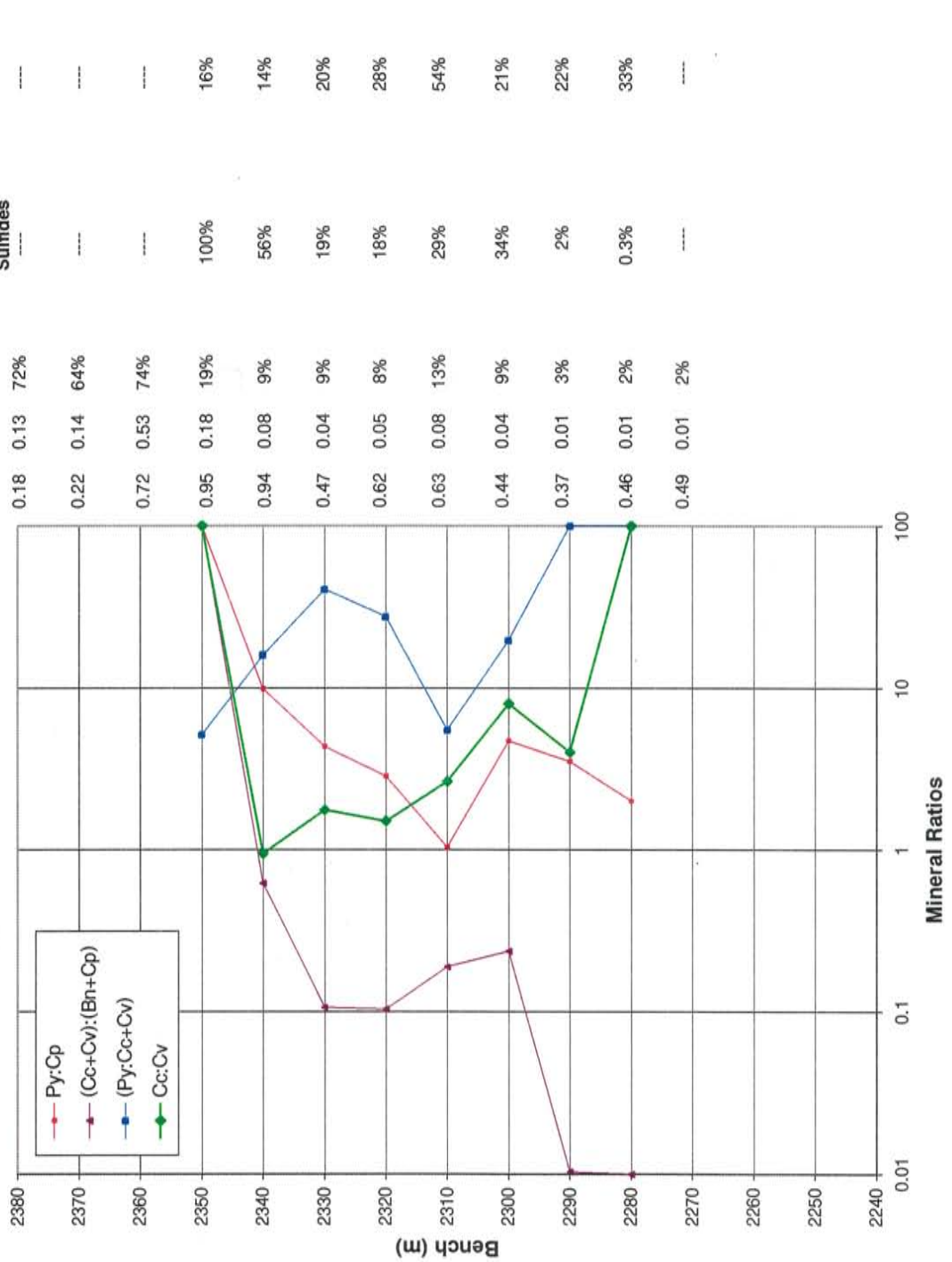
CuT	CuS	%REC	%Cu in Supergene Sulfides	%Cu Sulfides
0.36	0.24	67%	---	---
1.16	0.92	79%	---	---
0.58	0.48	83%	---	---
0.35	0.26	74%	---	---
0.86	0.38	45%	97%	57%
0.92	0.05	5%	19%	32%
0.92	0.03	3%	19%	35%
0.99	0.03	3%	9%	55%
0.68	0.02	2%	3%	37%
0.66	0.02	3%	4%	32%
0.60	0.02	3%	3%	34%
0.62	0.01	2%	0.1%	43%

DDH-02-08

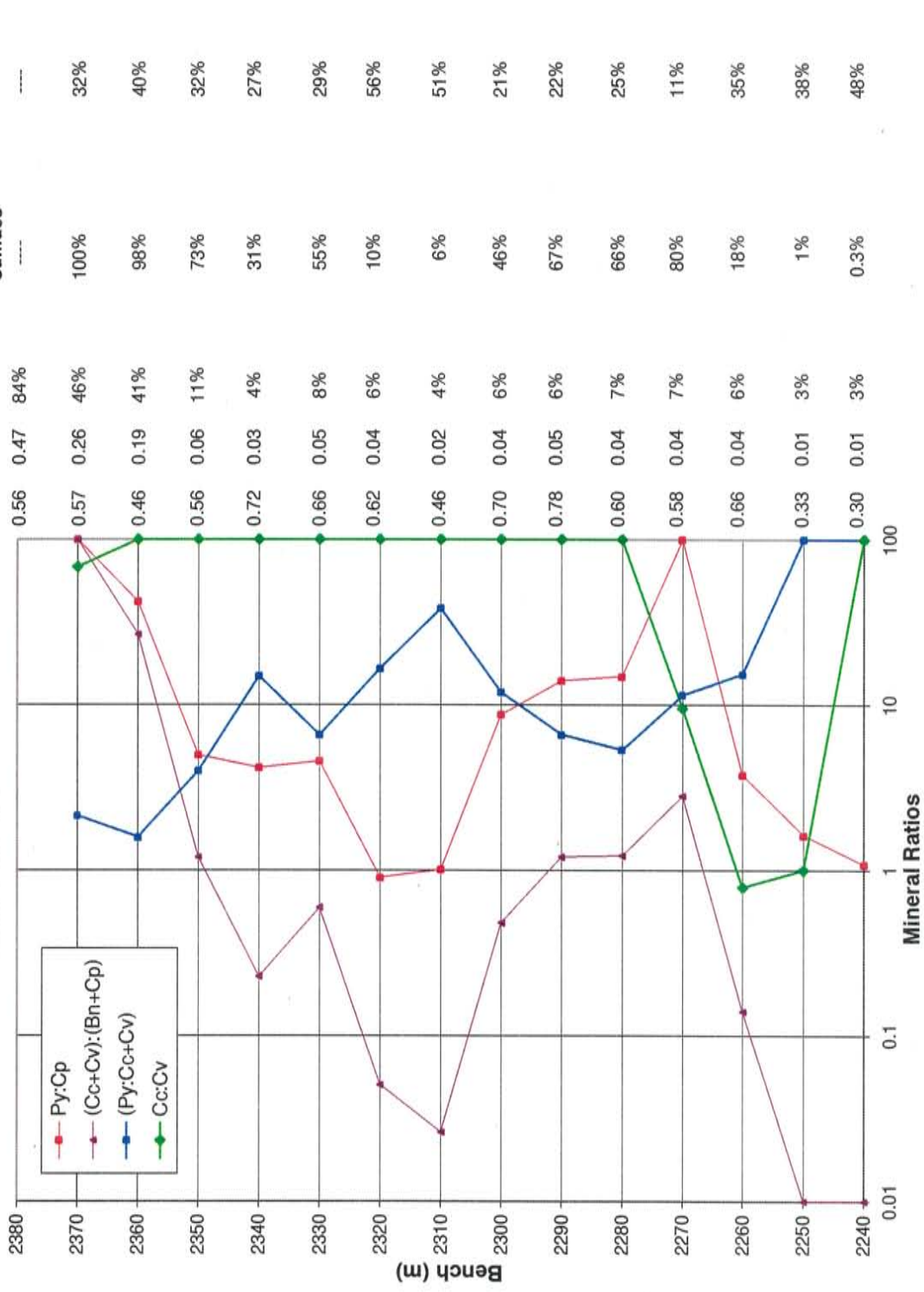


CuT	CuS	%REC	%Cu in Supergene Sulfides	%Cu Sulfides
0.82	0.58	71%	---	---
0.46	0.36	78%	---	---
0.46	0.27	59%	---	---
0.26	0.14	54%	---	---
0.17	0.07	41%	---	---
0.53	0.13	25%	90%	9%
0.59	0.05	8%	42%	12%
0.47	0.03	6%	35%	18%
0.36	0.02	6%	2%	11%
0.36	0.01	3%	2%	7%
0.35	0.03	9%	19%	14%
0.43	0.03	7%	13%	20%

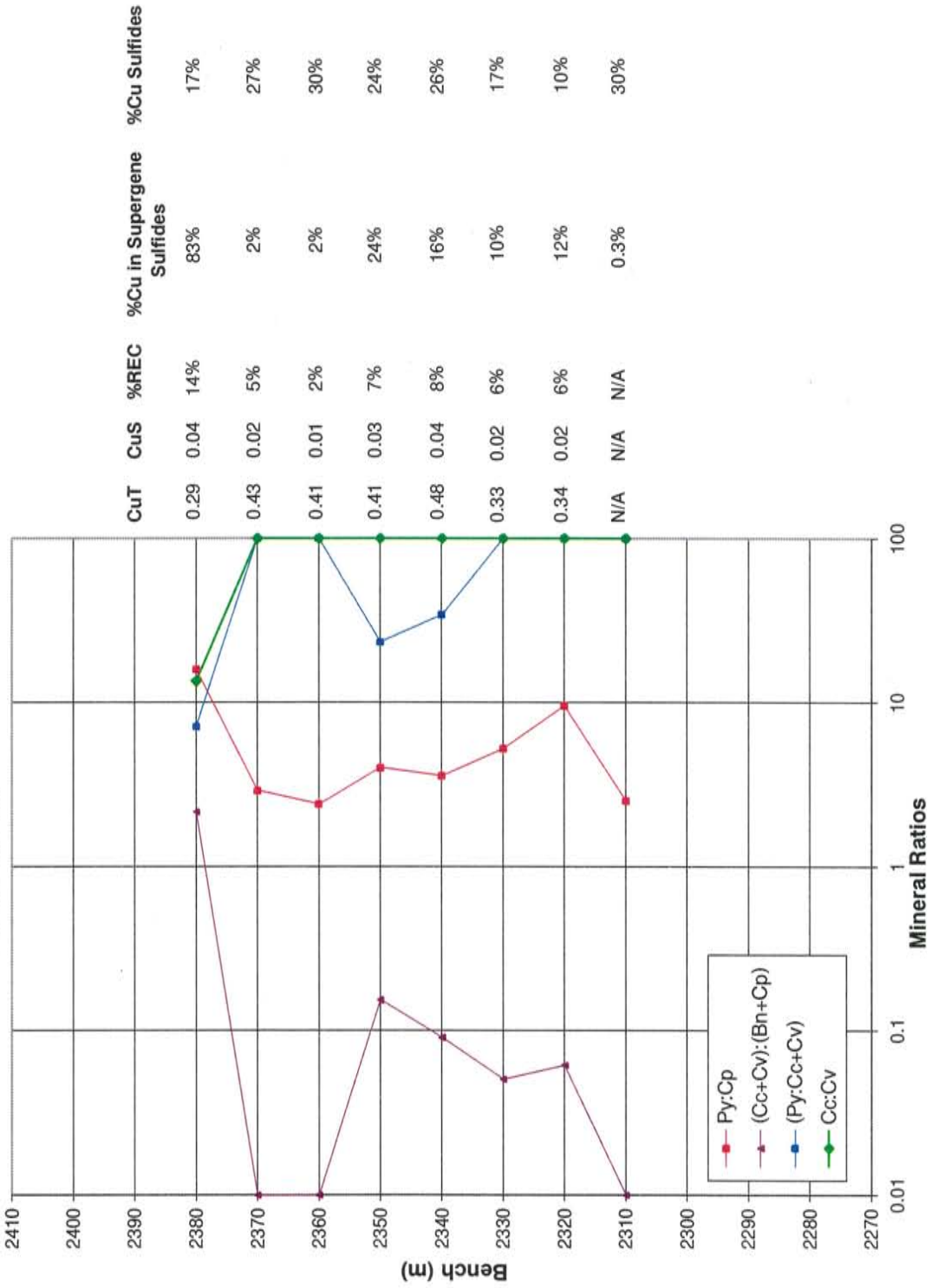
DDH-02-11



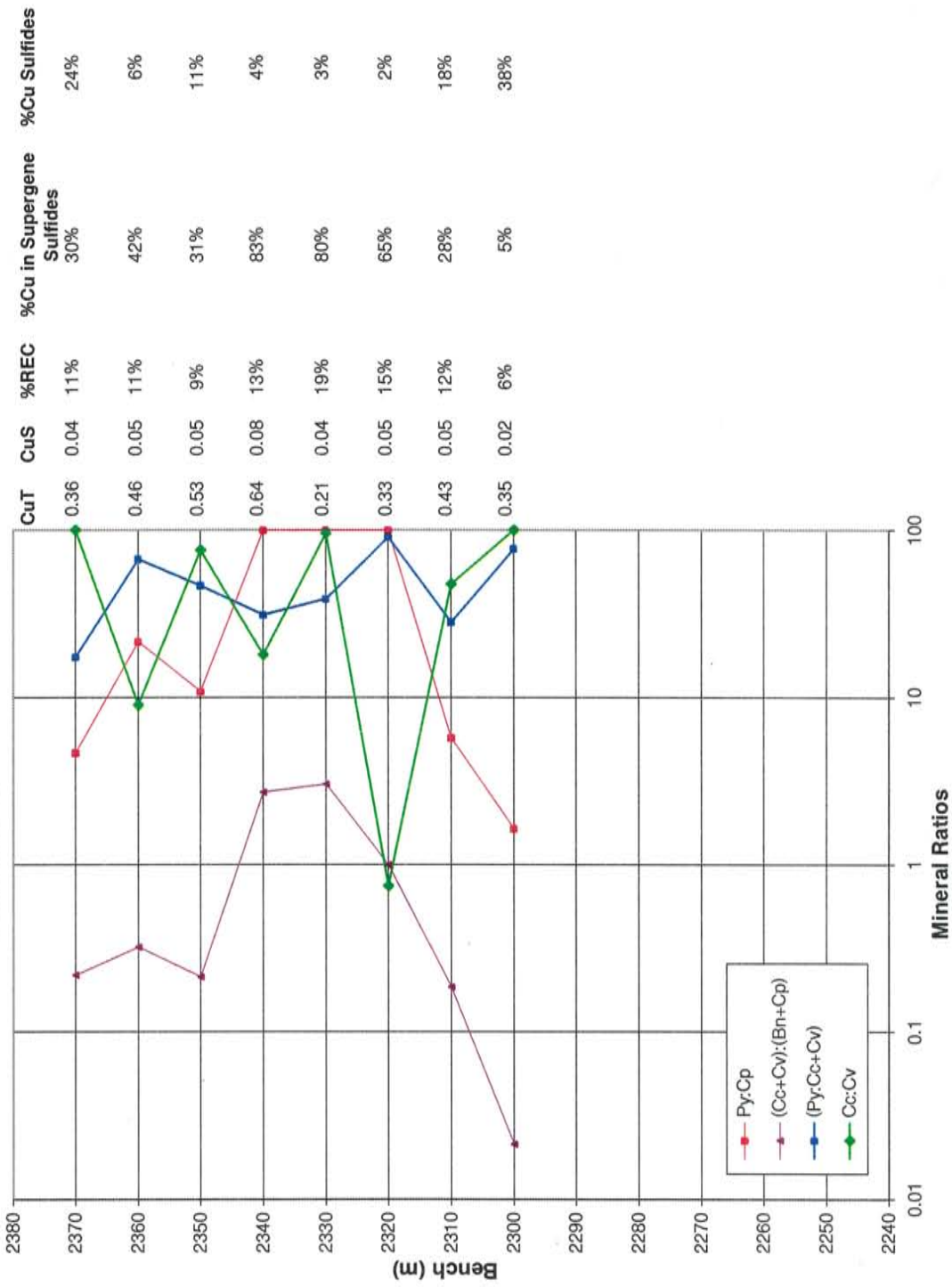
DDH-03-09



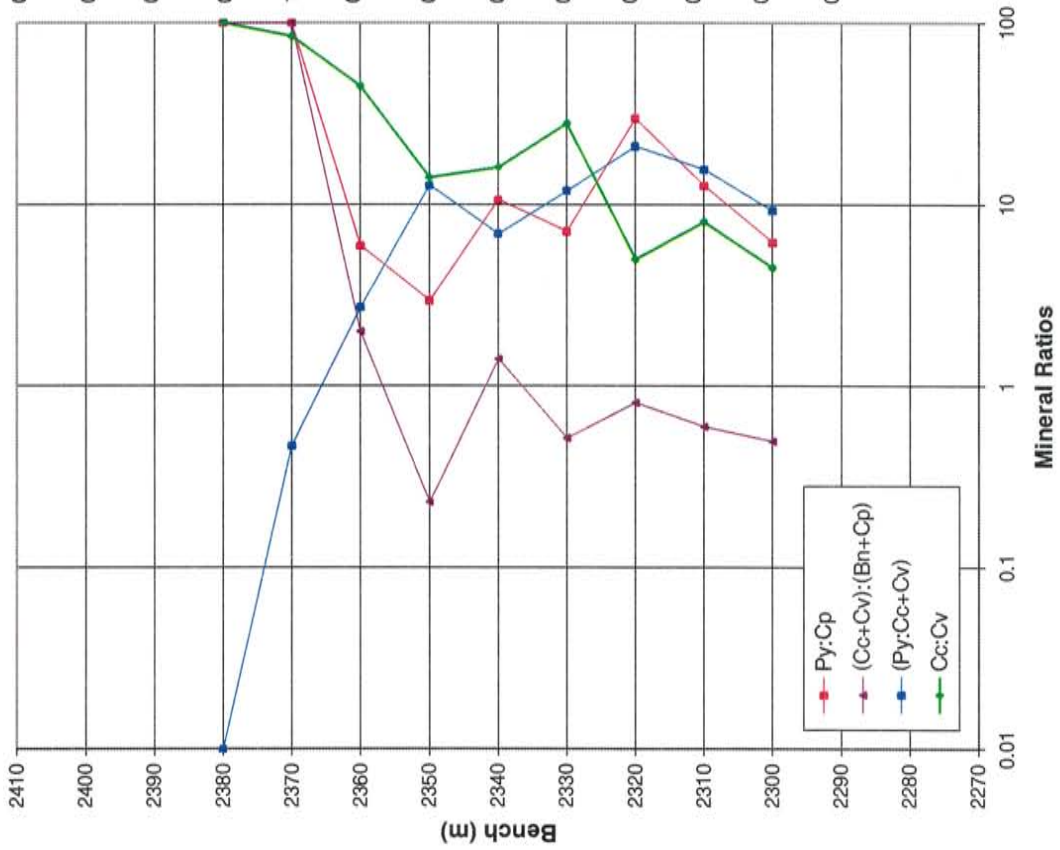
DDH-03-13



DDH-03-14

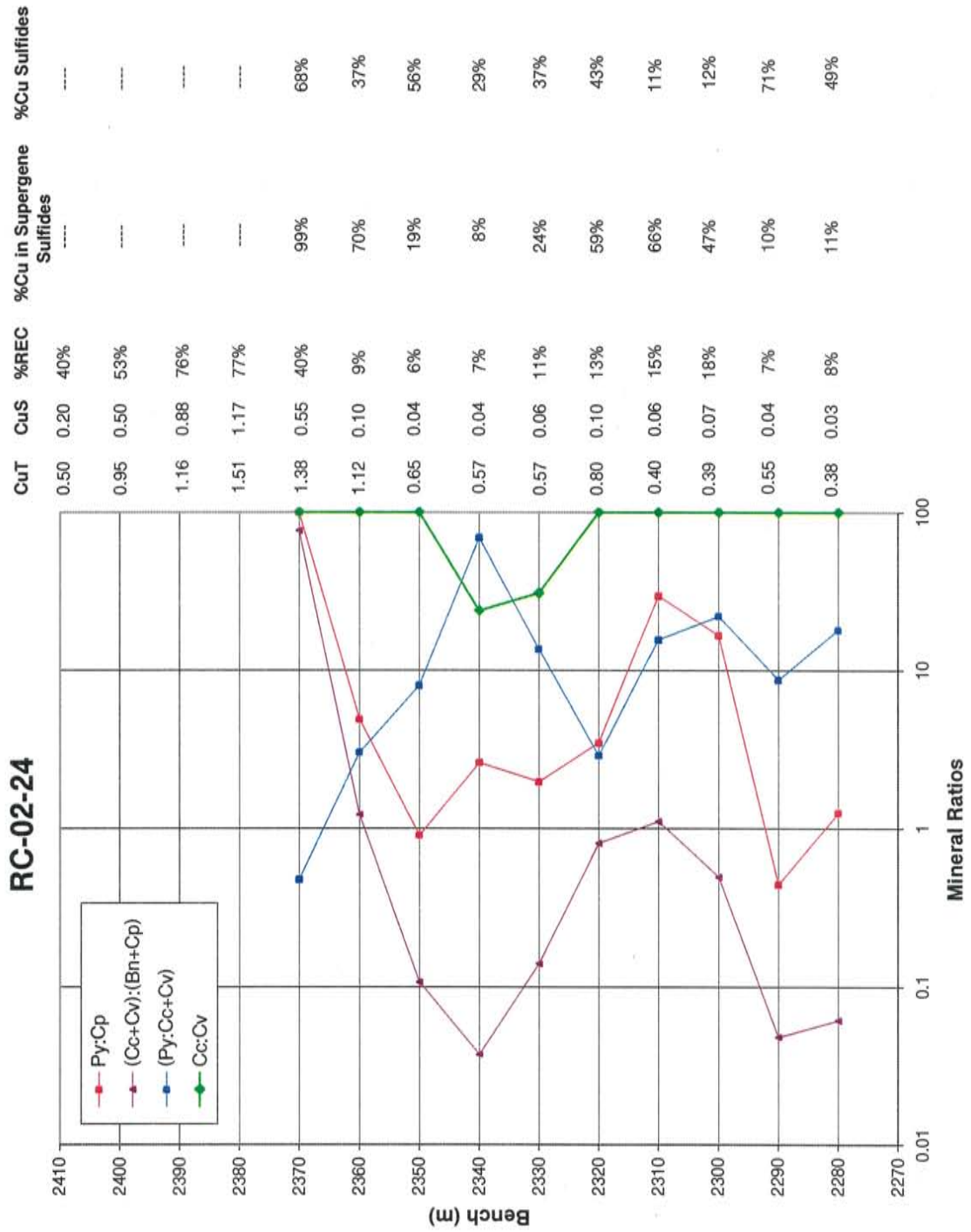


RC-02-21

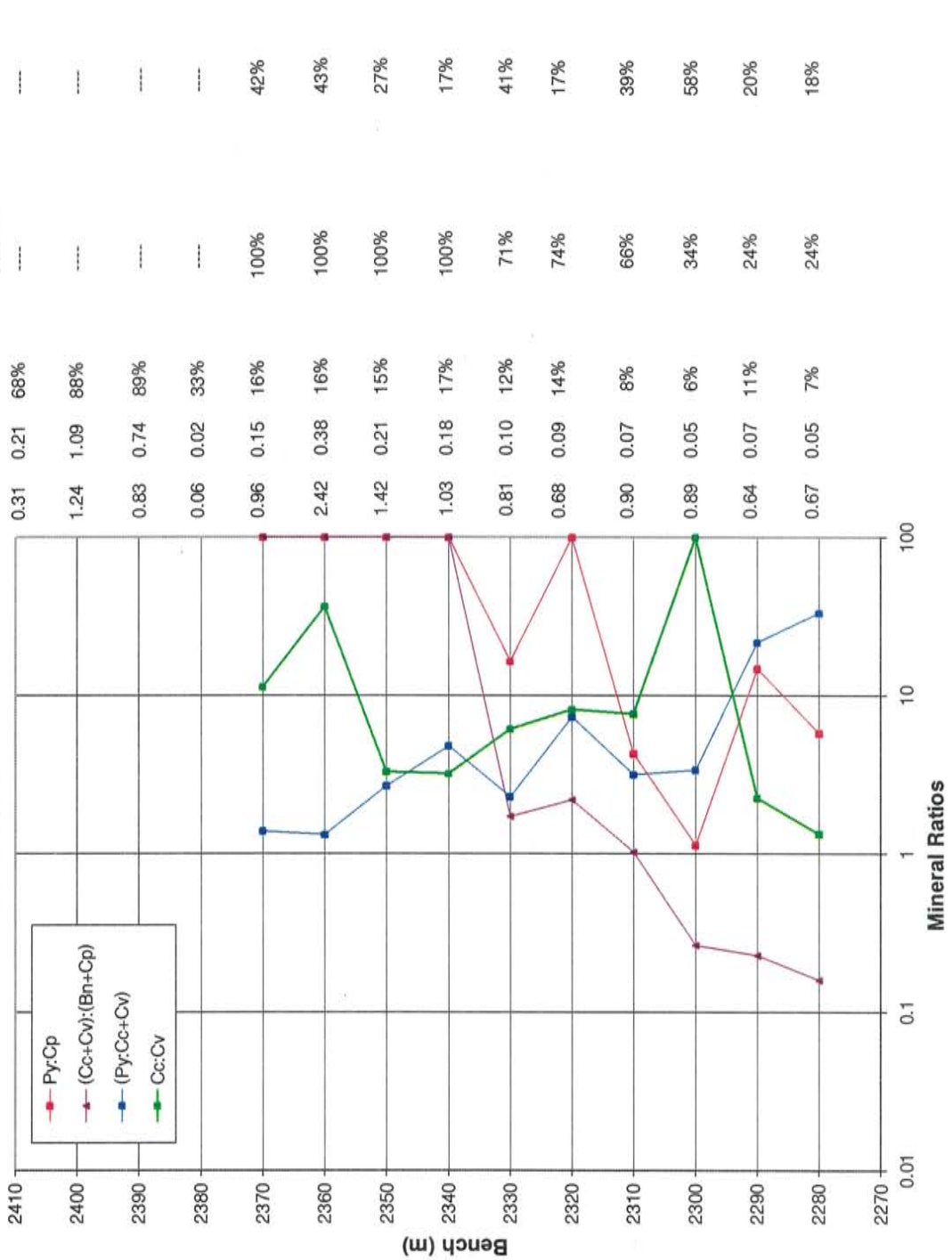


CuT	CuS	%REC	%Cu in Supergene Sulfides	%Cu Sulfides
0.19	0.13	68%	---	---
0.89	0.80	90%	---	---
0.59	0.54	92%	N/A	N/A
0.65	0.61	94%	100%	100%
1.25	1.09	87%	100%	68%
0.83	0.11	13%	81%	36%
0.52	0.04	8%	34%	30%
0.55	0.04	7%	75%	20%
0.51	0.04	8%	51%	20%
0.42	0.05	12%	57%	10%
0.66	0.06	10%	53%	15%
0.61	0.06	10%	48%	25%
0.38	0.05	13%	---	---

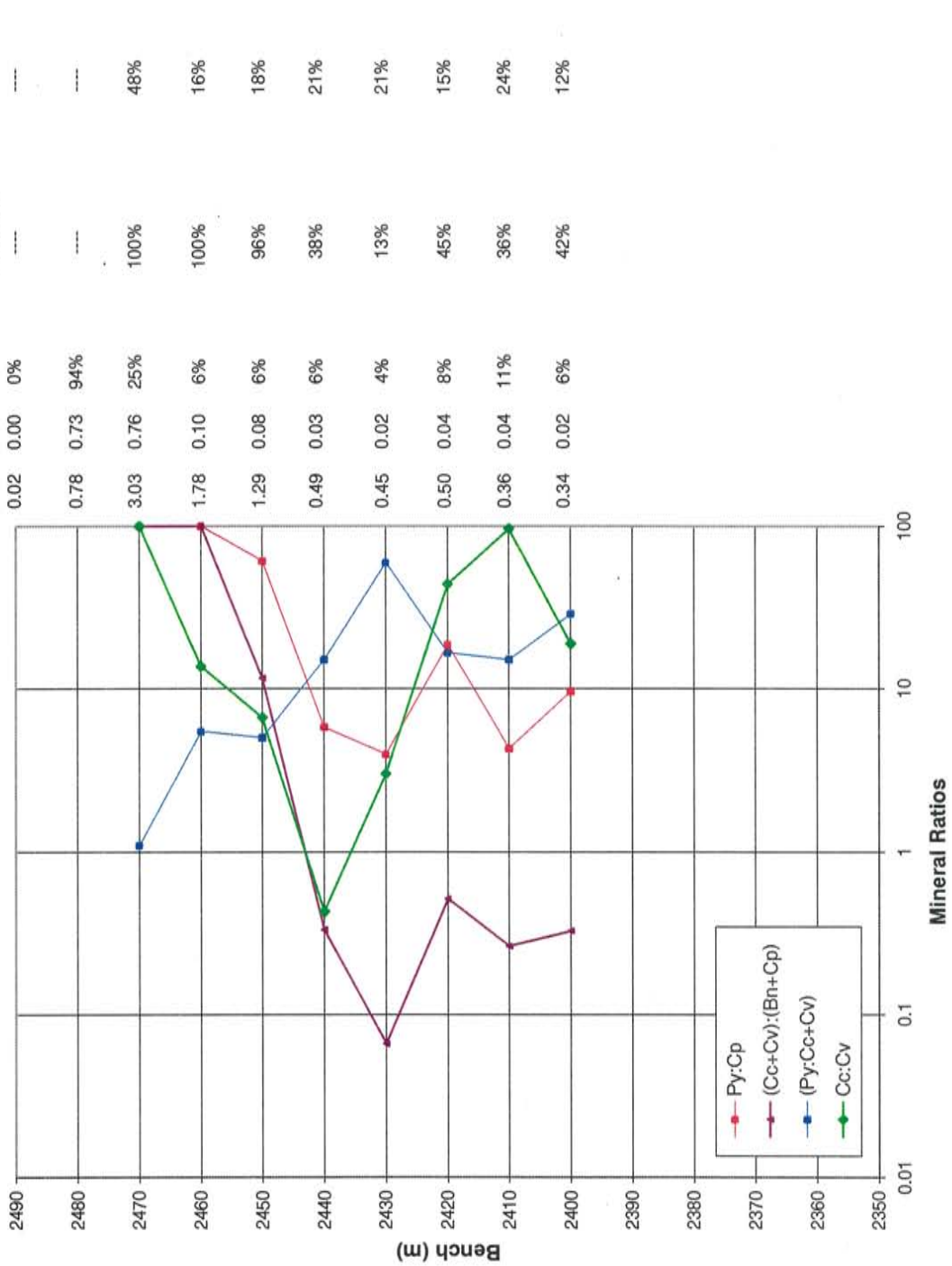
RC-02-24



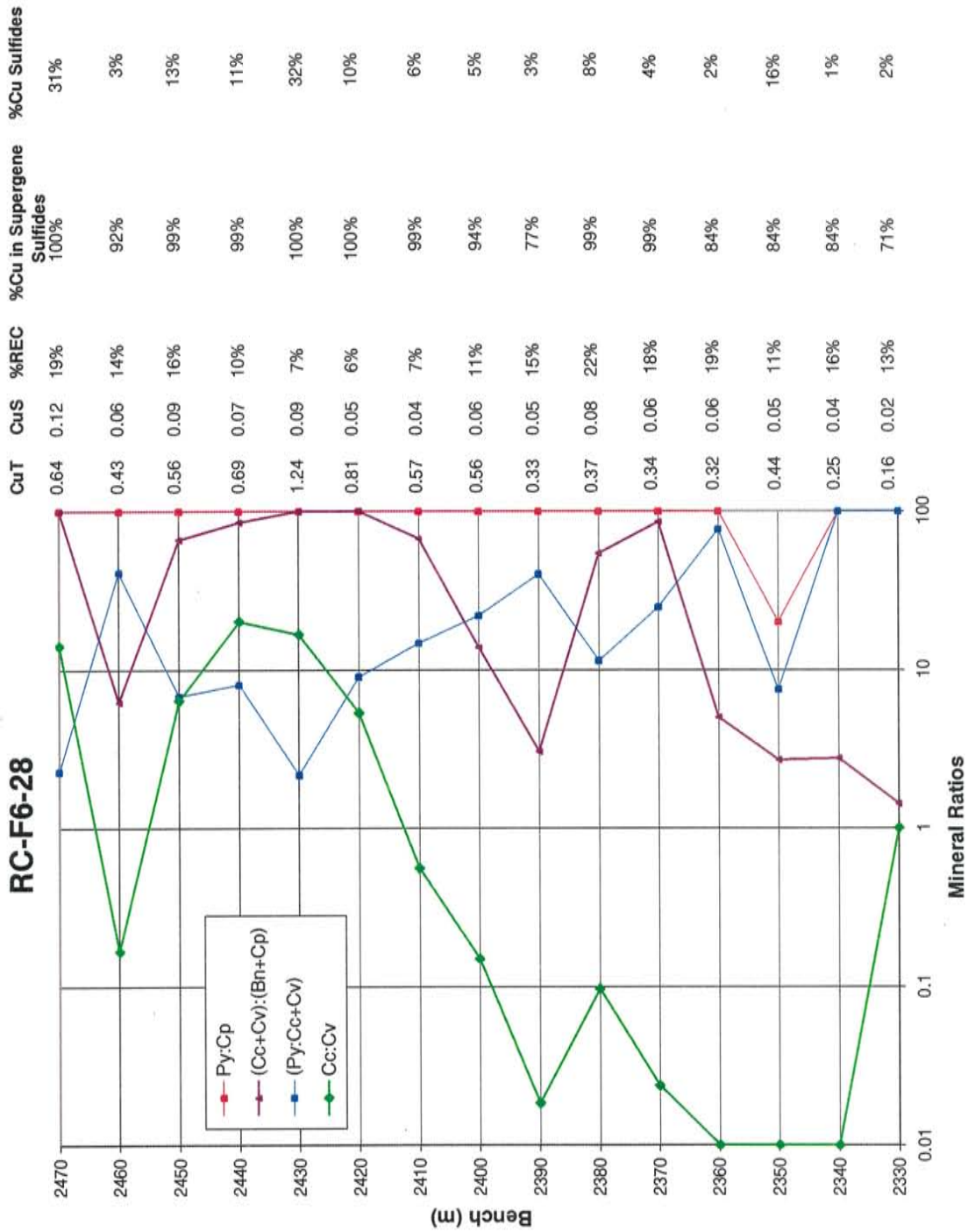
RC-02-30



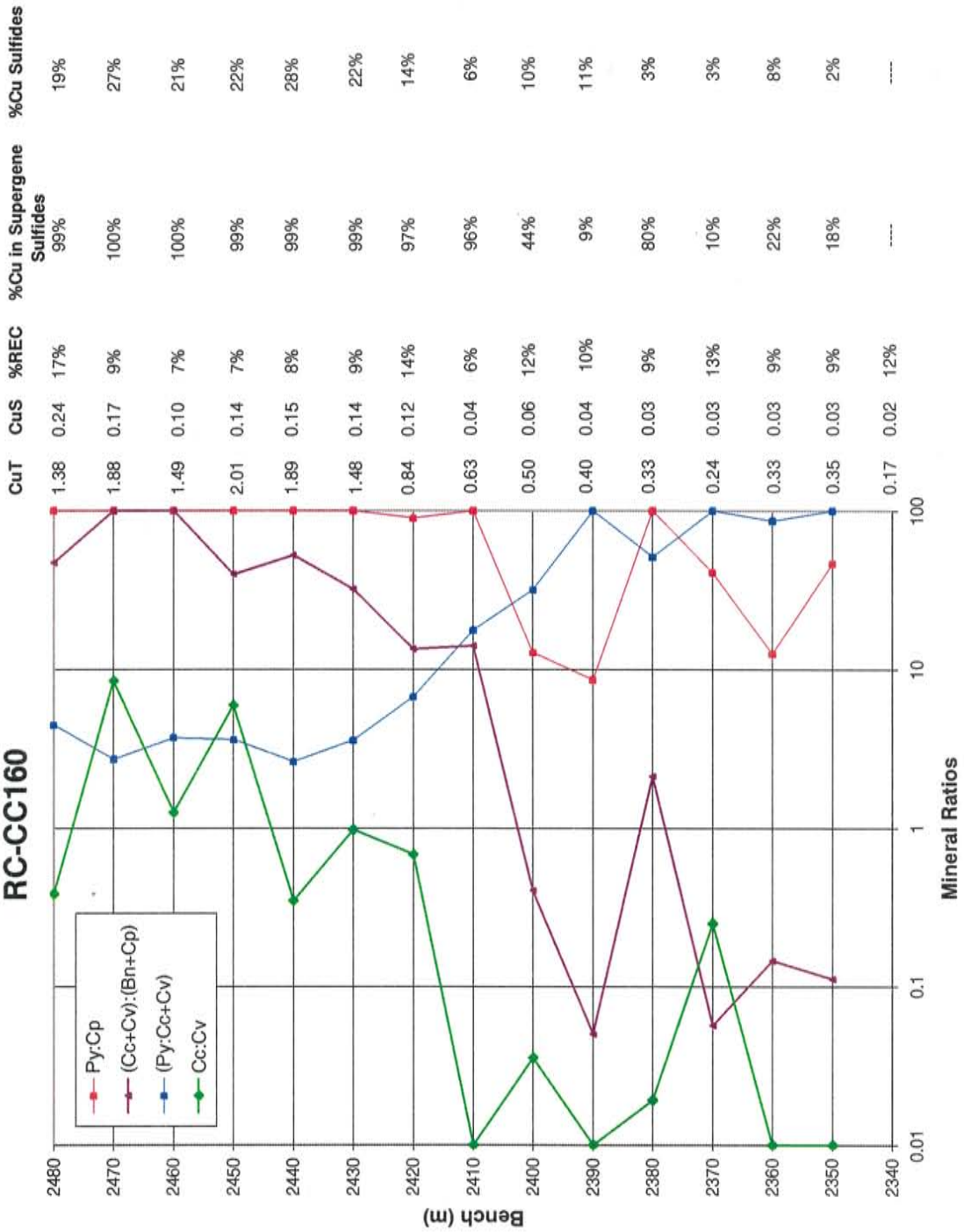
RC-F6-17



RC-F6-28



RC-CC160

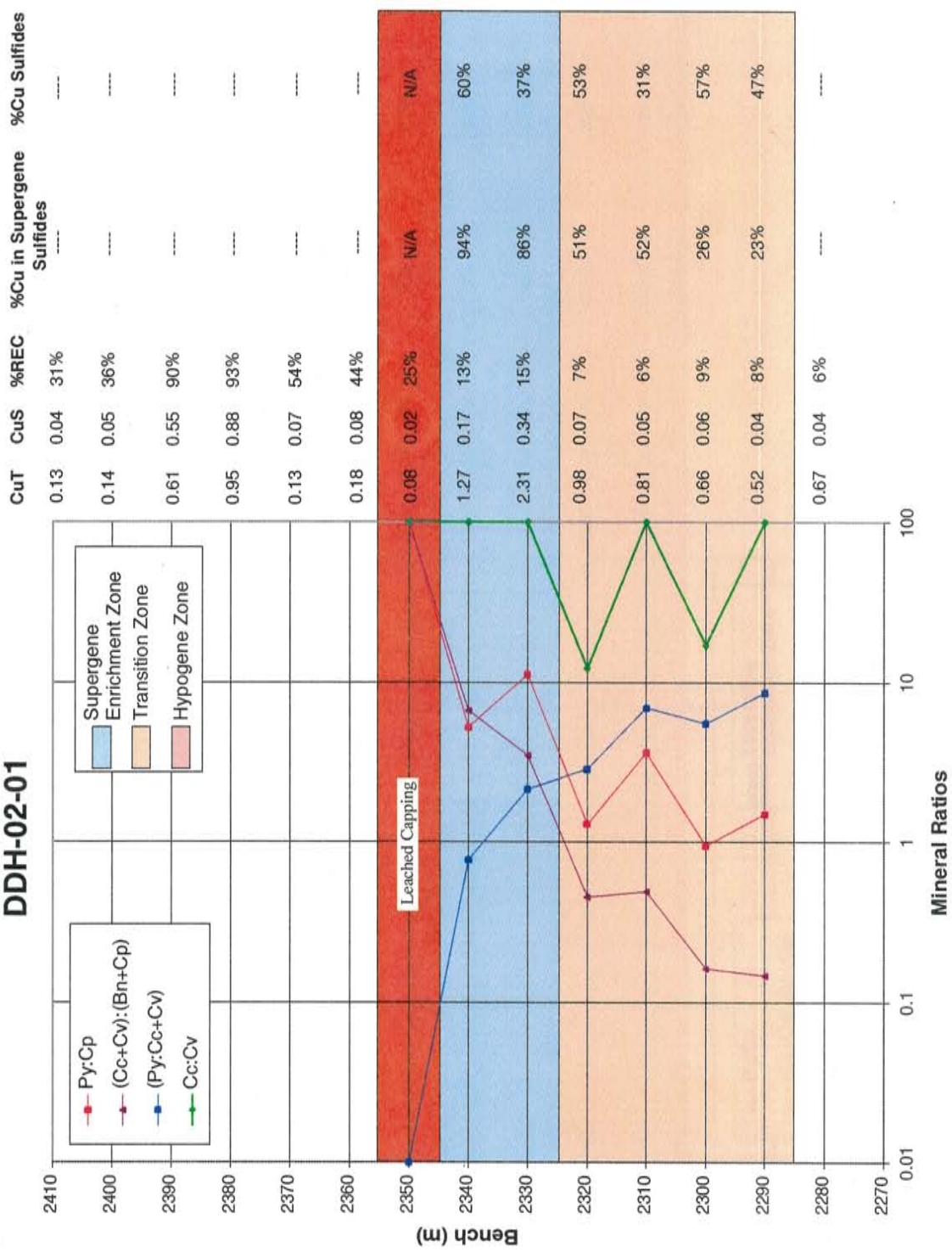


APPENDIX B

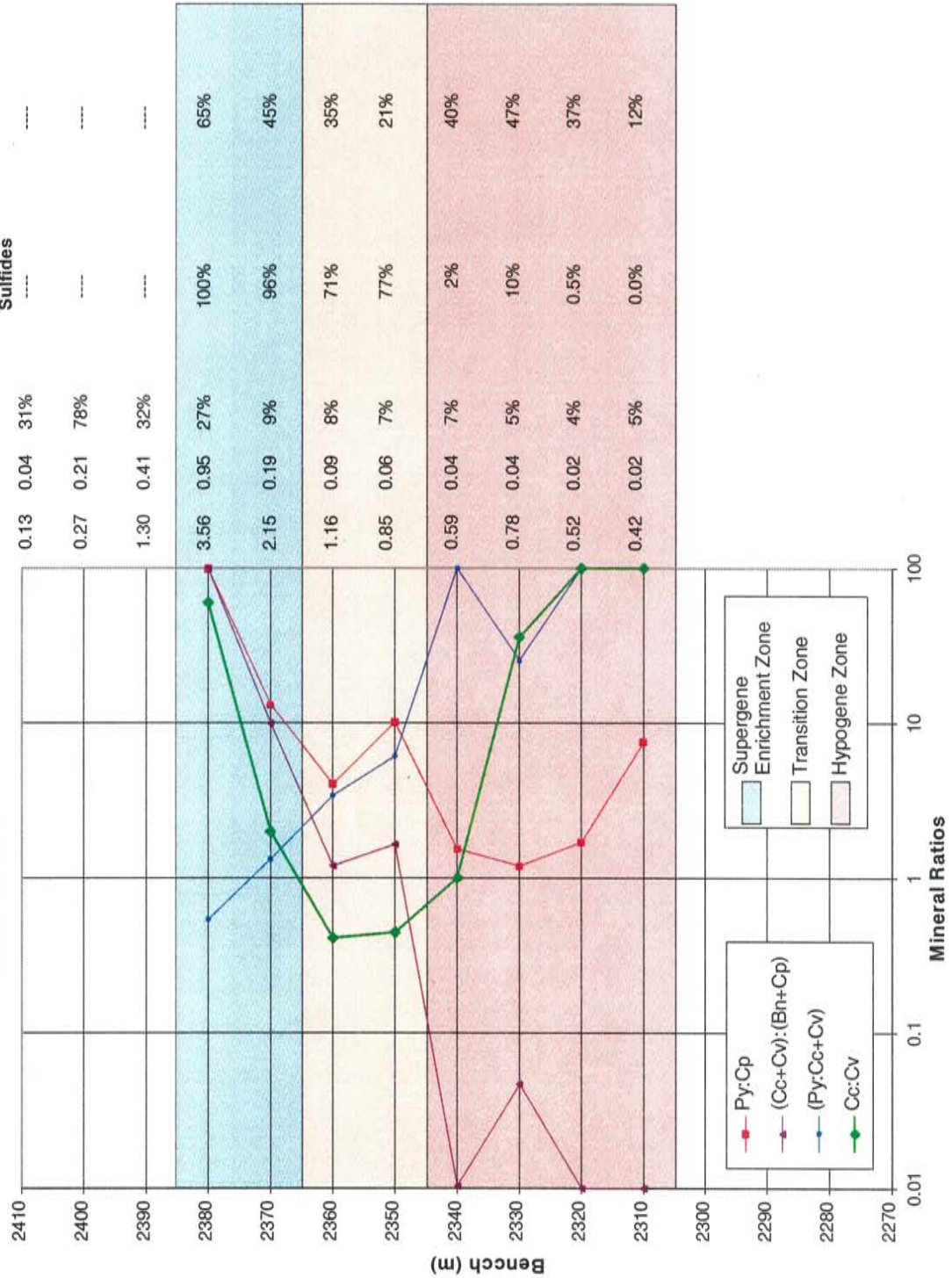
Interpreted mineral ratio diagrams for the below mentioned drill holes illustrating the relationship between the selected mineral ratios, percent copper in supergene sulfides, and the relative percent copper sulfides to the interpreted mineral zones.

Drill Holes: DDH-02-01, DDH-02-03, DDH-02-04, DDH-02-08, DDH-02-11, DDH-03-09, DDH-03-13, DDH-03-14, RC-02-21, RC-02-24, RC-02-30, RC-F6-17, RC-F6-28, and RC-CC160.

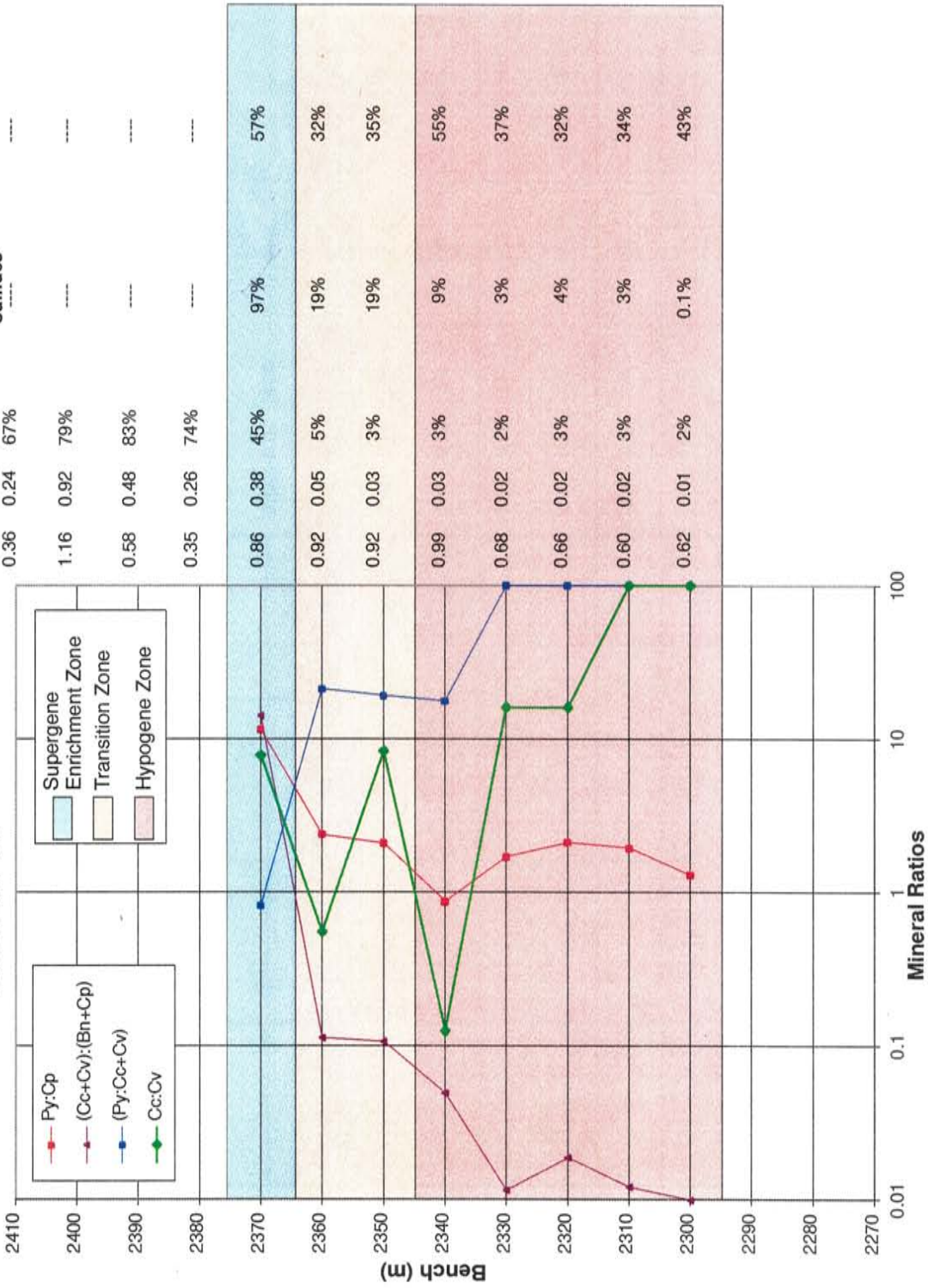
DDH-02-01



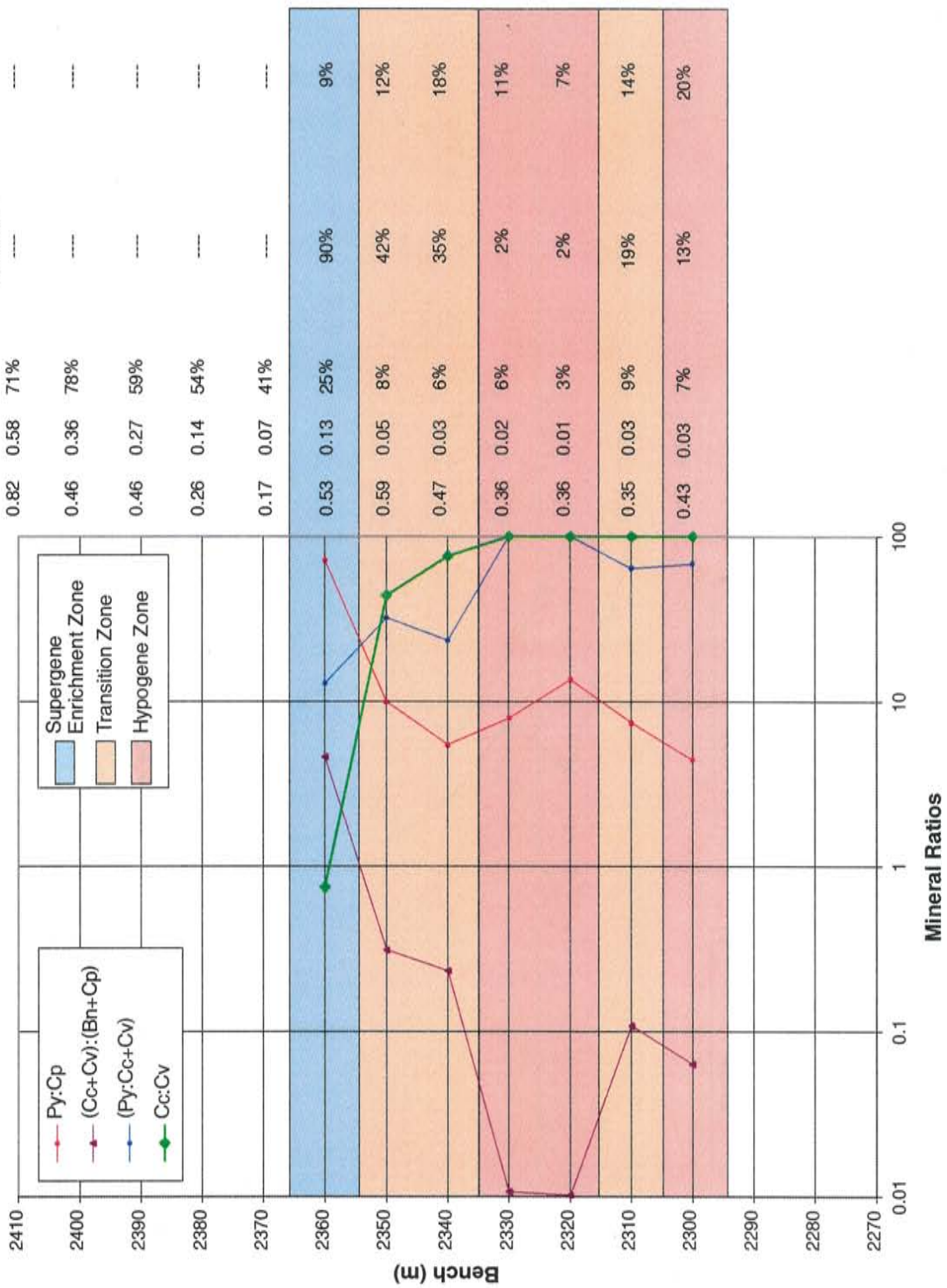
DDH-02-03



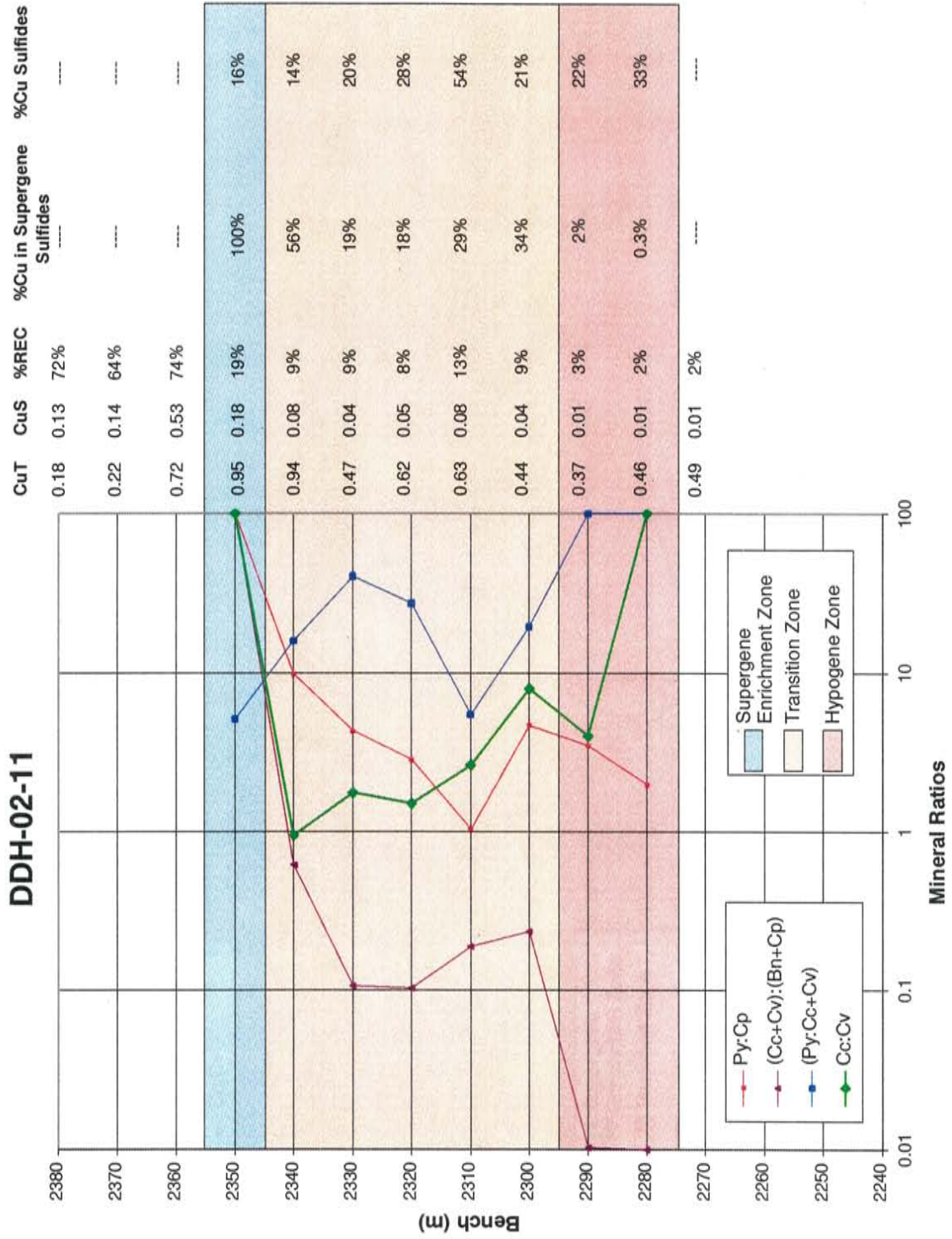
DDH-02-04



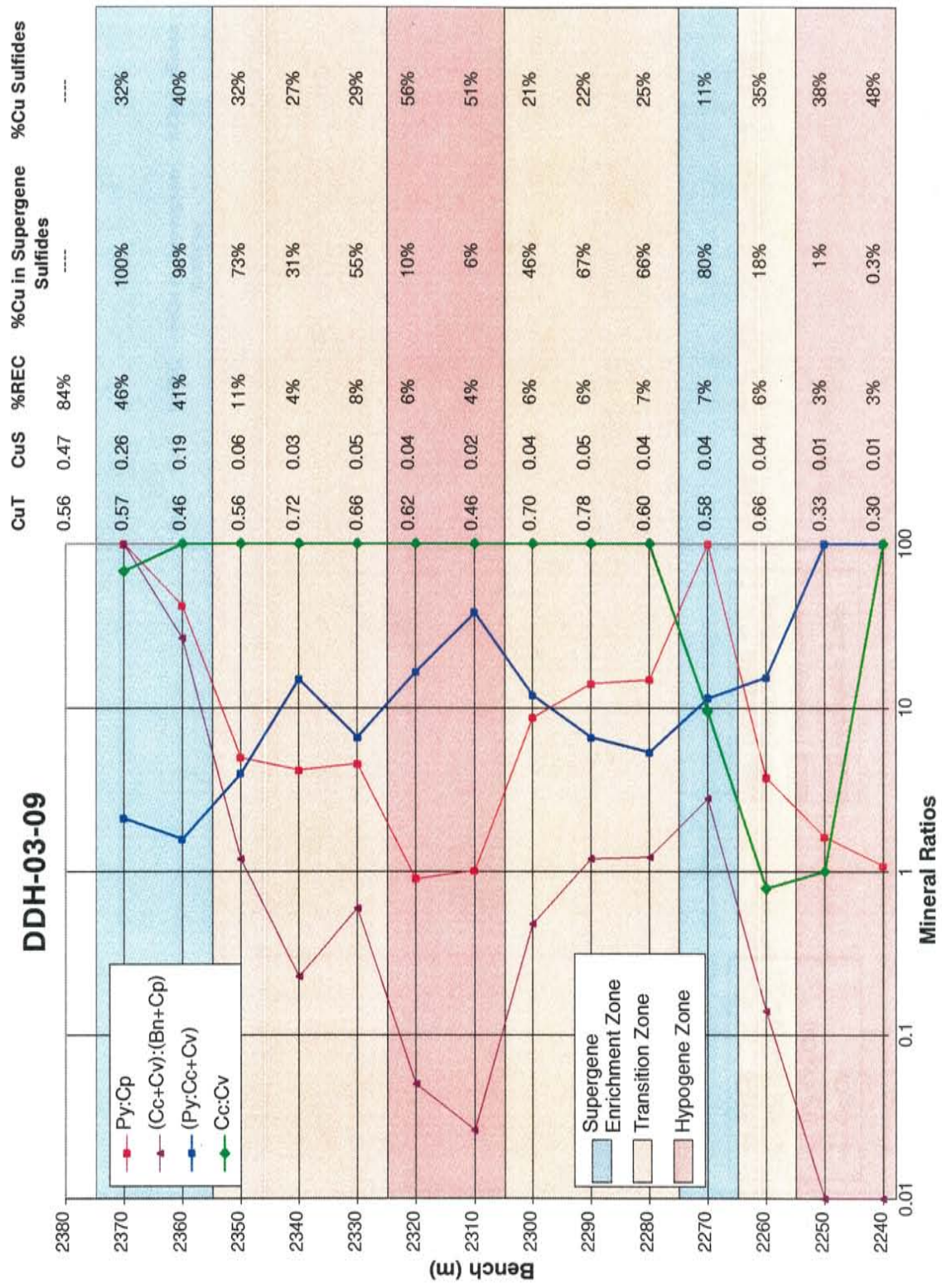
DDH-02-08



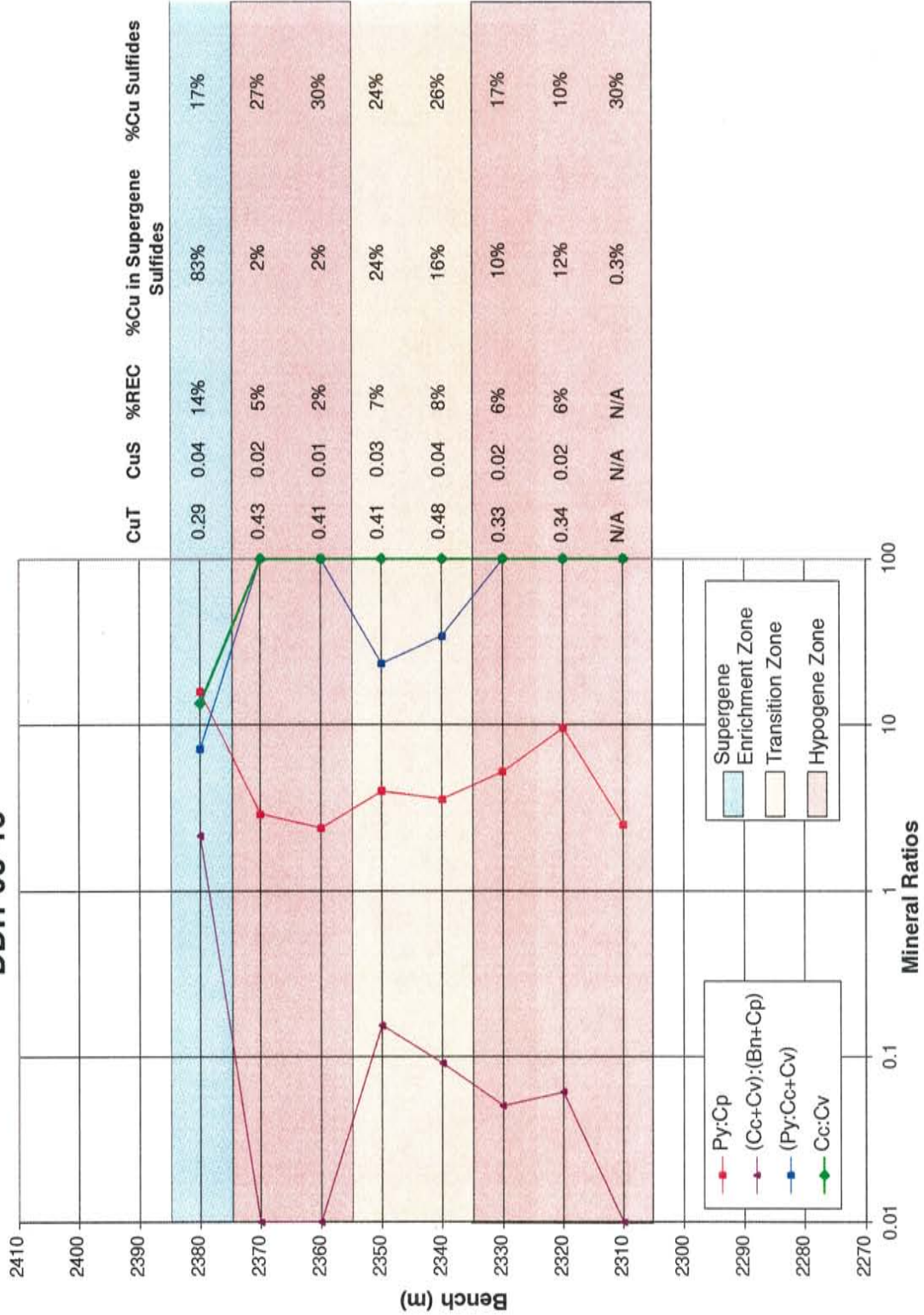
DDH-02-11



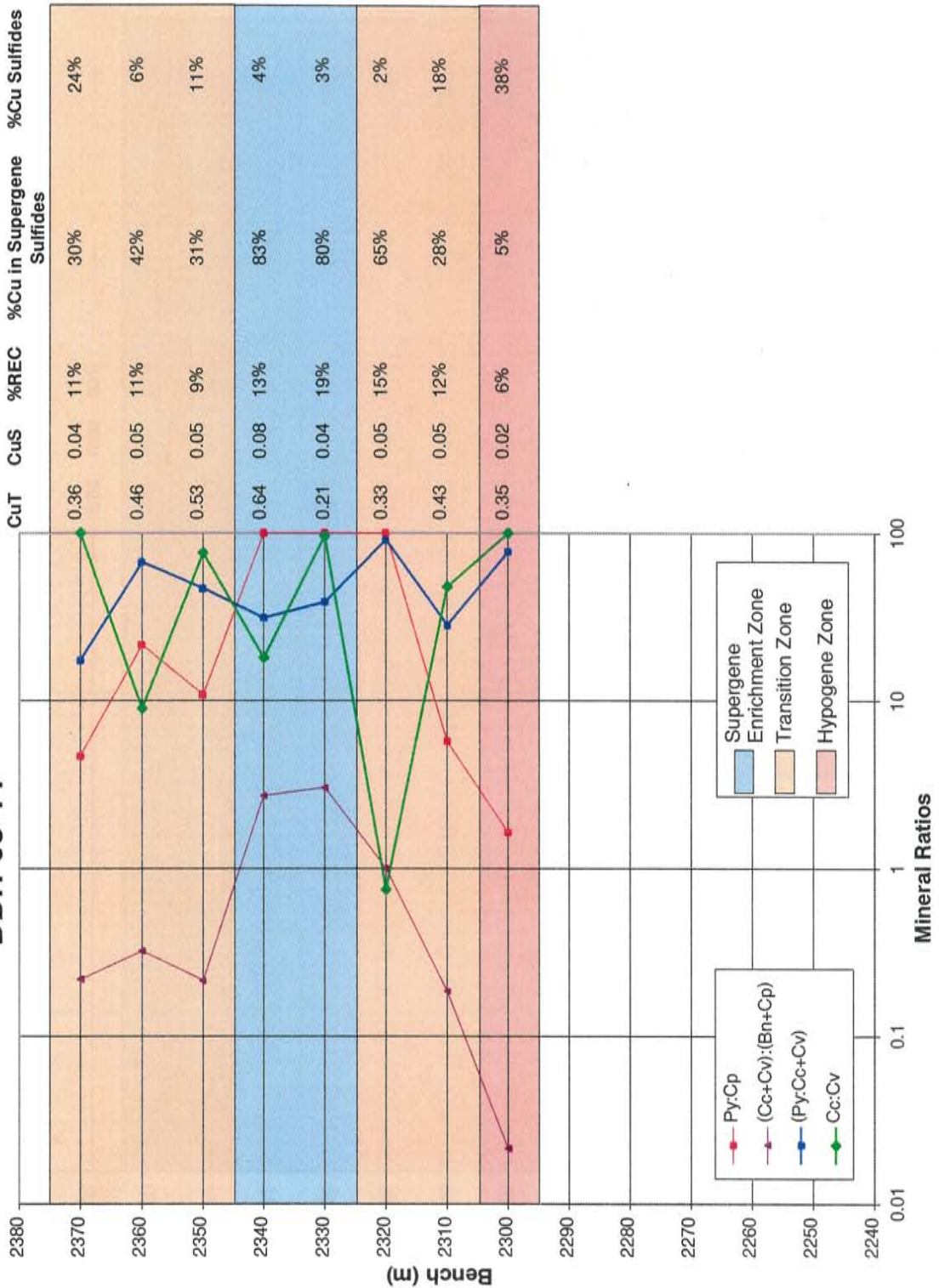
DDH-03-09



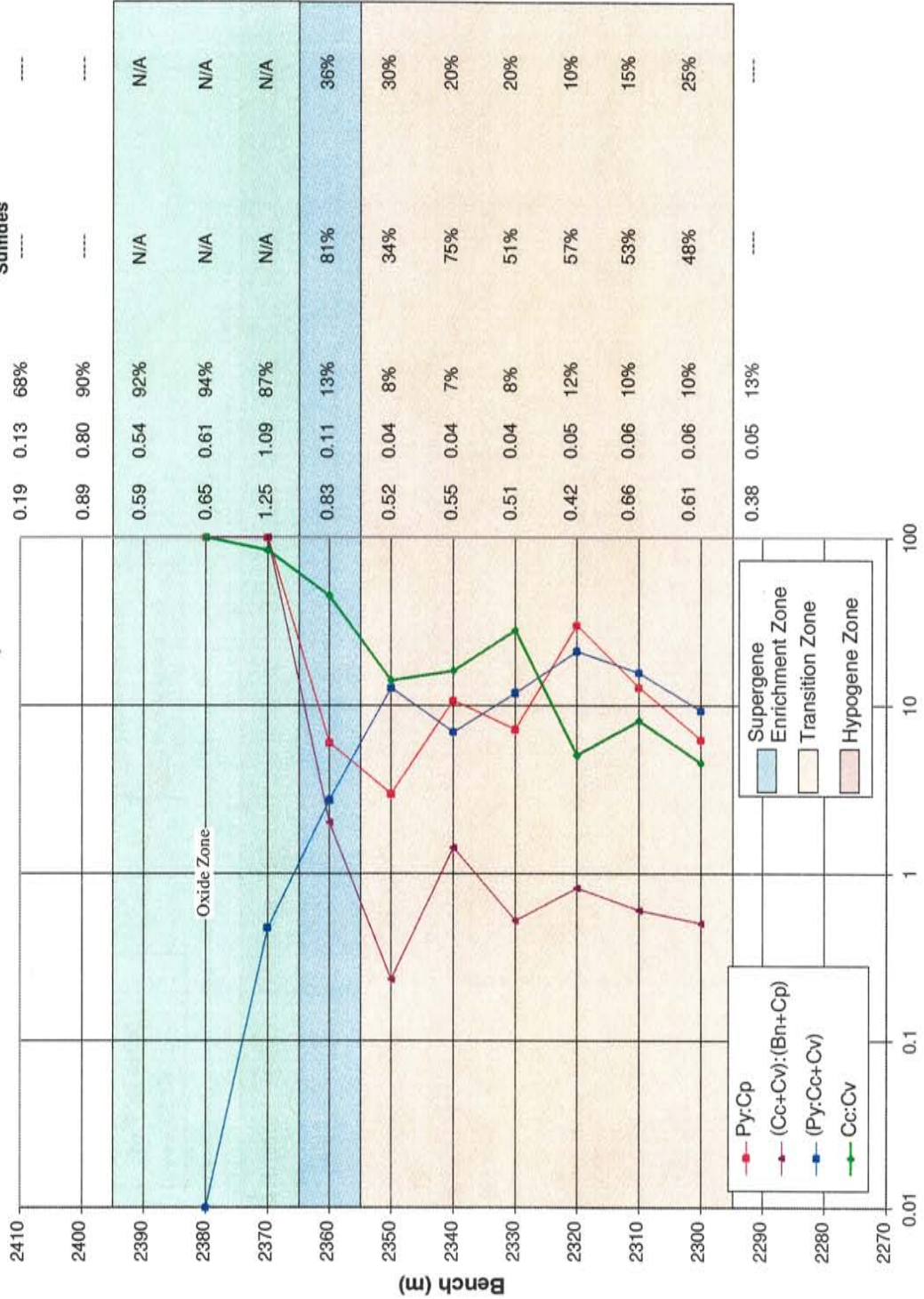
DDH-03-13



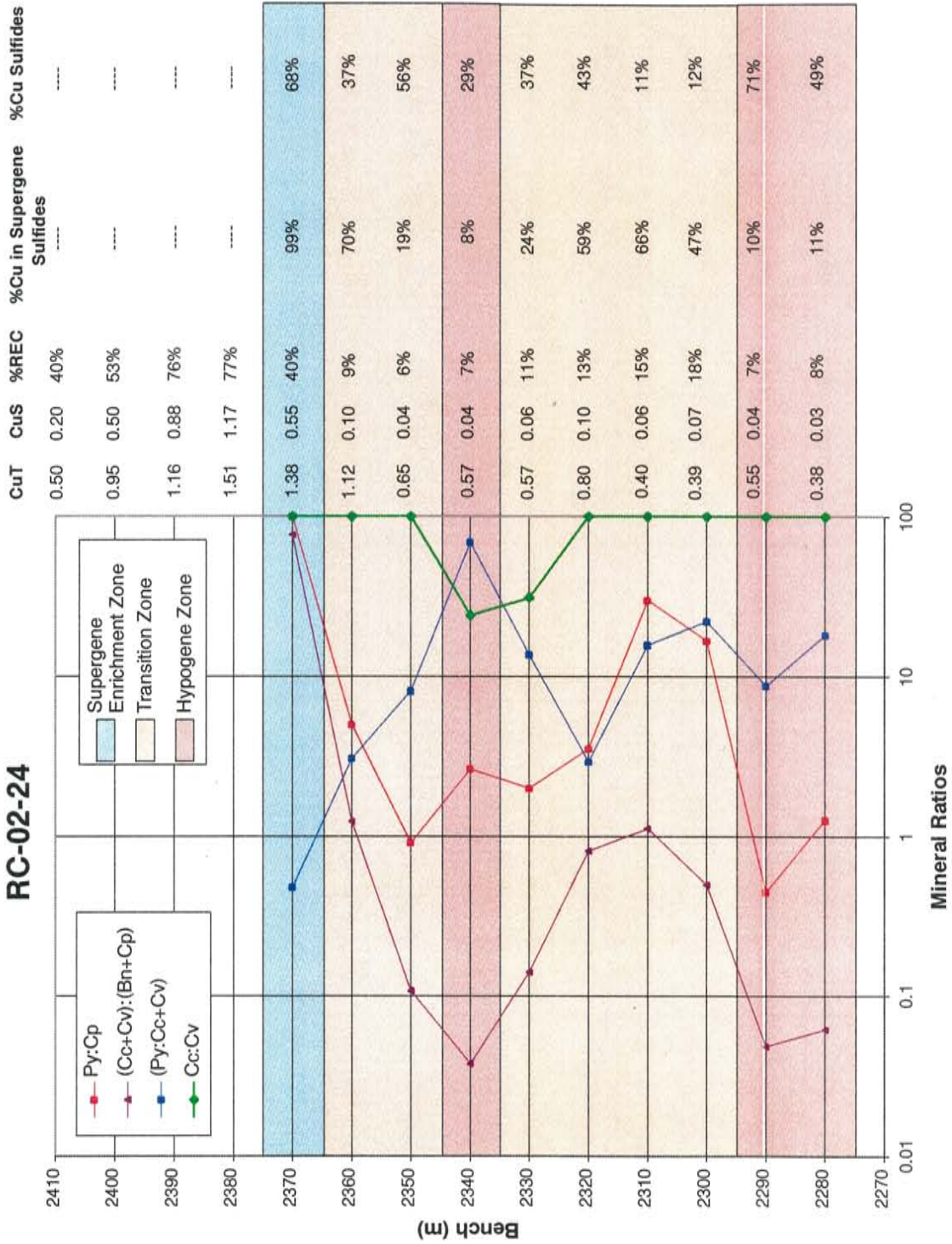
DDH-03-14



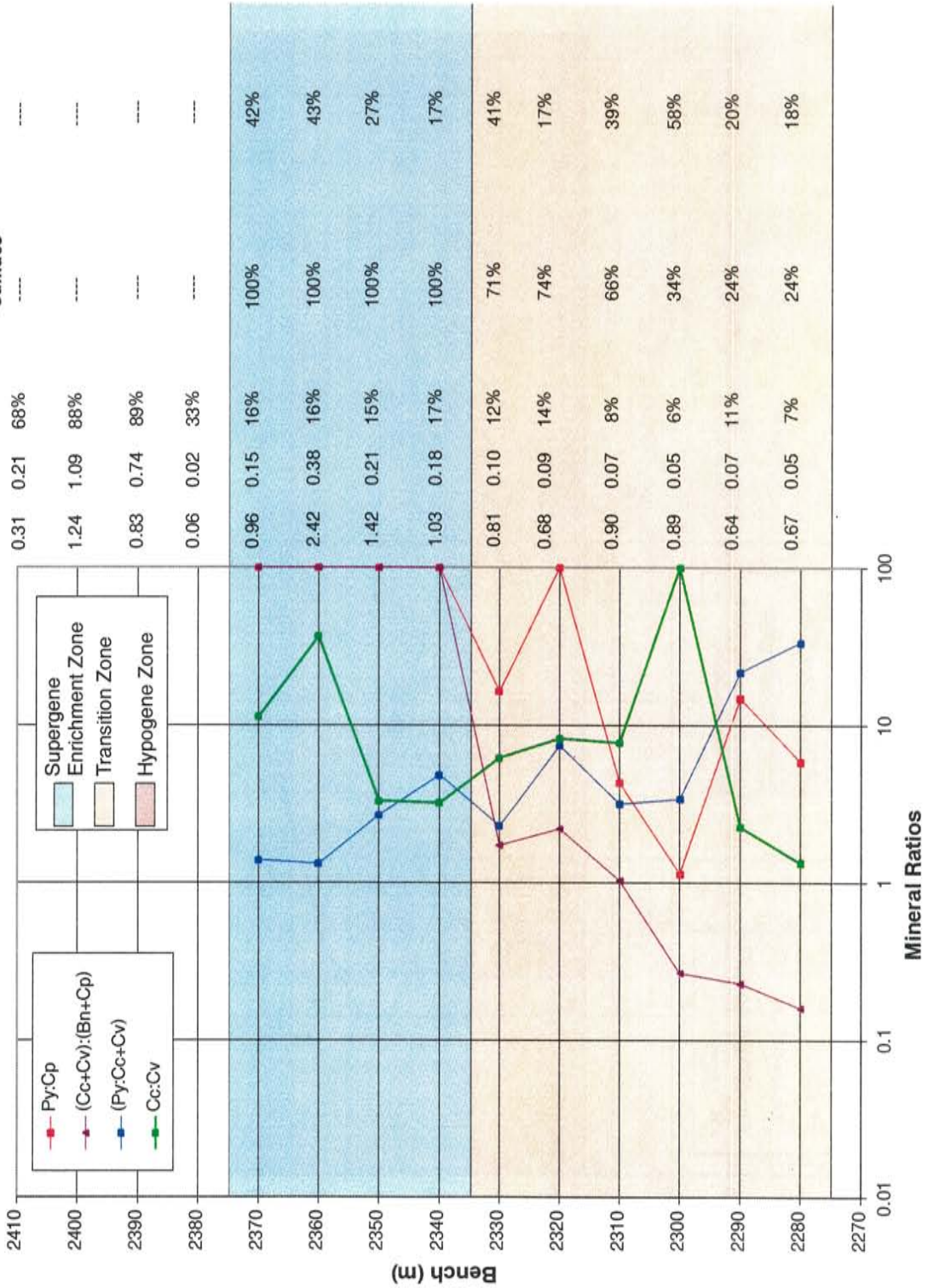
RC-02-21



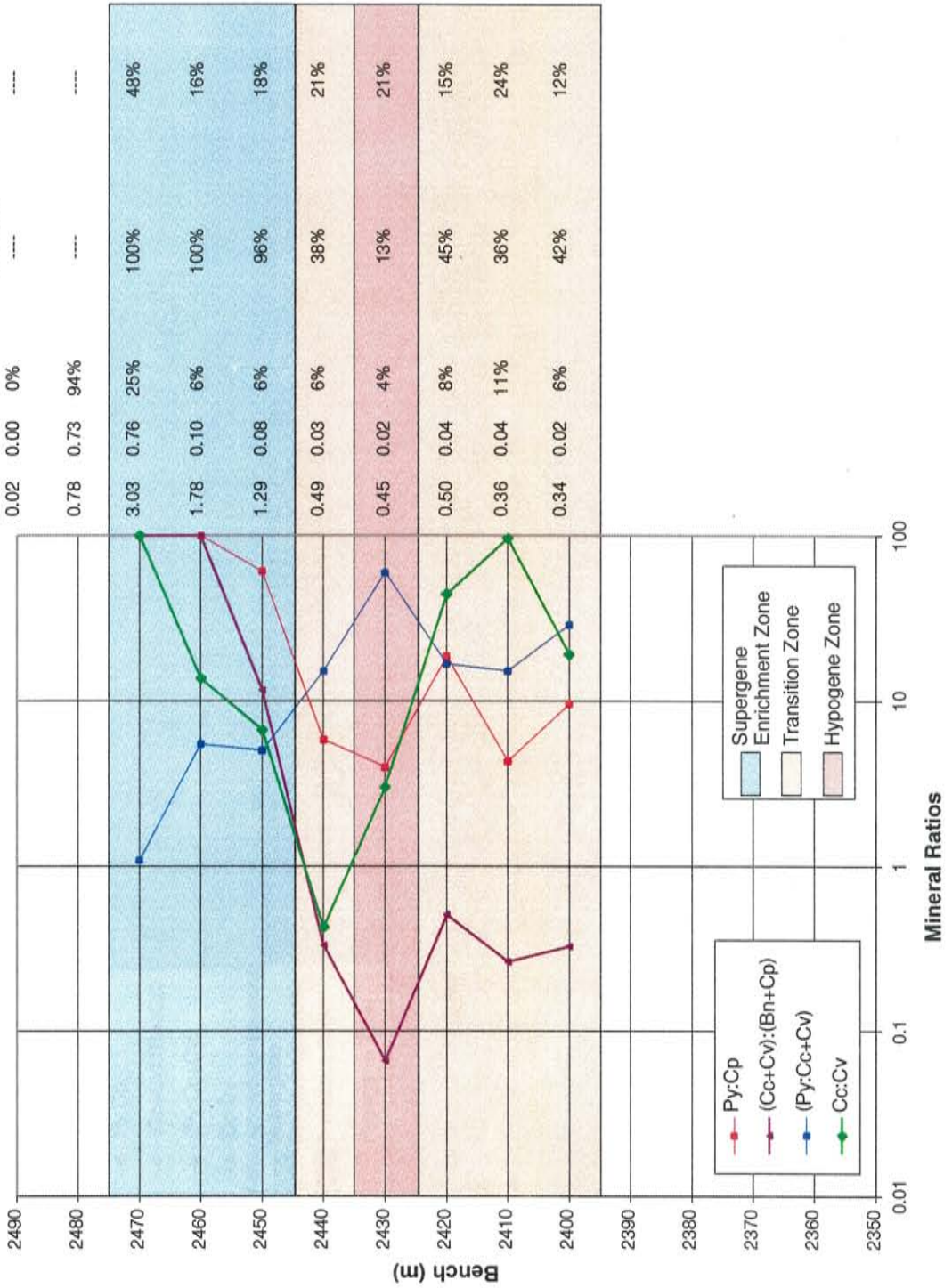
RC-02-24



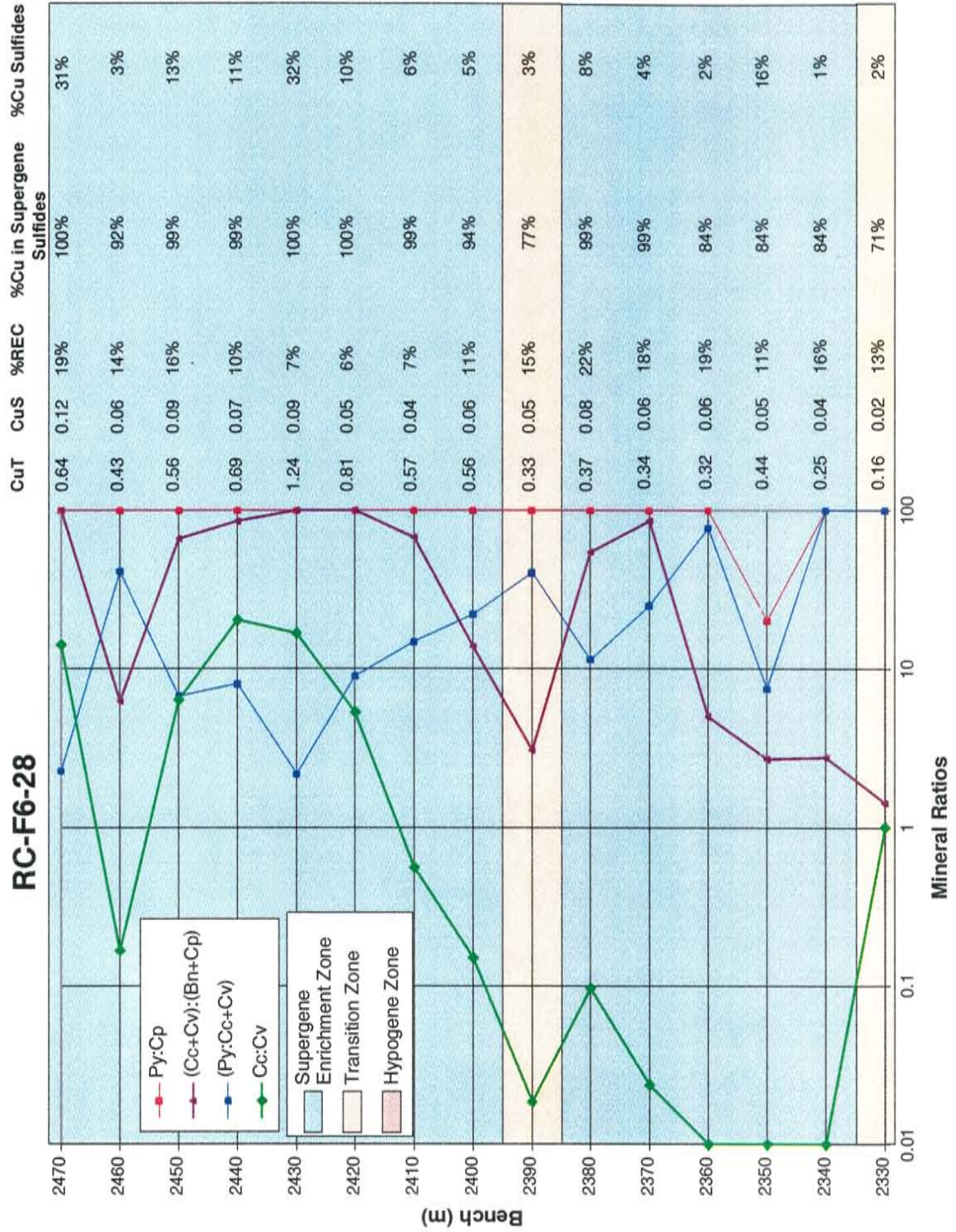
RC-02-30



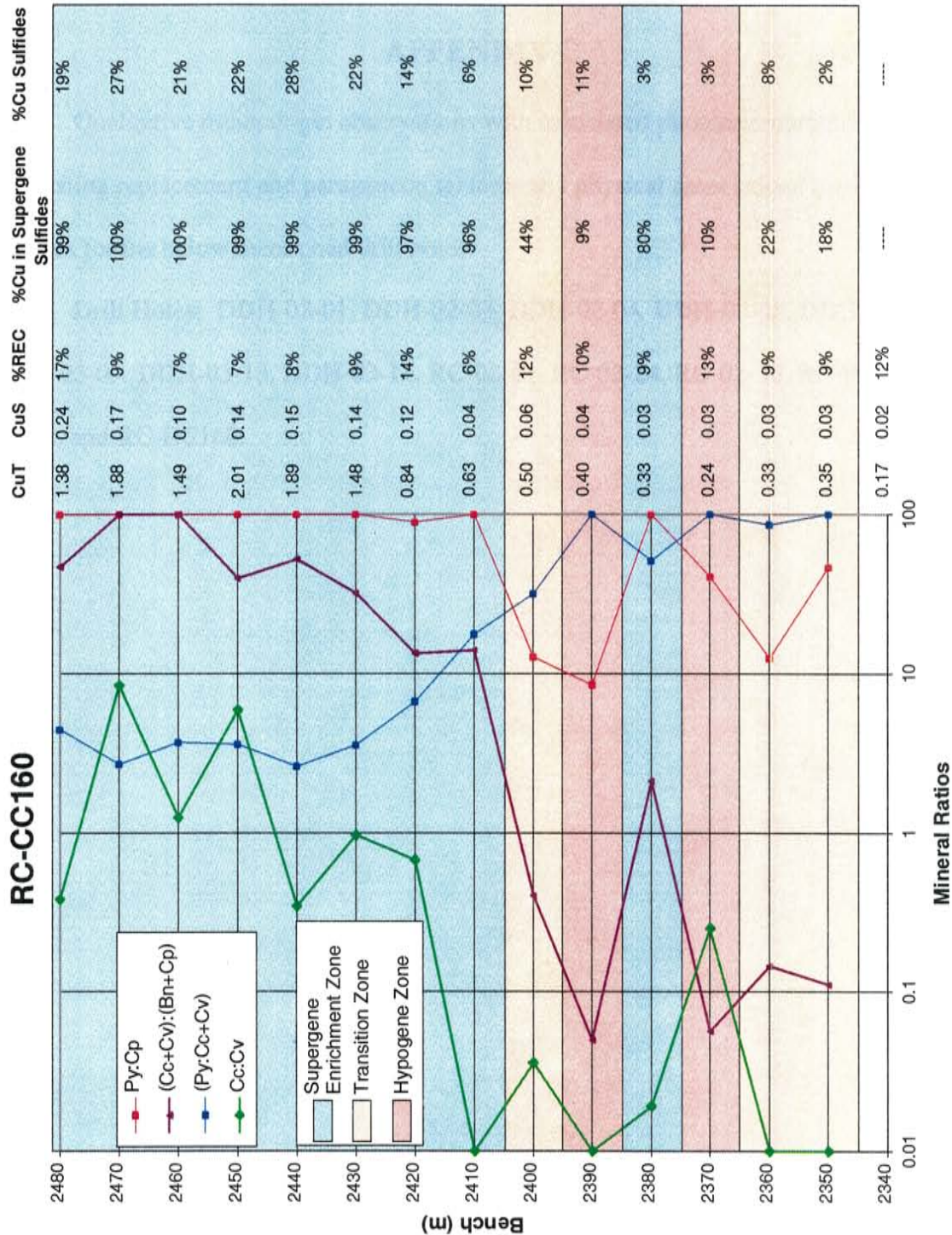
RC-F6-17



RC-F6-28



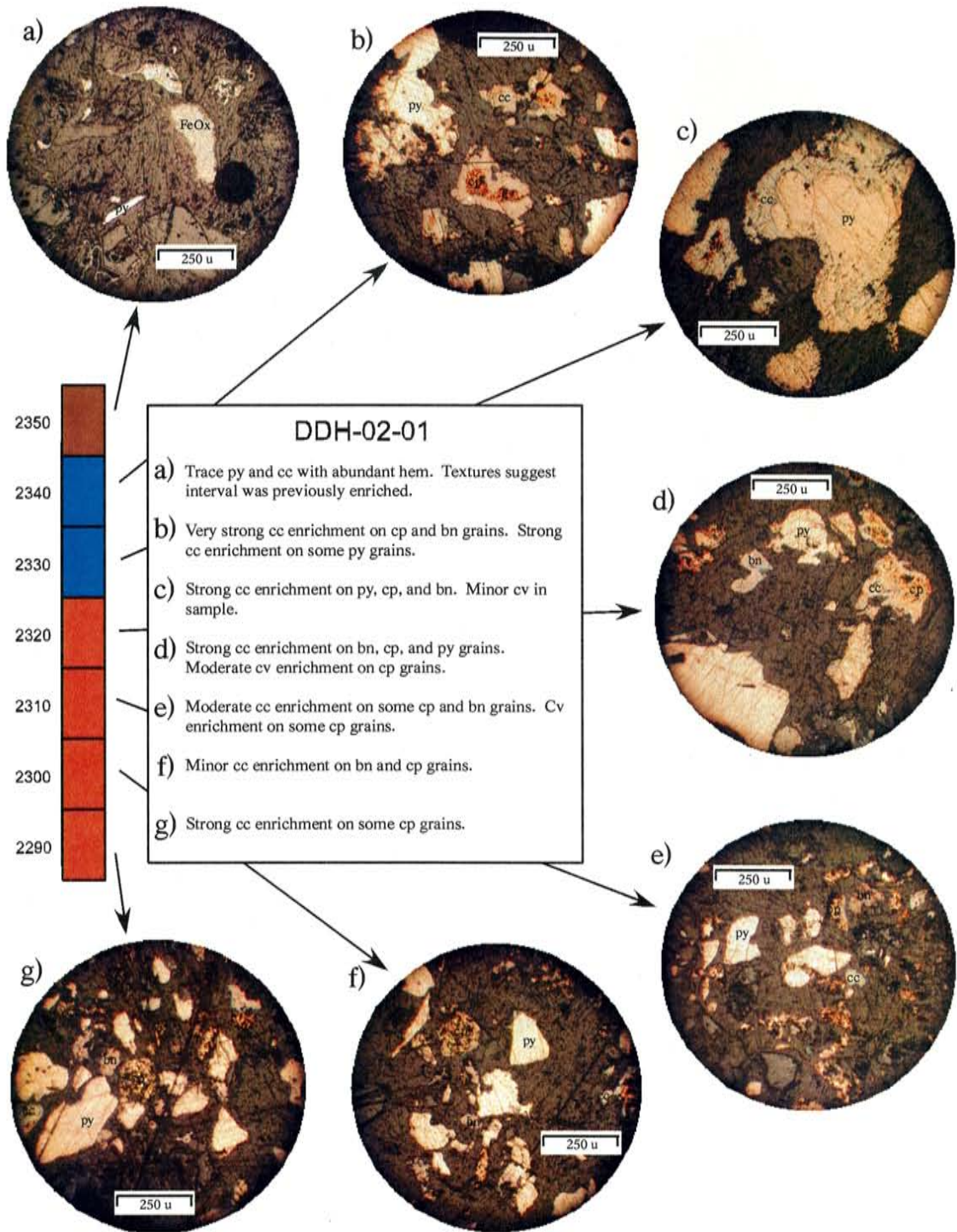
RC-CC160

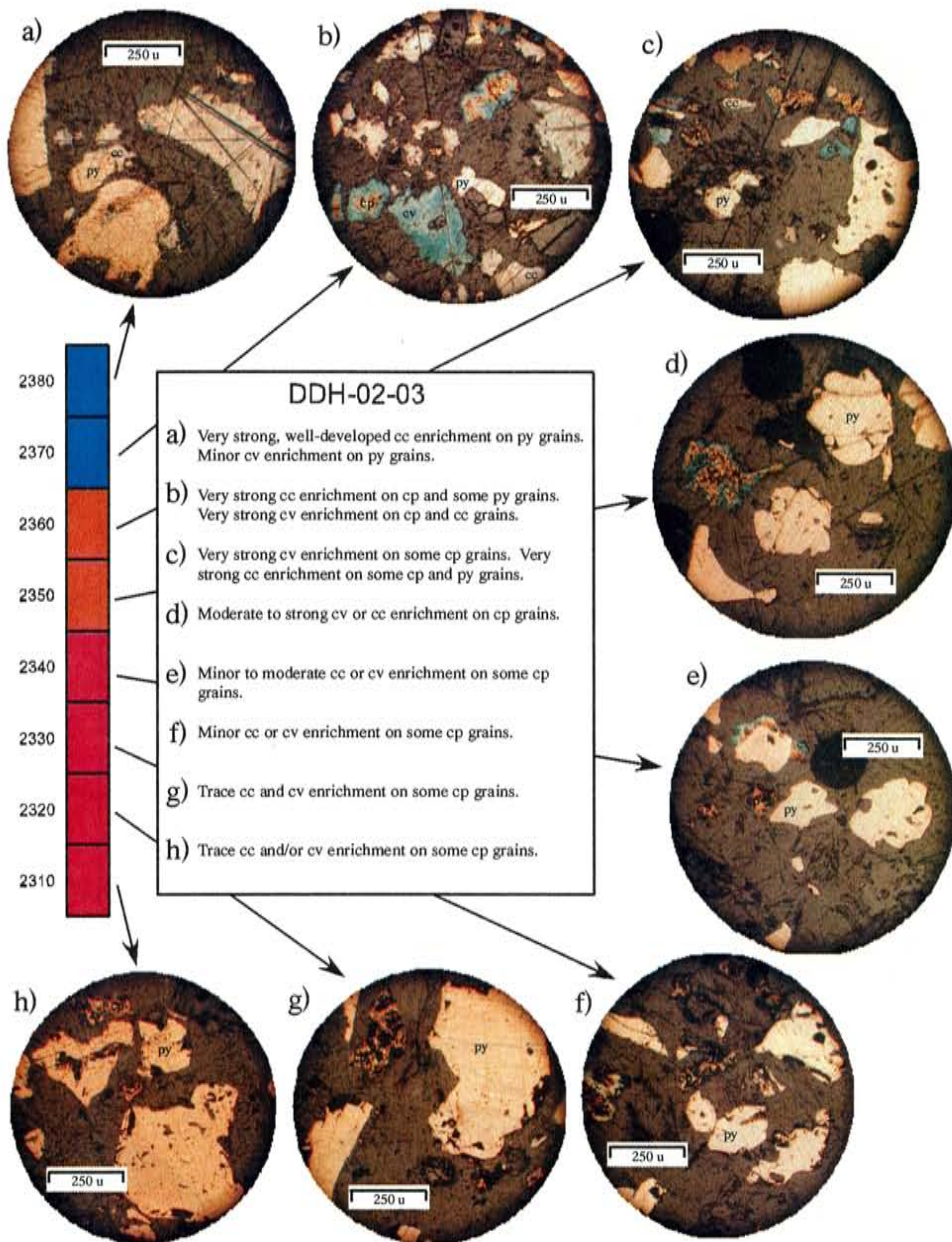


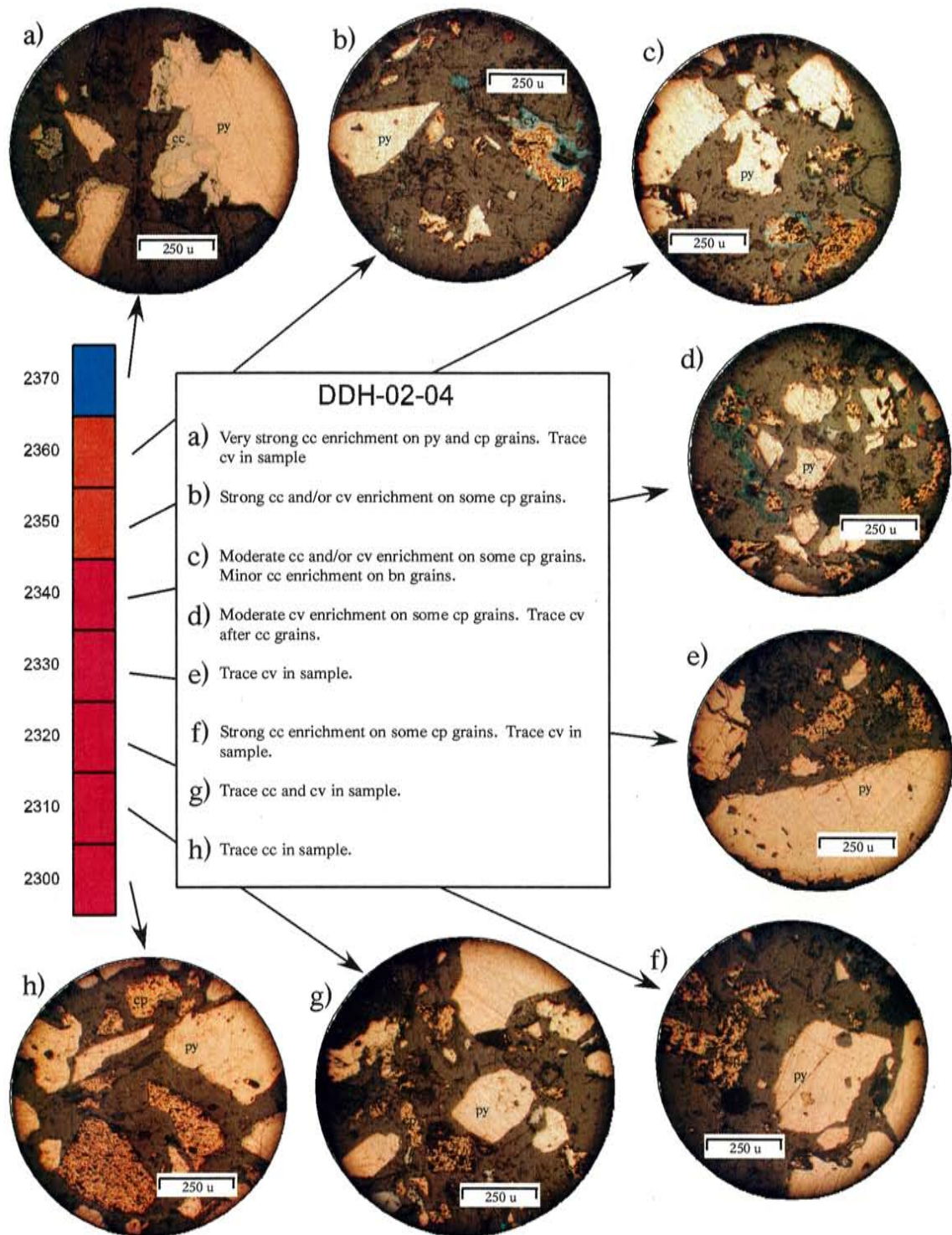
APPENDIX C

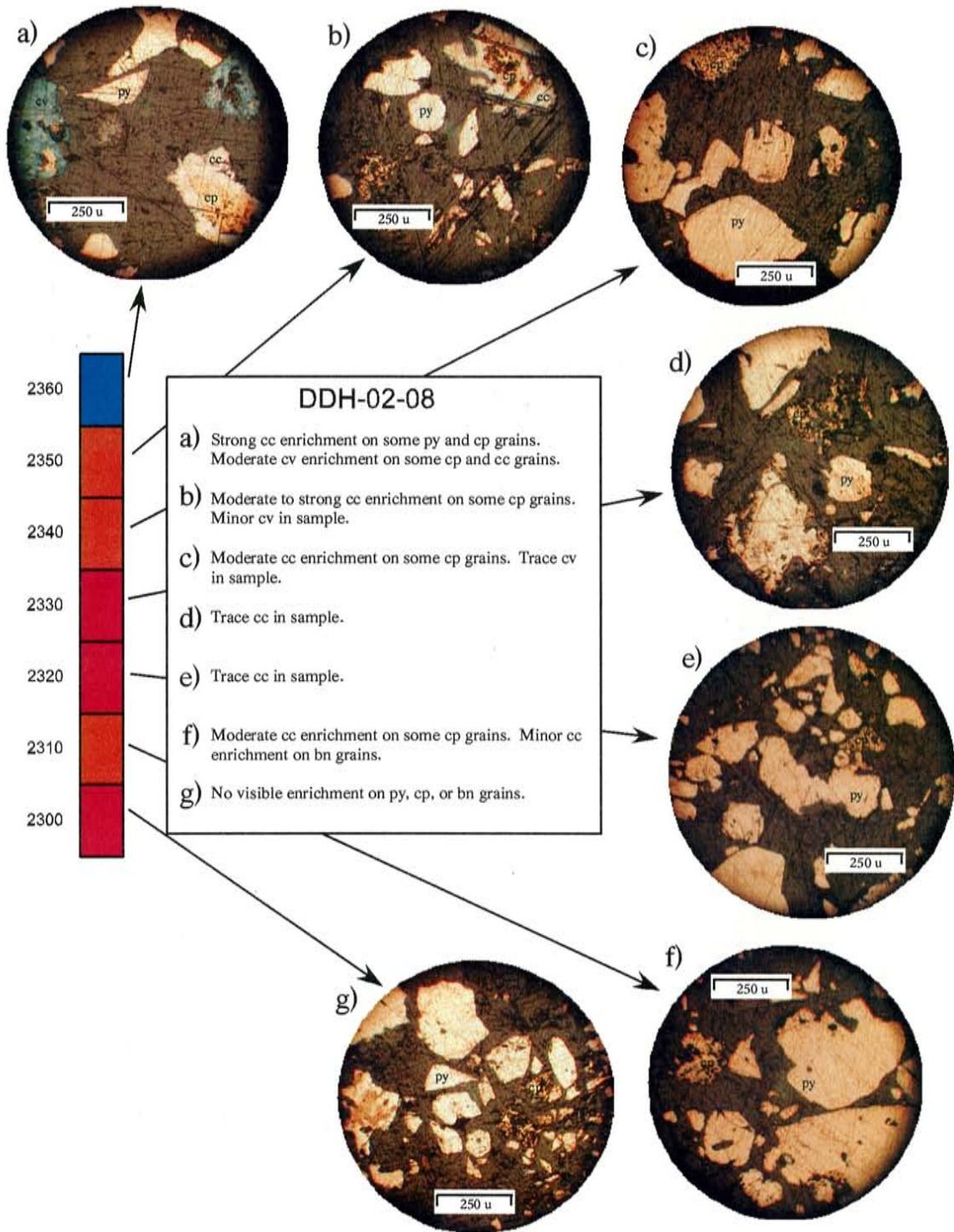
Qualitative mineralogic observations with associated photomicrographs illustrating replacement and paragenetic textures and physical associations between sulfides for the below mentioned drill holes.

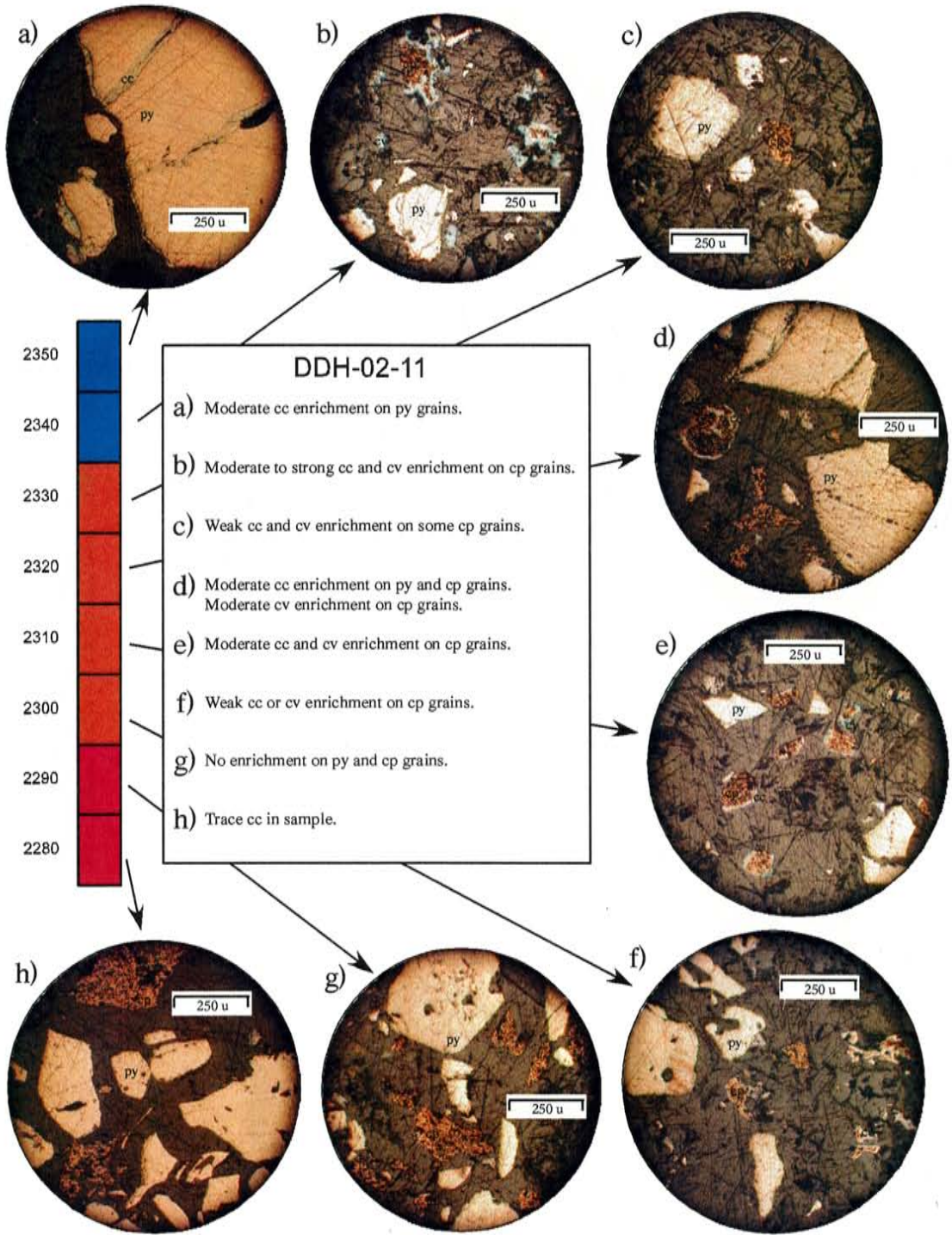
Drill Holes: DDH-02-01, DDH-02-03, DDH-02-04, DDH-02-08, DDH-02-11, DDH-03-09, DDH-03-13, DDH-03-14, RC-02-21, RC-02-24, RC-02-30, RC-F6-17, RC-F6-28, and RC-CC160.

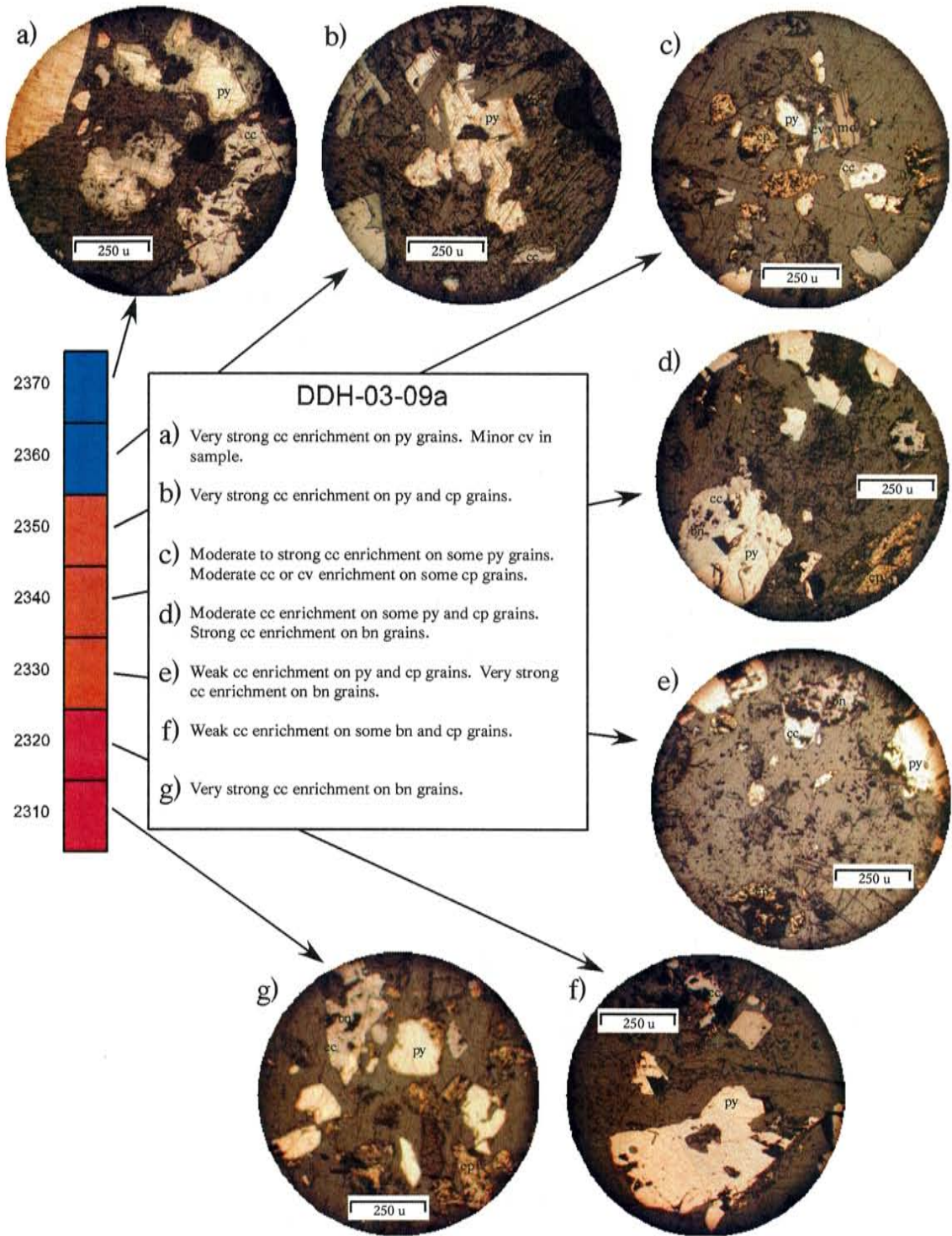


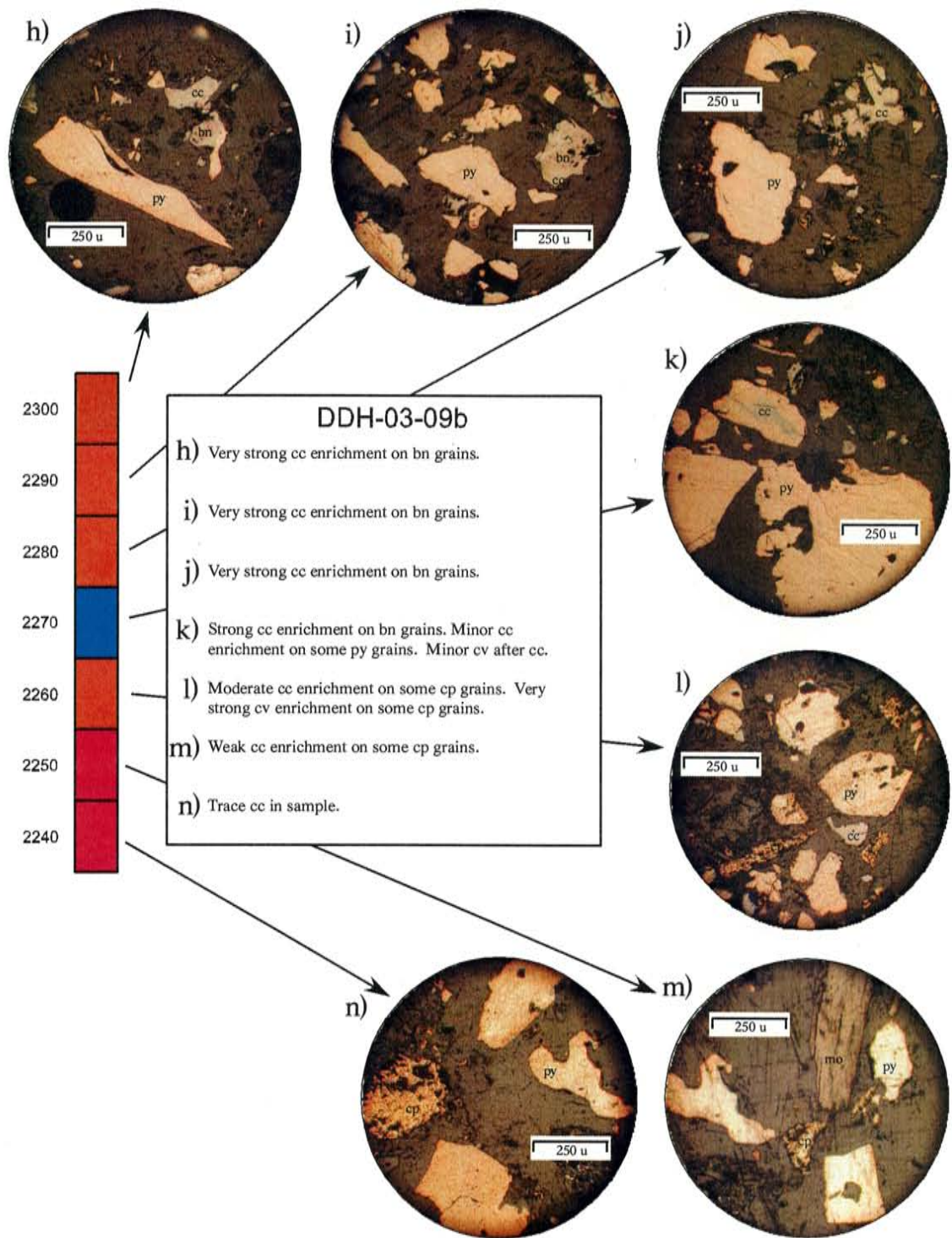


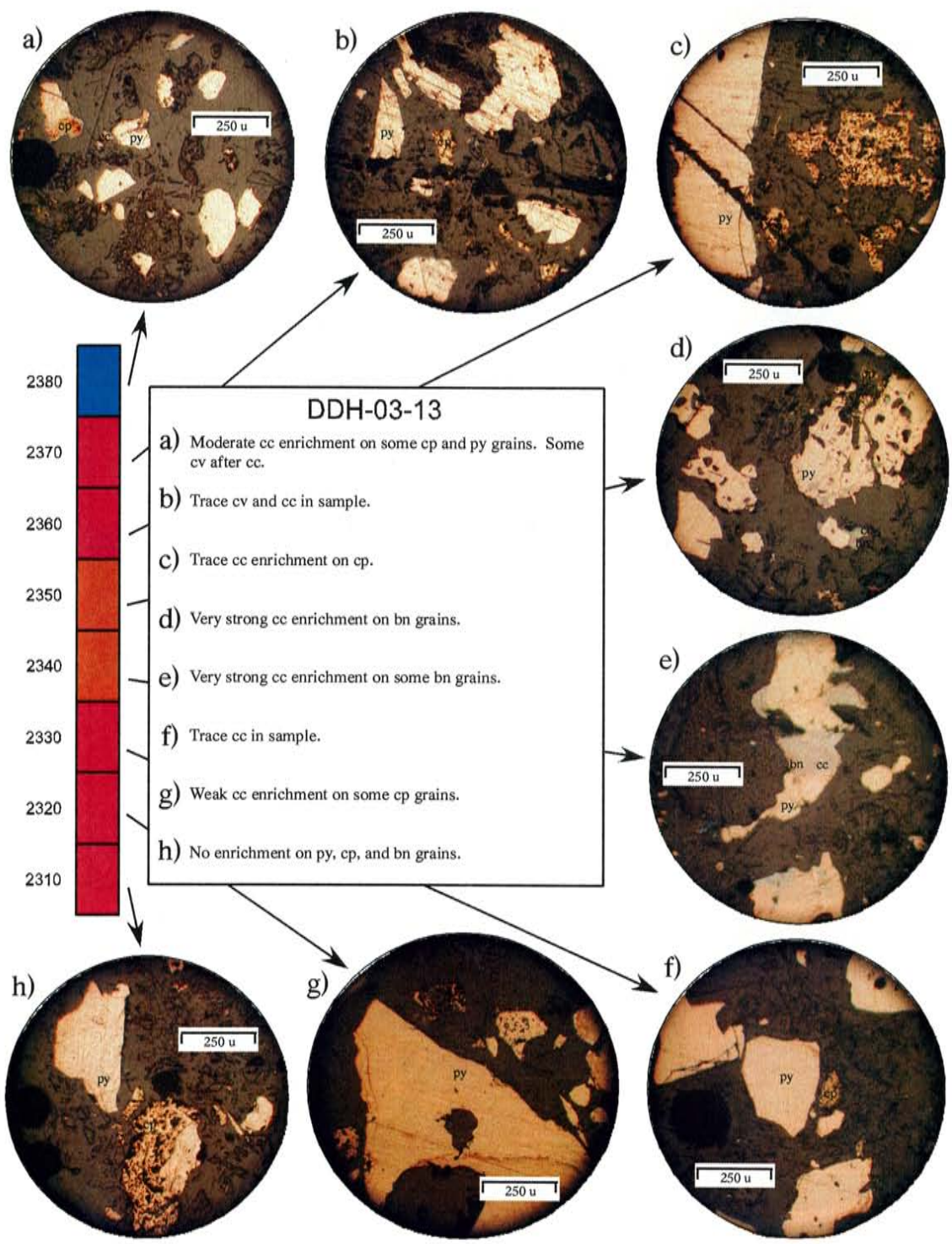


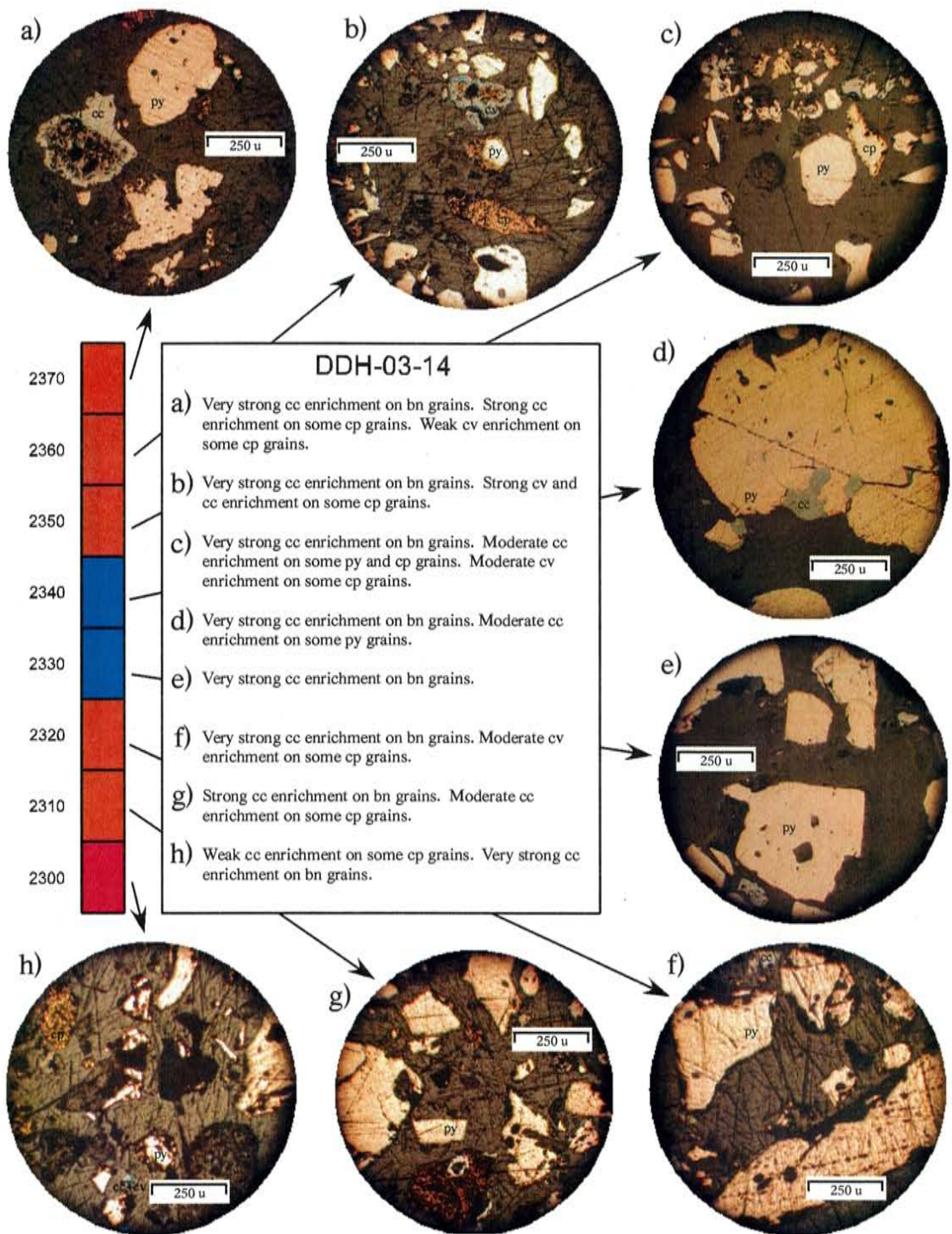


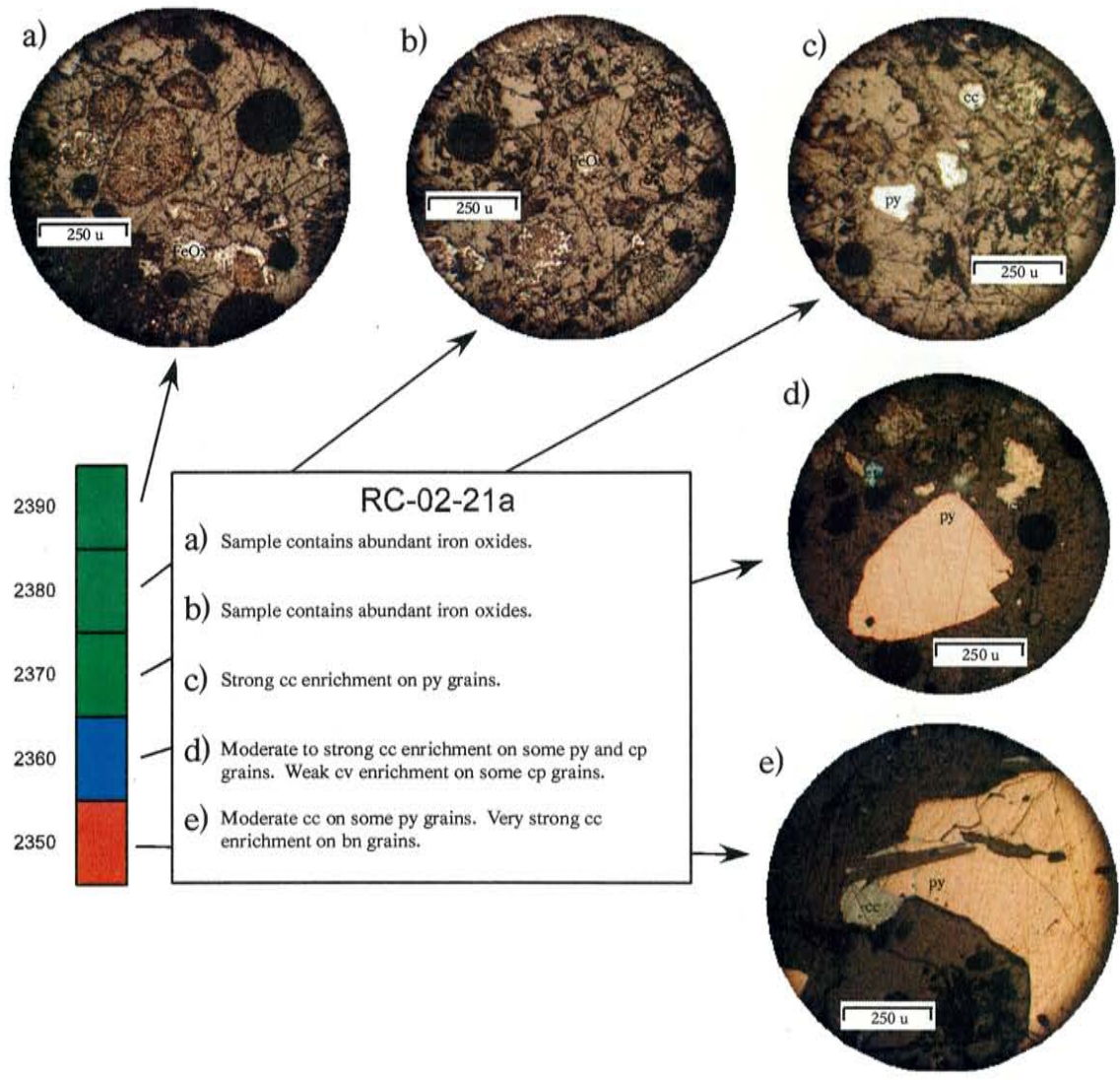


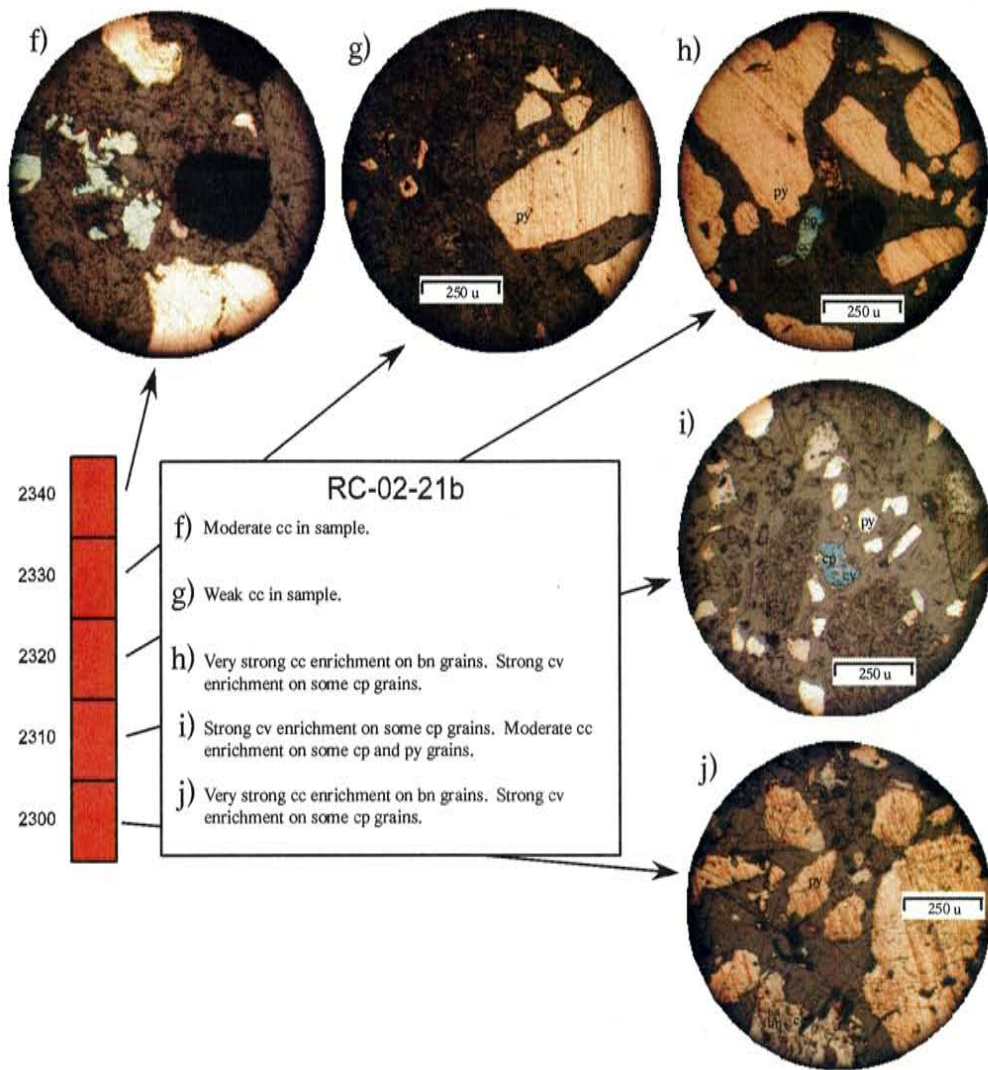


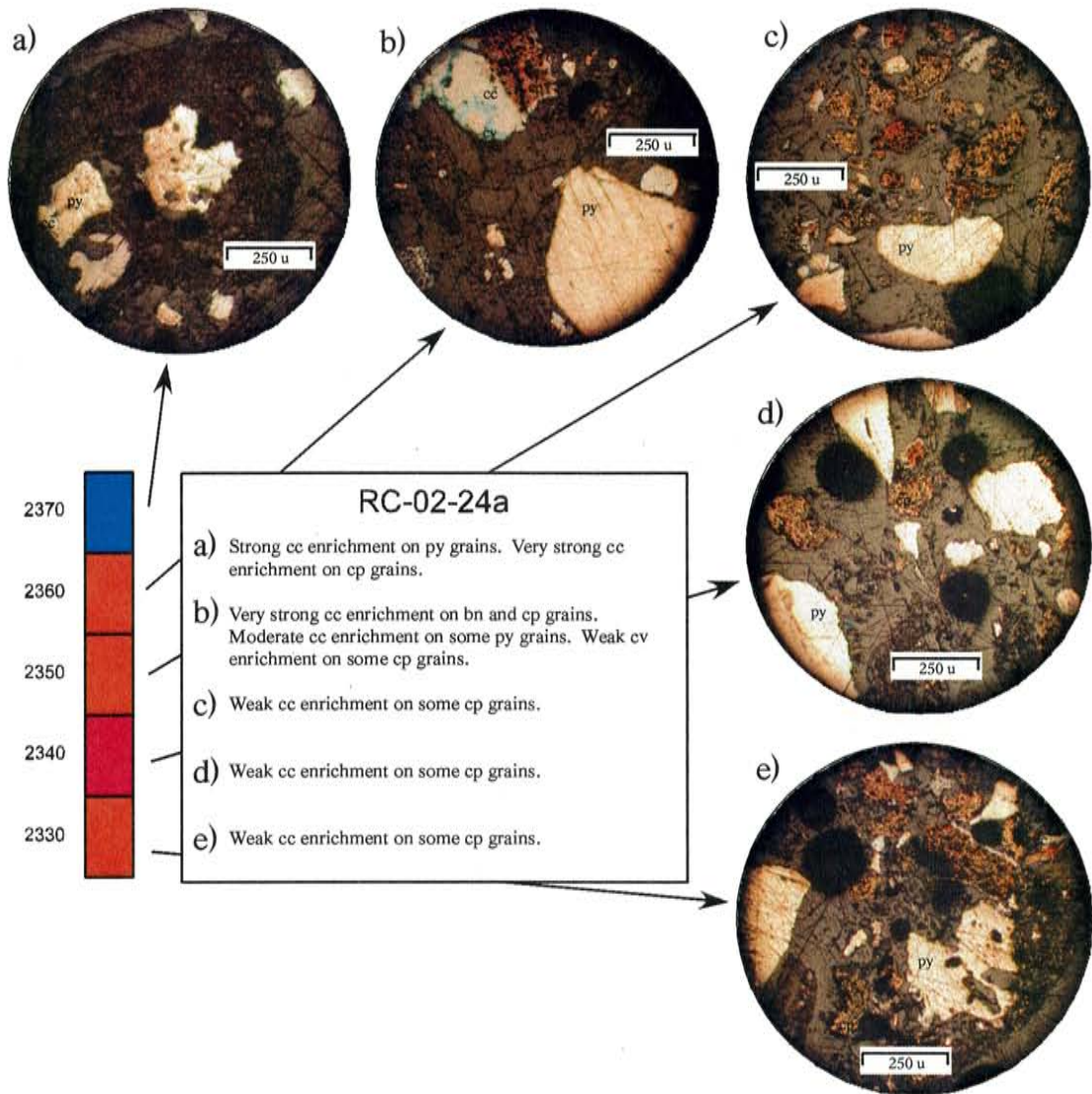


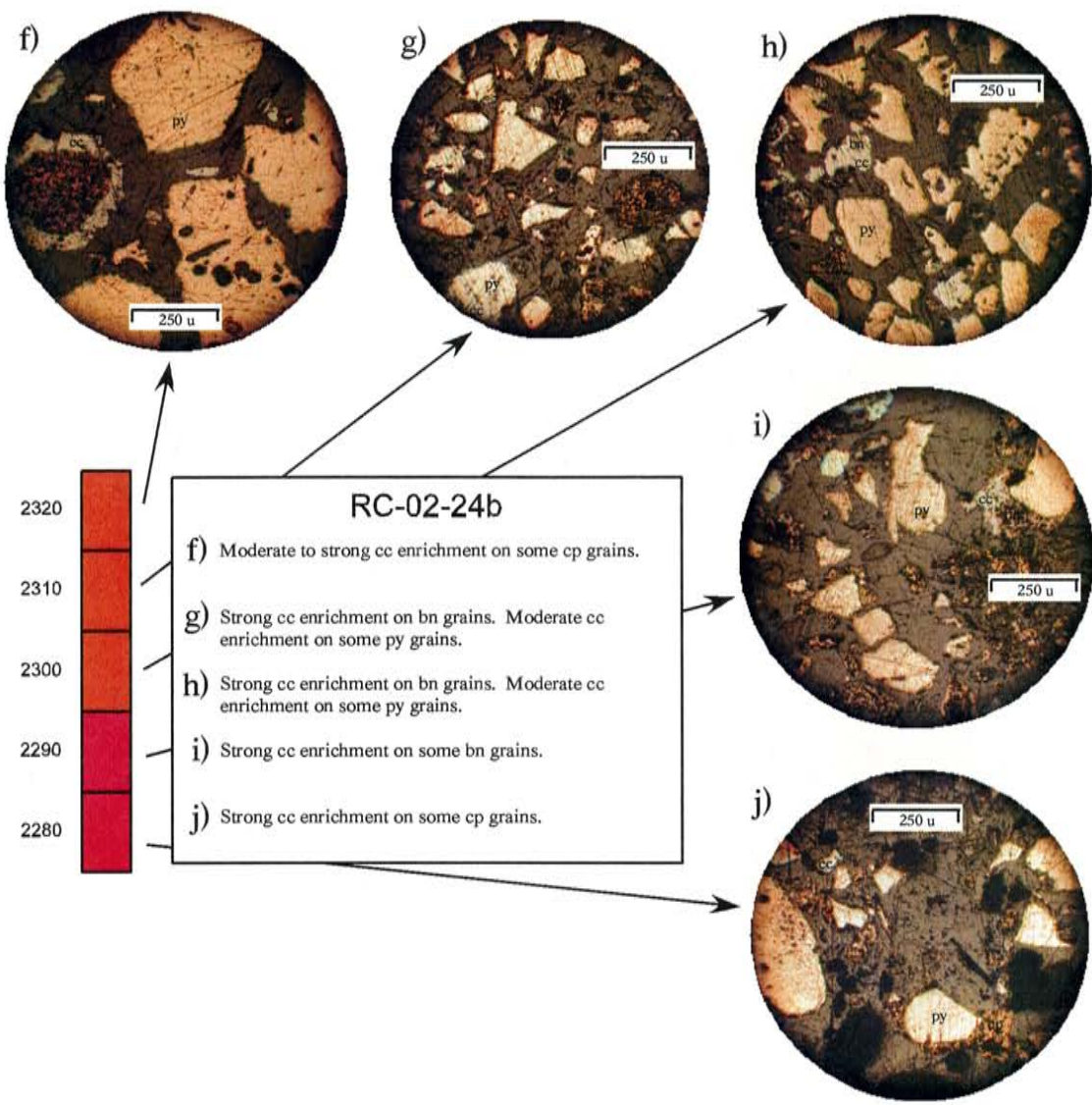


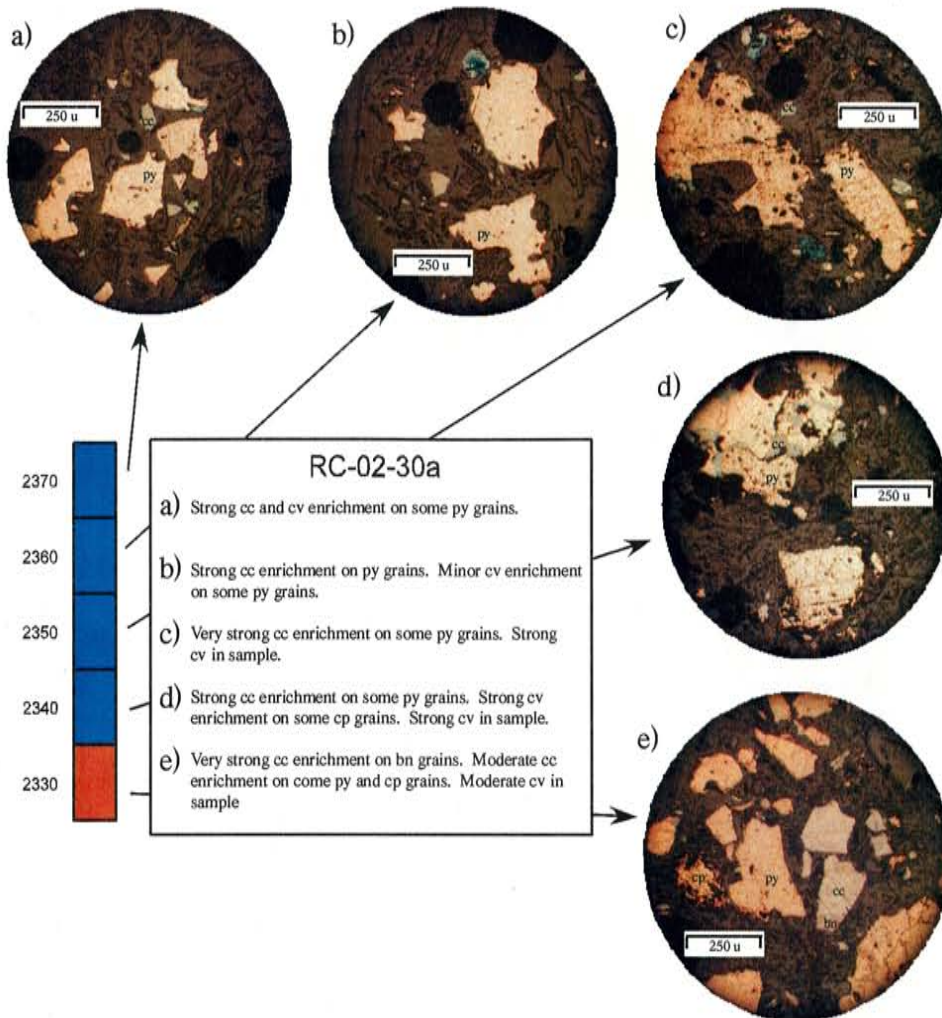


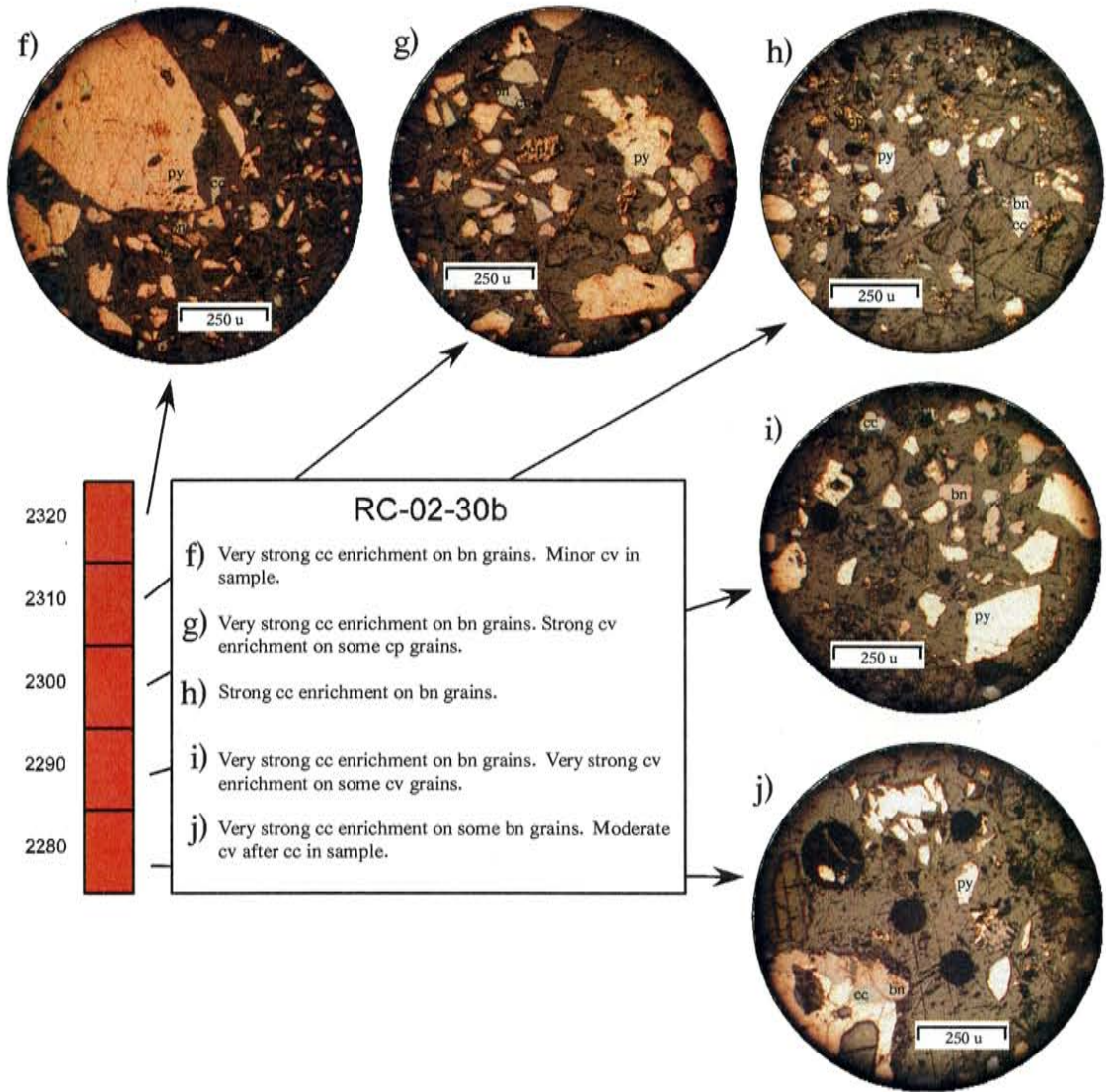


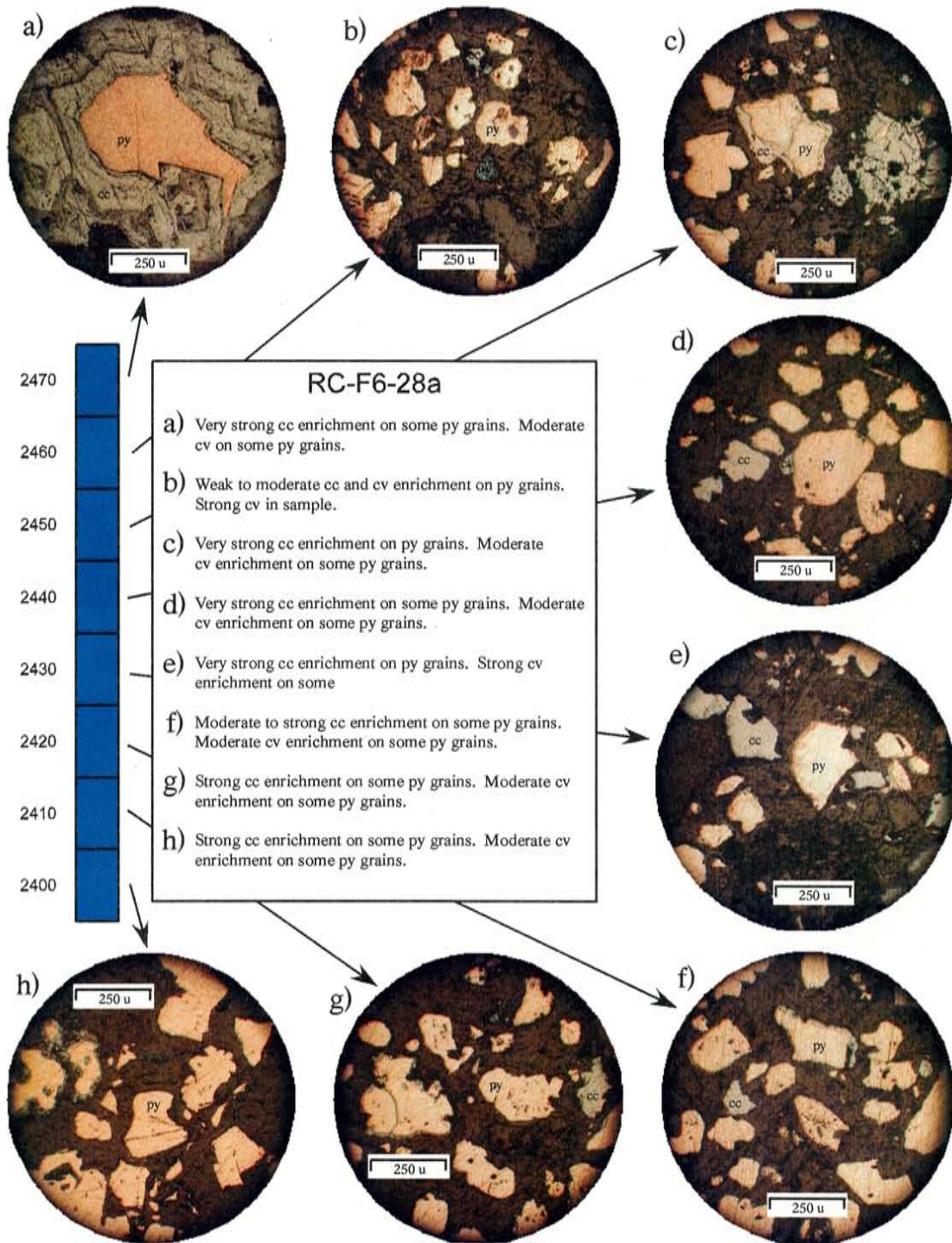


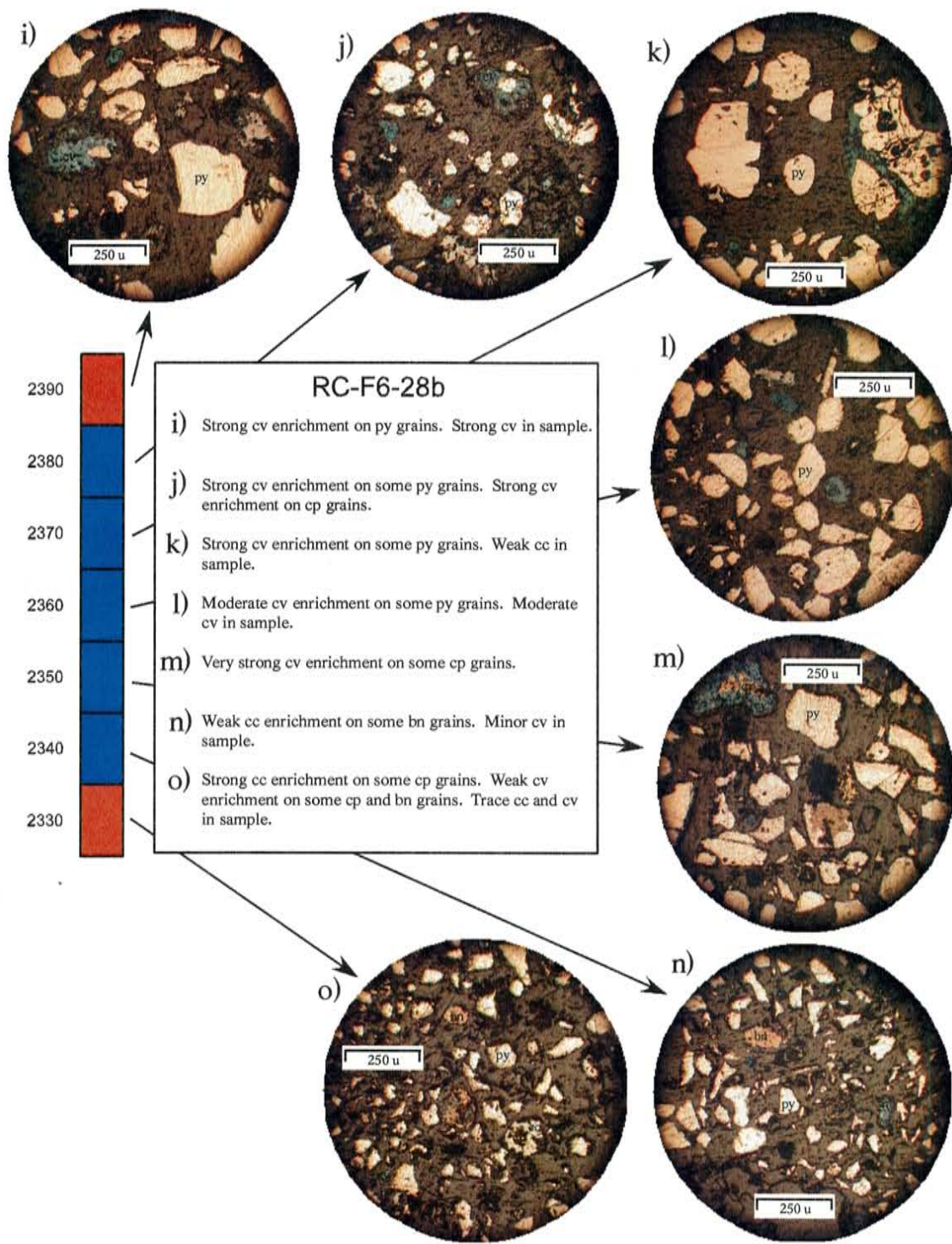


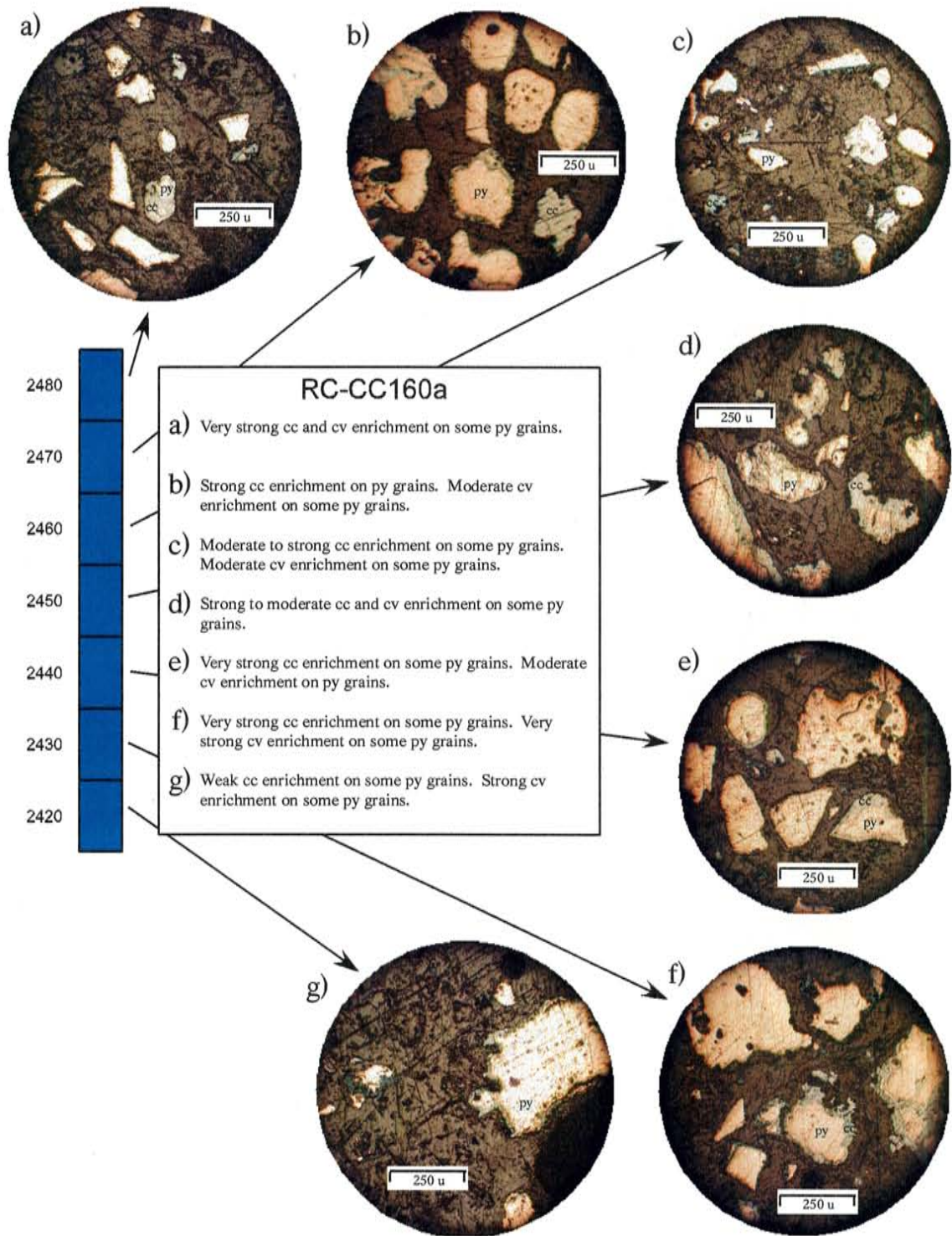


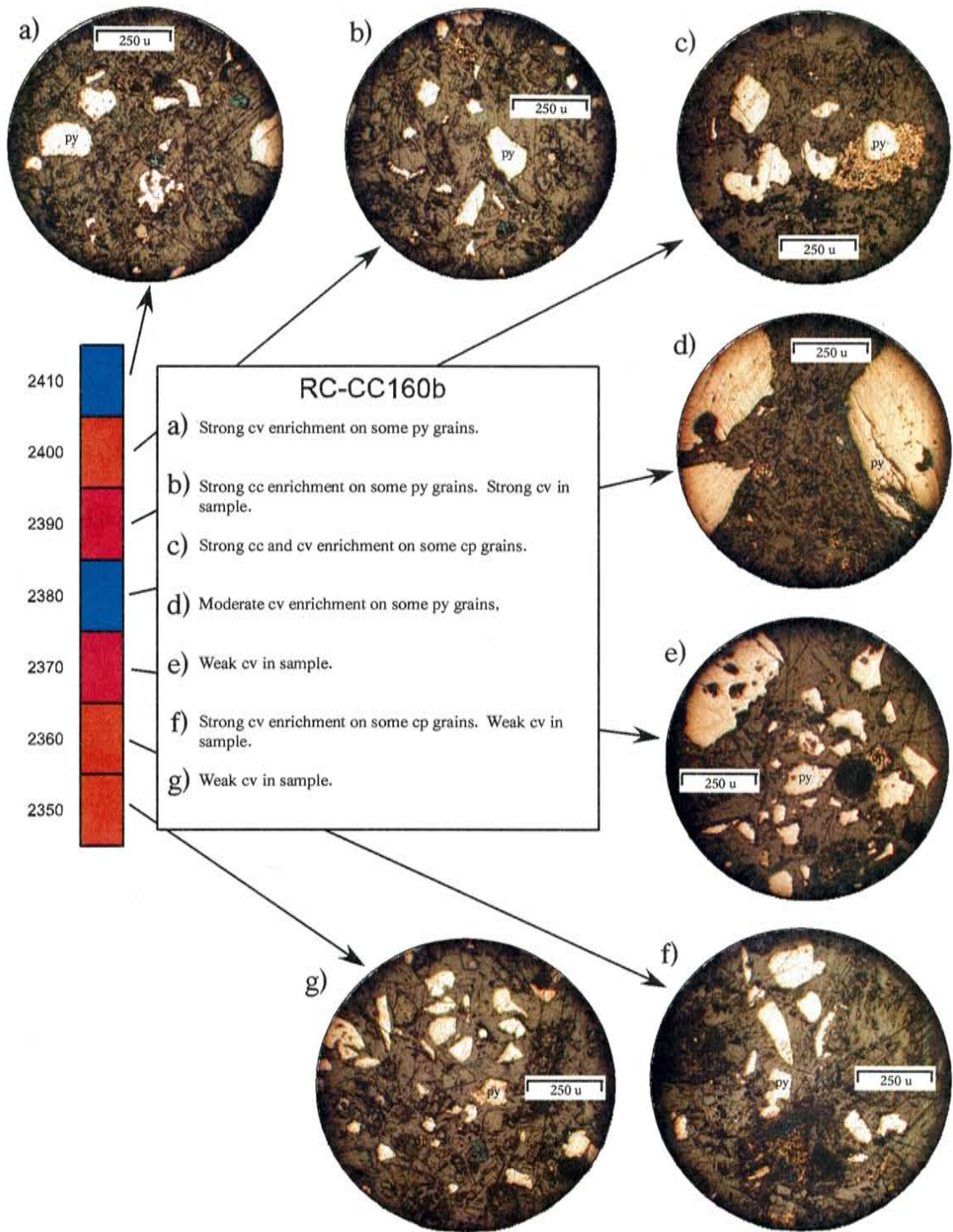










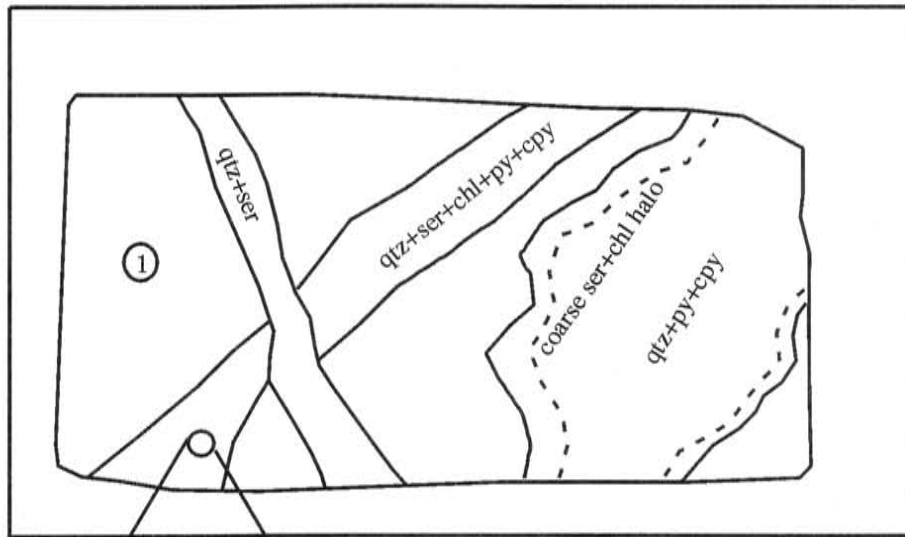


APPENDIX D

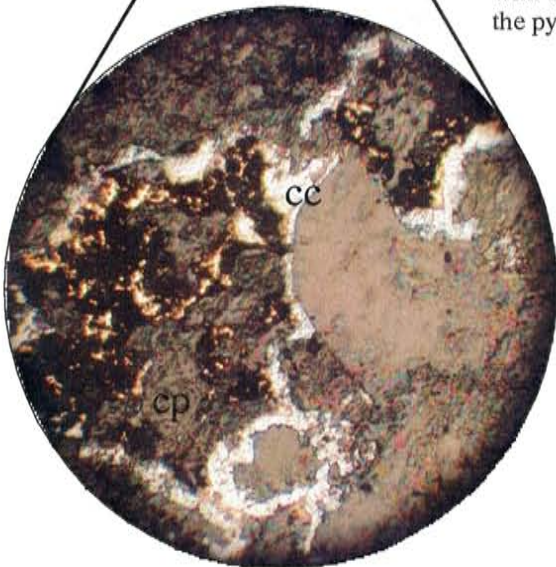
Reflected and transmitted-light petrographic results with photomicrographs for the below mentioned samples.

Samples: DDH-02-01-230.30, DDH-02-01-246.70, DDH-02-01-279.20, DDH-02-03-192.60, DDH-02-03-200.90, DDH-02-03-206.30, DDH-02-03-215.10, DDH-02-03-224.50, DDH-02-03-243.60, DDH-02-04-195.80, DDH-02-08-253.00, DDH-02-11-221.50, DDH-03-09-79.00, DDH-03-09-100.65, DDH-03-09-124.00, DDH-03-13-58.50, DDH-03-14-27.00, DDH-03-14-43.00, DDH-03-14-49.00, DDH-03-14-69.00, and DDH-03-14-78.00.

DDH-02-01-230.30m



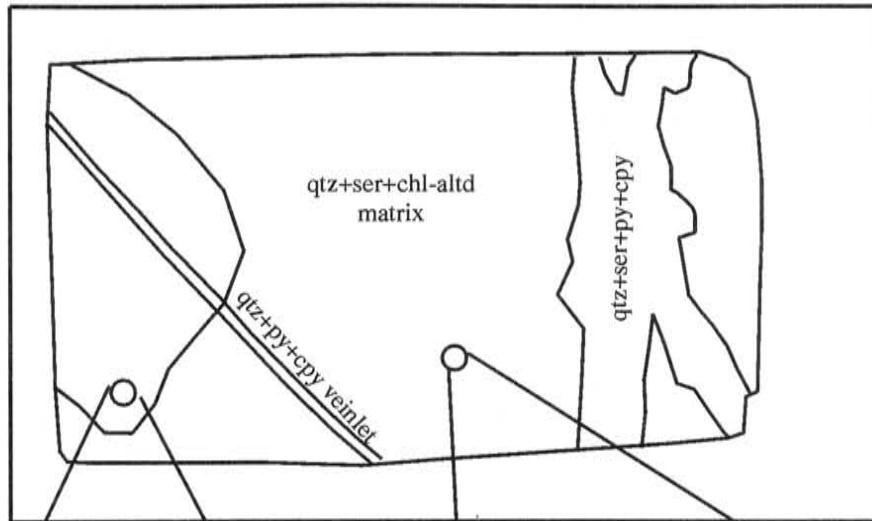
- ① Early potassic alteration is overprinted by ser+chl+qtz alteration. This later ser+chl alteration is associated with the development of veins that also introduced the py+cpy mineralization.



Strong Cc enrichment on cp and py.

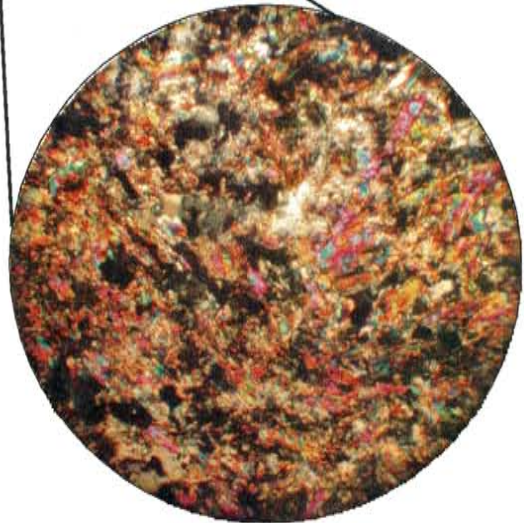
Field of view = 1,250 microns.

DDH-02-01-246.70m



Hypogene cp is replaced by
supergene bn and cc+cv.

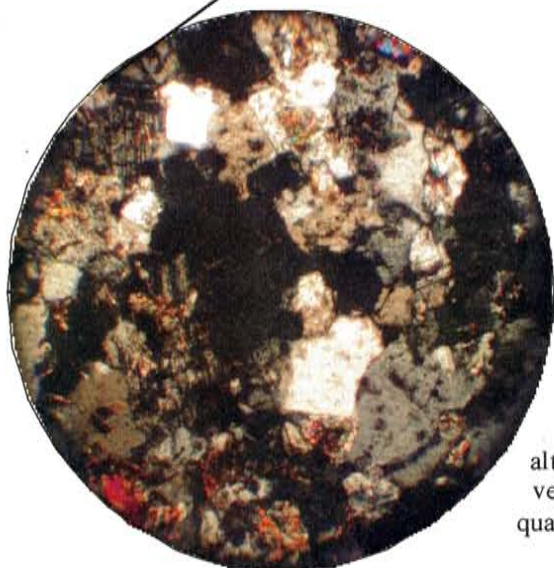
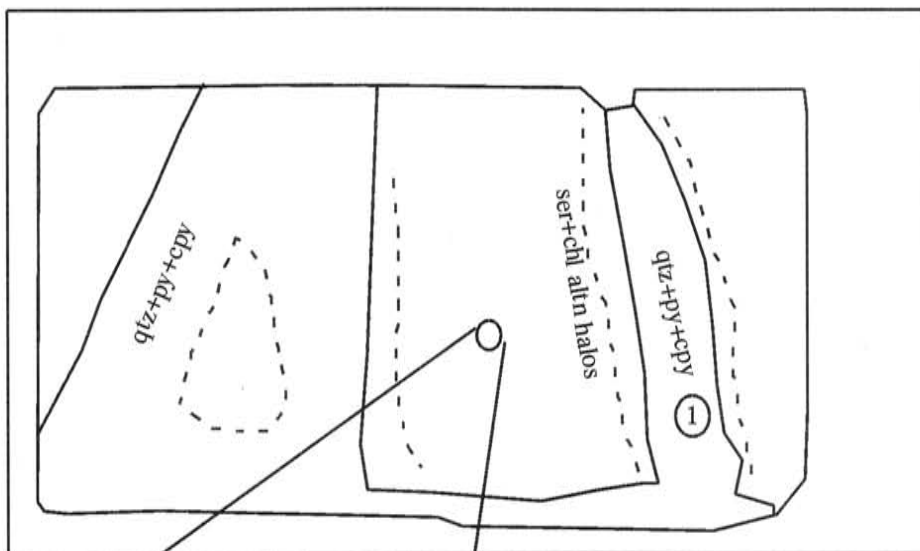
Field of view = 75 microns.



Strong qtz+ser altered matrix
Photomicrograph taken with
poles crossed.

Field of view = 1,250 microns.

DDH-02-01-279.20m

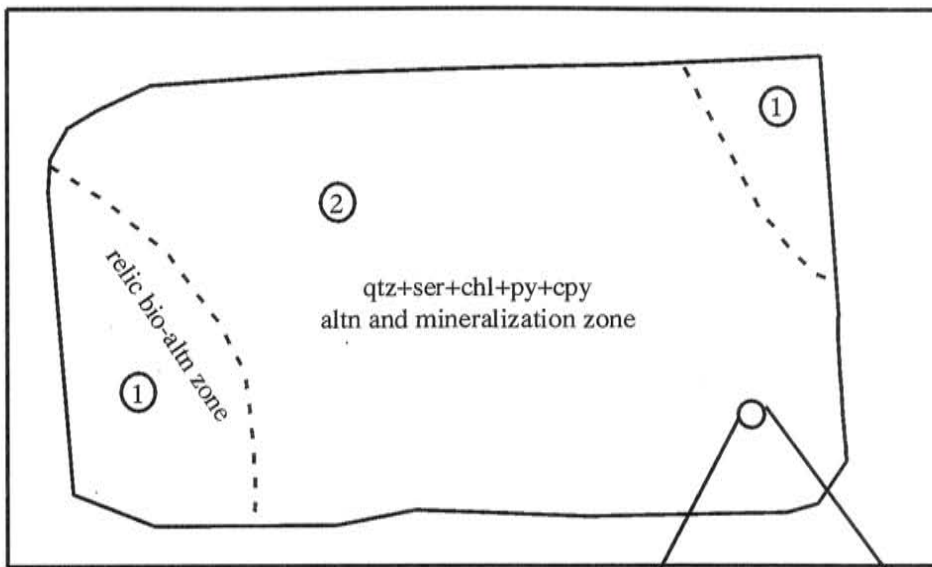


- ① py+cp+bn hypogene mineralization is associated with the development of qtz+ser+chl veins. Some cp shows weak cc/cv enrichment, bn is strongly enriched and has thick cc coatings.

Photo micrograph of the least altered groundmass. Groundmass is very crowded and contains abundant quartz and plagioclase fsp with accessory sphene/titanite.

Field of view = 1,250 microns.

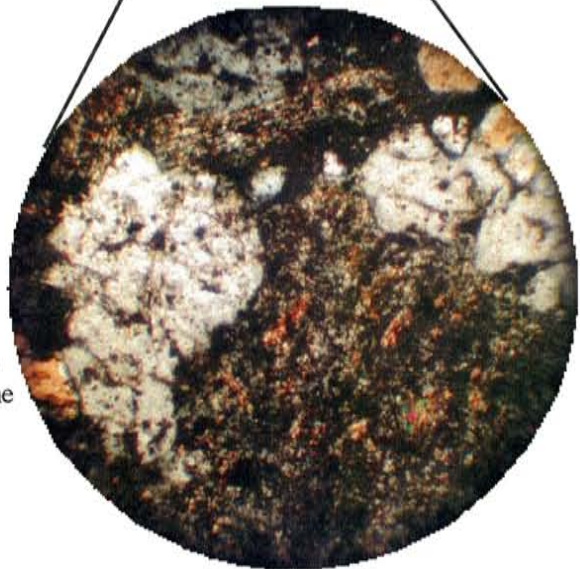
DDH-02-03-192.60m



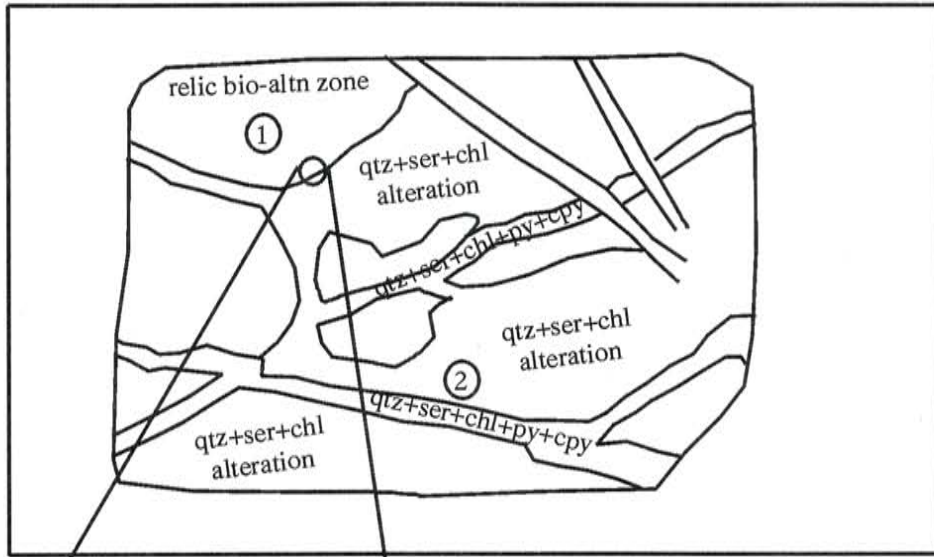
- ① These zones contain minor relic secondary biotite that has been over-printed by a ser-chl alteration.
- ② Disseminated cp+py mineralization was introduced during the ser-chl event. This sample shows no enrichment on hypogene sulfides.

Photo micrograph of the groundmass which generally contains relic 3,600 to 700 micron plagioclase phenocrysts. The remaining groundmass is altered to fine-grained sericite.

Field of view = 1,250 microns.



DDH-02-03-200.90m

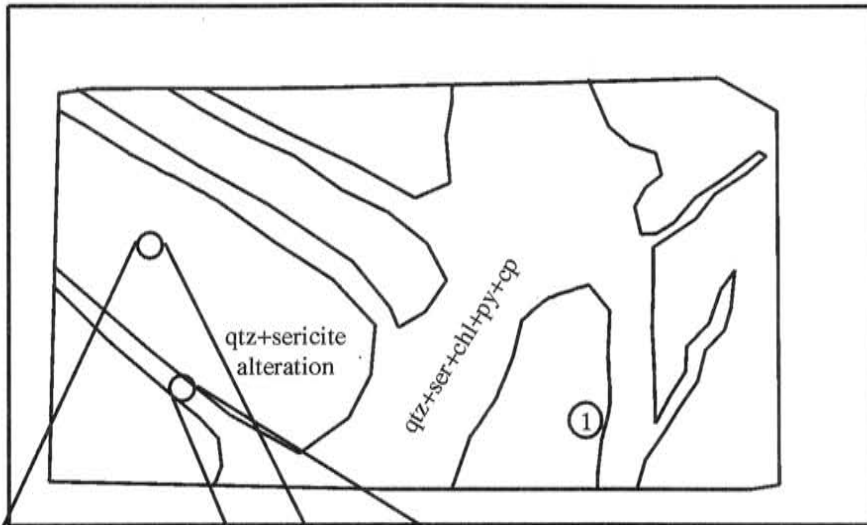


- ① This zone contains minor relic secondary biotite that has been over-printed by a ser-chl alteration.
- ② Disseminated cp+py mineralization was introduced during the ser-chl event. This samples shows cv enrichment on cp.

Photo micrograph of the groundmass. Where qtz+ser+chl veins cut the bio altered rock bio is altered to sericite and chlorite.

Field of view = 1,250 microns.

DDH-02-03-206.30m



① Hypogene py+cp mineralization shows no enrichment.



Photo micrograph of the groundmass that has been altered to 100 to 125 micron quartz grains is a matrix of fine-grained white phyllo silicate or sericite.

Field of view = 1,250 microns.

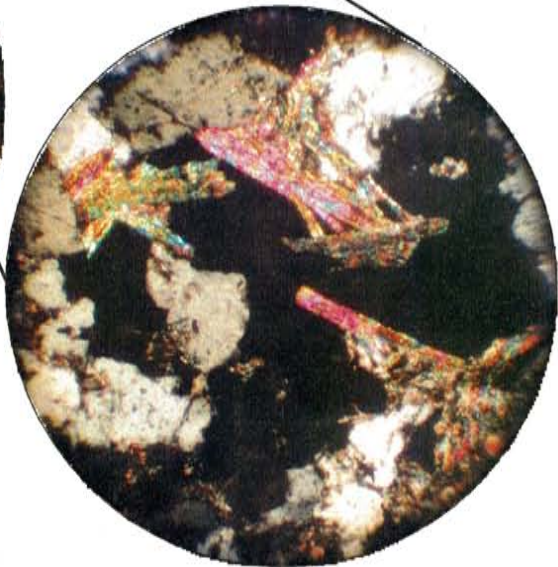
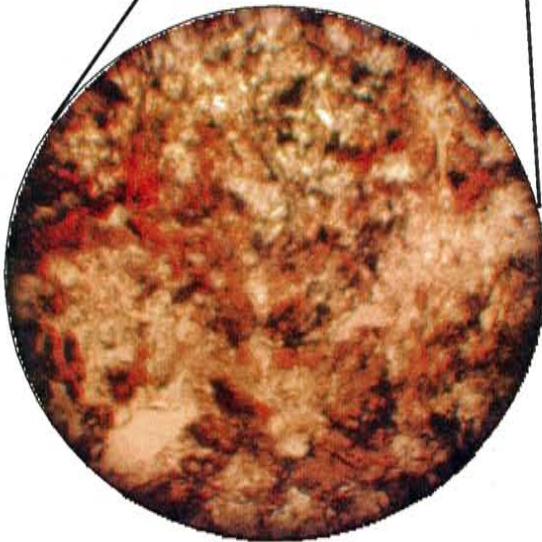
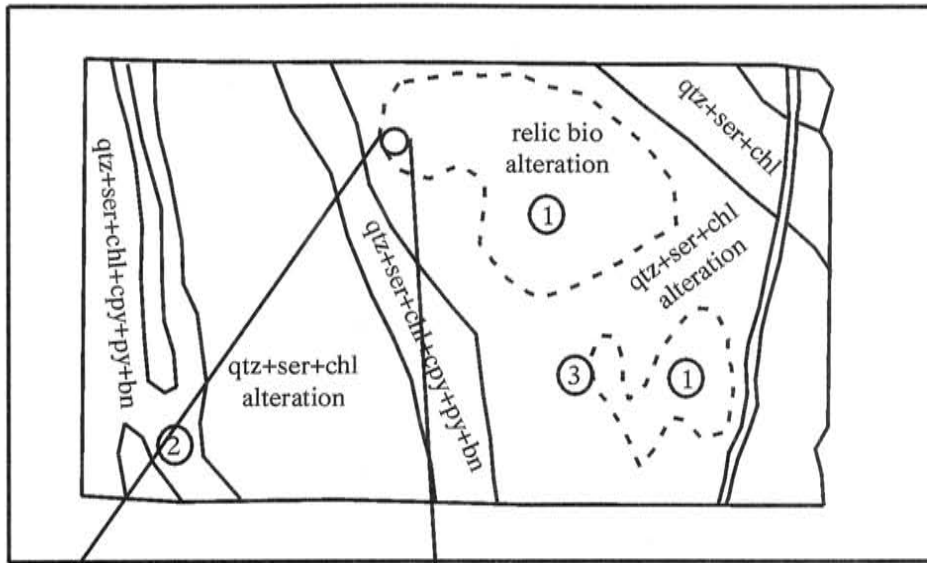


Photo micrograph of the qtz+ser+chl vein. Sericite becomes very coarse within the vein. Chlorite, not in view, is commonly found along vein margins as clusters.

Field of view = 1,250 microns.

DDH-02-03-215.10m



- ① This zone contains minor relic secondary biotite that has been over-printed by a ser-chl alteration.
- ② Vein and disseminated cp+ minor bn mineralization. This hypogene assemblage is not enriched by any supergene sulfides.
- ③ Where recognisable, the groundmass contains a few percent 2,400 to 1,000 micron plagioclase phenos; 1,000 micron phenos are more common. Also a percent 200 to 300 micron qtz-eyes and bata qtz.

Photo micrograph of the groundmass.
Where qtz+ser+chl veins cut the bio
altered rock bio is altered to
sericite and chlorite.

Field of view = 1,250 microns.

DDH-02-03-224.50m

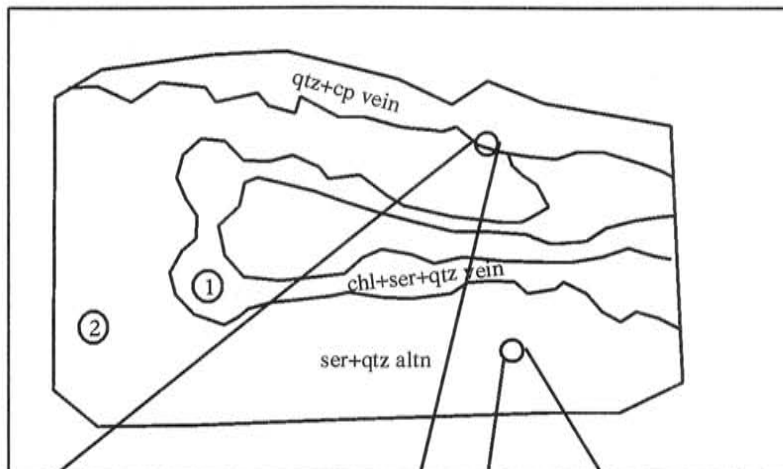


Photo micrograph of the contact between the groundmass and the qtz+cp vein. cp is found in the center of the vein. There is no altn halo associated with this vein.

Field of view = 1,000 microns.

- ① This zone contains clusters of chl intergrown with ser probably as part of a vein.
- ② The moderately ser+qtz altd groundmass contains 400 to 1,200 micron qtz-eyes and 800 micron bata-qtz, large 3,200 to 1,800 micron plagioclase and microcline phenocrysts. This sample does not have a fine-grained groundmass, rather it appears to have a crowded texture.

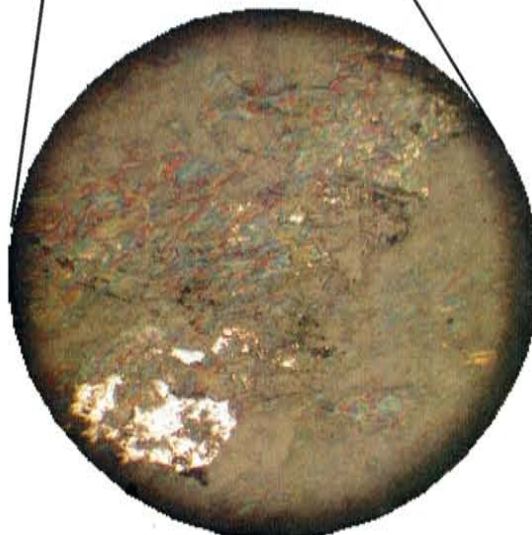
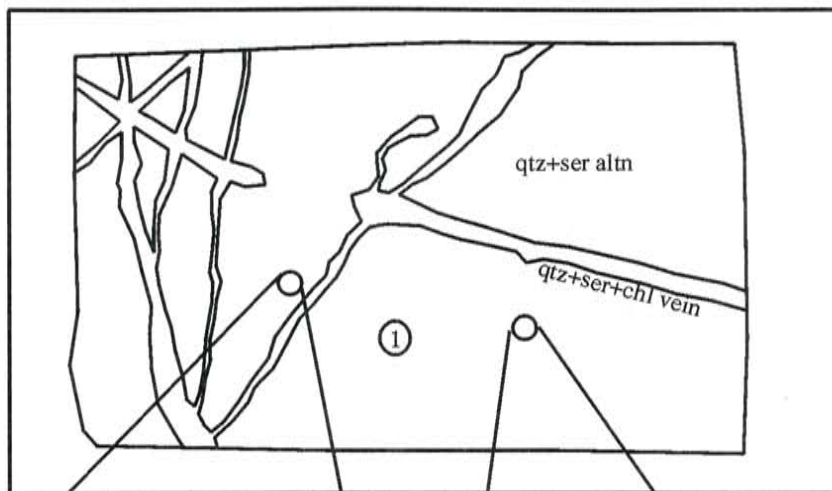


Photo micrograph of the minor disseminated py+cp mineralization. No visible enrichment on hypogene sulfides.

Field of view = 400 microns.

DDH-02-03-243.60m



- ① Strong qtz+ser alteration has affected the sample. The groundmass is composed of fine-grained ser clusters separated by micro veinlets of qtz.



Photo micrograph of py+cp+bn mineralization associated with the development of qtz+ser+chl veins. There is no enrichment on hypogene sulfides.

Field of view = 400 microns.

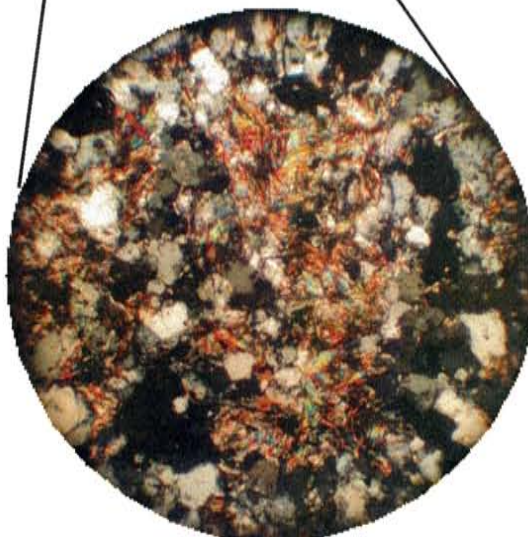
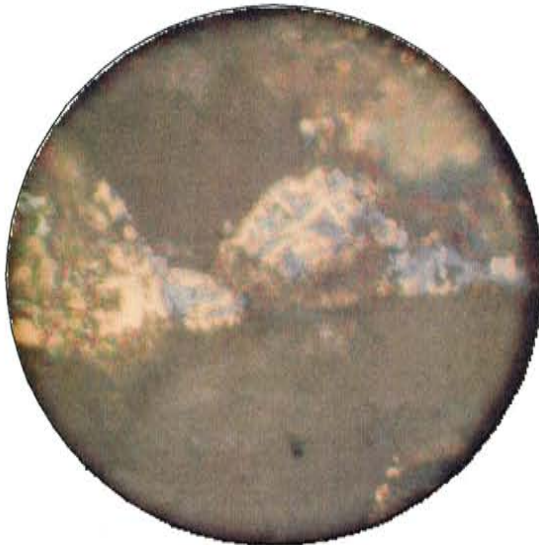
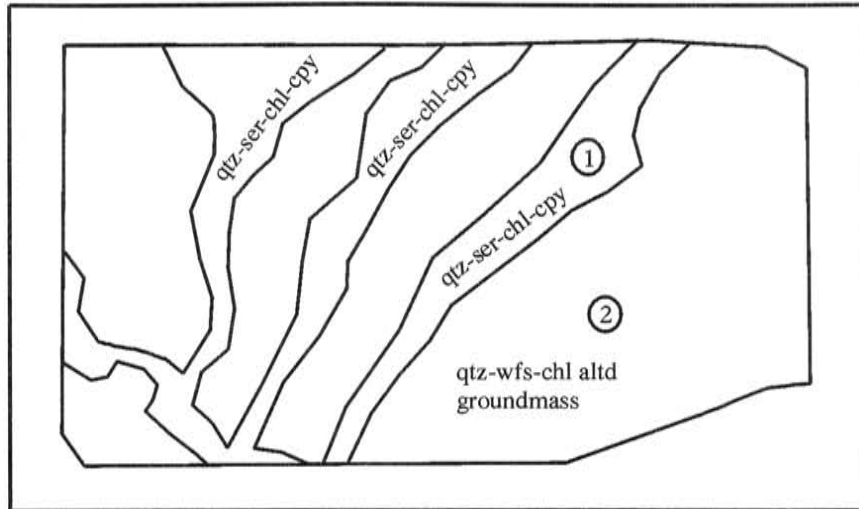


Photo micrograph of qtz+ser altd groundmass.

Field of view = 400 microns.

DDH-02-04-195.80m



- ① Photomicrograph of chalcopyrite mineralization found in vein centers. Here the chalcopyrite can have trace cv/cc enrichment.

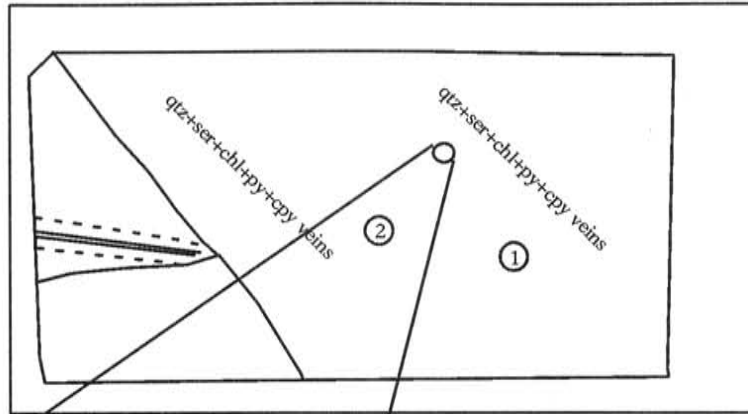
Field of view = 100 microns



- ② Photomicrograph of 1 to 2 mm fsp phenos that have been altered to white phyllo silicate (wfs). The groundmass has been altered to qtz+wfs+chl.

Field of view = 1,000 microns

DDH-02-08-253.0m

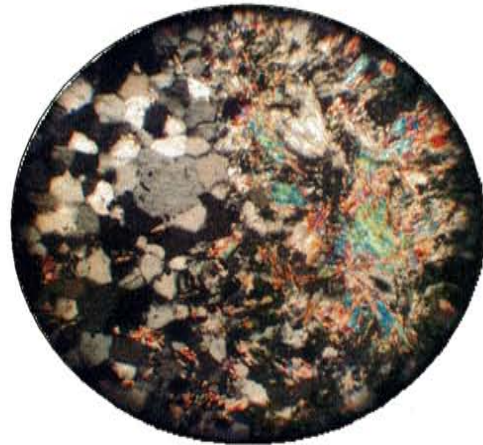


All relic textures within the sample have been destroyed. This sample shows coarse qtz+ser+chl+py+cpy veins developed with alteration halos containing very coarse ser+chl. These veins are well developed in this section.



Photomicrograph of chalcopyrite mineralization. Most enriched chalcopyrite grains are associated with veins.

Field of view = 400 microns



② Photo micrograph of the very coarse ser+chl altered matrix.

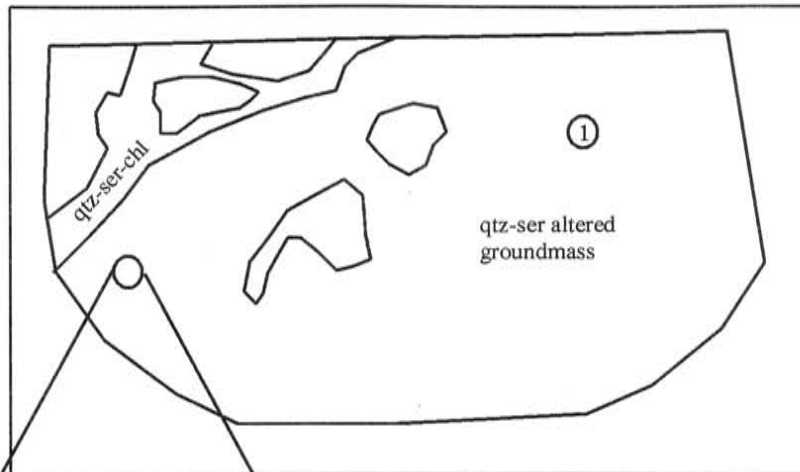
Field of view = 1,000 microns.



① Photomicrograph of pyrite-chalcopyrite mineralization. Where this occurs as disseminated mineralization little to no enrichment is observed.

Field of view = 1,000 microns

DDH-02-11-221.50m



- ① Well-preserved qtz-fsp porphyry. Section contains abundant 1 to 2 mm fsp phenos and 0.5 mm qtz-eyes and bata qtz phenos too.

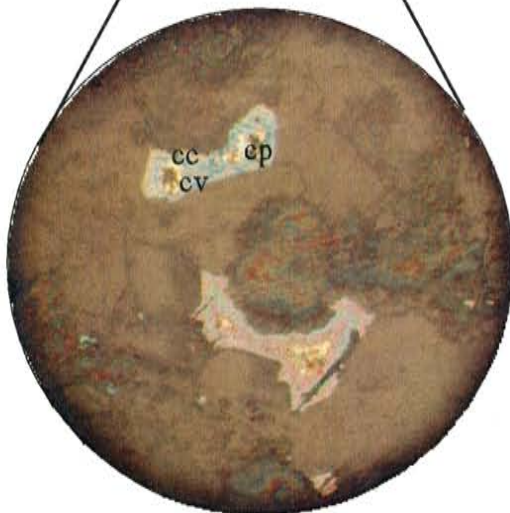
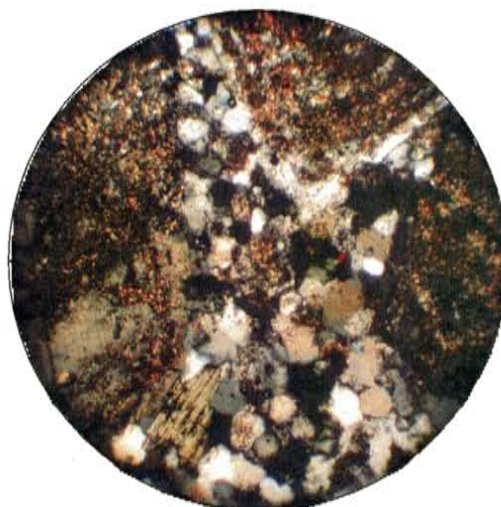


Photo micrograph of moderate to very strongly developed cv and cc enrichment on chalcopyrite grains (transition zone). Mineralization is developed in moderate qtz-ser-chl altered porphyry.

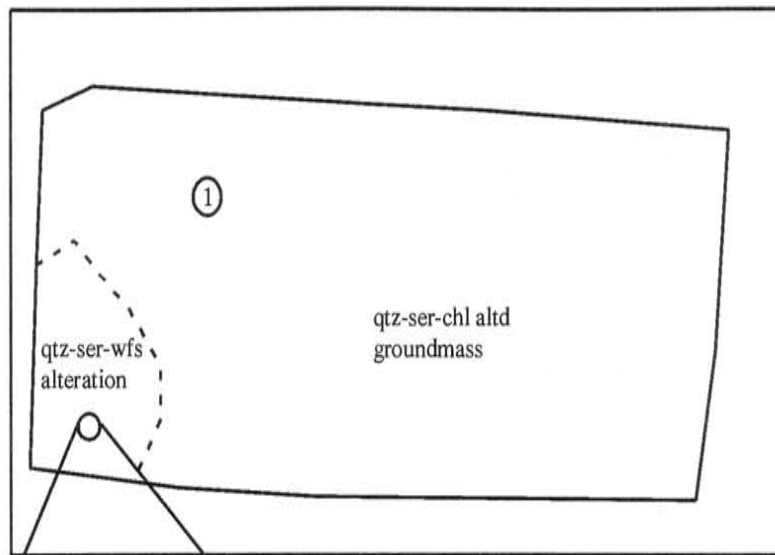
Field of view = 400 microns



Photomicrograph of qtz-fsp phenos in a granular qtz-ser altered groundmass.

Field of view = 1,000 microns

DDH-03-09-79.00m

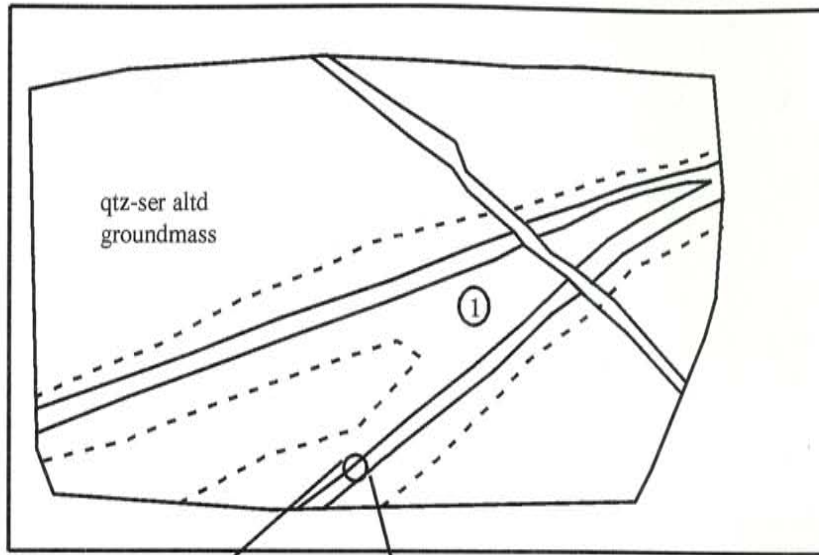


- ① Strong qtz-ser-(chl) alteration where chlorite seems to occur more proximal to veins. Sericite also becomes more coarse within veins. Relic phenocrysts are not present, original texture of rock has been destroyed during alteration.

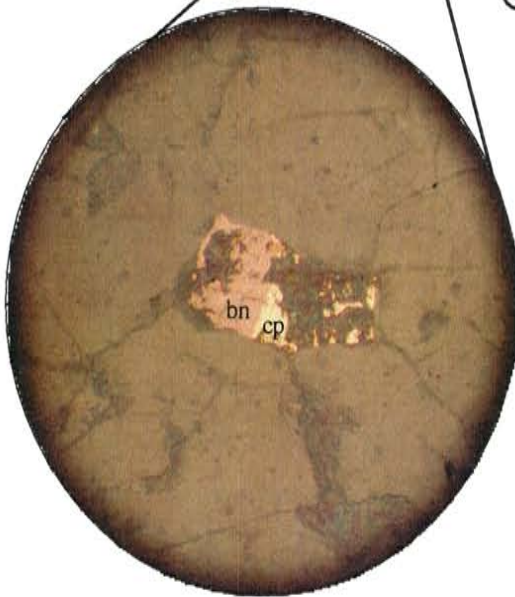
Locally there is some cc enrichment on bn grains. This only occurs within the qtz-ser-wfs altd zone. Overall hypogene py-cp-bn mineralization and unenriched.

Field of view = 400 microns.

DDH-03-09-100.65m



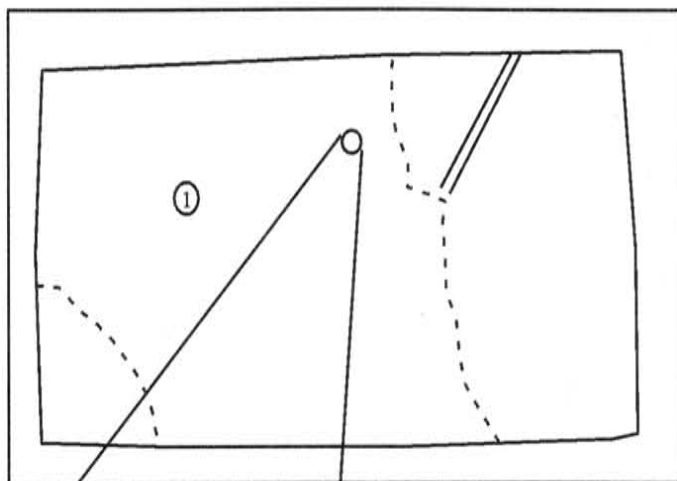
- ① Quartz-sericite veins with coarse sericite within veins and fine sericite within vein halos. Sample is completely recrystallized.



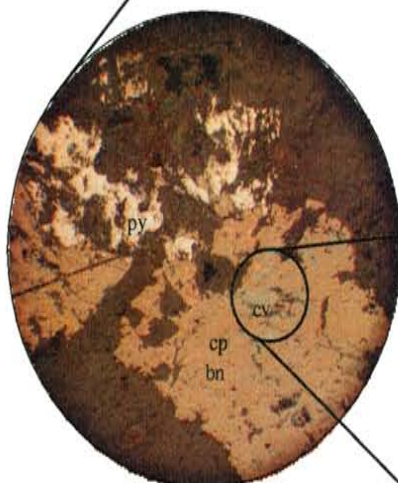
Py-cp-bn mineralization is associated with development of veins. There is some minor cc/cv enrichment, not pictured, that occurs within veins.

Field of view = 400 microns.

DDH-03-09-124.00m

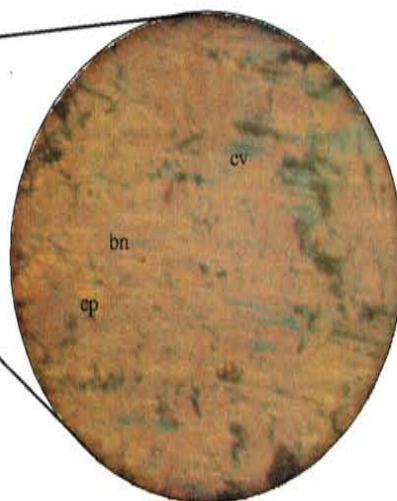


- ① This zone contains coarse and fine-grained sericite + quartz. this alteration is associated with numerous veins and veinlets. Overall py-bn-(cp) mineralization is associated with the development of qtz-ser veins. there is only trace enrichment in this sample.



Photomicrograph of a bornite grain with chalcopyrite developed along the crystal boundaries (?) with covellite.

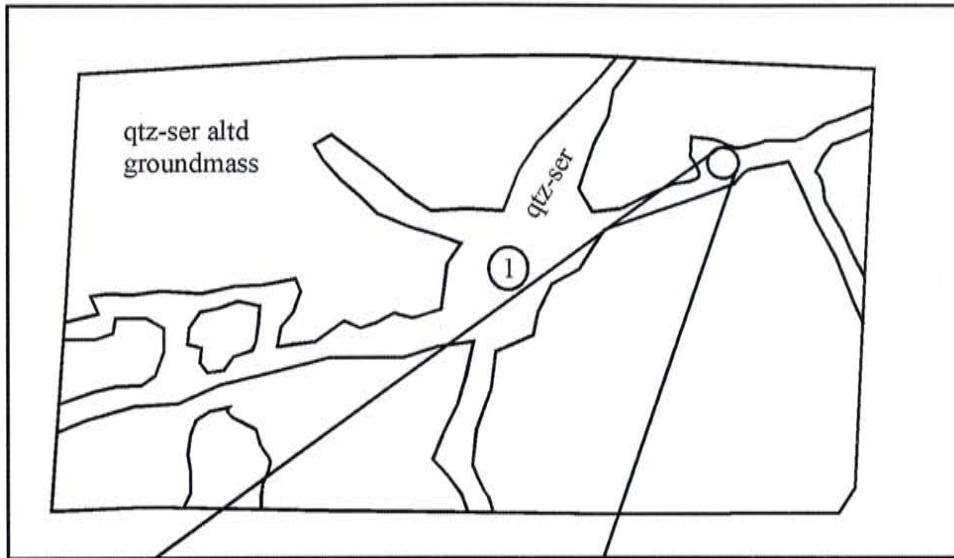
Field of view = 400 microns.



Close-up of the inter-growth textures seen in the photo to left.

Field of view = 100 microns.

DDH-03-13-58.50m

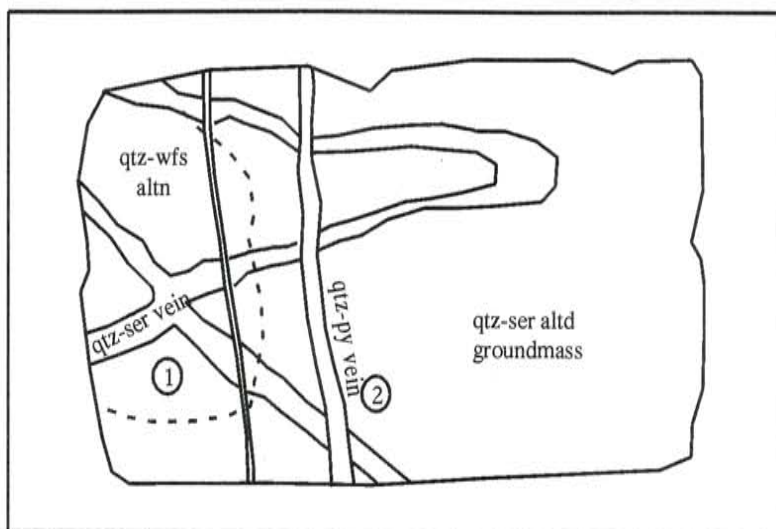


① Quartz-sericite veins cut section and are associated with the development of strong qtz-ser alteration of the groundmass. No relic textures are preserved.

Photomicrograph of py-cp mineralization developed throughout the sample. Locally there is somecc/cv enrichment, but overall this is weak.

Field of view = 400 microns.

DDH-03-14-27.00m

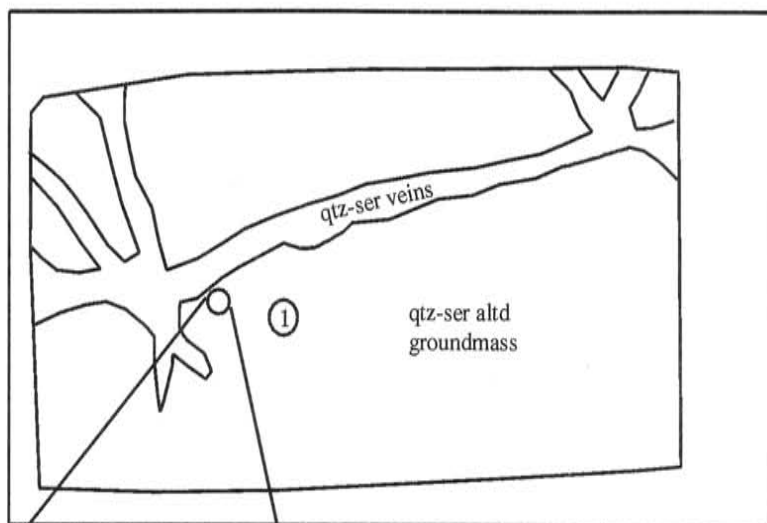


- ① This zone shows qtz-wfs alteration with minor fine-grained sericite.
- ② Most of the groundmass is altered to qtz-ser associated with qtz-ser veins. Sample shows a later set of linear qtz-py veins.

Photomicrograph of essentially py only mineralization with some cc enrichment developed throughout the sample. Locally there is some bn and cp.

Field of view = 400 microns.

DDH-03-14-43.00m

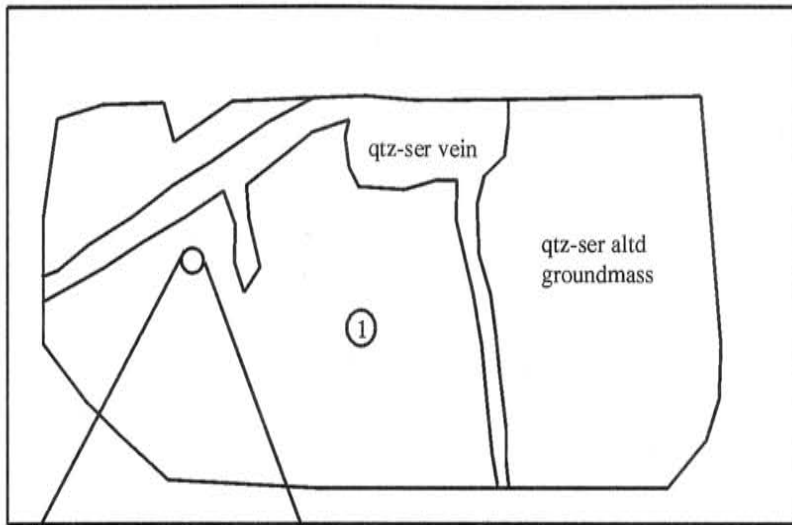


- ① Quartz-sericite veins cut section and are associated with the development of strong qtz-ser alteration of the groundmass. No relic textures are preserved.

Photomicrograph of py mineralization developed throughout the sample. There is no enrichment in this section.

Field of view = 400 microns.

DDH-03-14-49.00m



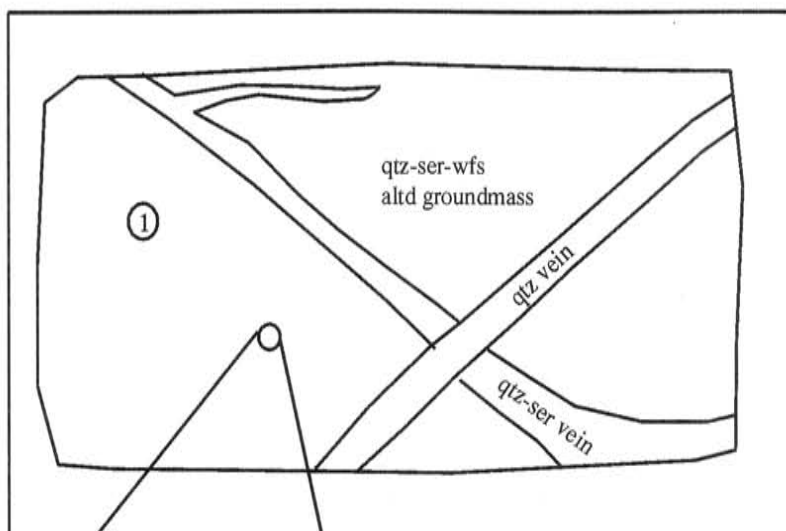
- ① Strong pervasive qtz-ser alteration of groundmass associated with the development of qtz-ser veins. Sericite is very coarse.



Photomicrograph of py mineralization developed throughout the sample. Mineralization is associated with veins. No enrichment on py grains.

Field of view = 1,000 microns.

DDH-03-14-69.00m



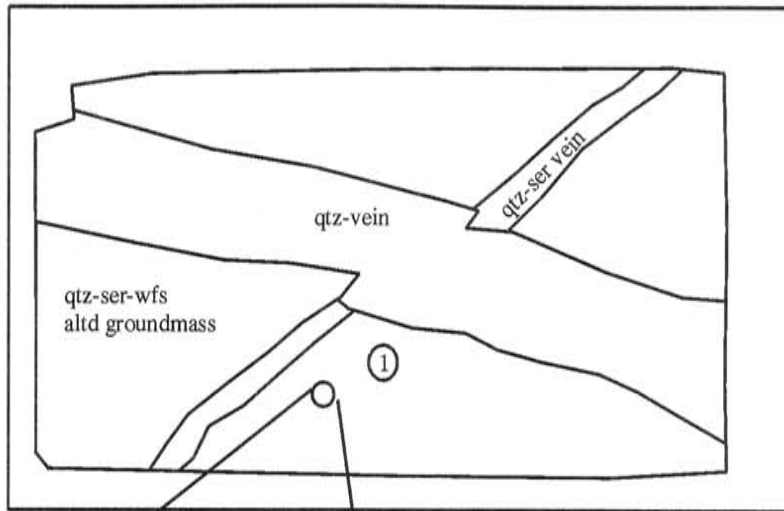
- ① Strong pervasive qtz-ser-wfs alteration of groundmass associated with the development of qtz-ser veins. A later quartz veins cuts earlier veins. No mineralization is associated with the later qtz-vein.



Photomicrograph of cp-bn mineralization developed throughout the sample. Overall there is py and cp-bn mineralization is associated with veins. Pyrite is not seen in contact with cp or bn in this section. No enrichment of hypogene sulfides.

Field of view = 400 microns.

DDH-03-14-78.00m



- ① Strong pervasive qtz-ser-wfs alteration of groundmass associated with the development of qtz-ser veins. A later quartz vein cuts earlier veins. No relic textures are preserved.



Photomicrograph of cp-mo mineralization developed in the sample. Overall there is strong cp-py mineralization developed in this section. Little to no enrichment of hypogene sulfides.


Field of view = 400 microns.

APPENDIX E

Drill hole columns showing the relationship between lithology “A”, alteration “B” to the occurrence of the defined mineral zones “C”. Lithologic units, alteration types and paragenetic relationships presented in these columns represent observations made during drill core inspection, thin section and grain-mount petrographic study, and previous drill core logs for the below mentioned drill holes.

Drill Holes: DDH-02-01, DDH-02-03, DDH-02-04, DDH-02-08, DDH-02-11, DDH-03-09, DDH-03-13, DDH-03-14, RC-02-21, RC-02-24, RC-02-30, RC-F6-17, RC-F6-28, and RC-CC160.

Explanation

 Cerro Empexa Fm. (?) andesitic lavas and volcaniclastics.

 Feldspar porphyry


 Quartz-feldspar porphyry/Igneous Bx.


 Argillic Alteration

 Qtz + White Phyllosilicate (sericite) alteration.

 Qtz + Chlorite + White Phyllosilicate alteration.


 Biotite + Magnetite alteration


 Remnant "pods" of Biotite + Magnetite alteration.


 Remnant zones of Qtz + Chlorite + White Phyllosilicate alteration.

 LC Leached Cap.

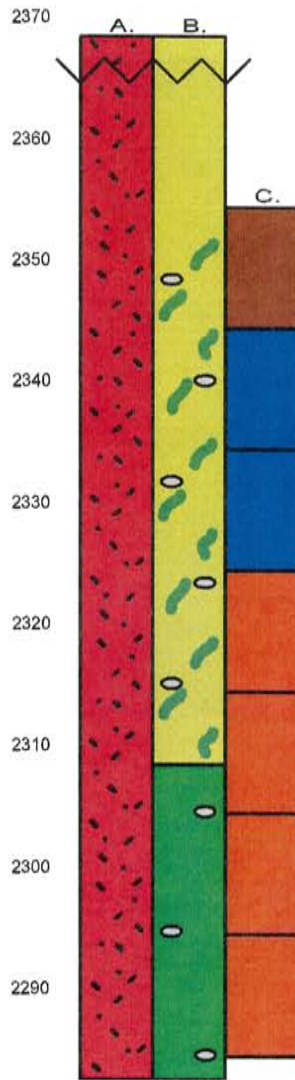
 OX Copper Oxides.

 S >80% Cu in Supergene Sulfides.

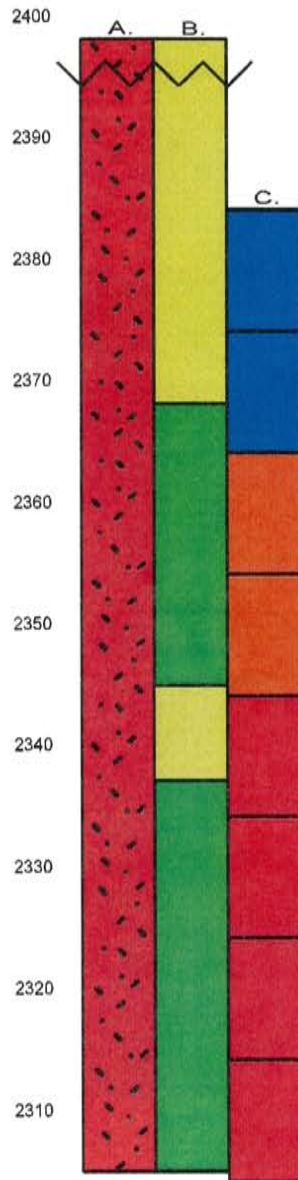
 T <80% -> 15% Cu in Supergene Sulfides.

 H <15%-0% Cu in Supergene Sulfides

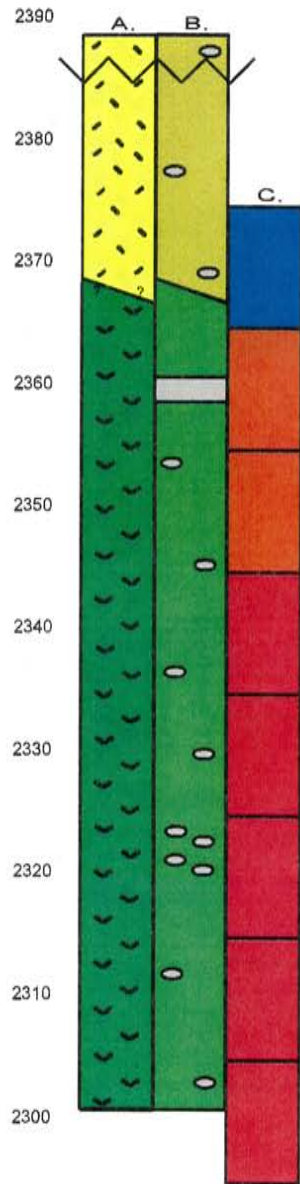
DDH-02-01



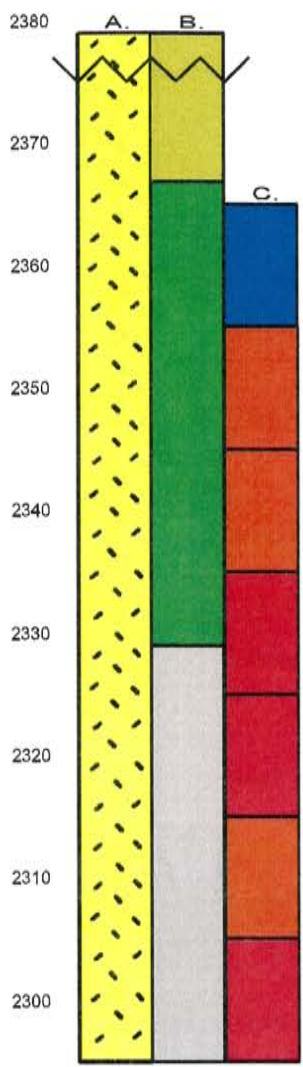
DDH-02-03



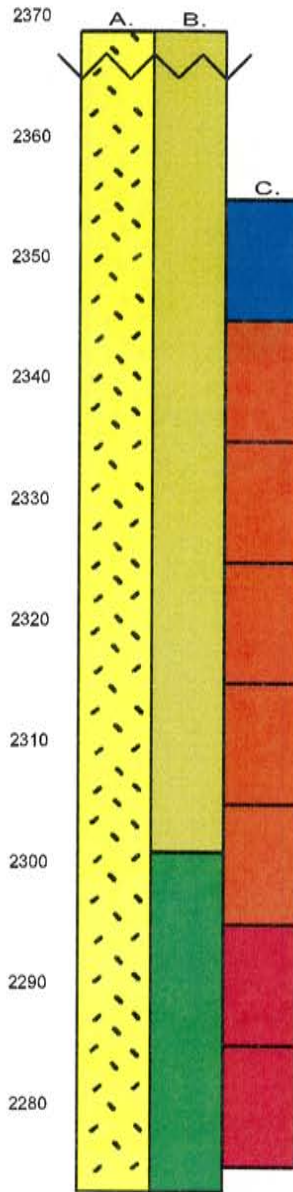
DDH-02-04



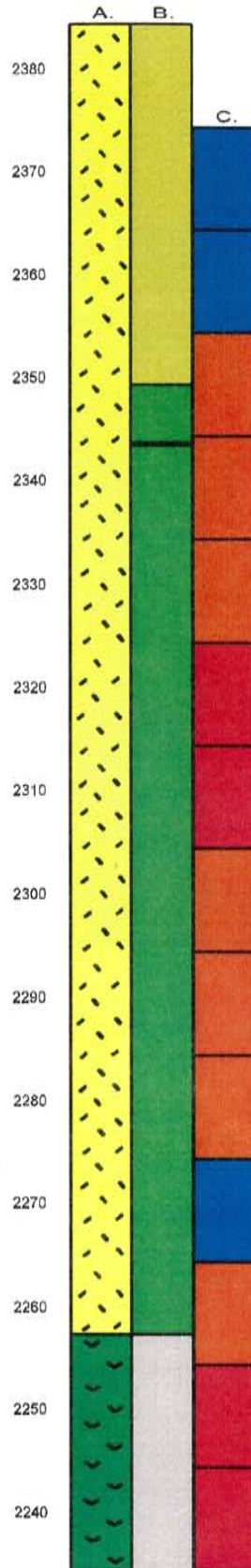
DDH-02-08



DDH-02-11



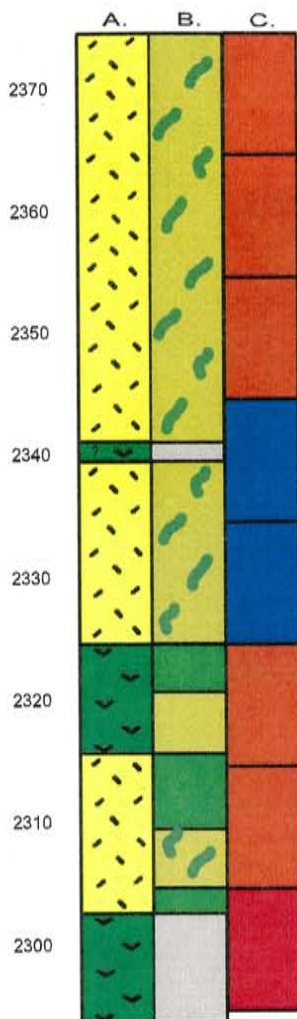
DDH-03-09



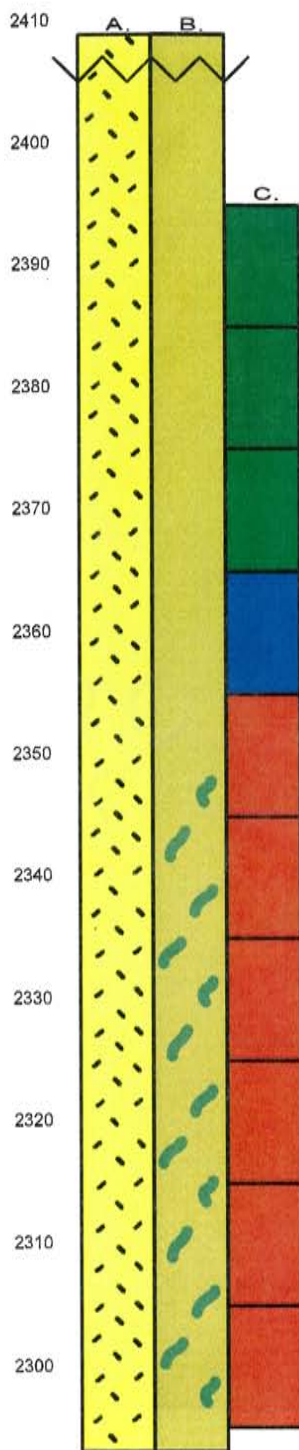
DDH-03-13



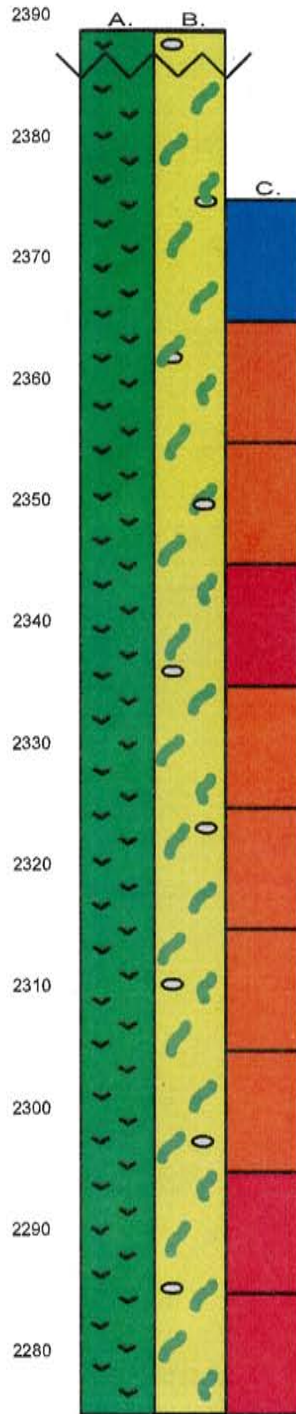
DDH-03-14



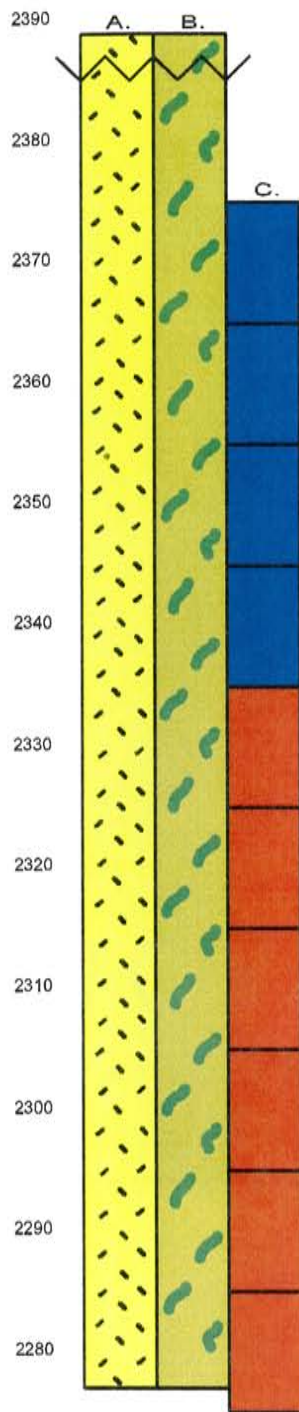
RC-02-21



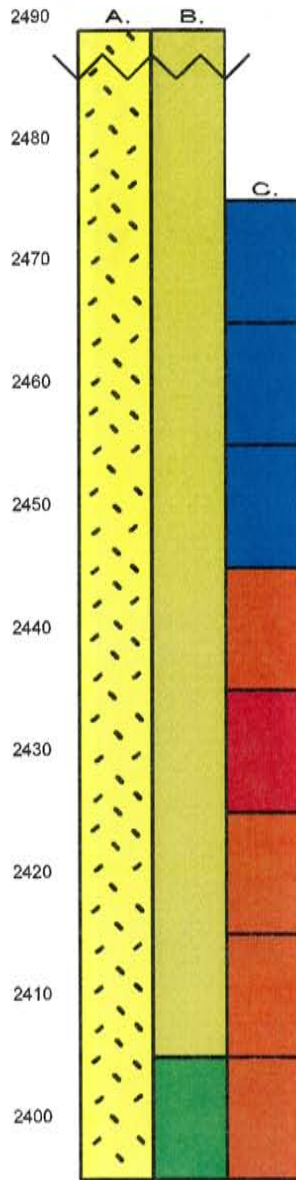
RC-02-24



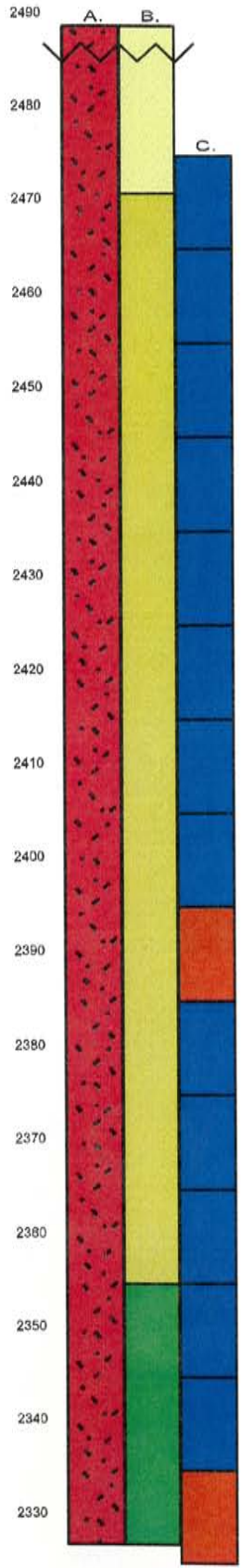
RC-02-30



RC-F6-17



RC-F6-28



RC-CC160

